UNIVERSITY OF SOUTHAMPTON

FACULTY OF ENGINEERING, SCIENCE & MATHEMATICS

School of Engineering Sciences

Analysis of the Propulsion and Manoeuvring Characteristics of Survey-Style AUVs and the Development of a Multi-Purpose AUV

by

Alistair Robin Palmer

Thesis for the degree of Doctor of Engineering

September 2009

UNIVERSITY OF SOUTHAMPTON

ABSTRACT

FACULTY OF ENGINEERING, SCIENCE AND MATHEMATICS
SCHOOL OF ENGINEERING SCIENCES

Doctor of Engineering

ANALYSIS OF THE PROPULSION AND MANOEUVRING CHARACTERISTICS OF SURVEY-STYLE AUVS AND THE DEVELOPMENT OF A MULTI-PURPOSE AUV

By Alistair Robin Palmer

Autonomous Underwater Vehicles (AUVs) are a developing technology with multiple applications including oceanographic research, military missions and commercial activities such as oil and gas field exploration. The reported research covers two main areas, namely, the assessment of the survey performance of AUVs and the development of the next generation of multi-purpose AUVs.

The performance characteristics of long range survey-style AUVs are examined and improvements in performance are sought through the use of hybrid devices. Hybrid devices are defined as those that provide both propulsion and manoeuvring forces. Two devices were chosen for detailed investigation; a vectored thruster and a collective and cyclic pitch propeller. The manoeuvring performance of both devices was found to be insufficient to justify the additional engineering complexity associated with them.

The aim of the next generation of AUVs is to be able to combine long range survey capabilities with low speed investigation of the environment encountered. An assessment of a likely mission profile and a review of the available design options demonstrate that maintaining the survey efficiency of the AUV is of principal importance. Therefore the investigation focuses on approaches to the addition of low speed control to an existing survey-style AUV design using propeller based thrusters. Externally mounted thrusters and through-body tunnel thrusters are reviewed and new experimental investigations are reported to provide insight into the performance characteristics on a survey-style AUV hull form.

The main body of the experimental programme characterises forward and aft mounted tunnel thruster performance over a range of forward speeds and small yaw angles. The results are used to develop a new, simple modelling procedure representing the performance of tunnel thrusters on an AUV which facilitates the incorporation of the characteristics of tunnel thrusters into numerical simulations of AUV performance. Such a simulation is used to examine approaches to undertaking the transition phase between high speed survey and low speed manoeuvring operation. The results demonstrate the advantageous nature of undertaking a smooth interchange between control approaches considering both the vehicle performance and the energy demands.

In loving memory of

Gregory David Palmer

(1981 – 2003)

Contents

List of Figures

Photographs used in this thesis are credited to the references provided in the captions, where applicable.

List of Tables

Declaration of Authorship

I, Alistair Robin Palmer, declare that the thesis entitled

'Analysis of the Propulsion and Manoeuvring Characteristics of Survey-Style AUVs and the Development of a Multi-Purpose AUV'

and the work presented in the thesis are both my own, and have been generated by me as the result of my own original research. I confirm that:

- this work was done wholly or mainly while in candidature for a research degree at this University;
- where any part of this thesis has previously been submitted for a degree or any other qualification at this University or any other institution, this has been clearly stated;
- where I have consulted the published work of others, this is always clearly attributed;
- where I have quoted from the work of others, the source is always given. With the exception of such quotations, this thesis is entirely my own work;
- I have acknowledged all main sources of help;
- where the thesis is based on work done by myself jointly with others, I have made clear exactly what was done by others and what I have contributed myself;
- parts of this work have been published as:

  Modelling Tunnel Thrusters for Autonomous Underwater Vehicles
  Palmer, A.R., Hearn, G.E. and Stevenson, P.
  Proceedings of the IFAC Workshop on Navigation, Guidance and Control of Underwater Vehicles (NGCUV), Killaloe, Ireland, 8-10 April 2008

  Thruster Interactions on Autonomous Underwater Vehicles
  Palmer, A.R., Hearn, G.E. and Stevenson, P.
  Proceedings of the 28th ASME International Conference on Ocean, Offshore and Arctic Engineering (OMAE2009), Waikiki, Hawaii, USA, 31 May–5 June 2009

  Experimental Testing of an Autonomous Underwater Vehicle Equipped with Tunnel Thrusters
  Palmer, A.R., Hearn, G.E. and Stevenson, P.
  Proceedings of the First International Symposium on Marine Propulsion (smp'09), pp569-575, Trondheim, Norway, 22-24 June 2009

  A Theoretical Approach to Facilitating Transition Phase Motion in a Positively Buoyant Autonomous Underwater Vehicle
  Palmer, A.R., Hearn, G.E. and Stevenson, P.
  Transactions of the Royal Institution of Naval Architects 2009 (Accepted, to appear)

Signed: ……..

Date:…….

Acknowledgements

I would like to thank my supervisors, Grant Hearn and Peter Stevenson, for their assistance and advice during the completion of this research. I am very grateful to have had the opportunity to work with them and gain from their areas of expertise and differing approaches, which I believe has produced a more rounded research project.

I would like to thank all those who have contributed to the University of Southampton AUV project, especially Maaten Furlong and Alex Phillips, which has provided me with some of the most entertaining and enlightening experiences of my time at the university. I would also like to thank all those I have shared an office with, and although he was lucky to escape that particular fate, a certain Austrian whose beverage reciprocation ceases only at seven.

Finally, I would like to thank my family and Em for sharing the excitement, the successes and, of course, the setbacks during my time completing this research.

Nomenclature

In the main text a 'prime' (e.g. x') denotes a non-dimensional quantity and a 'dot' (e.g. $\dot{x}$) denotes a time derivative, where appropriate.

a	Jet velocity decay model coefficient
a_m	Propeller axial inflow factor
A	Representative area (m^2)
b	Jet velocity decay model coefficient
b'_j	AUV stern propeller model coefficients (j=1, 2,…,9)
B	Buoyancy (N)
$\overline{BG}$	Vertical distance between centre of gravity and centre of buoyancy (m)
c	Tunnel thruster model coefficient
C	Static merit coefficient
C_D	Drag coefficient
C_{DET}	Drag coefficient for an external thruster
C_{DTT}	Drag coefficient for the additional drag caused by a thruster tunnel
C_F*, C_X*, C_Y*	Force coefficient for force F, X, Y
C_L	Lift coefficient
CoA	Centre of action of force (m)
CoA_S	Centre of action of suction force (m)
C_P	Tunnel thruster model coefficient
C_T	Thrust coefficient
d	Diameter (m)
d_f	Thruster quadratic damping ($kg.m^{-1}$)
D	Drag force (N)
D_A, D_F	Measured drag forces from aft, A, and forward, F, force blocks (N)
$D_{I\%}$	Percentage increase in vehicle drag
D_{PUL}	Drag force per unit length ($N.m^{-1}$)
E	Energy (Whr)
F	Force (N)
F_A, F_F	Measured side forces from aft, A, and forward, F, force blocks (N)
F_S	Suction force (N)
F_T	Thruster force (N)
F_V	Force on vehicle (N)
g	Acceleration due to gravity (= $9.81 m.s^{-2}$)
g_1, g_2,..., g_6	Tunnel thruster model coefficients

G	Steepness of thruster rotational speed allocation for pitch control
G_x	Linear momentum flux (kgm.s^{-2})
G_φ	Angular momentum flux (kgm^2.s^{-2})
h	Separation between vehicle and thruster (m)
i	Subscript representing a time step
I_{YY}	Pitch moment of inertia (kgm^2)
J	Advance coefficient
J_0, J_1	Bessel functions of the first kind
J_m	Motor inertia (kgm^2)
k	Ratio of the angular and linear velocities in a jet
k_0	Ratio of propeller rotational speed to vehicle speed at self propulsion
k_4, k_5	Tunnel thruster model coefficients
k_6	Pitch control allocation factor
K_3	Tunnel thruster model coefficient (kgm)
K_n	Motor speed constant (kgm^2.s^{-1})
K_F	Tunnel thruster force coefficient
K_N	Tunnel thruster moment coefficient
K_Q	Propeller torque coefficient
K_T	Propeller thrust coefficient
K_{Tn}, K_{Tp}, K_{Tt}	Thrust coefficients for nozzle, n, propeller, p and total, t, forces
l	Vehicle length (m)
l_p	Moment arm for experimental measurements (m)
l_T	Tunnel length (m)
L	Lift force (N)
m	Mass (kg)
m_f	Mass of fluid in control volume (kg)
M_{SS}	Pitch moment due to quantity SS (Nm)
n	Rotational speed (s^{-1})
n'	Propeller rotational speed ratio
N	Moment (Nm)
N_P	Number of panels
N_{SS}	Yaw moment due to quantity SS (Nm)
N_S	Suction moment (Nm)
p, q, r	Angular velocity components about x, y, z axes (rad.s^{-1})
p_B	Blade pitch (deg)
Δp_B	Differential in blade pitch (deg)
P	Power (W)

P_d	Pitch demand (rad)
P_{dL}	Pitch demand limit (rad)
P_S	Shaft power (W)
Δp	Pressure difference (Pa)
Q	Torque (Nm)
Q_m	Motor torque (Nm)
r_f	Fluid exchange rate (kg.min^{-1})
r_j	Jet half width (m)
r_p	Propeller radius (m)
r_{T1}, r_{T2}	Tunnel radius at location 1, 2 (m)
R	Turning radius (m)
R_B	Propeller blade radial force (N)
Re	Reynolds number
Re_e	Effective Reynolds number
R_j	Non-dimensional jet radius
ΔR_B	Differential in radial force across propeller hub (N)
s	Propeller slip ratio
S	Planform area (m^2)
SHP	Shaft horsepower (hp)
S_W	Swirl number
t	Time (s)
t_R	Running time (hr)
T	Thrust force (N)
T_1, T_2	Thrust force from thruster 1, 2 (N)
$T_{n\|n\|}$	Model coefficient for thruster characteristics
$T_{n\|u\|}$	Model coefficient for thruster characteristics
T_v	Transverse force from vectored thruster (N)
ΔT	Differential in blade thrust across propeller hub (N)
ΔT_T	Tunnel thruster thrust loss (N)
u, v, w	Velocity components in x, y, z directions (m.s^{-1})
u_c	Jet centreline velocity (m.s^{-1})
u_j	Average jet velocity (m.s^{-1})
u_m	Maximum jet velocity (m.s^{-1})
u_p	Velocity at propeller plane (m.s^{-1})
u_{req}	Required forward speed (m.s^{-1})
u^*	Mid-transition speed (m.s^{-1})

U	Flow velocity ($m.s^{-1}$)
U_c	Critical speed for control surface depth control ($m.s^{-1}$)
V	Swept volume (m^3)
x, y, z	Distance in longitudinal, transverse and vertical directions (m)
x_B	Longitudinal centre of buoyancy (m)
x_G	Longitudinal centre of gravity (m)
x_l	Moment arm for propeller about vehicle centre (m)
x_P	Moment arm for propeller blade about propeller hub (m)
x_S	Moment arm for suction force about vehicle centre (m)
x_T	Moment arm for thruster force about vehicle centre (m)
x_v	Moment arm for vectored thruster about vehicle centre (m)
X	Force in the surge or longitudinal direction (N)
X_{SS}	Surge force due to quantity *SS* (N)
Y	Force in the sway or transverse direction (N)
Y_{SS}	Sway force due to quantity *SS* (N)
z	Vertical distance (m)
z_B	Vertical centre of buoyancy (m)
z_G	Vertical centre of gravity (m)
Z_{SS}	Heave force due to quantity *SS* (N)

Greek Symbols

α	Angle of attack (rad)
α_0, α_1	Coefficients for linear approximation to thrust characteristics
β	Advance angle (deg)
γ	Jet path in a crossflow model coefficient
δ	Deflection angle (rad)
δS	Sternplane deflection angle (rad)
$\Delta\sigma$	Transition steepness
ε	Effective roughness height of a surface (m)
ζ	Bendemann merit coefficient
η	Efficiency
θ	Pitch angle (rad)
κ	Index representing time step at the end of the transition zone
μ	Thruster angle (deg)
υ	Kinematic viscosity (for seawater = $1.09 \times 10^{-6} m^2.s^{-1}$)
ξ	Jet path in a crossflow model coefficient

ρ	Density (for seawater = 1025kg.m^{-3})
$\sigma_{i,S}$	Proportion of depth control at time step i undertaken by tunnel thruster (S≡TT) or control surfaces (S≡CS)
τ	Thruster efficiency
χ	Radial angular co-ordinate (rad)
ψ	Yaw angle (rad)
ω	Jet path in a crossflow model coefficient
∇	Volume (m^3)

Mathematical Symbols

$\hat{=}$	Defined as ($a \hat{=} b$ implies a 'is defined as' b)

Abbreviations

Vehicle names are not included in this list.

ACCEL	ACCELeration
AST	Anti-Suction Tunnel
AUV	Autonomous Underwater Vehicle
CAD	Computer Aided Design
CCPP	Collective and Cyclic Pitch Propeller
CFD	Computational Fluid Dynamics
CS	Control Surfaces
DC	Direct Current
DNS	Direct Numerical Simulation
DVL	Doppler Velocity Log
GPS	Global Positioning System
HYD	HYDrodynamic
HYDST	HYDroSTatic
IMO	International Maritime Organisation
ITTC	International Towing Tank Conference
MARIN	MArine Research Institute Netherlands
NACA	National Advisory Committee for Aeronautics
NERC	Natural Environment Research Council
NOC,S	National Oceanography Centre, Southampton
PID	Proportional Integral Derivative
PIV	Particle Image Velocimetry
PROP	PROPeller
RANSe	Reynolds Averaged Navier Stokes equations
RB	Rigid Body
ROV	Remotely Operated Vehicle
TT	Tunnel Thruster
USB	Universal Serial Bus
UUV	Unmanned Underwater Vehicle
VBD	Variable Buoyancy Device
V/STOL	Vertical/Short Take-Off and Landing

Chapter 1 – Introduction

1.1 General Background on Underwater Vehicles

Following the presentation of some general background information on underwater vehicles to allow some appreciation of the challenges they present, the scope of the research and the achievements attained are listed prior to indicating the organisation of the rest of the thesis.

Underwater vehicles are being used in an ever increasing number of applications ranging from scientific research to commercial and leisure activities. Most of these tend to be used for a specific application; consequently, there is a wide variety of underwater vehicles in operation. These vehicles can be categorised into several different groups according to their particular characteristics. One of these characteristics is the method of control and the groups used in this category are defined as illustrated in Figure 1.1.

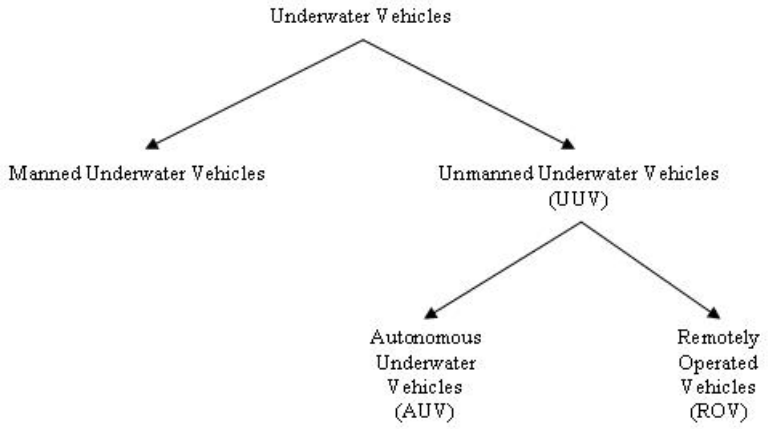

Figure 1.1 – Underwater Vehicles Categorised by Control Method

This work focuses on Unmanned Underwater Vehicles (UUVs) and more specifically Autonomous Underwater Vehicles (AUVs). AUVs have onboard control systems that use the information recorded by sensors to determine the demands to be sent to the vehicle actuators to complete the defined missions. The reliance on these components dictates a need for a robust design. A constraint on the use of an AUV is the limited energy supply that can be carried onboard. Most AUVs use batteries of various types to provide both propulsion and hotel power. Therefore the total energy available is limited by the available volume (or weight) for batteries and the energy density of the chosen batteries.

These two characteristics of AUVs heavily influence the design choices during the development of an AUV. The autonomous nature of the vehicle means that key design factors include reliability, robustness and controllability. The limited energy available

means that the energy cost associated with the various choices is a key factor in the design evaluation process. The combination of these factors dictates that the design cycle for an AUV is highly iterative.

In contrast, Remotely Operated Vehicles (ROVs) operate with a connection to a surface station, either on land or on a surface vessel. This connection is used to provide a communication link between the vehicle and a human operator, allowing human control, rapid data transfer and a much larger power supply. On most ROVs the control system is part human, part automatic; some elements of the control system are undertaken using automatic control (for example depth control) allowing the human operator to concentrate on the intricacies of the particular task. The larger power supply allows the designer (and operator) to design (use) the vehicle with less consideration for the energy required and this freedom also allows redundancy to be built into the design, for example in thruster configurations, which is not found on energy limited AUVs.

Within the AUV group there are subgroups of vehicles [1] which are split according to their particular application. The vehicles in these subgroups have common features and one particular subgroup contains the AUVs whose primary application is to undertake survey missions. These vehicles are often characterised in terms of the range achievable – the combination of vehicle endurance and speed – as this provides a measure of their survey performance capabilities. The vehicle range allows an assessment of the design of a vehicle incorporating the propulsive efficiency and the energy storage capacity. To maximise the range of survey vehicles the design focuses on combining a hydrodynamically shaped hull form and a high efficiency propulsion system with the ability to carry sufficient energy alongside the mission dependent payload. These design factors result in a common survey vehicle design comprising a torpedo-shaped (or similar) hull form with a stern mounted propeller and control surfaces (rudder and hydroplanes) to provide control at speed.

The required range of a vehicle can significantly influence the characteristic features of an AUV during the design of the vehicle. For example, the design of a short range AUV requires less emphasis on propulsive efficiency and energy usage. This freedom allows the short range AUV designer to include more energy consuming devices and to optimise for the mission requirements. Whereas the key to successful long range AUV design is a compromise between functionality limitations and mission range requirements and hence greater emphasis on hydrodynamic efficiency.

Common survey-style AUVs employ a stern mounted propeller and control surfaces for control. The propeller is used to provide a longitudinal thrust force giving control over the forward speed of the vehicle. The control surfaces, usually mounted in a cruciform arrangement, provide forces that enable the vehicle to pitch or yaw. However, the forces generated by the control surfaces are dependent upon the external flow velocity over the surface and will only provide the required control when the vehicle forward speed is sufficient.

Survey vehicles tend to be ballasted to be positively buoyant. This ensures that the vehicle rises to the relative safety of the surface should the propulsion system fail. To overcome the positive buoyancy at survey speeds, the hydroplanes generate a downward hydrodynamic force so that the vehicle operates at a small (nose-down) pitch angle. Operating at a pitch angle reduces the survey efficiency by increasing the drag of the vehicle. However, this approach allows for active buoyancy control without the substantial energy demands of alternative systems, see Section 3.5.

There are several vehicles that fit into the category of survey-style AUVs. These include HUGIN [2], Remus [3] and ISE Explorer [4] as illustrated in Figures 1.2(a), (b) and (c) respectively. All three of these vehicles exhibit some of the standard features of survey-style AUVs. However, it is interesting to note the differences between the vehicles despite their common characteristics, for example, the differing tail section designs.

Most AUVs are application specific. Improving performance has led to a greater desire to use AUVs for more complex and varied missions. Rather than have the AUV travel over a predefined route undertaking a limited surveying task in an assigned area, it would be beneficial to allow more in-depth localised scientific measurements over longer timescales than the cruising advance speed allows. This type of mission requires a multi-purpose vehicle, that is, one capable of combining efficient long range survey operation with low speed interaction; an investigation style task more commonly associated with ROVs.

For a survey-style vehicle to undertake this type of mission some low speed control is required to overcome the limitations of the conventional control surfaces. Manoeuvring forces are required, in addition to an ability to control the positive buoyancy, at low speed. The choice of approach to provide this additional control represents a key design choice in the development of a multi-purpose AUV. This must be considered in terms of the impact on the survey efficiency of the vehicle versus the low speed performance offered by the adopted approach.

(a)

(b)

(c)

Figure 1.2 – Photographs of Survey-Style Autonomous Underwater Vehicles
(a) HUGIN 3000, Length: l = 5.5m, Length to diameter ratio: l/d = 5.5 [2];
(b) Remus 600, l = 3.25m, l/d = 10 [3];
(c) ISE Explorer, l = 5m, l/d = 7.35 [4].

The following sections introduce the scope of the research undertaken to assist in the development of a multi-purpose AUV.

1.2 Scope of Research

The reported research is limited to the examination of survey-style AUVs. This limitation focuses the work on hydrodynamically shaped vehicles with an emphasis on survey efficiency and the energy cost associated with design choices. Approaches employed in

other fields of engineering, including other types of underwater vehicle, are assessed to examine their applicability to a survey-style AUV.

This research programme uses the Autosub family of AUVs as basis vehicles. These AUVs are developed and operated by the Underwater Systems Laboratory at the National Oceanography Centre, Southampton (NOC,S) with funding provided by the Natural Environment Research Council (NERC). The Autosub family currently consists of Autosub 3, the third generation of the original Autosub and a newer vehicle, Autosub6000. The particulars of these vehicles are given in Table 1.1 with photographs in Figure 1.3. Both vehicles have torpedo shape hull forms with an open single screw stern mounted propeller and four aft control surfaces in a cruciform arrangement [5]. Autosub 3 has undertaken many survey missions across the oceans and has investigated under ice caps [6]. Autosub6000 was developed using the experience obtained with the Autosub family and incorporates secondary battery technology to aid missions to depths of up to 6000m [7].

Table 1.1 – Autosub Family Particulars

	Autosub 3	**Autosub6000**
Length (m)	7.0	5.5
Maximum Diameter (m)	0.9	0.9
Length to Diameter Ratio	7.8	6.1
Flooded Mass (kg)	3600	2800
Depth Rating (m)	1600	6000
Design Speed ($m.s^{-1}$)	1.75	1.7

(a)   (b)

Figure 1.3 – Photographs of the Current Autosub Family
(a) Autosub 3 [6];
(b) Autosub6000 [7].

The calculations undertaken in this research refer directly to Autosub 3, due to the substantial amount of data available for this vehicle. However, the hydrodynamic

similarities between Autosub 3 and Autosub6000 mean that the conclusions of this work are applicable to both vehicles.

The initial focus of this research is an assessment of the performance of a survey-style AUV with respect to the propulsion and manoeuvring systems. Approaches to improving this performance are then considered through the enhancements offered by hybrid devices. That is, the improvements in performance offered by devices that offer a combination of propulsion and manoeuvring capabilities are considered.

The second part of the reported research focuses on next generation AUV development. These AUVs will be multi-purpose vehicles capable of combining efficient long range survey operation with low speed interaction and investigation style tasks. This development is considered in terms of how to add the necessary low speed manoeuvring and control capabilities to a survey-style AUV. An analysis of the available options for the low speed control is undertaken and the performance of an AUV with these modifications is considered.

This research work focuses on the practical and hydrodynamic issues of AUV propulsion and manoeuvring systems. A substantial influence on the performance of these systems is the control system used. However, the complexities of these control systems are beyond the scope of this work. Therefore, where appropriate simple control systems are developed and used to facilitate the simulation of the influence of other features on the performance of the whole system.

1.3 New Contributions

The new contributions to the development of AUVs and the exploration of the oceans include:

- The assessment of the performance of a collective and cyclic pitch propeller based on a survey-style AUV propeller design using the boundary element method.
- An analysis of the choices for low speed manoeuvring and buoyancy control for survey-style AUVs.
- An experimental assessment of the performance of a through-body tunnel thruster on a survey-style AUV body across a range of forward speeds and yaw angles.

- The development of modelling procedures for through-body tunnel thrusters to enable the assessment of the performance of, and to aid the design of control systems for, multi-purpose AUVs through the use of numerical simulations.
- The assessment of the performance of a survey-style AUV during the transition between high speed survey operation and low speed manoeuvring, including the interchange between control approaches focusing on the performance of the vehicle and the impact of different approaches.

1.4 Relevance to the Industrial Sponsor

This Engineering Doctorate research has been co-supervised and funded by the Underwater Systems Laboratory at the National Oceanography Centre, Southampton as the industrial sponsor. To put this research into context it is important to understand the relevance and importance to the industrial sponsor. Hence this research has focused on survey-style AUVs, as developed at NOC,S, and has used the Autosub family of AUVs as the basis vehicles.

The work undertaken on AUVs at NOC,S is funded by the Natural Environment Research Council (NERC) under the Oceans 2025 contract [8]. The Oceans 2025 contract is a NERC funded five-year programme of marine research which aims to:

> "…improve our understanding of how the ocean behaves, how it is changing, and what this means for society."

The Oceans 2025 contract is split into 10 themes. Theme 8 is 'Technology Development'. One of the aims of Theme 8 is to:

> "Provide distinctive measurement and observation platforms that meet science needs and cannot be sourced from industry, focussing on autonomous underwater vehicles and platforms for deep and long-range, long-endurance operation."

Theme 8 has four work packages. Work package 8.2 has a specific objective relevant to this research work:

> "To complete construction of Autosub6000 and test a basic version at sea followed by devising the software and hardware systems needed to make the vehicle agile and highly programmable, able to contribute to science experiments in water depths to 6000m."

The research work undertaken forms part of the efforts to develop survey-style AUVs to make them more agile and facilitate science experiments up to 6000m depth.

1.5 Organisation of Thesis

The thesis is arranged into four further chapters prior to some concluding remarks, references and appendices. Chapter 2 examines the performance of existing survey-style AUVs and considers the potential of hybrid propulsion and manoeuvring devices as a means of enhancing the survey capabilities. Chapter 3 introduces the requirements for a multi-purpose AUV and discusses the associated challenges and available options. Chapter 4 considers the performance of the chosen low speed control approach, propeller based thrusters, and reports the results, conclusions and modelling approaches developed using experimental testing. Chapter 5 implements the chosen low speed control approach on a survey-style AUV and assesses the resulting performance during the transition phase between survey and low speed operation and during low speed manoeuvres.

Chapter 2 – Assessment of Survey Performance

2.1 Introduction

The primary task of the AUVs under consideration in this research is surveying areas of the seas and oceans. These survey missions are undertaken for a variety of reasons including oceanographic research, commercial activities such as exploration of oil and gas fields and military missions such as surveillance and mine-sweeping. These missions have similar profiles giving a large number of AUVs with similar characteristics but different origins and design philosophies. The performance of a survey-style AUV on a typical mission will be discussed before examining possible approaches to enhancing this performance.

2.2 Survey Performance Characteristics

Survey-style AUVs are a group of vehicles with common characteristics that enable them to undertake survey missions in an efficient manner. These characteristics include a hydrodynamically shaped hull form and underactuated propulsion and manoeuvring control. The rationale behind these choices will become apparent when a common mission profile, such as a lawnmower survey, is considered.

2.2.1 Lawnmower Survey

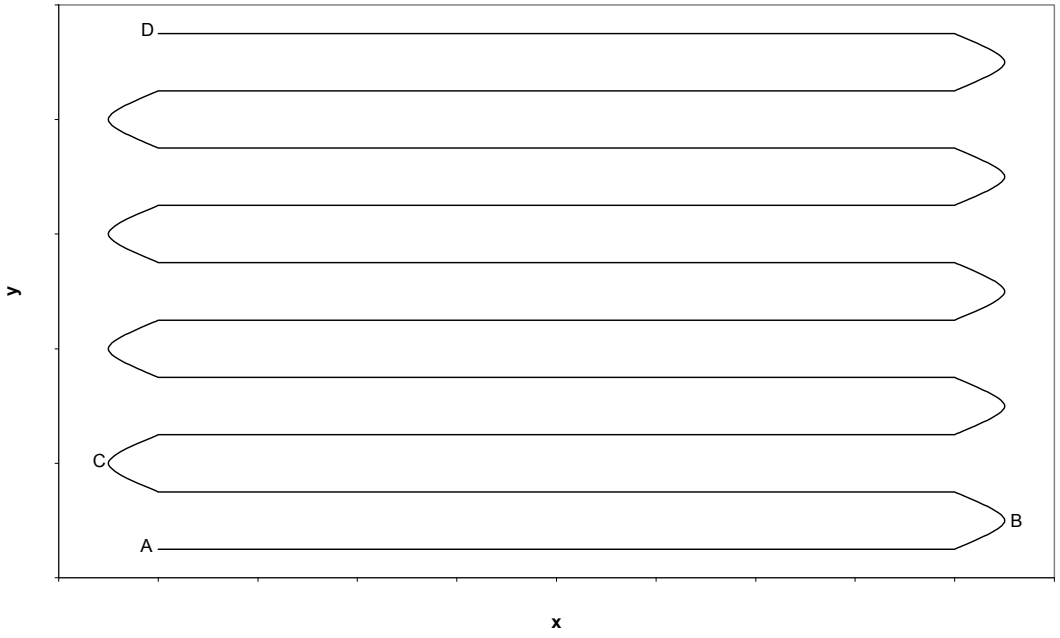

Figure 2.1 – 2-D Lawnmower Survey Mission Profile

A 2-D lawnmower survey mission profile is illustrated in Figure 2.1. The vehicle travels from a starting position, A, in a straight line over a chosen length with a 180º turn at the end of the line, B. The vehicle then returns along a parallel line, offset from the previous line by a known distance (as a function of the manoeuvrability of the vehicle), and makes another 180º turn at the end of this line, C. This process is repeated until the desired area has been covered, D. The survey can be carried out at a constant depth or with a variable depth profile along each line of the mission. A mission profile of this type enables the generation of a detailed map of the area (in whatever terms are desired) in a logical and efficient manner.

The features of a lawnmower survey mission profile can be used to explain the common characteristics of a survey AUV. In the following discussion the environment around the AUV is idealised as an infinite body of undisturbed (that is, without currents) homogeneous seawater. The vehicle will undertake the mission at a given speed, that is, with a constant demand on the rear propulsor (as a function of the particular method of control employed). The vehicle will spend the majority of the mission travelling in one particular direction, forwards, with only a relatively small proportion of the mission time spent turning.

The features of this mission profile dictate that an efficient approach to completing the mission is to use a vehicle with a hydrodynamically shaped hull form, optimised for the predominant direction of motion, with a high efficiency propulsor, such as a propeller optimised for the survey speed condition. A low power manoeuvring system, with a minimal impact upon survey efficiency, capable of controlling the vehicle yaw and pitch at the selected advance speed is required. These characteristics are chosen to minimise the power required to cover a particular distance, which allows the vehicle to maximise the achievable range, and hence survey as large an area as possible.

Two other common design features employed on survey-style AUVs include the addition of more control surfaces [4] and the use of twin screw propulsion [9]. The additional control surfaces are mounted forwards of the rear control surfaces to enhance manoeuvrability, assist in depth and pitch control at low speeds and aid rapid changes in depth. The use of twin screw propulsion is common on flatfish shaped AUVs and provides manoeuvring forces in the horizontal plane through a differential between the operating points of the two screws. This means the AUV requires less control surfaces. However, the efficiency of a twin screw propulsion system is lower than that of a single screw system [10].

Since this research focuses on a basis survey AUV design incorporating a hydrodynamically shaped hull form, a single screw rear propeller and a stern mounted cruciform of control surfaces, operational and performance characteristics of such AUVs are discussed next.

2.2.2 Characterisation of Survey Vehicle Performance

An operational characteristic of a survey vehicle is the achievable range (the product of vehicle speed and endurance). Most AUV manufacturers and operators will provide details of the maximum vehicle range or the endurance of the vehicle at given speeds. In addition, AUVs may be characterised by size, weight, depth rating, payload capacity and the sensor packages available. Most manufacturers and operators do not provide manoeuvring performance measures for survey vehicles. For those that do, standard naval architecture definitions including turning circle diameter are used.

The given set of AUV characteristics provides the potential user with sufficient information to select an appropriate vehicle for a particular mission. For a survey vehicle performance indicators beyond these simple measures are not of any great importance.

2.3 Propulsion and Manoeuvring Systems

To enhance propulsion and manoeuvring system performance on an AUV it is important to understand the individual component performance characteristics and how each component interacts with one another. This understanding provides insight into how changes to the individual systems will affect the overall vehicle performance. As a first step, the components of the propulsion and manoeuvring systems are introduced together with identification of those factors that affect their performance during survey operation.

2.3.1 Propulsion System

The propulsion system components, in terms of the straight line forward speed performance, are schematically represented in Figure 2.2.

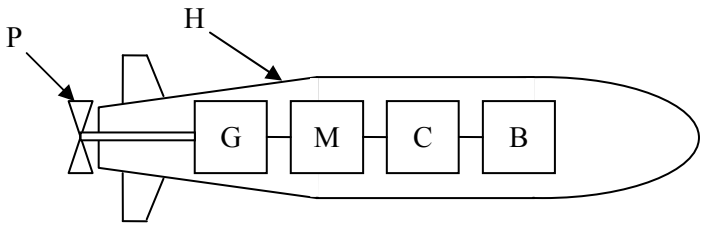

Figure 2.2 – Schematic Illustration of the Propulsion System
(P: Propeller, H: Hull form, G: Gearing and Shafting, M: Motor, C: Motor controller, B: Batteries)

The performance characteristic factors for the cited key components are briefly discussed next.

2.3.1.1 Batteries

The batteries provide both propulsion and hotel power. For a survey vehicle the propulsion power demand imposes a constant load on the batteries. The performance of the batteries is dependent upon how they are managed and the loads applied to them. To maximise the performance of the batteries the propulsion load should be kept as consistent as possible, with minimal spikes in the demand.

2.3.1.2 Motor Controller

The motor controller forms the link between the high level control, which determines what the vehicle is doing at a given point in time, and the physical implementation of the task. The motor controller takes as input a demand from the high level control, which is likely to be a forward speed, and converts this into an operating point for the motor. The control variable selected is a function of the complexity desired. There are two common options. Firstly, to control the power (current) provided to the motor or, secondly, to control the rotational speed of the motor. The former approach is the simpler, as it is easier to manage the battery load and provides a good way of maintaining constant vehicle speed through the water. The latter approach is more complex, but can provide greater control over the performance of the propulsor. Both options may incorporate a feedback loop, which in turn requires some sensor capability on the motor.

2.3.1.3 Motor, Gearbox and Shafting

The motor uses the energy stored in the batteries to rotate the shaft and hence turn the propeller. The motor should be designed/selected to operate at its most efficient when the shaft rotational speed matches that required to give the desired vehicle speed. A survey vehicle generally operates as a steady state system; hence the dynamic performance of the motor is of little importance. Therefore, the motor performance can be represented using simple models [11]. Any gearing and the necessary shafting will create losses. These need to be accounted for in the system performance analysis.

2.3.1.4 Hull Form

The hull form is a hydrodynamic fairing enclosing the AUVs internal components. The hull form is the primary cause of the drag force that needs to be overcome to propel the vehicle at the chosen speed. The drag is a function of the hull geometry, the vehicle speed and the angle of attack of the vehicle. The form of the hull is a function of the design shape, the appendages (including those that are mission dependent) and the hull surface condition.

The vehicle drag is also influenced by the propeller generated pressure distribution. In turn, this pressure distribution is a function of the complex flow conditions at the propeller plane generated by the flow over the upstream hull form.

The drag of the hull form can be characterised using empirical formulae, experimental testing or Computational Fluid Dynamics (CFD) simulations. Each approach has differing levels of accuracy, complexity and cost. The vehicle drag, D, is usually expressed in terms of a drag coefficient, C_D, at a given Reynolds Number as a function of the angle of attack, α. In this study a volumetric representation is adopted:

$$D = 0.5\,\rho\,\nabla^{2/3}\,U^2\,C_D\,. \tag{2.1}$$

2.3.1.5 Propeller

The propeller is a device consisting of several blades. The rotating blades accelerate the fluid along the propeller axis, resulting in a thrust force acting in the opposite direction. Propeller performance is a function of the blade rotational speed and the flow into the propeller [10]. For the majority of the mission, the propeller will be operating at a constant

rotational speed, subject to a constant inflow profile (in this idealised environment), and thus should be optimised for this particular condition.

Propeller performance can be characterised using various theoretical approaches or using experimental testing. Again these approaches have differing levels of accuracy, complexity and cost. Propeller performance is usually given in the form of a non-dimensional propeller chart, which shows how the thrust, torque and efficiency vary as a function of the inflow speed and blade rotational speed [10].

2.3.1.6 Performance Assessment of the Propulsion System

The complete performance of the propulsion system is commonly characterised in terms of the efficiency of the system, that is, the ratio of the useful power output to the power input required. The power input is the product of the voltage and current supplied by the batteries. The power output is the product of the propeller generated thrust and the resultant speed of the vehicle. However, there are other factors that are important when analysing the overall impact of the propulsion system on the vehicle. These include, amongst others, the vibrations induced by the propeller on the hull, the noise generated by the system and the internal space required.

2.3.2 Manoeuvring System

The manoeuvring system components, in terms of the vehicle turning performance, are illustrated in Figure 2.3.

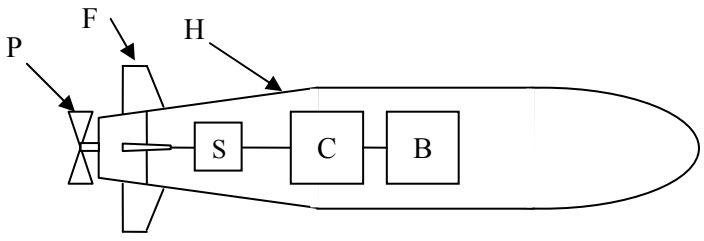

Figure 2.3 – Schematic Illustration of the Manoeuvring System
(P: Propeller, F: Control Surfaces, H: Hull form, S: Servos, C: Servo controller, B: Batteries)

Without revisiting details discussed in the previous propulsion section, the factors affecting the performance characteristics of the manoeuvring system are now briefly discussed.

2.3.2.1 Batteries

The manoeuvring system requires only a small amount of power to adjust the deflection angle of the control surfaces. Therefore battery performance should not significantly influence the manoeuvring system performance.

2.3.2.2 Servo Controller and Servos

The controller forms the link between the high level control and the physical implementation of the demands. The control approach adopted converts the input demand into a control surface deflection angle to be sent to the servos. These demands are a function of the desired operational mode and the selected manoeuvre. The performance of the servos dictates the responsiveness of the control surfaces and the accuracy with which the control surfaces achieve the commanded deflection angle.

2.3.2.3 Hull Form

The hull form (and the physical properties of the vehicle) dictates the response of the vehicle to the control surface generated forces. The naked (unappended) hull form is unstable. Thus control surfaces are added to provide both stability and manoeuvring capabilities. This stability means that once the vehicle is travelling in straight line motion, it will resist any attempt to deviate from this condition. This resistance needs to be overcome by the control surface forces generated. Thus to assess the performance of the system requires an understanding of the response of the vehicle to these forces.

Vehicle response is commonly characterised theoretically using dynamic equations of motion. In manoeuvring studies the forces acting on the system are usually represented as a series of hydrodynamic coefficients. These coefficients can be determined using empirical relationships, experiments or CFD simulations.

2.3.2.4 Propeller

The propeller performance will vary as a function of the changing inflow profile caused by the manoeuvre. Further performance variations could arise depending upon the control strategy used for the propeller. This is a function of whether the rotational speed of the propeller remains constant or not.

2.3.2.5 Control Surfaces

The control surfaces are symmetric aerofoil shapes. They generate a lift force when positioned at an angle to the flow. The magnitude of the lift is governed by the differing pressure distributions of the flows over the upper and lower surfaces of the aerofoil. For a given aerofoil, the lift generated is a function of the flow velocity over the surface and the deflection angle. The control surface also causes a drag force at all angles of attack (including zero) as a function of the flow velocity and deflection angle. The moment generated on the vehicle by the control surfaces is a function of the location of the control surfaces. That is, to maximise the turning moment generated the control surfaces should be mounted as far aft on the vehicle as possible, giving the largest moment arm possible [12].

Aerofoil characteristics have been extensively studied using wind tunnel testing, hence data for commonly used sections is widely available [13]. Experimental and CFD approaches can also be used to characterise the performance of aerofoil sections. The performance is expressed in terms of lift and drag coefficients, C_L and C_D respectively, (for a particular Reynolds Number) as a function of the angle of attack, α, thus

$$L = 0.5 \rho S U^2 C_L$$

and (2.2)

$$D = 0.5 \rho S U^2 C_D .$$

2.3.2.6 Performance Assessment of the Manoeuvring System

The complete performance of the manoeuvring system is usually provided in terms of simple manoeuvring measures such as the vehicle's turning circle diameter. Such metrics can be determined through experimental trials, CFD simulations or estimated using equations of motion (provided that sufficient information is available about the performance of the control surfaces and the response of the hull).

In the complete analysis of the manoeuvring system it is necessary to include the influence of the internal space required, the overall dimensions of the vehicle, the drag generated when not generating lift (at zero deflection angle) and the effect of the control surfaces on the flow into the propeller.

2.3.3 Complete Performance Assessment

The components of the propulsion and manoeuvring systems have been analysed in some detail in previous work [14, 15, 16, 17]. This literature identifies approaches to analysing each component individually, which can be combined to offer some insight into overall system performance. A more complete system performance can only be accurately predicted by modelling the entire system to ensure all component interactions are included. This more thorough approach increases the complexity and cost of an experimental or computational analysis programme. It is therefore common to attempt to model the components of each system individually whilst accounting for the remaining system influences in simple ways. This approach is exemplified in the use of a single wake fraction to account for the influence of the hull form on the inflow velocity to a propeller.

Using this simplified analysis it is possible to develop an understanding of the operation of the complete system and to gain insight into performance variations caused by design parameter changes. This approximation of the interactions between components provides a suitable basis for the design and development of an AUV. When using the insight gained from this simplified analysis it is important that the influence of the assumptions used and weaknesses of the approach adopted are understood. As a simple example it is important to understand how the variation of the magnitude of the selected wake fraction influences the determined propeller performance and the uncertainties introduced by this simplified representation of the inflow profile.

The components of interest in this study are the external components that interact with the flow to generate propulsion and manoeuvring forces. The performance of these components, the propeller and the control surfaces, will be considered next.

2.4 AUV Propeller Performance

The performance of a typical AUV propeller can be examined using experimental techniques and computational approaches. For this work a computational approach was adopted to facilitate the rapid assessment of the influence of a variety of different parameters. The chosen approach is the boundary element method.

The boundary element method belongs to the same family of analysis techniques as the lifting line and lifting surface methods [18]. These methods are based on the classical hydrodynamic ideas of modelling the potential flow around bodies using fluid singularities.

In potential flow, the fluid is assumed incompressible and inviscid and the flow is assumed to be irrotational. The main differentiating factor between these methods is the approach to modelling the distribution of circulation on the propeller blade. The boundary element method is the most physically representative of this family of methods as the full blade geometry is modelled using vortex elements. (Lifting line and lifting surface methods model the blade as either a line or surface of vortex elements with source and sink distributions to simulate the blade thickness.) This level of complexity means that these problems are solved using panel methods [19]. Panel methods represent a structure using a distribution of N_P panels placed over the body surface. This enables the required surface integrations to be computed as the solution of a set of N_P algebraic equations, which reduces the computational expense and allows these simulations to be performed quickly on a personal computer [20].

Potential flow does not recognise the shearing influence of fluid viscosity and so provides a simplification of the full Navier-Stokes equations. Limitations of this approach are that viscous effects have to be approximated (for example, as skin friction) and the onset of blade stall is not modelled. Hence the results have to be analysed within these limitations. Viscous effects are included in models using the complete Navier-Stokes equations and the approximate Reynolds Averaged Navier Stokes equations (RANSe) simulations; however the computational effort makes these approaches less attractive.

The current Autosub propeller is modelled using the in-house boundary element code, Palisupan [21]. This code has been used on a wide range of problems and has undergone extensive experimental validation (see [22]). The propeller is modelled as a single blade with a helical fraction of the hub to take advantage of the inherent symmetry. The propeller geometry is constructed from a standard propeller table and a propeller section for each specified radius. The details of the propeller are given in Appendix A1. Additionally, a wake model is required to account for the jump in potential at the trailing edge of the propeller blade. This wake is modelled using a fixed helical shape of user defined length. The panel distributions for the blade, hub and wake are selected to achieve a force convergence with the characteristics of the flow in mind. The generation of the propeller geometry files and the panel distributions are undertaken using script based procedures for ease of development. For further details on the code used and the modelling procedures adopted see [23].

Once the geometry has been modelled a solution is calculated as a function of the rotational speed of the propeller and the inflow profile. To include the influence of the hull form on the inflow profile a simulation of the flow over the Autosub hull form was performed using

Palisupan. This calculation procedure involves an iterative solution of the (non-lifting) potential flow over the body and a boundary layer model based on flat plate boundary layer theory [24]. The nominal wake profile at the propeller plane was extracted from this solution and applied to the propeller blade. The wake profile is assumed axisymmetric, thus neglecting the influence of the control surfaces on the wake profile, for details see Appendix A2.

The forces and moments generated by the propeller were calculated across a range of advance coefficient, J, and are plotted in Figure 2.4 using the following non-dimensional coefficients for the thrust, T, torque, Q, and efficiency, η:

$$J = \frac{U}{nd}$$
$$K_T = \frac{T}{\rho n^2 d^4}$$
$$K_Q = \frac{Q}{\rho n^2 d^5} \qquad (2.3)$$
$$\eta = \frac{JK_T}{2\pi K_Q}$$

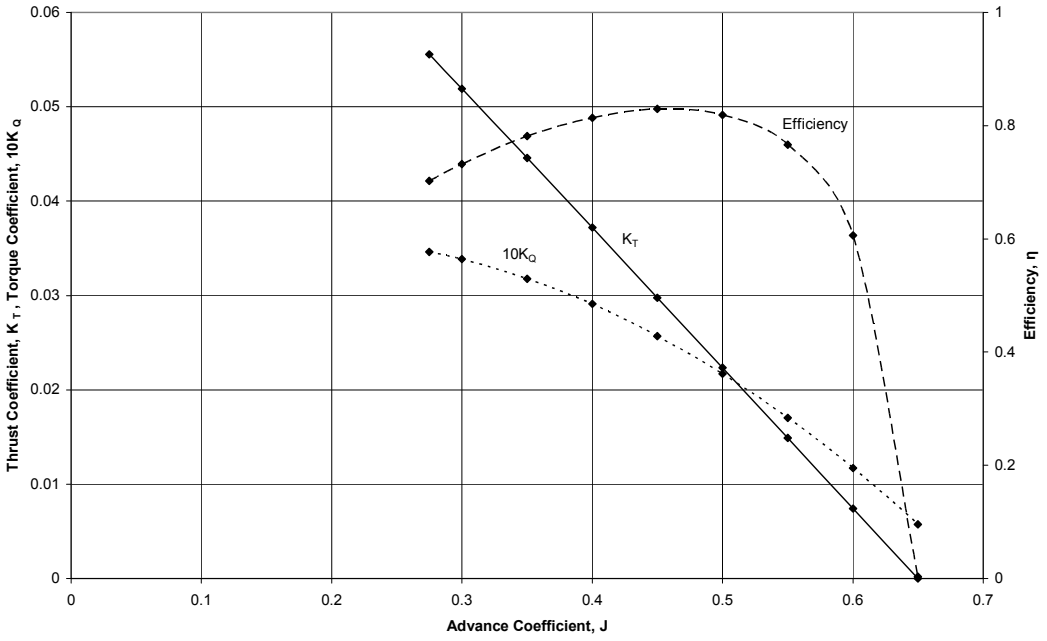

Figure 2.4 – Autosub Propeller Chart

(Solid line shows K_T, dotted line shows $10K_Q$ and dashed line shows efficiency)

The propeller demonstrates standard propeller characteristics, that is, a reduction of thrust and torque with increasing advance coefficient up to a point at $J = 0.65$ where the propeller generates no thrust force. Furthermore, the chart shows an optimal operating point, in terms

of efficiency, at J = 0.46, which corresponds to the propeller being optimised for survey speeds at the design rotational speed. This model of the propeller blade will be used as the basis of the investigation into the performance of hybrid devices.

2.5 Control Surface Performance

The performance of the control surfaces (rudder and hydrofoils) could be investigated using a computational approach similar to that used for the propeller. However, an experimental investigation into the performance of the control surfaces was undertaken during the design phase of Autosub [25]. A series of captive manoeuvring trials were used to assess the performance of three sets of control surfaces and the selection of the chosen control surfaces was based upon the measured results. Therefore, a comprehensive body of experimental data characterising the performance of the control surfaces, including the interaction with the hull is available [25].

The performance of a control surface is usually given in terms of the lift and drag coefficients. However, to analyse the performance of the complete manoeuvring system the forces and moments generated by the control surfaces are given in the form of the hydrodynamic derivatives used in the equations of motion, so that they are compatible with the coefficients for the hull form. These coefficients are similar to the lift and drag coefficients, but assume that the lift and drag varies linearly with deflection angle. This assumption is valid as long as the onset of stall is avoided.

The turning performance of the vehicle is characterised in terms of the turning radius. Equation (2.4) can be used to calculate the turning radius based on the linearised equations of motion in the horizontal plane with the assumption of a steady turning rate. The coefficients used in Equation (2.4) are non-dimensional (as indicated by a prime) with the values adopted given in Appendix A3.

$$R' = \frac{1}{r'} = \frac{(-Y'_r + m')N'_v - (-N'_r + m'x'_G)Y'_v}{(Y'_\delta N'_v - N'_\delta Y'_v)\delta} \tag{2.4}$$

The theoretically predicted turning performance of the vehicle with an increasing deflection angle at survey speeds, calculated from Equation (2.4), is shown in Figure 2.5. The turning radius is given in non-dimensional form as the number of vehicle lengths, l, required to make the turn. These results show that at the higher control surface deflection angles the turning radius for the vehicle tends towards twice the length of the vehicle.

Having introduced key standard propeller concepts and turning circle radius, a necessary appreciation for survey operation, the next step is to consider how propulsion and manoeuvring performance improvements might be achieved. These results provide a basis performance standard to which the manoeuvring performance of the hybrid devices can now be compared.

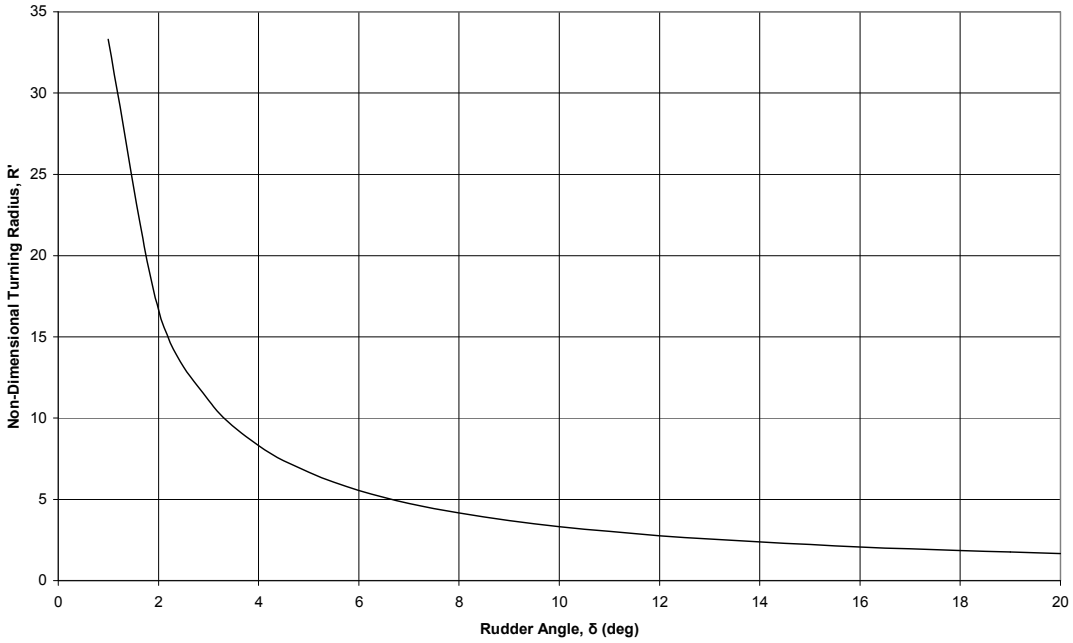

Figure 2.5 – Turning Performance of Autosub using the Rudder

2.6 Performance Improvements

Having outlined the propulsion and manoeuvring system components employed on a survey-style AUV the discussion will ultimately focus on an examination of potential improvements in performance. Performance improvements can be sought in a variety of ways. Typically propulsion system improvements could be sought through increases in system efficiency, reduced vibrations, etc (for example [26]). Achieving such improvements necessitates greater understanding of the individual systems and how they interact with each other to enable detailed integrated design solutions. Rather than focus on improvements to existing systems (through detailed analysis of the interactions between the systems) analysis is to be undertaken of alternative hybrid systems – systems which combine both propulsion and manoeuvring capabilities. A limited number of these hybrid systems have been reported in the published literature. This study seeks to determine whether these systems could offer potential performance improvements for a large, long range, survey-style AUV like Autosub.

The performance of the associated internal components of the systems is assumed known and to be represented by simple models (where necessary). In what follows external components will be examined in terms of their interaction with the surrounding fluid to generate propulsion and manoeuvring forces.

2.6.1 Hybrid Devices

In the context of propulsion and manoeuvring for a survey-style AUV, hybrid devices are those whose principal mode of operation is the generation of a propulsion force with a secondary mode providing additional forces for manoeuvring and control. There are two basic ways of achieving this using a single device. Firstly, to direct the principal propulsion force in a direction such that the distinct resolved components generate propulsive and manoeuvring forces. Secondly, to generate forces in additional directions in combination with the principal propulsive force. The most common approach used on surface vessels is the first approach, for example, an azimuthing propulsor.

Hybrid devices may not offer superior performance when compared with the individual propulsion or manoeuvring systems but they may offer other potential benefits such as a reduction in vehicle drag or improved propeller inflow through the reduction or removal of the control surfaces.

The majority of active force generation approaches used on marine vehicles are propeller based. Hybrid propeller based devices include a vectored thruster and a collective and cyclic pitch propeller. Another approach to generating both propulsion and manoeuvring forces from a single device is to appeal to the currently developing field of biomimetics [27]. The aim of this approach is to mimic behaviour observed in nature to efficiently generate and control forces, for example, flapping foils which aim to mimic fish fins [28]. The size of this field, its developmental nature and its distinction from the other approaches means that it is deemed to be outside of the scope of this investigation.

The two available propeller based hybrid devices that could potentially improve the performance of a survey-style AUV are vectored thrusters and collective and cyclic pitch propellers. These two devices will be considered next.

2.6.2 Vectored Thrusters

A current vehicle which uses a hybrid device is the Bluefin AUV [29], presented in Figure 2.6. The stern mounted vectored thruster provides the required propulsion and manoeuvring forces.

Figure 2.6 – Photograph of the Bluefin-21 AUV [29]

A vectored thruster can orientate the propeller jet in a particular direction. The device is mounted in place of the normal stern propeller. The resolved components of the resultant thrust provide the propulsion and manoeuvring forces for the vehicle. Vectored thrusters tend to employ a duct around the propeller to enhance the lateral force generation capabilities of the device (and to protect the propeller). The use of vectored thrusters is similar to the azimuthing and podded propulsors used on tugs and ferries to enhance the manoeuvrability. (Vectored thrusters can also be used in alternative thruster configurations to increase the manoeuvrability options available from a given number of thrusters.)

The major limitation of this device is the angular range over which the force can be directed. Angular range is restricted by the stern mounting and the actuation approach adopted. The actuation options include directing the propeller and duct using two internally mounted arms [30], exploiting the properties of magnetic couplings [31], the use of a parallel kinematics machine (robotic arms) [32] and a smart materials approach. In the last approach the propeller duct is actively shaped to direct the propeller jet [33]. These options have various advantages and disadvantages. The most common approach uses two internally mounted arms as this is the simplest and most mechanically robust approach but does limit the actuation to a single plane.

2.6.2.1 Vectored Thruster Performance

A relatively straightforward approach to examining vectored thruster performance would be to calculate the expected thrust force for the given inflow and rotational speed and then determine the components of this thrust force as a function of the thruster angle [34, 32]. In this simple model the off-axis component of the inflow is ignored. Figure 2.7 demonstrates this approach for normal operation (with no thruster angle) and for operation with a thruster angle, μ.

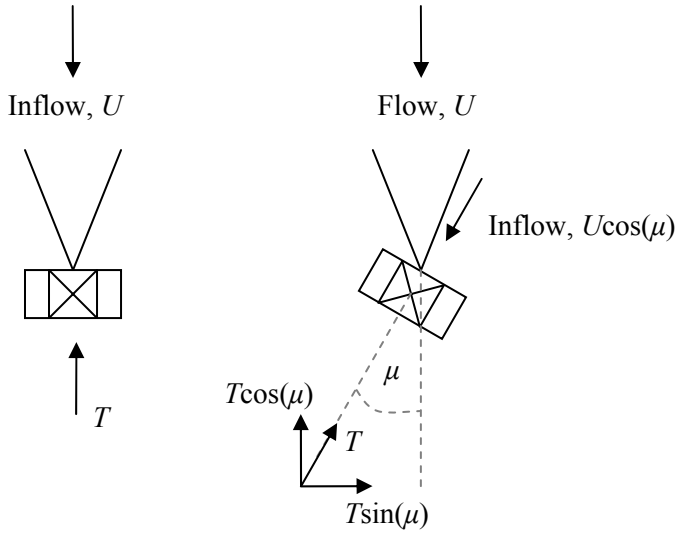

Figure 2.7 – Simplified Performance Assessment Approach for a Vectored Thruster

There are several complications regarding the performance of a propeller in these conditions. These include:

- The performance of a propeller with an inclined inflow (including the off-axis component).
- The influence of the duct.
- The nature of the inflow as a function of the flow over the body.
- The design of the particular device (mounting) in question.

The performance of a vectored thruster at an angle of incidence to the flow has been examined experimentally [35]. The results show that the thrust angle (angle of the resultant force) does not necessarily correspond to the thruster angle (the angle of incidence of the thruster). This is due to the variations in the performance of the propeller in an inclined flow and the influence of the duct. As a consequence of this complexity, open water thruster performance is usually characterised using fits to experimental data [36].

The performance of two different designs of vectored thruster attached to an AUV body has previously been investigated [35, 37]. The first design has an internally actuated vectored thruster attached to the rear of a torpedo shaped vehicle, similar to the Bluefin AUV. Experimental testing of this vehicle demonstrated the influence of the hull form by showing different force responses from the vectored thruster compared to a thruster operating at an angle of incidence in open water. Particle Image Velocimetry (PIV) testing was used to identify the reasons for this differing performance. The principal cause was determined to be the occurrence of flow separation near the inlet of the thruster duct. Figure 2.8 provides the thrust angle recorded experimentally, plotted against the thruster angle [35]. For comparison purposes the same data is plotted for a ducted thruster operating in open water as calculated from [36] at the same advance coefficient.

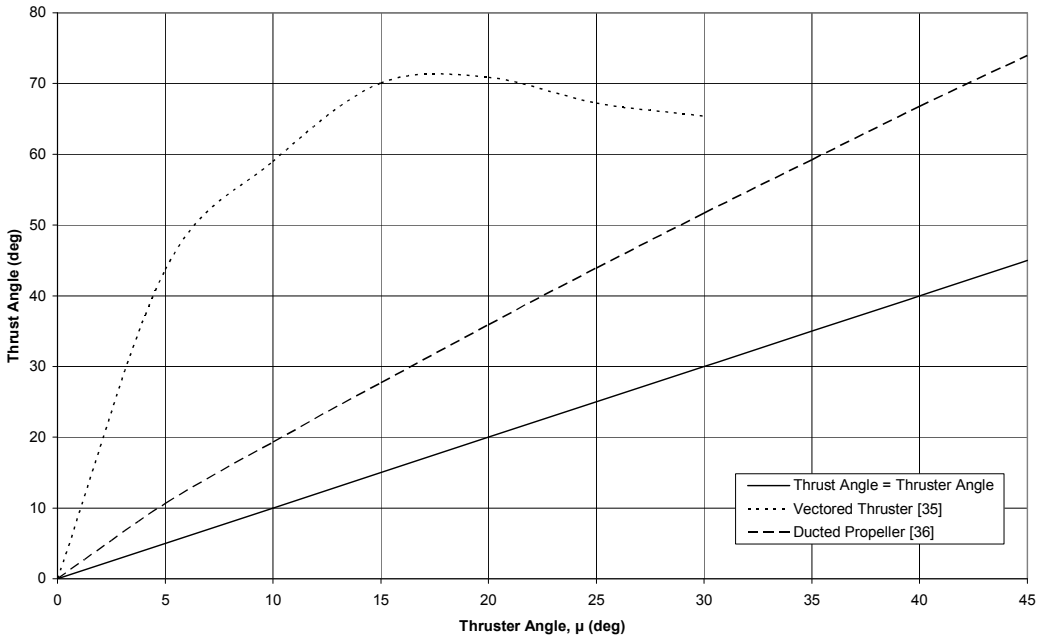

Figure 2.8 – Variation of Thrust Angle as a function of Thruster Angle for a Vectored Thruster

Figure 2.8 clearly demonstrates the invalidity of the assumption that the thrust angle coincides with the thruster angle. In fact the thrust angle is always greater than the thruster angle. The primary reason for this is the influence of the duct, which generates a force perpendicular to the propeller axis when operating with a non-zero thruster angle. The relationship between the thrust angle and the thruster angle illustrated in Figure 2.8 illustrates the difficulty in modelling the performance of a vectored thruster. Furthermore, the dependence of the performance on the separation phenomena (observed using PIV testing) increases the complexity of modelling this device.

The second vectored thruster AUV design is based on the principle that vehicle drag can be reduced using boundary layer control techniques [37]. The vehicle has a laminar flow hull shape. Towards the rear of the vehicle suction is applied to the boundary layer to prevent flow separation. The removed boundary layer fluid is then used as the inflow to the thruster. CFD simulations and PIV testing were used to demonstrate the performance of the hull form. This showed that no separation occurred before the inlet to the thruster. Therefore, with this design being less affected by the surrounding flow, it may be more accurate to assume that the forces can be derived from the components of the thrust vector; however no results were provided to facilitate verification of this assumption.

2.6.2.2 Predicted Autosub Vectored Thruster Performance

If a vectored thruster were to be installed on Autosub the operator would need to know how well the device will perform to enable control system development. To address this need a series of calculations have been completed using various assumptions. The performance of the vectored thruster is considered in terms of the turning radius achieved. For the vectored thruster the steady turning radius can be calculated using a slightly modified version of Equation (2.4), namely:

$$R' = \frac{1}{r'} = \frac{(-Y'_r + m')N'_v - (-N'_r + m'x'_G)Y'_v}{(T'_v N'_v - T'_v x'_v Y'_v)}. \tag{2.5}$$

The hull form coefficients from Appendix A3 are used in the calculation, with $x'_v = l/2$. These parameter values include an interaction effect with the control surfaces, which is assumed to be small.

The calculation is performed using three different ways of estimating the generated total transverse force, T_v. The different approaches used are:

1. Using the linear assumption that thrust angle is equal to thruster angle, as adopted in [32, 34], with,
    a. the thruster assumed to be an open propeller generating a constant force along the thruster axis (for all thruster angles) equal to the vehicle drag at survey speed with zero deflection angle. (From Figure 2.7, $T = D$.)
    b. the thruster assumed to be an open propeller generating a variable force which has a constant magnitude component along the vehicle's longitudinal axis equal to the drag at survey speed with zero deflection angle. (From Figure 2.7, $T\cos(\mu) = D$.)

2. Using the data provided by [36] for ducted thrusters operating in open water with a constant operating point equal to the drag at survey speed with zero deflection angle. (Thruster rotational speed, n = const, giving $T = D$ at $\mu = 0$.)

In these calculations the AUV drag, D, is calculated using Equation (2.1) with $C_D = 0.045$ ($\alpha = 0$) [38]. Unfortunately, the results presented in [35] are for a limited number of operational conditions which are restricted to low forward speeds (low advance coefficient). Hence no calculation using this data is possible. The resulting calculations are provided in Figure 2.9 alongside the turning radii using the rudder. In Figure 2.9 the horizontal axis shows the deflection angle of the control surface, δ, or the thruster angle, μ, as appropriate.

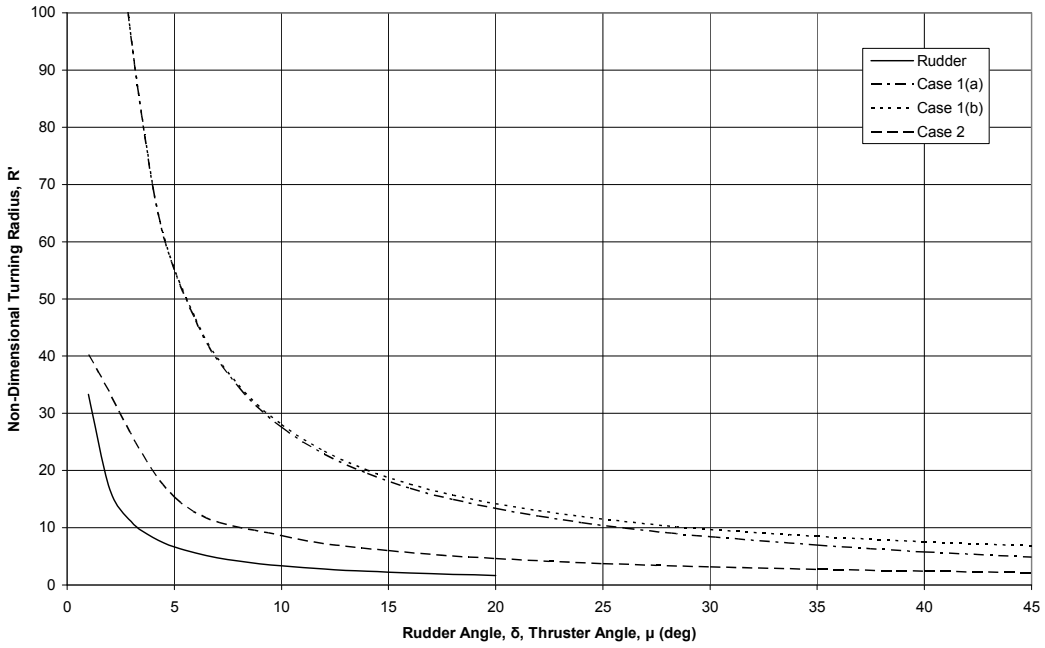

Figure 2.9 – Turning Performance of Autosub using a Vectored Thruster

These results show that a large deflection angle is required for the vectored thruster to match the performance of the rudder. Cases 1 (a) and (b) are very similar and quite different to Case 2 thus demonstrating the importance of the duct in enhancing the side force generated. Despite the influence of the duct, the performance demonstrated by Case 2 does not match the performance of the rudder. Furthermore, the thrust generated along the vehicle's longitudinal axis in Case 2 drops off considerably at thruster angles beyond 20º.

The implication of the thrust angle data of Figure 2.8 is that a vectored thruster operating behind a vehicle provides greater turning abilities than the ducted thruster operating in open water. This assumes that sufficient magnitude of turning force is still generated in these conditions. The large resultant thrust angles also indicate a significant decrease in force

along the longitudinal axis similar to Case 2. These unknown performance characteristics indicate that further investigation would be required.

The variations in the performance of a vectored thruster and the large number of variables mean that no common performance characteristics have been published. To undertake the required further investigations a number of approaches could be adopted including CFD, experiment or both. The complex, and unknown, flow conditions associated with this device mean that it would be difficult to validate the accuracy of a CFD model. Furthermore, the importance of separation phenomena would require a full viscous solution, which further increases the complexity and cost. Therefore, the initial characterisation of such a device would need to be carried out using an experimental approach, which could provide detailed force data for a range of operating conditions and also insight into the flow phenomena occurring. This data and insight could then be used to develop CFD techniques to model the performance of a vectored thruster.

2.6.3 Collective and Cyclic Pitch Propellers

The alternative option to directing the propeller jet is to use the propeller to generate forces in directions other than the primary propulsion direction. During normal operation a propeller blade generates forces in the axial direction (thrust) as well as forces in the radial and tangential directions. The forces in the radial and tangential directions are considerably smaller than the axial force. The radial force generated by a blade is cancelled out by a force generated by the opposite blade (for an even number of blades).

The forces generated by a propeller blade are a function of the blade pitch. Hence resultant forces in the radial direction, ΔR_B, can be developed through differentials in the radial forces generated by opposite blades. These differentials are caused by variations in the pitch of the blades during a revolution, see Figure 2.10. A propeller that uses this technique to generate additional forces is called a collective and cyclic pitch propeller (CCPP).

$$\Delta R_B = R_{B2} - R_{B1}$$
$$\Delta T = T_2 - T_1$$
$$\Delta p_B = p_{B2} - p_{B1}$$

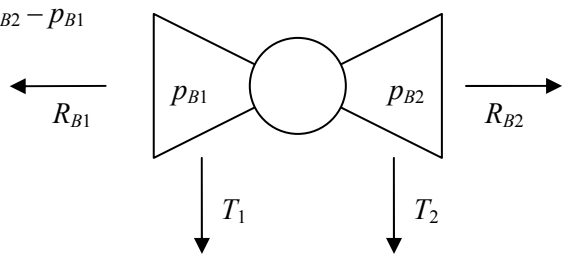

Figure 2.10 – Diagram showing the Forces Generated by the Blades of a CCPP

A CCPP is effectively a propeller that offers three modes of operation:

- As a fixed pitch propeller, optimised for a particular operational condition.
- As a collective pitch propeller, allowing the pitch of the propeller blades to be actively set to allow in-service performance optimisation across a range of operational conditions.
- As a cyclic pitch propeller where the pitch of the blades varies in a cyclic pattern during each revolution. This pitch variation creates differentials in the forces generated across the propeller hub and hence generates manoeuvring forces.

The operation of a CCPP is similar to that of a helicopter rotor and hence the swash plate arrangement is one approach to achieving these pitch variations [39]. The application of cyclic pitch propellers has been demonstrated on submersibles [40] and on surface vessels [41]. One of the first applications of the principles of cyclic pitch to a submersible was made using many-bladed propellers with the blades mounted around the centre of the vehicle. This device inspired the development of a working prototype of a propeller, using a swash plate arrangement, mounted as a rear propulsor [39]. The forces generated were found to be sufficient to control an underwater vehicle. Another example of the practical implementation of a CCPP on an underwater vehicle is given in [42]. On surface vessels CCPPs have been investigated in terms of the achievable manoeuvring performance [41] and as a means of reducing propeller induced vibrations and cavitation [43]. The latter is achieved by adjusting the pitch of the blades as a function of the cyclic variations in the propeller inflow field.

2.6.3.1 Collective and Cyclic Pitch Propeller Performance

The performance of a CCPP is dependent upon the force differentials generated by each propeller blade pair. To determine what these differentials are, it is necessary to calculate the forces generated by a propeller blade over a range of blade pitch. These forces can be determined using the boundary element method. These estimated forces can be used to form a model of this device.

The collective and cyclic pitch propeller will be modelled in a quasi-static manner. The single propeller blade model developed will be used to calculate the variations in the forces and moments as a function of the propeller blade pitch. The use of the existing propeller blade ensures that the performance of the CCPP in the fixed pitch mode is suited to the primary task, that is, survey propulsion. This means that no attempt has been made to tailor the design of the propeller blade to the generation of manoeuvring forces.

The forces and moments generated by a two-bladed propeller undergoing cyclic pitch motions are determined by assuming that the forces and moments at any instantaneous time are equal to those calculated using the boundary element code. This ignores any dynamic effects caused by the continual changes in blade pitch. The interaction between the blades was assessed to determine the influence of one blade on the other as a function of the difference in blade pitch. These tests showed that there was only a small interaction between the blades and that the magnitude of the interaction did not vary significantly as a function of blade pitch. This result was to be expected, given the small blade area ratio and large propeller hub.

The forces on the single propeller blade calculated at design pitch give an indication of the relative magnitudes of the forces generated by the propeller. The radial and tangential forces are approximately 10% and 20% of the thrust respectively. This calculation, and the subsequent analysis of the CCPP, was carried out using the axisymmetric inflow profile determined from the flow over the hull form, see Appendix A2. (Radial variations in the inflow profile were not found to have a significant impact on the manoeuvring performance when compared with a uniform inflow profile.)

The variation in pitch is centred about the design pitch and has a range of 10º. This small range is used to attempt to ensure that the changes in pitch are achievable in reality and to attempt to avoid the occurrence of blade stall. The variation of pitch is idealised as a sine wave, with maximum and minimum pitch corresponding to the 3 o'clock and 9 o'clock positions respectively, to give a resultant yawing moment. The blades have design pitch at the 12 o'clock and 6 o'clock positions resulting in no pitching moment and ensuring the continued generation of an appropriate forward propulsive force.

The calculations of the performance due to the changes in pitch are undertaken using different geometry files for each pitch value. A new geometry file is generated for each pitch angle in the range in question, at an increment of 1º, using the script files for the original propeller blade. The same panel distribution is adopted for each pitch angle investigated.

2.6.3.2 Theoretical Predictions of CCPP Performance

Throughout a revolution the thrust generated by the complete propeller is constant as the reduced thrust generated by the lower pitch blade is compensated for by the increased thrust from the higher pitch blade. The torque is not constant throughout the revolution and

follows the variations in pitch in a non-linear manner, giving corresponding decreases in hydrodynamic efficiency. The loss of efficiency is greater for larger pitch changes, with the efficiency loss of the order of 10% when operating at the maximum pitch range of 10º.

The ability of a CCPP to manoeuvre an AUV can be calculated using the linearised equations of motion in a similar manner to the rudder. In this case the Equation (2.4) becomes:

$$R' = \frac{1}{r'} = \frac{(-Y'_r + m')N'_v - (-N'_r + m'x'_G)Y'_v}{(\Delta R'_B N'_v - (\Delta R'_B x'_l + \Delta T' x'_P)Y'_v)} . \tag{2.6}$$

Here $\Delta R'_B$ and $\Delta T'$ are calculated as indicated in Figure 2.10, with R_B and T for each blade assigned according to the blade pitch on each. The coefficients for the hull form given in Appendix A3 are used, thus these include an interaction effect with the control surfaces, which is assumed to be small.

The turning moment generated by the CCPP is made up of two components (see Figure 2.10). The first of these is the difference in radial force generated, ΔR_B, and the second of these is the difference in axial force generated, ΔT. The difference between the radial forces is much smaller than the difference between the axial forces. However, when considering the moments generated, this disparity is reduced by the much greater moment arm for the radial forces in comparison with the axial forces. The turning radius is calculated using the maximum differences in radial and axial forces and thus represents the maximum achievable performance in this condition.

The effectiveness of a CCPP as a manoeuvring device at survey speeds (in comparison with the rudder) is expressed in terms of the calculated turning radii of Figure 2.11. In Figure 2.11 the horizontal axis corresponds to either the deflection angle of the rudder, δ, or the pitch difference between the blades, Δp_B, as appropriate.

The turning radii for the control surfaces and the CCPP differ considerably with the performance of the control surfaces outstripping the CCPP. The trends exhibited by the CCPP show that a large pitch difference would be required to begin to match the turning performance offered by the control surfaces. The calculated performance shows that the CCPP is capable of providing some control forces but these forces are insufficient to offer suitable performance to consider the device as a combined propulsion and manoeuvring device for a survey-style AUV.

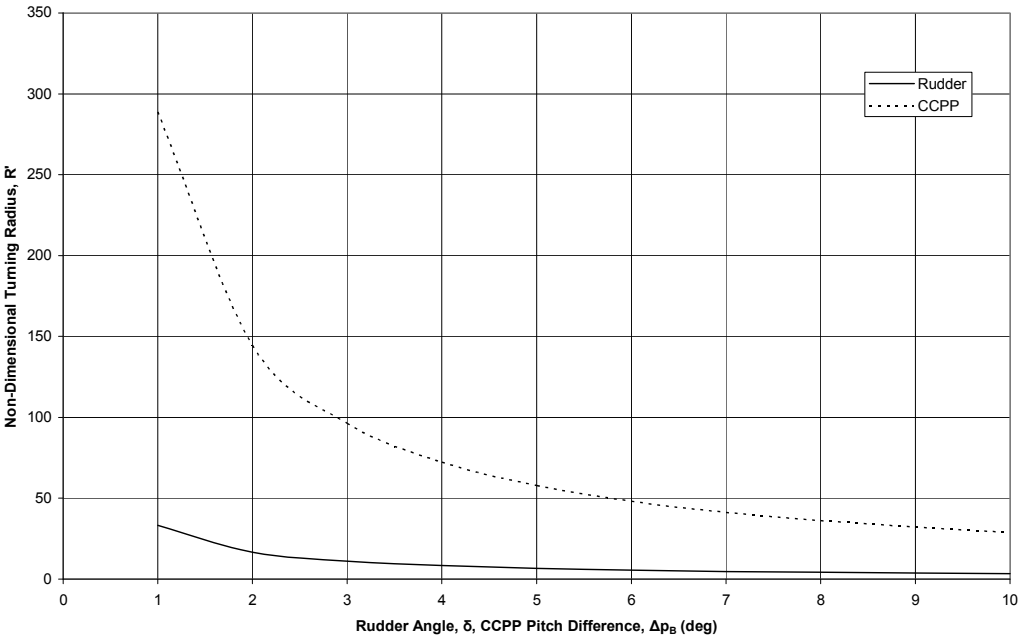

Figure 2.11 – Turning Performance of Autosub using a CCPP

2.6.3.3 CCPP Performance Enhancement

The CCPP has been shown to be unsuitable as a combined propulsion and manoeuvring device using this propeller blade design. The calculations performed for the CCPP used the Autosub propeller blade without any attempt to optimise for manoeuvring performance. Whilst optimisation of the blade design is still not the aim of this study, the performance of the CCPP can be enhanced in a simple manner. The application of a rake angle to the blade gives an increase in the radial forces generated without a significant decrease in the axial force. (A rake angle is commonly applied to propeller blades for a variety of reasons, including increasing the clearance around the propeller and to influence the trim of small high speed surface craft.)

A series of simulations were undertaken to assess the influence of a rake angle on the forces generated by the propeller blade. The results indicate a decrease in thrust of approximately 12%, coupled with a five-fold increase in radial force at a rake angle of 20º. The turning performance of a CCPP at survey speeds with a 20º rake angle is shown in Figure 2.12 demonstrating a considerable improvement in turning performance. However the performance of the control surfaces is still far superior to that of the CCPP.

Therefore the conclusion of this initial study into the performance of a CCPP as a combined propulsion and manoeuvring device is that a new blade would need to be designed

specifically for this application. This should lead to an improvement in the performance of the CCPP as a manoeuvring device but is likely to cause a decrease in the primary performance required of the device, that is, efficient survey propulsion force generation.

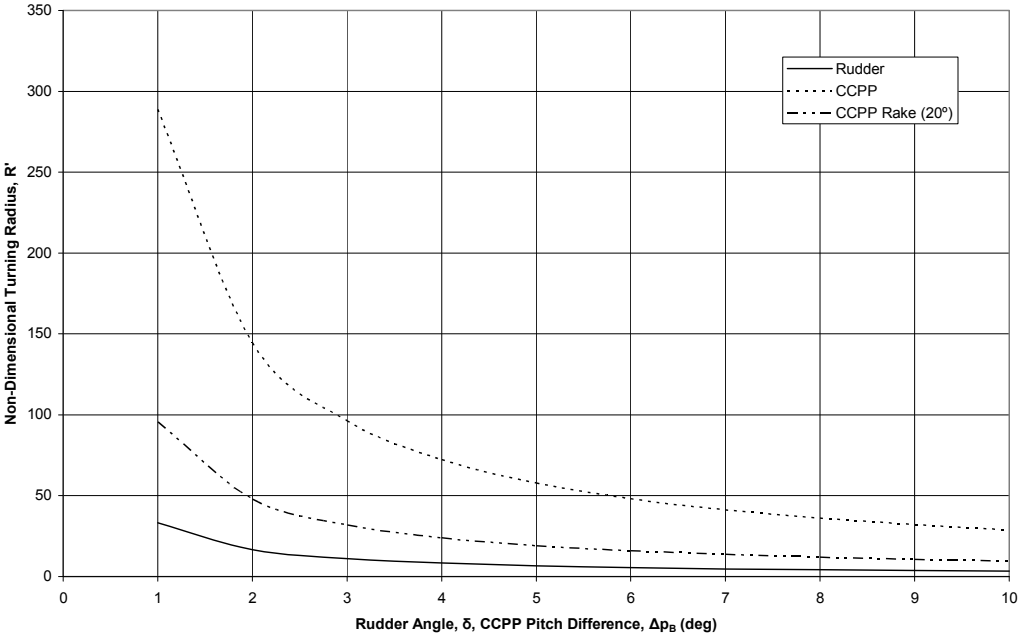

Figure 2.12 – Turning Performance of Autosub using a CCPP with a 20º Rake Angle

2.6.4 Additional Performance Factors

It has been discussed that the performance of a device in its primary operation is not the only issue to consider. It is also important to consider the total impact of a hybrid device. This discussion is undertaken working with the assumption that the devices in question offer suitable propulsion and manoeuvring performance.

A vectored thruster or a CCPP would remove the need for control surfaces for manoeuvring, which would reduce the drag of the vehicle and improve the flow into the propeller by giving an axisymmetric inflow profile. However, control surfaces will still be required for stability. The reduction in drag is estimated to be at most 6% of the total drag (ignoring interaction effects) [44]. This does not represent a significant saving.

Both devices would require considerable internal space to allow for the actuators required to orientate the propeller or provide the cyclic pitch changes. (The choice may be significantly influenced by the impact on payload versus propulsion space.) Furthermore, these actuation processes would increase the total power requirement (and hence battery capacity), and the

losses in these mechanisms would further reduce the efficiency of the devices. The performance of the device would also be dependent upon the accuracy and reliability that the orientation or pitch changes could be implemented.

A significant drawback of these devices is the complexity of the systems involved and the increased likelihood of failure due to the large number of moving parts required. These issues represent significant stumbling blocks relating to the implementation of either a vectored thruster or a CCPP on a deep diving survey-style AUV.

2.7 Concluding Remarks

The characteristics of survey-style AUVs have been examined and explained by considering a typical mission profile. The component parts of the propulsion and manoeuvring systems on an AUV have been discussed. The performance of the propeller has been modelled using a boundary element code and the performance of the rudder has been described using existing experimental data. This analysis was undertaken to facilitate the assessment of hybrid devices for an AUV. Hybrid devices are defined as those that offer both propulsion and manoeuvring capabilities.

A review of the available hybrid devices has been undertaken and two were selected for further analysis due to the potential benefits proffered. The performance of a vectored thruster has been assessed using experimental data and a model of a collective and cyclic pitch propeller has been constructed based upon the propeller model developed using the boundary element code. However, the performance of these two devices was found to be insufficient, in comparison with the existing control surfaces, to justify the additional engineering complexity required.

Chapter 3 – Development of Multi-Purpose AUVs

3.1 Introduction

The majority of AUVs are application specific, meaning that they are designed for a particular type of mission and thus may not be suited to, or may not be able to undertake, other types of mission. As part of the development of AUVs, there is a desire to enable them to undertake more complex missions involving different regimes of operation. A particular type of multi-purpose vehicle is one capable of undertaking deep ocean survey missions combined with low speed, more detailed, investigations of the environment as points of interest are discovered.

3.2 Multi-Purpose AUVs

To begin the development of such a vehicle it is important to understand how the vehicle will be used. The sample mission profile provided in Figure 3.1 initially reflects the survey mission of Section 2.2 until, at point E, the vehicle detects a feature of interest.

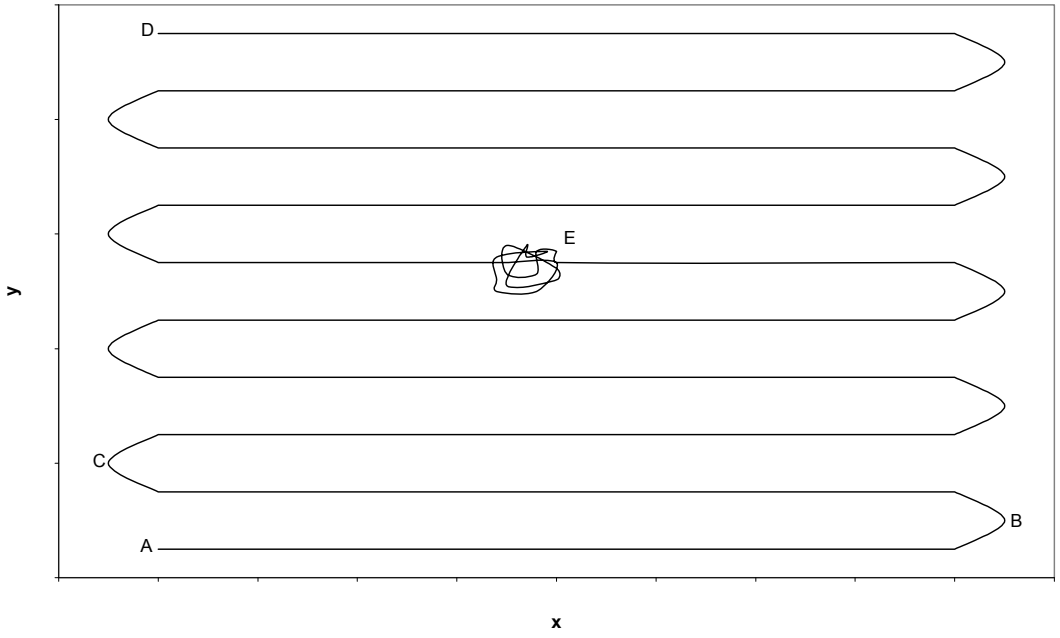

Figure 3.1 – Multi-Purpose AUV Mission Profile

The vehicle then begins to investigate the feature of interest, undertaking the tasks necessary to complete the objectives of the given mission, before continuing with the original survey pattern. The investigation around point E is different to survey operation in the following ways:

- The investigation is carried out at translation speeds much lower than normal survey speeds and without a predominant direction.
- The investigation requires the vehicle to hover and to maintain position and attitude regardless of prevailing environmental conditions, for example, currents.
- The investigation requires individual control over five degrees of freedom (excluding only roll) to provide far greater agility than during survey operation to enable the achievement of mission objectives.

These differences present challenges to the designer of the AUV. Table 3.1 emphasises the requirements for the new multi-purpose AUV, in comparison with the basic survey AUV.

Table 3.1 reinforces the need for additional low speed control over sway, heave, pitch and yaw motions sufficient to maximise the range of manoeuvring options for a survey AUV to become a multi-purpose AUV. It is assumed that the rear propulsor can maintain sufficient control over surge motion throughout the speed range. Furthermore, passive roll control will remain sufficient during low speed manoeuvring tasks.

Rather than have direct control over each degree of freedom, vehicle control in some degrees of freedom can be achieved by using combinations of actuators. For example, the control of sway motion using a combination of surge and yaw control. Taking this approach yields a less manoeuvrable vehicle, but would still facilitate greater interaction and exploration of a feature of interest than is currently available with a survey-style configuration. This less manoeuvrable vehicle would require a smaller number of actuators than if the direct control approach is adopted.

In this research the focus is placed upon developing a vehicle with direct manoeuvring control over the required five degrees of freedom. The design of systems facilitating direct control could then be used to develop a vehicle using a combined control approach.

The main component of the mission illustrated in Figure 3.1 is the survey mission. The investigations undertaken at low speed represent a small proportion of the mission. Thus it would be inappropriate to make design choices focussing on the low speed performance without considering the impact on survey efficiency. In fact, the survey efficiency impact of a particular approach is likely to be a key deciding factor (given the dominance of the survey component of the likely mission profile). Therefore, a key aim in the development of a multi-purpose AUV is to add low speed manoeuvring capabilities without unduly compromising the survey performance.

Table 3.1 – Survey and Multi-Purpose Vehicle Requirements

	Survey Vehicle		**Multi-Purpose Vehicle**	
	Existing Control Capability	**Application**	**Required Additional Control Capability**	**Additional Application**
Surge	Controlled by propeller throughout speed range	Survey speed propulsion	None	Low speed manoeuvring control
Sway	None	Not Applicable	Control at low speed	Manoeuvring for investigation tasks
Heave	None	Not Applicable	Control at low speed	Depth control at low speed and manoeuvring for investigation tasks
Roll	Passive control	None	None	None
Pitch	Controlled at speed by control surfaces	Depth control	Control at low speed	Manoeuvring for investigation tasks
Yaw	Controlled at speed by control surfaces	Heading control	Control at low speed	Manoeuvring for investigation tasks

The challenges relating to the addition of the low speed control can be split into the two required planes of control. The horizontal plane comprising of sway and yaw control and the vertical plane comprising heave and pitch control. The addition of sway and yaw control simply requires force generation capability in the horizontal plane. The options for generating these forces will be discussed later.

The control over heave and pitch motions requires the ability to generate forces in the vertical plane, however, this plane is complicated by the weight – buoyancy balance. Most survey AUVs are ballasted to be positively buoyant to ensure that they rise to the relative safety of the surface should any part of the propulsion system fail. When travelling at survey speeds the buoyancy is controlled by operating at a small nose-down pitch angle, controlled by the hydroplanes. The differences between the flow over the upper and lower sides of the vehicle generate a downwards force to counteract the upwards force due to the positive buoyancy.

At low speeds the depth control approach used during survey operation is infeasible. The downwards force generated by the flow over the vehicle is a function of the flow speed and hence at lower speeds a larger pitch angle is required. The control surface generated forces also suffer from this speed dependence. Consequently at lower speeds these forces become insufficient to maintain the required, larger, pitch angle. Therefore the addition of low speed control for the vertical plane requires the addition of both low speed buoyancy control and low speed manoeuvring control.

An obvious solution to the problem of buoyancy control is to neutralise the buoyancy and adopt a different safety net, for example, a drop weight system. However, for a deep diving AUV the fluctuations in fluid density and the differing compressibility of the water and components of the vehicle can lead to substantial changes in buoyancy that are difficult to predict especially when exploring uncharted waters [45]. This means that some form of active depth (buoyancy) control is required throughout the speed range.

There are two approaches to controlling the depth of the vehicle over the entire required speed range. The first option is to use a method that is capable of controlling the buoyancy throughout the entire speed range. The second option is to interchange between methods of control as a function of the operational speed. The first option is much simpler to implement and control, however, the decision must also be based upon the levels of energy required.

The primary operating mode for the multi-purpose AUV is long range survey-style operation. This dictates the importance of energy efficiency in the design choices. Therefore a depth control system with a low power requirement is necessary for this phase of operation. This explains why control surfaces are currently used on survey-style vehicles. Operating the vehicle at a small nose-down pitch angle causes a small increase in drag requiring a corresponding small increase in thrust from the stern propeller. This leads to a small increase in propulsion power requirement compared to zero pitch operation.

Alternative survey speed depth control approaches include variable buoyancy systems and utilising the force generation capabilities of thrusters. However, variable buoyancy systems are only commonly used on shallow diving underwater vehicles as the power requirement increases with operating depth due to increase in ambient pressure. The use of thrusters for survey speed depth control also has a consistently high energy requirement. Given the high energy requirements of these alternative depth control systems, it is clear that neither a variable buoyancy system nor the thrusters can compete with the control surfaces at survey speeds. Thus, different approaches for depth control in the different regimes of operation must be explored, see Section 3.5.

Provision of a different depth control approach for the different speed regimes creates a further challenge for the designer. This new challenge is a transition phase between survey speed control surface control and the alternative low speed control approach. The key issue in this phase is how the vehicle approaches the interchange between control strategies. The impact the chosen approach has on the overall performance of the vehicle will be discussed in greater detail in Chapter 5.

To enable appropriate consideration of the available options it is necessary to identify the ranges of operation for both depth control and low speed manoeuvring control. This will be considered next.

3.3 Operating Ranges

An appreciation of the operational conditions is important to ensure suitable selection of actuator designs, subject to efficient energy utilisation. Significant differences between the requirements of vertical and horizontal plane control have already been cited. The next step is consideration of the speed ranges and forces involved.

3.3.1 Speed Ranges

The entire speed range, from zero speed hover to maximum survey speed, will be split into three regimes of operation. These ranges will be defined using a pair of limits. The lowest practical speed at which acceptable survey-style depth control can be achieved using the control surfaces will be used to help define these limits. The upper limit is defined as the lowest practical speed for normal survey operation. The lower limit defines a maximum speed for low speed operation. Outside of these limits, depth and manoeuvring control are undertaken using a single individual approach. Between these limits defines a transitional range to allow the interchange between one method of control and the other. The control difficulties in this transitional range dictate that normal operation is not recommended in this speed range.

The absolute limit of control surface depth control is a function of the design of the vehicle, the particular design of the control surfaces used and the maximum control surface deflection angle allowed. This functionality allows scope for developments in the design of the survey speed depth control system, which may improve the overall performance of the vehicle. The critical speed for the vehicle, U_c, below which control surface depth control can no longer be maintained, can be calculated using the linearised equations of motion in the vertical plane for a positively buoyant AUV. The vertical plane equations of motion can be rearranged to yield:

$$U_c^2 = \frac{M'_w lB + mg\overline{BG}Z'_w - BZ'_w l\left[\frac{M'_w}{Z'_w} - \frac{M'_\delta}{Z'_\delta}\right]}{Z'^2_w 0.5\rho l^3\left[\frac{M'_w}{Z'_w} - \frac{M'_\delta}{Z'_\delta}\right]}. \tag{3.1}$$

This equation expresses the critical speed as a function of vehicle buoyancy, B, and the variation of the critical speed is illustrated in Figure 3.2. The derivatives used in Equation (3.1) are given in Appendix A4.

Autosub is ballasted to be a minimum of 0.3% positively buoyant. For Autosub this corresponds to a minimum force of around 100N. The buoyancy is a function of the density of the water, and the relative compressibility of the water and vehicle, and thus cannot be considered constant.

Hence, with the buoyancy, B, variable, it is clear from Figure 3.2 that it is necessary to define a wide range of transitional speeds to ensure control is maintained throughout the mission. Equation (3.1) is likely to underestimate the actual critical speed for the vehicle,

since the derivatives used do not account for Reynolds Number effects and the onset of stall. The values calculated are used to assign the operational speed ranges defined in Table 3.2.

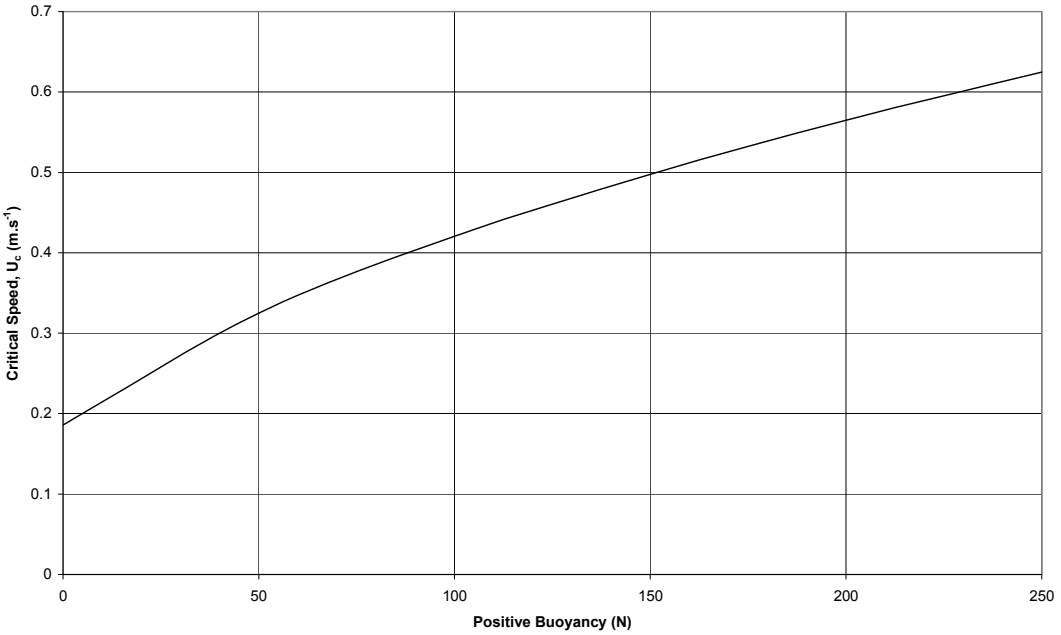

Figure 3.2 – Variation of the Critical Speed, U_c, for Control Surface Depth Control as a function of Positive Buoyancy for Autosub 3

Table 3.2 – Multi-Purpose AUV Speed Ranges

Mode of Operation	Speed Range
Survey	$> 1.0 m.s^{-1}$
Transition	$0.5 – 1.0 m.s^{-1}$
Low Speed Manoeuvring	$< 0.5 m.s^{-1}$

3.3.2 Required Forces

To analyse the performance of the chosen systems it is necessary to estimate the order of magnitude of the forces required to enable Autosub to operate at low speeds. The minimum amount by which Autosub is ballasted positively buoyant is approximately 100N. However, with this value variable it is important to consider much larger forces and here forces up to 200N will be considered.

To estimate the forces required to manoeuvre Autosub at low speeds, a simple manoeuvre will be considered. The chosen manoeuvre is pure sway translation, that is, steady sideways motion in the horizontal plane (which is analogous to pure heave translation). The steady state drag force on the vehicle is estimated using a strip theory approach, which accounts for

the variations in the shape of the hull form. A strip theory formulation slices the vehicle into equal length sections and the drag on each section is estimated assuming the section is a 2-D cylinder. The influence of section length on the calculated drag force was investigated to ensure that the results are independent of the chosen section length. The drag force per unit length for each section is defined as [46]:

$$D_{PUL} = 0.5\rho U^2 dC_D, \text{ where } C_D = f(\mathrm{Re}_e, \varepsilon/d). \tag{3.2}$$

The drag coefficient for each section is determined as a function of an effective Reynolds Number, Re_e, (which in turn is a function of the surface roughness and the turbulence in the flow), and the surface roughness of the cylinder, ε. The results of this calculation across the low speed manoeuvring speed range are plotted in Figure 3.3.

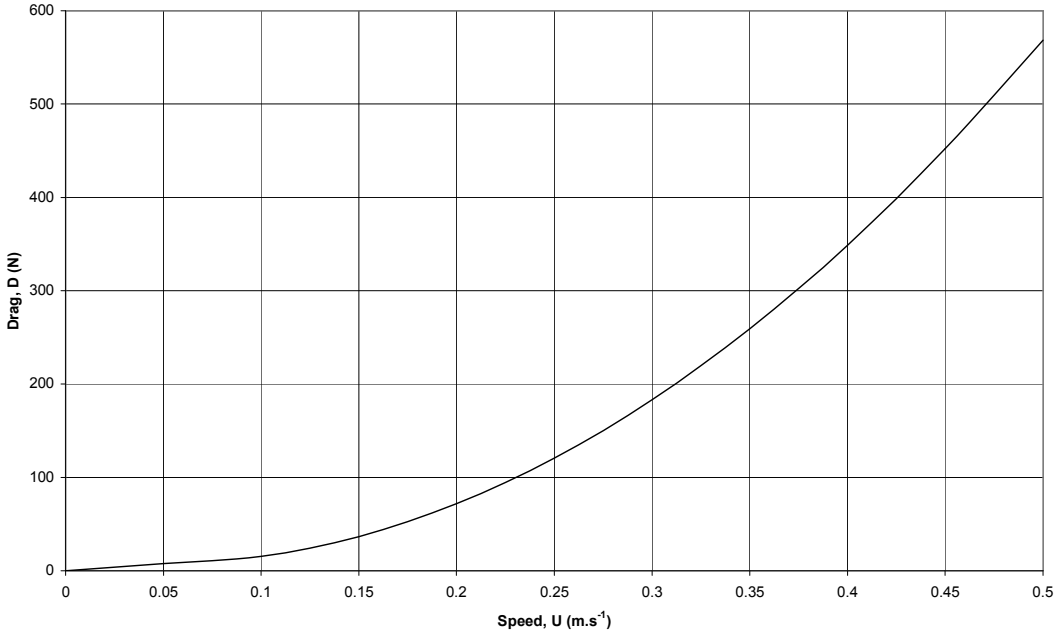

Figure 3.3 – Variation of Drag Force for Pure Sway Motion of Autosub 3 as a function of Translation Speed

The forces required to propel Autosub in a pure sway manoeuvre are quite considerable and will require a large amount of power to realise. (It should be recalled that the translation forces in the vertical plane need to be offset by the magnitude of the positive buoyancy force as appropriate). For comparison purposes the estimated drag of Autosub at survey speeds is approximately 166N. Therefore it is obvious that designing an efficient system is an absolute necessity in order to enable Autosub to undertake low speed manoeuvres.

3.4 Potential Control Solutions

The preceding discussion has highlighted the propulsion and manoeuvring requirements for a multi-purpose AUV and identified the operating ranges for the vehicle. The key development required is the addition of low speed control. The following discusses the potential options.

There are two planes of operation to consider. The horizontal plane requires only low speed manoeuvring control. The vertical plane requires low speed depth and manoeuvring control. In terms of internal space use and energy demands it would be more efficient to select a depth control method capable of providing low speed manoeuvring control. Whilst a combination of approaches might be possible, the demands on the internal space may become too large.

To control the buoyancy there are two options. The first of these is to neutralise buoyancy and provide a buoyancy control system. The second approach is to generate a force in the vertical plane that counteracts the positive buoyancy force. Clearly, both methods meet the criterion requiring active control over buoyancy.

The remaining low speed control requirements dictate a need to generate forces in particular preferred directions. The most common method of providing these forces is the use of propeller based thrusters, either through the use of ROV-style underwater thruster units or the use of through-body tunnel thrusters.

Other options include vertical axis propellers [10], cyclic pitch systems, jet based systems and biomimetic devices. However, these devices have drawbacks regarding engineering complexity and the additional developments required to improve operability and reliability.

Internal actuation is another possible group of available options that includes gyroscopic control [47] and moving mass systems [48]. However, these systems only provide control over the orientation of the vehicle and use the stern propulsor to provide manoeuvring forces. Thus these systems would not be able to hold the vehicle attitude in a cross-current (for example) and hence would limit vehicle operation.

The inherent autonomy of an AUV and the potentially hostile environments in which they operate dictate a necessity for robust and reliable design choices. Essentially the less commonly used options proffered have drawbacks concerning their robustness and

reliability. Hence they are not considered suitable for use on a multi-purpose AUV. Therefore this work will focus on the assessment of existing and well developed technologies, which in this case provides two options, namely, variable buoyancy systems and propeller based thrusters.

3.5 Assessment of Available Options

To assess the viability of the available options for the development of a multi-purpose AUV it is important to highlight the factors that influence the decisions. The first factor is how well the proposed approach can undertake the primary task of low speed control. This is defined in terms of the manoeuvres that the approach would enable the vehicle to undertake, how well these manoeuvres could be performed, the ease of controllability and the associated energy demands made. The second of these factors is the impact on the design of the vehicle as a whole. This addresses the internal space required, the location of the device (in terms of conflicting space requirements) and the impact on the overall vehicle dimensions. The third factor is the influence on the survey efficiency, which focuses on the additional drag generated and the influence of the addition of the new devices on the flow around the vehicle.

These factors will now be briefly considered in the analysis of two different groups of device that have so far been identified.

3.5.1 Variable Buoyancy Systems

A variable buoyancy system is a device that regulates the buoyancy of a vehicle by interchanging fluids of differing density. These devices are mounted inside the vehicle and consist primarily of fluid storage tanks and pumping equipment. Multiple devices can be employed to facilitate control over trim (pitch) in addition to depth. These devices can only provide control in the vertical plane. They do not have any direct influence on the external flow characteristics of the vehicle.

3.5.1.1 Depth Control and Manoeuvrability

Variable buoyancy systems require electrical power to drive the pumps that interchange the fluids. The rate of fluid exchange determines the responsiveness of the device in terms of the rate of change of the buoyancy balance. These systems are commonly used on shallow diving vehicles, but are not usually found on deep diving AUVs (excluding buoyancy driven

gliders). This is due to the cost and size required to overcome the ambient pressure encountered at depth [49].

To illustrate these difficulties, an existing variable buoyancy system is used to provide some quantitative information about the power requirements and resulting performance. The chosen system is the University of Aberdeen Oceanlab's Variable Buoyancy Device (VBD) [50], whose main selling point is that it is designed to operate at depths up to 6000m; a necessity for a multi-purpose AUV. The VBD offers depth control alongside dynamic and static trimming capabilities (with multiple devices). The VBD is 0.75m in length with a 0.75m diameter and offers a buoyancy payload of 30kg. These specifications would be suitable for Autosub. However, the VBD has a fluid exchange rate of 1kg.min^{-1}, which roughly corresponds to the gradual application of 10N.min^{-1}. Such a low fluid exchange rate would offer insufficient manoeuvring performance for a vehicle the size of Autosub. This low responsiveness is placed in context when recalling that propeller based thrusters can produce a much larger force with a response time measured in seconds.

The primary reason for the low fluid exchange rate is the power required to exchange fluids. The specification for the VBD gives a power consumption of 1.5kW for a constant pumping speed. The VBD uses a hydraulic pump to exchange fluids and the power consumption, P, can be estimated using:

$$P = \frac{nV\Delta p}{\eta}. \tag{3.3}$$

Here n is the rotational speed of the pump, V is the swept volume, Δp is the difference in pressure across the pump and η is pump efficiency. The power required is proportional to both the fluid exchange rate and the pressure difference across the pump. This can be used to explain the increasing power required by the VBD as depth increases for operation at a constant pump speed, as illustrated in Figure 3.4. The variations in efficiency shown in Figure 3.4 are due to the proportionally high frictional losses in both the hydraulic and water circuits at low operating pressure (shallow water) [50].

To determine the power requirement for a low speed manoeuvre a simple example is considered. The data in Figure 3.3 shows that to undergo pure heave at 0.25m.s^{-1} requires a force of 120N. A fluid exchange rate, r_f, of 1kg.min^{-1} dictates that the VBD would need to operate for 12.2mins ($120/r_f g$ mins, from a neutrally buoyant condition) to achieve the required force. Hence the energy consumption, shown in Figure 3.5 as a function of depth, is calculated using the measured input power from Figure 3.4 and the estimated pumping time.

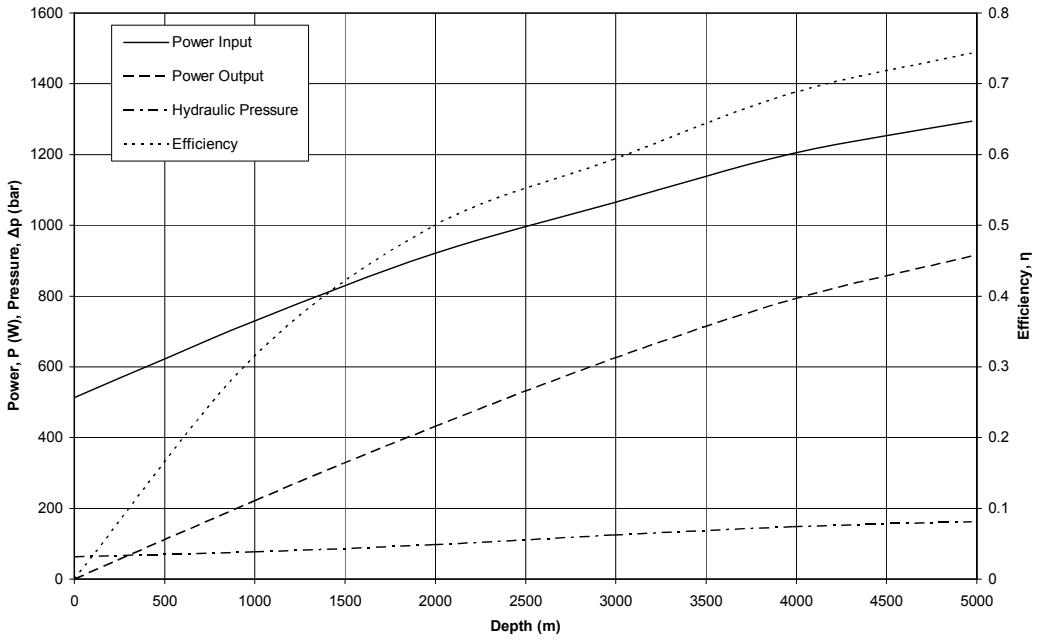

Figure 3.4 – Performance of the Aberdeen Variable Buoyancy Device at Constant Pumping Speed as a function of Operating Depth [50]

This energy requirement is not prohibitive for a large survey AUV. However, the responsiveness of the vehicle would be unacceptable given that it takes approximately 12mins to reach the required force. To improve the responsiveness would require a considerable increase in required power, as implied by Equation (3.3). That is, to halve the response time would require double the energy and to reduce the response time to an acceptable level would increase the energy requirements to a prohibitive level.

Other variable buoyancy systems in use on underwater vehicles include the Seahorse AUV system, which has a fluid exchange rate of $9kg.min^{-1}$; however insufficient details of the power requirement are provided [49]. The Seahorse AUV is typically used in shallow waters (up to 350m) and hence the power required will be considerably lower than for the VBD. The 4000m rated MBARI ROV uses a variable buoyancy system with a 3.7kW (5hp) motor, which provides a fluid exchange rate of approximately $3kg.min^{-1}$ [51]. These other systems confirm the conclusion that the power requirement for low speed manoeuvring control would be unsustainable on an energy limited AUV.

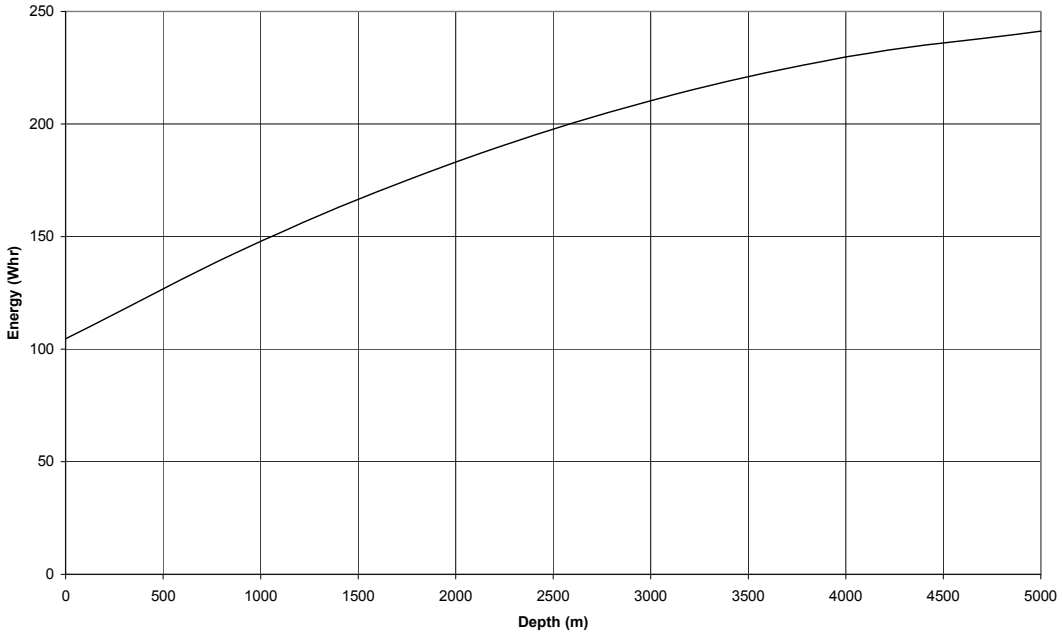

Figure 3.5 – Variation of the Energy Consumption of the Aberdeen VBD as a function of Operating Depth for a Buoyancy Change of 120N

3.5.1.2 Design Impact

The impact of a variable buoyancy device on the design of the vehicle could be quite considerable as the device would require significant amounts of internal space. The space required is also location sensitive, that is, the variable buoyancy devices must be placed in specific locations to allow the device to control the depth (and trim) of the vehicle. For a twin device design the devices would need to be placed with one at each end of the vehicle. These locations may be available, but the size of the devices would have a significant impact on the payload space available and the design of the vehicle may need to be significantly altered to accommodate these devices.

3.5.1.3 Survey Efficiency Impact

In favour of the use of a variable buoyancy system is the impact on survey efficiency. The system itself would not cause an increase in drag unless the vehicle is required to increase in size to carry the system. The survey performance of the vehicle would improve, since the vehicle could operate at level trim throughout the operational range. Operating at level trim reduces the required propeller load and thus corresponds to a (small) reduction in propulsion power. An estimate of the increase in propulsion power required to operate at a trim angle has been made using the equations of motion for the AUV. This estimate has been compared

with the power required to overcome a small buoyancy error. Figure 3.6 shows the length of time that the vehicle would need to operate for, in the trimmed condition for a range of operating depths, to use the same amount of energy as required by the VBD to overcome a given buoyancy error. That is, Figure 3.6 shows the required running time estimated using

$$t_R = \frac{(\text{VBD pumping power at depth}) \times (\text{Time to correct buoyancy error})}{\text{Additional propulsion power to operate in trimmed condition}}. \qquad (3.4)$$

These results show that the vehicle would need to operate for a considerable length of time in a given condition to recover the energy used to overcome small buoyancy errors. The large amounts of power required to run the VBD for a short period of time, relative to the small increase in propulsion power required to operate in the trimmed condition, lead to the large increase in running time for small buoyancy errors. The in-service buoyancy errors are likely to be small as once the vehicle is neutrally buoyant then changes in buoyancy will only be caused by changes in the density of the surrounding water and the differing compressibility of the water and the vehicle. (It is important to note that small changes in buoyancy can have considerable consequences for the performance of the vehicle, for example, in a coastal area subject to freshwater inflow where the vehicle may not be sufficiently buoyant to reach the surface.) No account is made of the change in depth incurred due to the low responsiveness of the VBD. These results show that it is more efficient to operate in the trimmed condition if small changes in buoyancy are likely to be encountered. This conclusion highlights the option of using a variable buoyancy system to initially neutralise the buoyancy and then operate in the trimmed condition to accurately control the in-service buoyancy.

Another option that could be used as part of a combined system is passive buoyancy. Passive buoyancy consists of materials such as syntactic foam and silicone oil, which compress at a higher rate than seawater. Thus it is possible to tune the vehicle to be approximately neutrally buoyant within a predetermined depth range if sufficient volume of material can be carried onboard. This tuning reduces the magnitude of any buoyancy error to be corrected and thus reduces the required energy consumption.

3.5.1.4 Summary

The systems examined here serve to demonstrate that a variable buoyancy system can be used to assist the depth control and improve the survey performance of the AUV. However, the power requirements for a variable buoyancy system are too large for the device to be used as a low speed manoeuvring system and the system represents an inefficient approach to fine depth control when subject to small buoyancy errors. Variable buoyancy systems are

large and the incorporation of the system may require a complete redesign of the vehicle. In conclusion variable buoyancy devices would be an option for shallow diving AUVs but they are not suitable for deep diving vehicles.

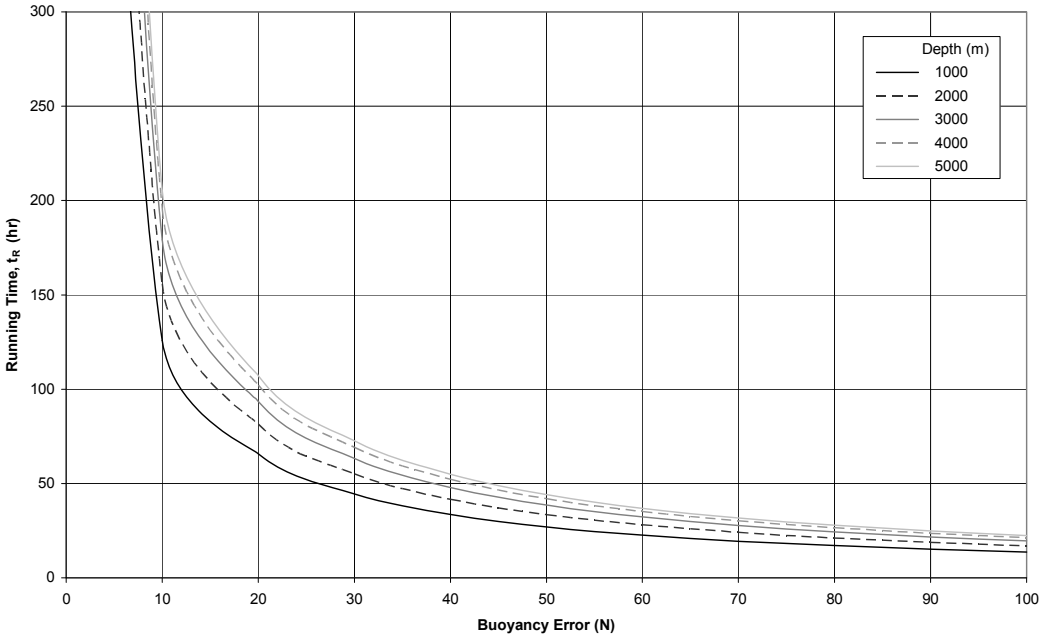

Figure 3.6 – Variation of Required Mission Time to overcome the Equivalent Aberdeen VBD Energy Requirement as a function of Buoyancy Error

3.5.2 Propeller Based Thrusters

Propeller based thrusters are a commonly used actuator for underwater vehicles for conventional survey propulsion, see for example, HUGIN [2], and also for directional control, see for example, Nereus [45]. The reasons for this are their reliability, responsiveness, simplicity and ability to generate forces throughout the operational range of the vehicle. There are many options to consider when selecting a propeller based thruster. In this discussion two groups of device will be considered. These are external thrusters and through-body tunnel thrusters.

3.5.2.1 Depth Control and Manoeuvrability

The power required to generate forces from a propeller based thruster can be estimated using the following equations:

$$P = 2\pi mQ = \frac{TU}{\eta}. \tag{3.5}$$

Thus an estimate of the power, P, can be made once the required thrust, T, is known, assuming a suitable efficiency, η. However, when the vehicle is stationary, the velocity, U, is zero and hence the efficiency of the thruster is zero, using standard definitions, despite a thrust force still being produced. To overcome this problem a momentum theory based relationship can be used to estimate the required power, (for details see Appendix A5):

$$P = T\sqrt{\frac{1}{2}}\sqrt{\frac{T}{\rho A}}\,. \tag{3.6}$$

This formulation gives an ideal value and, in reality, the constant, $\sqrt{1/2}$, will be much larger. Power requirements for thrusters at zero speed are easily obtainable from simple experiments and are often published by the manufacturer allowing a suitable relationship to be determined. However, Equation (3.6) allows an estimate of the power requirement to be made once the required thrust is known.

If a suitable thruster design is employed then the required forces should be achievable over the range of required conditions. The responsiveness of propeller based thrusters means that manoeuvrability should not present difficulties provided the dynamic effects of the thrusters can be controlled (see Section 4.2.1). The manoeuvrability offered by the thrusters is a function of the locations used (considering the moment arms) and the thruster type used. An external thruster can be a vectored thruster, which increases the number of manoeuvrability options offered by a particular thruster configuration. However, this flexibility is not possible using through-body tunnel thrusters.

3.5.2.2 Design Impact

The design impact of a propeller thruster is a function of the type of thruster used and the selected location. For an externally mounted thruster the design impact is minimal as the thrusters in question are usually self-contained units that require only a wired connection to the vehicle. However, externally mounted thrusters are likely to increase the overall dimensions of the vehicle, which not only places the thruster in a vulnerable location, but can also restrict the handling and operation of the vehicle. Through-body tunnel thrusters are also self-contained units, but do require internal space. However, the size of these thrusters, and the likely placement, dictates that it should be possible to provide this space without increasing the overall dimensions of the vehicle.

3.5.2.3 Survey Efficiency Impact

The survey efficiency impact of propeller based thrusters is a function of the location. For an externally mounted thruster the drag caused by the presence of the thruster can be quite considerable (see Section 4.3.2) and the influence of the presence of the thruster on the flow over the vehicle will also impact on the performance of the downstream components. These two problems represent a significant drawback to using externally mounted thrusters.

The survey efficiency impact of a through-body tunnel thruster is small providing the tunnel thruster is appropriately located, that is, as long as the tunnel entrances do not form significant barriers to the predominant direction of the flow (in normal survey operating conditions).

3.5.2.4 Summary

Propeller based thrusters offer a reliable and responsive solution to the problem of the additional low speed control for a multi-purpose AUV. Whilst the power requirements can be considerable the performance they offer and the inherent flexibility dictates that they warrant further investigation.

3.5.3 Device Choices

The preceding discussions present information demonstrating that variable buoyancy systems would offer insufficient performance to be used as a combined buoyancy control and low speed manoeuvring device. Therefore the development of a multi-purpose AUV will continue with propeller based thrusters providing the required additional control.

3.6 Concluding Remarks

The development of a survey-style AUV into a multi-purpose AUV provides the designer with demanding fundamental challenges. The options for providing the additional control have been reviewed. Due to the required performance for low speed manoeuvring the additional control will focus on the use of propeller based thrusters. The operational ranges and the required forces have been assessed and these will be taken forward into a more in-depth analysis of the performance of the selected systems.

Chapter 4 – Propeller Based Thrusters

4.1 Introduction

The development of a multi-purpose AUV requires the addition of low speed depth and manoeuvring control. Two particular groups of propeller based thruster have been identified as possible solutions to the required additional control – external thrusters and through-body tunnel thrusters. In general terms these two groups of thrusters are the same; they share common features and generate forces in the same way. The key differences are how they are integrated into the vehicle and how this integration influences their performance across the operational range of the vehicle.

This chapter introduces propeller based thrusters, discusses in detail the performance characteristics and undertakes the required analysis for the thruster types in question. Modelling procedures for the groups of thruster are also developed. Some general issues relating to the performance and selection of propeller based thrusters on a multi-purpose AUV will now be discussed before focussing on the two individual groups in detail.

4.2 AUV Thruster Performance

The performance characteristics of a propeller based thruster in open water can be obtained through experimental testing or using CFD approaches. The thruster performance can be represented using simple models that replicate the characteristics illustrated on a non-dimensional propeller chart (for example, see Figure 2.4). Using a linear approximation to the thrust characteristics [52]:

$$K_T = \alpha_0 + \alpha_1 J \,, \tag{4.1}$$

the thrust force generated, T, can be estimated using:

$$T = T_{n|n|} n|n| - T_{|n|u} |n| u \,, \tag{4.2}$$

with $T_{n|n|} = \rho d^4 \alpha_0$ and $T_{|n|u} = \rho d^3 \alpha_1$. A similar approach has been adopted using four quadrant performance characteristics [53]. With a known inflow condition, u, and rotational speed, n, models such as Equation (4.2) accurately replicate the steady state open water performance of a thruster. In open water conditions the flow velocity across the propeller plane is constant, however, the velocity profile for an installed thruster is likely to be non-uniform (as a function of the location of the thruster). Thus the performance of the thruster in the installed condition is unlikely to match the open water performance.

To overcome this inconsistency the thruster needs to be tested in the installed condition, allowing the thrust characteristics to be determined as a function of a measurable state, for example the speed of the vehicle. (On an underwater vehicle the speed is recorded using a Doppler Velocity Log (DVL) however the uncertainty in the estimate of the speed could lead to incorrect thrust predictions. This is only likely to be a problem if the DVL loses its bottom track.)

The experiments required to characterise the thruster in the installed condition are far more difficult and expensive than testing the thruster in open water. Thus an alternative solution is sometimes used. This solution involves developing a model of the thruster based on open water tests and tuning the coefficients using full scale mission data. This solution may not necessarily capture the true performance of the thruster but it provides a suitable solution for vehicle control.

Models of the form discussed can be used by a control system to predict the steady state performance of the thruster. During survey operation the performance of the propulsion system can be considered as steady state. However, during other modes of operation, for example low speed manoeuvring, the propulsion system cannot be considered as a steady state system as the demand is no longer constant. Hence the dynamic performance of the thruster needs to be considered. The following section introduces the issues relating to dynamic thruster performance.

4.2.1 Dynamic Thruster Performance

The ‘dynamic’ performance of a thruster refers to the response to a rapidly fluctuating input (demand) signal. The response of a thruster to a rapid change in demand is highly non-linear and can dominate the dynamics of an underwater vehicle, especially at low vehicle speeds [54]. The dynamics of the thruster can lead to a closed loop system, which is limited in bandwidth and prone to limit cycle. Such performance characteristics can lead to stable small amplitude oscillations about a desired position. This phenomenon could be problematic for tasks requiring high positional accuracy, for example, docking.

When a thruster receives a change in demand there is a finite time delay between the demand and the thruster achieving the desired steady state performance. The response of the thruster in this time delay is non-linear with the response time improving (shortening) with increasing demand. An overshoot in the force generated is also experienced during this time delay. These two factors limit the ability of the vehicle to accurately control itself at low

speed due to the difficulties in predicting (and controlling) the response of the thruster. These difficulties are particularly problematic for low speed, fine positioning, manoeuvres due to the required accuracy of the control forces and the frequency with which the direction of thruster rotation is reversed. An example time series of thruster performance is shown in Figure 4.1 to illustrate the characteristics described.

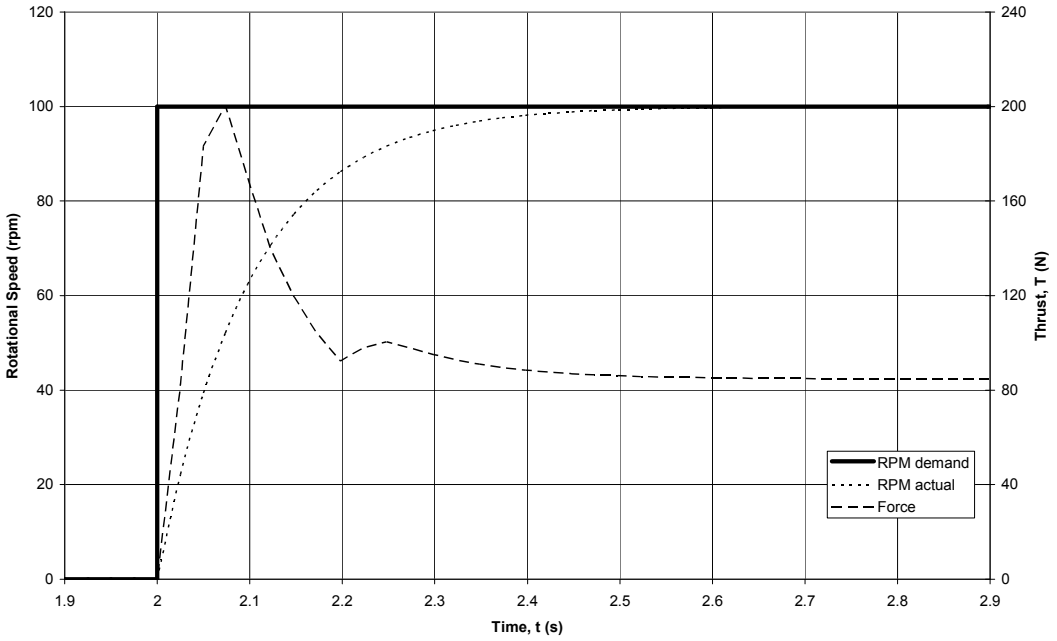

Figure 4.1 – Example Time History of Thruster Dynamic Response [54]

In Figure 4.1 a step change in demand rotational speed is made at time, t = 2s and the desired steady state performance is achieved at t = 2.5s. A large overshoot in force is experienced for a short time before a gradual reduction to the steady state value. It should be noted that the response characteristics of a particular thruster are unique.

To overcome the difficulties associated with controlling a vehicle at low speed, attempts have been made to incorporate the dynamics of thruster units into the models and control systems employed. The first model developed was a one-state model based on the thruster rotational speed [54]. This significantly improved the modelling accuracy but could not capture the overshoot in the thrust response, hence a two-state model was developed using the rotational speed, n, and the flow velocity at the propeller, u_p [55]. This two-state model is described using a representation of the motor dynamics to determine the rotational speed of the shaft:

$$J_m \dot{n} + K_n n = Q_m - Q \tag{4.3}$$

where J_m is the inertia of the motor, K_n is a motor speed constant and Q_m is the motor torque. In addition, a model of the flow dynamics at the thruster is used to determine the velocity at the propeller:

$$m_f \dot{u}_p + d_f (u_p - u)|u_p - u| = T \tag{4.4}$$

where m_f is the mass of fluid in the control volume and d_f is a quadratic damping coefficient. The resulting rotational speed and flow velocity are used to determine the thrust and torque from the propeller. The original two-state model used blade element relations to determine the thrust, T, and torque, Q. Subsequently, the model underwent several developments, including the addition of Fourier series relationships to determine the thrust and torque [56] and experimental validation [57]. However, the two-state model is only accurate at zero vehicle speed, hence the addition of a simplified model of vehicle dynamics was suggested in [52] to improve the modelling accuracy. More recent thruster models have included an alternative approach based on the Wiener-Hammerstein Cascade Model (currently only for zero vehicle speed operation) [58].

These models have facilitated the incorporation of the dynamics of a thruster into control systems enabling improvements in the low speed performance of underwater vehicles. For these models to accurately replicate the dynamic performance of the thruster requires the coefficients used to be tuned using experimental testing. An alternative practical 'solution' to the problem of thruster dynamics is to restrict the rate of change of the input demand. Restricting the rate of change of input demand negates the influence of the dynamics of the thruster and means that the performance of the thruster can be predicted using steady state models, for example Equation (4.2). This technique can be easily implemented as part of the thruster controller. The drawback to this approach is a reduction in the responsiveness of the thruster.

[58] provides an example of the rate of change of input demand that can be modelled using a steady state model. (The particular values are unique to each thruster and controller.) Using a sinusoidal variation of thruster demand [58] shows that the steady state model accurately replicates the thruster response with an oscillation frequency of π rads.s^{-1}, but cannot replicate the thruster response with an oscillation frequency of 6π rads.s^{-1}.

The control of thruster dynamics is an important issue in the control of underwater vehicles. However, since it is not the main focus of this work the analysis of the two chosen groups of thrusters will focus on the steady state performance of the thrusters without focussing on the dynamic performance in detail.

4.2.2 Thruster Operation Ranges

The operational range of a thruster imposes limits on the ability of the control system to manoeuvre the vehicle, especially at low speeds. A thruster will only operate within a particular range of rotational speeds. The top end of this range sets a limit on the maximum force achievable from a given thruster design. This maximum force gives a maximum speed at which the vehicle can move in a chosen direction or determines a maximum current in which the vehicle can hold position. Similarly, at the lower end the thruster will have a minimum rotational speed and thus a minimum achievable force. For a thruster designed to operate in both forward and reverse modes there will be a gap between the minimum forward rotational speed and minimum reverse rotational speed. The region between these two minima is known as a 'deadband', see Figure 4.2.

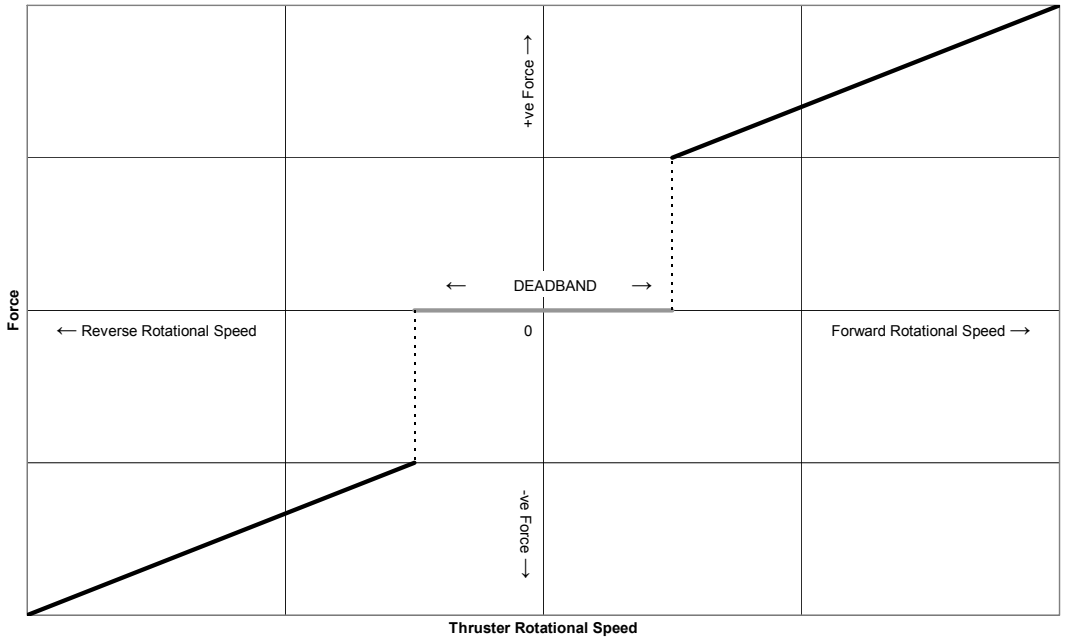

Figure 4.2 – Diagram illustrating the definition of a Thruster Deadband

If a demand rotational speed in the deadband region is requested then the controller will command the thruster to rotate at the minimum speed in the chosen direction. This deadband can cause difficulties in the control of underwater vehicles at low speeds due to the inability to smoothly transfer from generating a force in one direction to generating a force in the opposite direction. Furthermore, the limitations imposed by having a minimum achievable force can cause difficulties in precise positioning control. This deadband can be included in a model of the thruster and thus the response of the device predicted to improve the performance of the control system.

The models mentioned here only consider the performance of the isolated thruster and do not account directly for the interaction of the thruster with its surroundings. The performance of the two groups of thrusters identified onboard a vehicle will be discussed in detail in Sections 4.4 and 4.5. Next, the selection of the size and location of the chosen thrusters will be discussed.

4.3 Selection of Thruster Size and Location

Having addressed the general performance considerations for propeller based thrusters it is necessary to define a design specification for the thrusters to facilitate further examination of their performance. That is, the size and location of the device will influence its performance characteristics on a vehicle. These two specifications are linked to a number of other issues relating to the performance of the overall vehicle. These issues will be addressed next.

The exact selection of the size and location of a thruster is a compromise between several factors. These factors can be broadly categorised into three groups:

1. Manoeuvring performance.
2. Survey efficiency impact.
3. Power requirement.

The manoeuvring performance is a function of the location of the thruster, which determines the moment arm, and the forces induced on the vehicle by the thruster. The survey efficiency impact is primarily measured in terms of the change in vehicle drag as a consequence of the introduction of the thruster. This is a function of the location of the thruster (with respect to the shape of the vehicle) and the size of the thruster. The power requirement is a function of the design and efficiency of the thruster, the forces required and the size of the thruster. The compromise between these factors can be expressed in terms of the selection of the size and location of the thruster as follows:

1. The size of the thruster has to be selected as a balance between the forces required to achieve a given level of manoeuvrability, the power required to generate these forces and the additional drag this size of thruster incurs.
2. The location of the device has to be selected as a balance between maximising the moment arm, minimising the additional drag incurred and the practicalities of mounting the thruster at the preferred location.

To demonstrate these factors, the influence of the size of the thruster on the power requirement and the estimation of the vehicle drag will now be considered.

4.3.1 Power Requirements

The power required by a thruster to generate a given force at zero advance speed can be calculated using Equation (3.6). For this discussion the performance of the thruster is assumed to be ideal, as the interest here relates to the trends, rather more than the actual power values. Figure 4.3 shows the variation in required power to generate forces (T) appropriate to Autosub as a function of thruster diameter (solid lines) and the variation in required power as a function of thrust density (T/A, thrust per unit area, dashed lines).

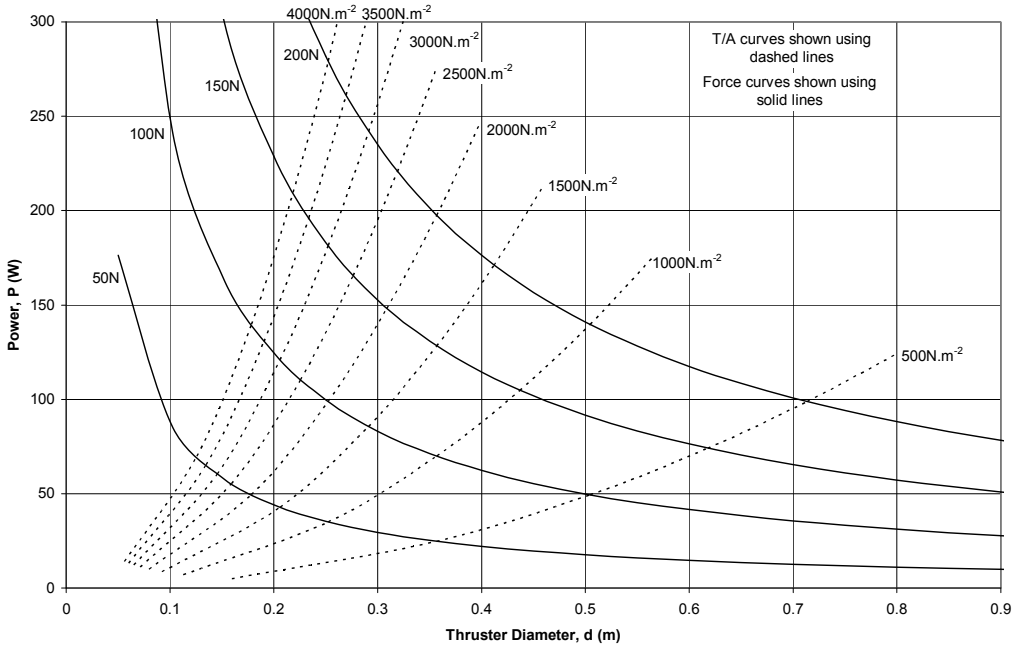

Figure 4.3 – Variation of Thruster Power Requirements as a function of Thruster Diameter and Required Force

Figure 4.3 shows the expected result that the power requirement reduces with increasing thruster size for a given force. These trends also show that there is a considerable power cost to reducing the size of the thruster beyond a certain thrust density threshold of the order of 2500N.m^{-2} (using ideal values).

4.3.2 Drag Estimation

The variation in vehicle drag due to addition of the thrusters is dependent upon the choice between external thrusters and through-body tunnel thrusters. The drag of the unmodified vehicle can be estimated using a drag coefficient, see Equation (2.1). The variation in vehicle drag caused by the two thruster groups will be considered in turn.

4.3.2.1 Estimation of External Thruster Drag

The increase in drag caused by the addition of external thrusters can be estimated by considering a pair of thrusters mounted on Autosub. In this estimate the drag of the mounting mechanism is ignored and any interaction effects are neglected. The addition of a pair of external thrusters of (individual) frontal area, A, will lead to a percentage increase in drag, $D_{I\%}$, given by:

$$D_{I\%} = 100\left(\frac{2AC_{DET}}{\nabla^{2/3}C_D}\right). \tag{4.5}$$

The selection of the drag coefficient C_{DET} is difficult given the unknown form of the thruster and the complexities of estimating the drag induced by the flow through the thruster (the thruster is assumed to be non-operational). Therefore a range of C_{DET} is used, based upon experimental results from a thruster characterisation test. The range chosen is $0.6 < C_{DET} < 1.0$. The increase in drag, for a range of thruster diameter and drag coefficient, C_{DET}, is given in Figure 4.4.

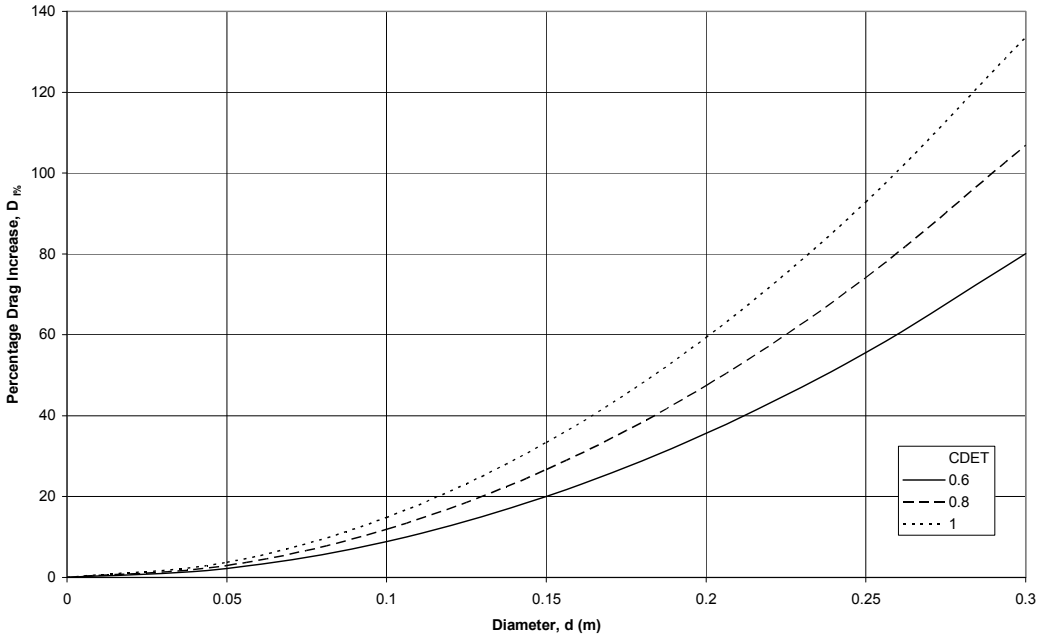

Figure 4.4 – Variation of Percentage Increase in Vehicle Drag due to the Addition of a Pair of External Thrusters as a function of Thruster Diameter

For a 20cm diameter thruster, with $C_{DET} = 0.8$, the percentage increase in drag (and hence propulsion power) is 47%. Figure 4.4 shows large increases in vehicle drag when using external thrusters. However, if the thrusters were used for survey propulsion (mounted as a pair on either side of a hydrodynamic hull form, as would be expected) then this increase in

drag would be offset by the removal of the low pressure region induced by a stern propulsor at the tail of the vehicle and an improvement in propulsive efficiency due to the uniform thruster inflow. The drag increase will be modified by the operation of the thruster and is generally considered as part of the power requirement to generate a required thrust force rather than as an increase in vehicle drag.

4.3.2.2 Estimation of Tunnel Thruster Drag

The drag increase caused by the addition of a tunnel thruster is different to that of an external thruster as the tunnel and vehicle cannot be considered separately. The addition of a tunnel alters the form of the vehicle and modifies the flow over the vehicle causing a variation in drag. Despite this, the variation in drag for surface vessels has been reported in terms of a drag coefficient for a tunnel which is added to the drag of the unmodified vessel. [59] gives a tunnel drag coefficient of 0.07 using the following standard definition (based on tunnel cross sectional area):

$$C_{DTT} = \frac{D}{0.5\rho A U^2} \tag{4.6}$$

[60] gives tunnel drag coefficients in the range 0.024 to 0.096 as an undefined function of the particular location of the thruster. [61] gives an increase in surface vessel drag of 10-12%. [61] notes the considerable influence of the various designs of tunnel fairings and notes the use of doors to 'close' the tunnel entrances at high speeds. The drag coefficients indicate a dependence on the size of the thruster and the ranges of tunnel drag coefficient indicate the influence of the particular design (for example, the entrance fairings). The percentage increase in vehicle drag caused by the addition of one tunnel thruster for a range of thruster diameter is shown in Figure 4.5 using a similar calculation to that given by Equation (4.5).

Figure 4.5 shows small increases in vehicle drag due to the addition of a tunnel thruster using the drag coefficients given in [59] and [60]. Notably, these increases are lower than those provided in [61].

The drag data presented so far is based on large surface vessels and the drag implications may differ for an AUV, given the differing hull shapes. The results of a series of resistance tests have been published for a flatfish AUV body [62]. The results are shown in Table 4.1 in terms of a non-dimensional hydrodynamic surge force coefficient, X'_{uu}, and this data actually shows a decrease in total drag for the vehicle with tunnels at low speeds.

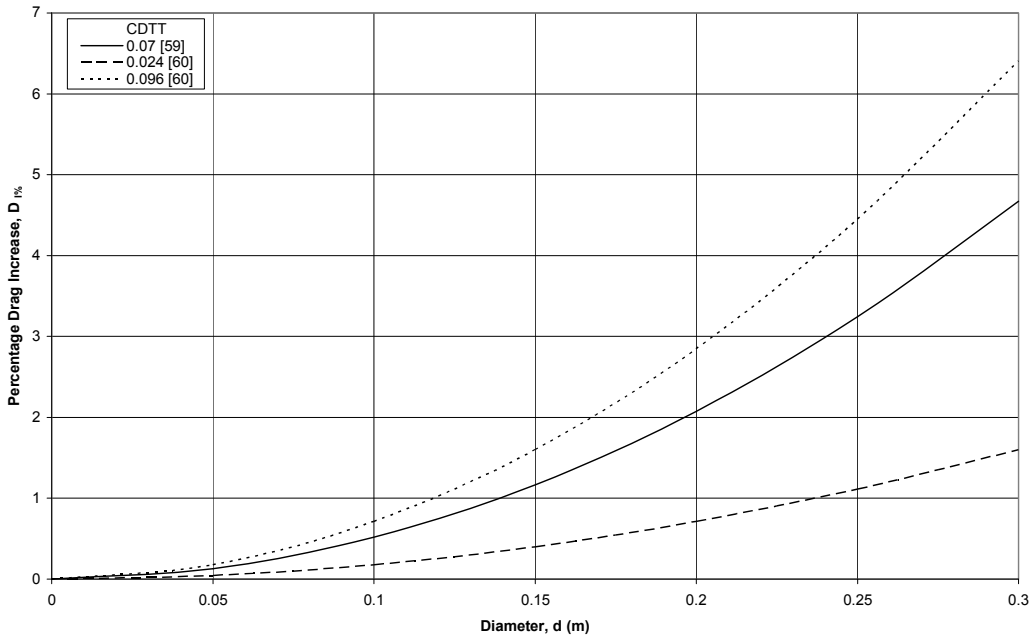

Figure 4.5 – Variation of Percentage Increase in Vehicle Drag due to the Addition of a Tunnel Thruster as a function of Thruster Diameter

Table 4.1 – Drag of Tunnel Thruster Openings on a Flatfish AUV

Forward Speed (m.s^{-1})	X'_{uu} **Smooth**	X'_{uu} **Tunnels**
0.3	-0.009	-0.008
0.6	-0.010	-0.008
1.0	-0.013	-0.013

Furthermore, [62] shows marginal decreases in vehicle drag at 1.0m.s^{-1} over a range of yaw angles covering ±20º. A single thruster was mounted on the flat sides of the AUV aft of the curved nose section. The comparison between the results shown in Table 4.1 and the data presented for surface vessels demonstrates the importance of sensible tunnel thruster placement. On a surface vessel, the shape of the hull form dictates that, to place the thruster near the bow, the tunnel is in a curved part of the hull form. This placement presents a direct blockage to the oncoming flow. However, on a torpedo shaped (or flatfish) AUV it is possible to place the thruster just aft of the nosecone in the flat parallel midbody, which reduces the drag impact of the tunnel but still places the tunnel near the front of the vehicle (to maximise the turning moment).

4.3.2.3 Drag Estimation Conclusions

The order of magnitude of these drag results indicates that the drag caused by the external thrusters has a significantly larger impact on the survey efficiency when compared to a tunnel thruster. This significantly larger impact means that the drag must take on a much greater importance in the design process of an external thruster AUV, however the options for reducing this drag penalty are limited. For a tunnel thruster AUV, with a sensibly placed tunnel, the drag impact is small and hence the design choices can be made based on the performance and power requirements.

4.3.3 Thruster Selection Conclusions

Given the differing orders of magnitude of the drag impact for the two types of thruster considered, it is difficult to select a common set of thruster dimensions for use in further analysis. Despite the apparent insensitivity of the tunnel thruster design and the relative substantial impact of the external thruster design a common thruster will be selected for the investigations solely based upon the power requirements.

Therefore for a vehicle of the size of Autosub, and given the forces required (see Section 3.3.2), the suggested thruster diameter is one quarter of the vehicle diameter, 0.225m. This value is determined using a thrust density of approximately $2500N.m^{-2}$ for the generation of a 100N force (from a single thruster). The location of the chosen thruster will remain a variable in the following analysis of the performance of the two groups of thruster identified.

4.4 External Thrusters

An external thruster is a propeller based thruster unit that is mounted on the outside of a vehicle. These thrusters are considered differently to the main rear propulsor as they are either used in addition to a rear propulsor or represent a significant design change to the existing considered survey vehicles. These two options have different operating regimes and, resultantly, employ different types of thruster. The former kind are similar in design and application to the thrusters employed on ROVs, that is, those specifically used for low speed tasks. The latter kind are used for both survey propulsion and low speed tasks and thus have a much wider operating range.

The key motivation in the design of a multi-purpose AUV is to develop a vehicle that combines the survey capabilities of a survey-style AUV and the low speed manoeuvrability

associated with ROVs. This motivation dictates a requirement to maintain the survey efficiency where possible. If the choice were made to add external thrusters to an existing survey-style AUV design then this would have a significant negative impact on the survey efficiency. The hydrodynamic shape of the vehicle would not readily facilitate the addition of the required thrusters in suitable locations to give a small survey efficiency impact. A vehicle using this approach could be developed but the resulting design would be more likely to be used in a different way. That is, used as a modular vehicle with different configurations for undertaking survey missions and low speeds tasks but resultantly unable to undertake both types of mission together. Vehicles of this kind tend to be hybrid AUV/ROVs. That is, vehicles capable of operating autonomously or remotely controlled. An example is the Redermor vehicle [63], see Figure 4.6.

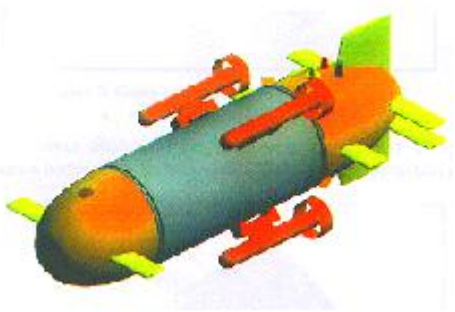

Figure 4.6 – CAD Representation of the Redermor AUV [63]

Thus to achieve the aims of a multi-purpose AUV using external thrusters requires a substantial redesign of the vehicle. This redesign involves using the external thrusters as both the main propulsion system and for low speed manoeuvring control. The redesign process would need to explore ways of incorporating the thrusters in such a way that they will provide an efficient approach to survey missions and also provide sufficient low speed control. One approach is to mount the thrusters on wings at the side of the vehicle. An example of this kind of vehicle is the Sentry AUV [48], shown in Figure 4.7.

The Sentry AUV is the replacement for ABE [64] and is designed to improve on the available performance by using a more hydrodynamic hull form and new battery technology. Sentry has four thrusters, each mounted on a wing at the side of the vehicle. Each combined thruster-wing actuator can be individually orientated to provide manoeuvring control and hover capability.

Figure 4.7 – Photograph of the Sentry AUV [48]

There are many configurations of thrusters that could be used and each possibility would need to be considered in terms of the manoeuvrability offered, the survey efficiency of the vehicle and the practicalities of the operation of the vehicle. The number of possible configurations is much larger when vectored thrusters are considered and the possibility of using combinations of tunnel thrusters and external thrusters on the same vehicle. Some simple example thruster configurations are illustrated in Figure 4.8.

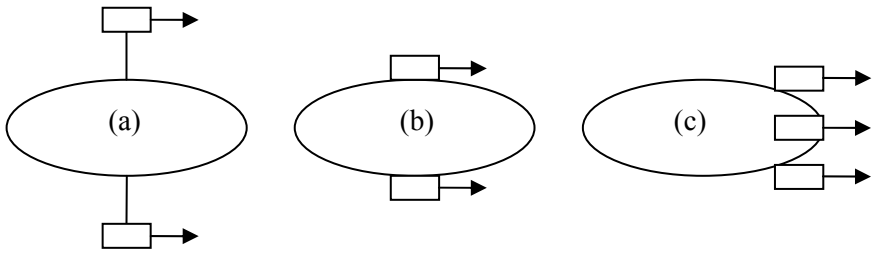

Figure 4.8 – Thruster Configurations: (a) pair of wing mounted thrusters; (b) pair of side mounted thrusters; (c) cruciform of four stern mounted thrusters.

A common feature of the thruster locations illustrated in Figure 4.8 is the exposed nature of the thrusters. Therefore, when using an open propeller, a practical design concern is the danger presented by a high speed rotating device in an exposed location, which could cause damage to the surroundings or be damaged itself. (Note that this risk is partially mitigated on the Sentry AUV by the span of the wings.) On low speed vehicles this risk is mitigated by placing a duct around the propeller as a shield. The presence of the duct can enhance the thruster performance at low speeds. However, this benefit reduces as vehicle speed increases. To mitigate this risk, this work will focus on the use of ducted thrusters.

4.4.1 Comparison with a Tunnel Thruster Vehicle

The designer of the multi-purpose AUV needs to choose between using external thrusters and using tunnel thrusters. The analysis of the performance of an external thruster as a survey propulsor is a relatively simple task due to the steady state nature of the operational conditions. However, the design configurations considered above, and the calculations of Section 4.3.2, indicate that the survey efficiency of the external thruster vehicle is likely to be lower than that of the tunnel thruster vehicle since the vehicle drag is likely to be greater.

This means that the low speed manoeuvrability performance would have to be significantly better than that of a tunnel thruster vehicle to make the external thruster an attractive option. Therefore the focus in the assessment of external thrusters is dominated by assessing how well the thruster configuration performs in terms of the low speed capabilities. At low speeds the operational conditions are highly variable, including non-uniform inflows and rapid changes in the direction of rotation. The performance of external thrusters and the difficulties associated with modelling them will be discussed in the following sections.

4.4.2 Open Literature Information

There is a large body of research on the design of external thrusters and their performance characteristics. The design research focuses on the design of the blades, the design of the duct and the influence of one on the other. The performance characteristics are commonly determined by experiment and are widely available, especially at zero speed of advance.

The design of external thruster units is similar to the design of any propeller with a uniform inflow profile. Example design procedures can be found in [10]. The design of the duct needs to be integrated into the design process for the propeller as the performance of one is dependent upon the other. There are various types of thruster technology employed including different ways of mounting the propeller blades and a choice of drive systems.

The research on performance characteristics consists of experimental results (e.g. [65]) and computational models using a variety of different approaches (e.g. [66]). There are two different types of characteristics, namely, open water characteristics, which focus solely on the performance of the thruster without any interference from other structures, and vehicle response characteristics which investigate the performance of the thruster when attached to a vehicle.

The open water characteristics of a thruster show how the thrust, torque and efficiency vary as a function of the operating conditions, normally with uniform axial inflow profiles. In a limited number of cases these characteristics extend to the performance of these devices in four quadrant operations and subject to off-axis and non-uniform inflows (e.g. [36]). These results are only available in a limited number of cases due to the difficulties in undertaking these experiments and difficulties in achieving accurate results using computational approaches.

The vehicle response characteristics are unique to the particular configuration of thrusters on a vehicle and hence are more complex to generalise and predict. The characteristics are dependent upon the complex interactions between the thruster (and any other thrusters) and the shape of the hull (and any other surrounding structures). Hence, these characteristics are usually determined by a specific set of experiments if required.

Examples of the available literature and the performance characteristics, both open water and vehicle response, will now be briefly discussed.

4.4.2.1 Open Water Characteristics

The open water characteristics of an external thruster are given in the form of a non-dimensional propeller chart. Alternatively manufacturers sometimes simply provide details of the thrust force generated as a function of the power drawn. An example data set of the performance of a series of ducted thrusters is given in [36]. This data is given in terms of standard thrust and torque coefficients with an additional duct thrust coefficient. Polynomial curve fits to the data are provided in terms of the advance coefficient, J, and the pitch-diameter ratio of the propeller, p_B/d. A sample performance curve for a ducted propeller is shown in Figure 4.9. The particular propeller is a Kaplan blade type Ka4-70 with $p_B/d = 1.0$ in a 19A duct.

This data shows similar trends to an open propeller (cf. Figure 2.4). However, it is important to note that the curves for the duct thrust, K_{Tn}, and resultant total unit thrust, K_{Tt}, show that the thrust generated by the duct becomes negative (a drag force) at $J = 0.65$ and this leads to the total thrust of the device becoming negative at $J = 0.78$ (despite the propeller still generating thrust). These performance curves demonstrate the influence of the duct in the thrust generation process and indicate why ducted thrusters are commonly used on vehicles operating at low speeds.

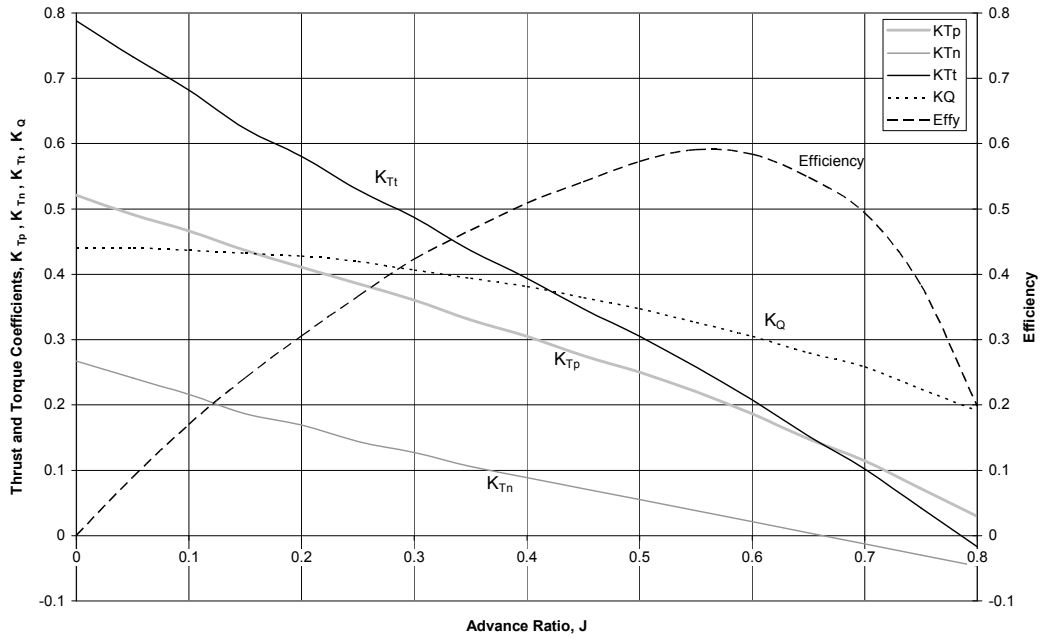

Figure 4.9 – Performance Characteristics of a Ka4-70 with p_B/d = 1.0 in a 19A Duct

In addition, data on the performance of the same thruster during four quadrant operation and subject to off-axis flows is presented. This data is given as a function of the advance angle, β, instead of the advance coefficient, J, to facilitate easy differentiation between the four quadrants of operation:

$$\tan(\beta) = \frac{U}{0.7\pi nd}. \tag{4.7}$$

Furthermore, the forces (thrust or longitudinal and transverse forces) and moments (torque and/or steering moment) are given using new coefficients since the standard K_T and K_Q definitions approach infinity as the rotational speed approaches zero. The force coefficients are of the form:

$$C_F^* = \frac{F}{0.5\rho\left[U^2 + (0.7\pi nd)^2\right]\pi/4\, d^2}. \tag{4.8}$$

The moment coefficients have an additional factor of $1/d$. Curve fits to this data are provided in [36] using Fourier series. Example performance curves in the range $0^\circ < \beta < 90^\circ$ showing the longitudinal force coefficient, C_X^*, and the transverse force coefficient, C_Y^*, for the same thruster as characterised in Figure 4.9 subject to an inflow angle of 30º to the thruster axis are shown in Figure 4.10.

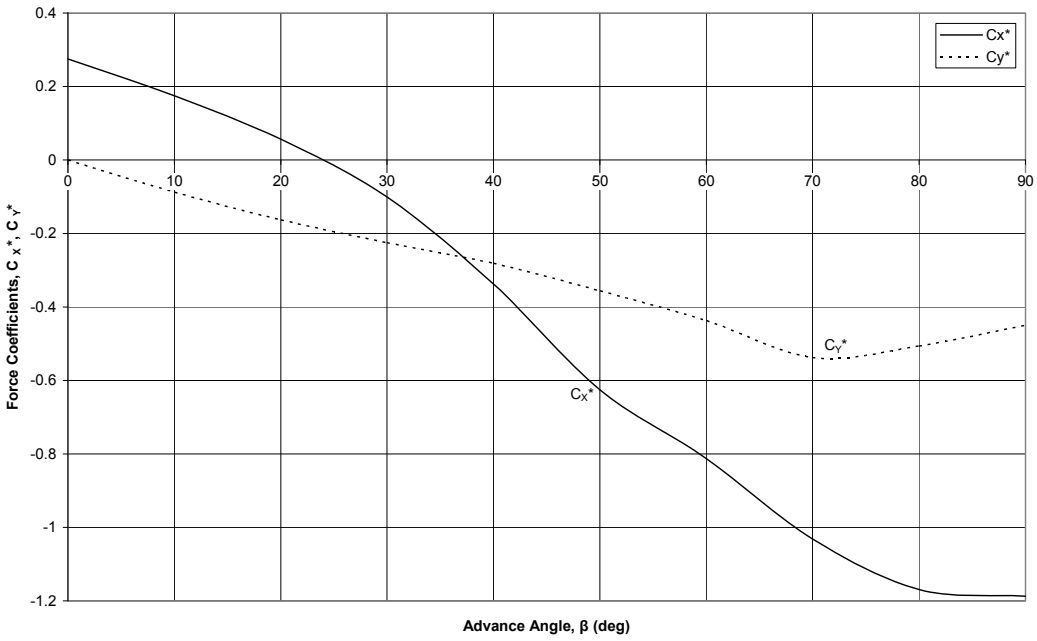

Figure 4.10 – Variation of the Forces generated by a Ka4-70 with p_B/d = 1.0 in a 19A Duct orientated at 30º to the Flow as a function of Advance Angle

This data shows the expected reduction in thrust at low values of β before the longitudinal force becomes negative and larger in magnitude at higher β values. The transverse force in this condition always acts in the same direction and has an approximately linear variation up to β = 70º before slowly reducing in magnitude at higher β values.

Other comprehensive data sets are available for different types of thruster including, for example, a podded propulsor [65]. However, most manufacturers do not provide such comprehensive performance data and if required this information must be determined by experimental testing.

A model of the performance of an external thruster on an AUV is required to aid in the assessment of the performance characteristics of an AUV equipped with external thrusters. The data and the curve fits provided in [36] mean that it is not necessary to develop a new performance model. (A computational model of thruster performance could be developed however the standard series form of the data and the breadth of the investigations in [36] mean that this data provides a more reliable option.) Therefore in the following sections the performance characteristics of a Ka4-70 with p_B/d = 1.0 in a 19A duct, taken from [36] and scaled appropriately, can be used as a representative external thruster.

4.4.2.2 Vehicle Response Characteristics

The key issue in understanding the response of the vehicle is to understand the actual forces induced by the operation of the thruster(s). It is known that the forces on a vehicle differ greatly from those measured on a thruster operating alone in open water. A thruster itself is usually considered as a black box, that is, the forces and moments generated by the thruster can be determined using the performance characteristics detailed above. To estimate the forces and moments from the thruster requires knowledge of the rotational speed and the inflow profile. To determine the forces and moments on the vehicle, it is important to consider any other effects the operation of the thruster may induce. These effects are dependent upon the inflow to and outflow from the thruster and how these flows interact with the vehicle. These interactions can induce considerable forces and moments on the vehicle, which can significantly affect the vehicle response.

The interactions between a thruster and its surroundings are commonly grouped into four categories:

1. Thruster – Waves
2. Thruster – Current
3. Thruster – Thruster
4. Thruster – Hull

These interactions are not mutually exclusive and could all occur together which further complicates the understanding of the response of the vehicle. For an AUV working at depth (depth greater than half the wavelength of the free surface disturbance) the interactions between the thruster and waves can be ignored. The influence of current on thruster operation takes two different forms, namely, the influence of an inflow component (which could be off-axis) and the interaction of the thruster outflow with the current. The influence of an off-axis inflow can be accounted for through appropriate definition of the inflow profile used in determining the thruster forces from the data presented above, provided the current velocity is known and a suitable data set is available. The interaction of the outflow with the current could cause a deflection of the thruster jet as a function of the relative strength of the outflow and the ambient flow. This deflection could lead to a different set of interactions to those expected without the influence of the current. However, for this work it is assumed that the AUV will not be working in waters with strong currents. Thus it is expected that the thruster outflow will dominate the ambient flow such that large deflections of the thruster outflow will not occur and can be neglected.

The remaining interactions, thruster – thruster and thruster – hull, can be considered in terms of the influences of the inflow and outflow. The details of these flows will now be briefly introduced.

4.4.3 Thruster Inflow and Outflow

A thruster is designed to generate a force that acts on a vehicle to produce the desired manoeuvre. However, the operation of this thruster generates inflow and outflow conditions, which can have an additional impact on the performance of the vehicle. The following considers these effects and addresses how they may be considered in the design and simulation of an AUV.

The flow into a thruster can be modified by the presence of a body near the thruster. The boundary layer between the free stream flow and the body consists of fluid moving with a lower velocity than the free stream velocity. If the thruster is operating in (or partially in) this boundary layer flow, this provides a non-uniform inflow profile for the thruster and hence affects the performance of the thruster. This effect is usually accounted for through the use of an averaged inflow profile, but can be accounted for in greater detail by calculating the performance of the thruster subject to the full 360º (2-D) flow profile.

The operation of an external thruster modifies the flow conditions both upstream and downstream of the thruster. The thruster accelerates the surrounding ambient fluid, with, appealing to momentum theory, half of the acceleration occurring upstream of the propeller plane and half downstream. The acceleration of the upstream fluid into the thruster induces a suction effect in this region. The accelerated jet flow downstream of the thruster induces another suction effect caused by the entrainment of the ambient fluid into the jet. If there are bodies in these regions around the thruster then the suction effects will act on these bodies and induce forces on them.

If a thruster jet of higher flow velocity than the ambient fluid flows directly onto a body, see Figure 4.11(a), then an increased force will be induced on that body. Furthermore, if a thruster jet becomes attached to a body, that is, the jet begins to flow along the surface of the body, see Figure 4.11(b), then the skin friction caused by the flow over the body increases. A jet flowing near a body is attracted towards the body by the pressure difference across the jet caused by the entrainment of the fluid into the jet (the Coanda effect). The increases in force are due to the higher flow velocity in the jet relative to the ambient fluid. The forces induced act against the desired thruster force giving a resultant force of ($T - D$) and hence

the effectiveness of the thruster is reduced. If the thruster jet flows into a second thruster then this jet will dominate the inflow conditions for the second thruster and affect its performance accordingly.

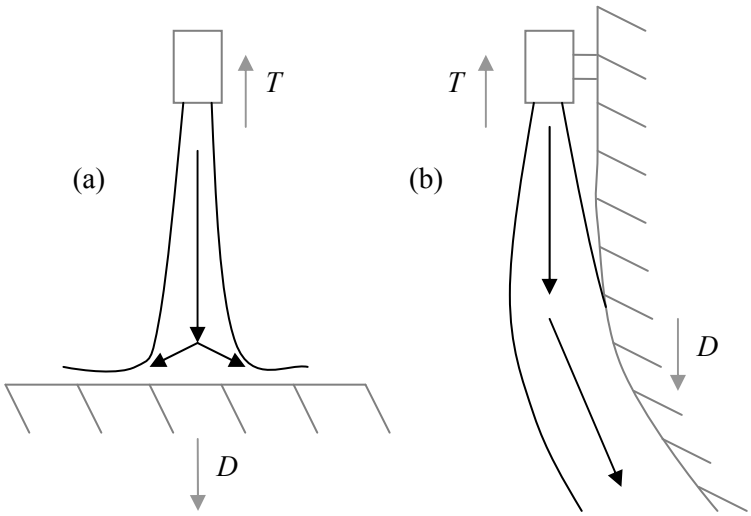

Figure 4.11 – Representations of Thruster Jet Flows:
(a) Thruster Jet Impinging on a Body; (b) Thruster Jet Attached to a Body.

These interactions are not unique to this particular scenario and occur on normal surface vessel stern mounted propulsion configurations. In this case the upstream suction effects cause an increase in vessel drag and are accounted for using a thrust deduction factor, usually of the order of a 10-20% increase in total drag [67]. The propeller jet flows downstream, away from the hull. Thus the only interaction is with a rudder (if present). The interactions between the rudder and propeller are complex and can be approached in a variety of ways, for examples see [22].

The development of the thruster jet as it flows downstream plays an important part in the interactions between a thruster and its surroundings. In order to be able to investigate these effects, it is necessary to understand how this flow develops. A thruster jet is a round jet with a swirl component caused by the rotation of the propeller blades. The characteristics and development of these jets will now be discussed.

4.4.3.1 Swirling Jets

A swirling jet is a round jet with a substantial tangential velocity component off the centreline of the jet. A swirling jet is characterised in a similar manner to a non-swirling jet, that is, in terms of the centreline velocity, u_c, and the half width, r_j – the radius of the jet at

which the velocity is half the centreline velocity. The velocity in the jet decays and the half width increases as the jet mixes with the surrounding fluid and develops downstream. These parameters are illustrated in Figure 4.12.

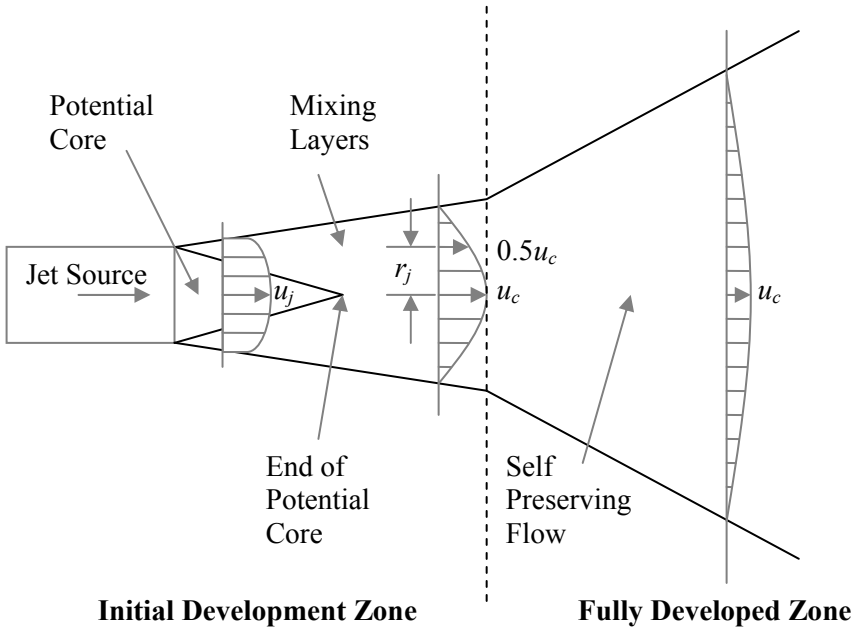

Figure 4.12 – Diagram illustrating the Development of a Swirling Jet

A swirling jet is also characterised by the amount of swirl within the jet. The level of swirl plays an important role in the development of the jet downstream. ([68] provides some good photographs of the flow of jets with varying levels of swirl.) The level of rotation in the jet is characterised by a swirl number, S_W, calculated as the ratio of the angular, G_φ, and linear, G_x, fluxes of momentum:

$$S_W = \frac{2G_\varphi}{G_x d} \tag{4.9}$$

The development of the jet, as illustrated in Figure 4.12, shows two distinct zones – the initial development zone and the fully developed zone. The initial development zone is the part of the jet where the swirl component has a significant influence on the mixing of the jet with the surrounding fluid. The swirl component decays rapidly in this initial development zone. The magnitude of the swirl component affects the development of the flow in terms of the spreading rate and the decay of axial velocity and can, for example, cause an area of reverse flow, or, for sufficiently high swirl, induce a phenomenon called vortex breakdown (where the jet potential core transitions into a wake type flow [69]).

In the fully developed zone the swirl component has decayed completely and the jet exhibits characteristics similar to a non-swirling jet. That is, the jet velocity profile downstream can be described using a similarity profile, for example [70],

$$\frac{u}{u_m} = \frac{1}{\left[1 + \left(\sqrt{2} - 1\right)R_j^2\right]^2}, \tag{4.10}$$

and the growth of the jet stabilises. However, the influence of the swirl on the development of the jet in the initial development zone is carried forward to the fully developed zone as observed in several experimental studies [71, 72].

4.4.3.2 Thruster Jets

A thruster jet can be considered as a swirling jet. However, there is a significant difference to those already discussed as the initial velocity profile does not take the form indicated in Figure 4.12. The actual velocity profile is influenced by the loading of the propeller blades and the presence of the hub, that is, with the maximum velocity around $0.7r_p$ and very low velocity on the centreline. This adds additional complexity to the initial development zone as the location of the maximum velocity in the jet moves to the centreline.

Thruster jets have been investigated in [73] and a simple model devised for thruster jet flow based on fits to experimental data for propellers and using results from published experimental and theoretical investigations into turbulent jets. The model provides a simplified representation of the flow, which does not necessarily accurately capture all of the important features and trends of the flow. Recent research on swirling jets has presented new results which provide greater insight into the complex structure of these jets (e.g. [71]). Attempts were made to incorporate these new results into a model of a similar form to the jet model from [73], however the large number of variables prohibits the development of a simple model suitable for this purpose. Simplifications based on experimental results could be adopted. However, the dependence of the development of the jet on the specific swirl distribution and method of swirl generation [74, 69] and the lack of far-wake propeller jet data meant that this approach could not be reliably employed.

Therefore, some basic information concerning the most important parameters in a thruster jet flow is presented to facilitate analysis of the likely interactions to be encountered on an AUV. This information concerns the spread of the jet and the decay of the maximum velocity within the jet, that is, 'global' jet parameters without dealing with the details of the velocity profile and structure of the jet.

4.4.3.3 Jet Spread

As the jet flows downstream, it mixes with the surrounding fluid. This mixing causes the entrainment of fluid into the jet, causing the jet to spread. An estimate of this jet spread is required when assessing the likelihood of interactions between the jet and other parts of the vehicle. In [73], a half-jet spread angle of around 8-10º is given, however it is known that the spread of a swirling jet is a function of the amount of swirl in the flow, which is characterised using the swirl number, S_W, which can be estimated for a propeller as:

$$S_W = \frac{2K_Q}{K_T}. \tag{4.11}$$

Most propellers generate a jet with a swirl number in the range $0.15 < S_W < 0.4$ under normal operating conditions (moderate and low J). Detailed studies of swirling jets have shown that the growth of the jet is non-linear in the initial development zone, with this growth enhanced by the amount of swirl [71]. The initial development zone is usually between four and six diameters long. In the fully developed zone, where the tangential velocity component has decayed, the growth becomes linear but maintains the enhanced growth rate caused by the swirl. Typical spread angles for swirling jets in the developed zone, as a function of swirl, range from approximately 5º for low swirl ($0 \leq S_W \leq 0.1$) up to approximately 8º for high swirl ($S_W > 0.3$) [71, 72]. For medium swirl ($0.1 < S_W \leq 0.3$) the growth rate scales with swirl. Experimental results from [73] show that the jet spread angle reduces with increasing advance coefficient, J, that is, when operating with co-flowing ambient fluid.

4.4.3.4 Maximum Velocity Decay

As a jet flows downstream, the maximum velocity in the jet decays. Theoretical arguments can be used to show that the decay of maximum velocity downstream in a turbulent jet will take the form [75]:

$$\frac{u}{u_m} = \frac{a}{[x/d]^b}. \tag{4.12}$$

In general, the value of a is set equal to 1. Theoretically, a non-swirling fully developed jet will decay with $b = 1$. Experimental data shows that swirling jets decay at slower rates, that is, $b < 1$. A study of available propeller jet data has shown that the best fit to the velocity decay is achieved using a variable value of b. Generally, b increases in the initial development zone before reaching a steadier value in the fully developed zone.

The selection of the coefficients (a and b) in Equation (4.12) is a function of the jet swirl and the advance coefficient, J. Experimental results for swirling jets in stationary flow show the decay coefficient, b, to increase with higher swirl. In the developed zone most swirling jets adopt a decay coefficient, which scales from weak swirl to high swirl, in the range $0.3 < b < 0.6$. As an example of how the decay coefficient varies with advance coefficient, experimental results from [73] give $b = 0.389$ for $J = 0$ and $b = 0.315$ for $J = 0.2$.

These simple details on the development of a thruster jet downstream will be used to assess the interactions discussed above.

4.4.4 Thruster Interactions

There is a small body of research on these interactions consisting of experimental results for specific surface vessels relating to particular offshore projects [76]. In some cases the results have been generalised to provide simple approaches to estimating the magnitude of the interaction concerned [77].

4.4.4.1 Thruster – Thruster Interactions

The interactions between a number of thrusters can be considered in terms of how the outflow of one thruster affects the performance of another. In simple terms, a thruster operating behind another will have an inflow which is dominated by the outflow of the forward thruster. This interaction must be accounted for to accurately determine the performance characteristics of the thruster configuration. This problem has been considered experimentally by many authors [76, 78]. However, in most cases the interactions investigated are between two thrusters operating in typical surface vessel configurations. These configurations tend to consist of a pair of azimuthing thrusters operating alongside each other in strong currents (and waves). Such configurations are unlikely to be used on a multi-purpose AUV primarily due to the shape of the AUV, the limited energy supply and the drag penalty such a configuration would incur. Therefore the focus is on an AUV type configuration with one thruster operating behind another as used on the Sentry AUV (see Figure 4.7) [48].

A set of experimental results for a pair of aligned thrusters (one behind the other) in stationary flow are shown in Figure 4.13 [79]. These results show how the thrust generated by the second thruster varies as a function of the separation between the thrusters. The thrust

from the second thruster decreases as the separation between the thrusters is reduced due to the higher inflow velocity at smaller separation distances.

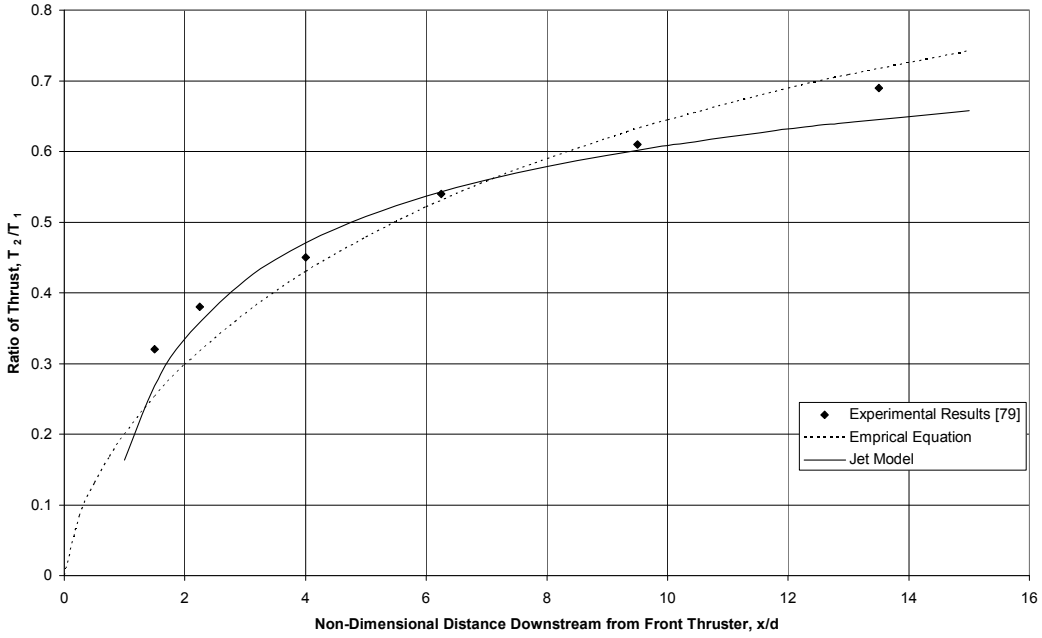

Figure 4.13 – Variation of Thruster Force as a function of Thruster Separation caused by Thruster – Thruster Interaction

An empirical equation was developed using these experimental results [79] to give the variation in thrust solely as a function of the separation, *x*:

$$\frac{T_2}{T_1} = 1 - 0.8^{\left[x/d\right]^{2/3}}, \tag{4.13}$$

as illustrated on Figure 4.13 (using a dotted line). This relationship accurately replicates the experimental results for operation at low and zero advance coefficients, *J*, as found in dynamic positioning applications. However, in this thruster – thruster interaction problem, higher *J* conditions may be experienced, for example, during survey operation. Therefore a model which accounts for these conditions is desirable.

The preceding discussion on thruster outflows outlined the difficulties in developing a simple model of the jet flow. Therefore a model will be developed using a jet velocity decay model and the open water characteristics for the thruster.

The average jet velocity far downstream of the forward thruster is given by:

$$u_j = \sqrt{u^2 + \frac{2T_1}{\rho A}}. \tag{4.14}$$

Here, u is the velocity of the ambient fluid or the velocity of the AUV on which the thruster is mounted. Examination of published experimental data (for example, [80]) shows that one diameter downstream is sufficiently far downstream for this relationship to apply. The velocity in the jet will decay with distance downstream. This decay can be estimated using:

$$\frac{u}{u_j} = \frac{a}{[x/d]^b} . \tag{4.15}$$

The resultant velocity is used to define an advance coefficient for the rear thruster. The thruster characteristics, in the form of an open water chart, can be used to determine the thrust produced by each thruster. The result of using this procedure is illustrated in Figure 4.13 (using a solid line) displaying good agreement with the experimental data. The agreement between the model and the experimental data reduces as x/d becomes large. However, this is less of a concern as the interaction becomes weaker in this region.

For $J = 0$, this model can be used to show that the interaction of two identical thrusters working with the same rotational speed is solely a function of the separation between the thrusters as implied by Equation (4.13). To accurately model the interaction at non-zero J, it is important to set the coefficients in the jet velocity decay model accordingly.

A study has been published which attempted to use a boundary element method to calculate the interactions between two aligned thrusters [81]. The developed model was unable to accurately capture the resulting flow conditions and thus the authors chose to model the interactions using the jet model from [73] in tandem with the boundary element method. The calculated inflow profile from the jet model was used as the input to the boundary element code to obtain the forces and moments from the propeller. The model shows good agreement with the experimental data from [79].

4.4.4.2 Thruster - Hull Interactions

If a jet from a thruster flows directly onto a body then there will be an increased force on the body due to the higher velocity in the jet (relative to the free stream). The magnitude of this effect has been considered in [73], [82] and [83]. [73] uses a jet model to determine the velocity of the impinging jet and derives force coefficients from experimental results. These force coefficients are, in general, larger in magnitude than those for steady uniform non-swirling flows. [82] uses flow visualisation results to determine the thrust in the jet and suggests a minimum separation of three to five thruster diameters between the thruster and any structure to avoid ‘substantial’ interaction effects. However, [83] presents data which shows that the thrust in the entire jet does not change substantially in the range between two

and four diameters downstream. This type of interaction is unlikely to occur on an AUV due to the location of the thrusters and the streamlined nature of the body, however the values given here can be used when considering configurations at the design stage.

Some of the possible configurations shown in Figure 4.8 and the Redermor vehicle shown in Figure 4.6 have external thrusters mounted close to the hull form. The motivating factors behind this choice are a desire to limit the survey efficiency penalty and to reduce the vulnerability of the thruster unit. However, the small distance between the thruster and the hull means that an interaction between the thruster induced flow and the hull is unavoidable. This interaction takes the form of a suction effect upstream of the thruster, a suction effect downstream of the thruster and the thruster jet will attach to the vehicle and then flow along the vehicle downstream. These effects combine to induce a lateral force, which pulls the vehicle in the direction of the thruster, and to induce a longitudinal force, which acts against the desired thrust force.

Previous investigations of these effects have been undertaken for dynamic positioning applications of surface vessels. These investigations include experiments to measure the thrust loss effects, however, these experiments tend not to cover the lateral forces induced. This is because most dynamic positioning thrusters are mounted on the bottom of a vessel, hence the suction effects induce a vertical force. However in dynamic positioning applications, vertical motions are dominated by the environmental conditions (free surface effects).

The thrust loss is discussed in [84] and gives a range of losses up to 25% of the desired thrust force, as a function of the proportion of the body length along which the jet flows. Free jet theory is used in [85] to show that the thruster jet will attach to the vehicle $6h$ downstream. Here h is the separation between the thruster axis and the body. A worst case scenario condition is described in [85] giving a 30% to 40% reduction of desired thrust. In this case the jet follows the line of the hull round the bilge and up to the free surface. It is shown experimentally in [73] that the thrust reduction in such a flow is a function of the radius of the bilge and the separation between the thruster and the bilge. The placement of external thrusters on an AUV, and the shape of AUV hulls, dictates that flows giving rise to the most severe thrust loss effects are unlikely to occur on an AUV.

The interactions between the induced flow due to the thruster and the vehicle are a function of the shape of the vehicle. For example, the induced forces on a cylindrical body, such as a torpedo-shaped AUV, are likely to be lower than those induced on a flat plate (due to the

differences in shape and hence separation between the jet and the body). The experimental research on dynamic positioning vessels has shown that abrupt changes in shape can lead to the detachment of a thruster jet from the body, resulting in a reduction of the induced friction effect. The slender hydrodynamic shape of AUV hulls means that this separation is unlikely to occur and the jet will remain attached for the entire downstream length of the vehicle.

To investigate the magnitude of the induced forces on an AUV, experiments were undertaken using a rim-driven thruster mounted close to a 0.357-scale large torpedo-shaped AUV (for further details, see Section 4.5.3.2). The thruster was mounted at the vehicle mid-height with the separation between vehicle and thruster, h, equal to one thruster diameter. Tests were undertaken with the thruster mounted at two different positions along the vehicle – at the junction between the nose and midbody (forward location) and at the junction between the midbody and tail (aft location). The tests were undertaken with the thruster operating in both directions (emitting a jet upstream and downstream) with the vehicle stationary. Figure 4.14 shows a schematic of the experiment and Figures 4.15 and 4.16 show the longitudinal and lateral forces recorded on the vehicle, respectively, as a percentage of the desired thrust force. For clarity versions of Figures 4.15 and 4.16 without error bars are provided in Appendix A6.

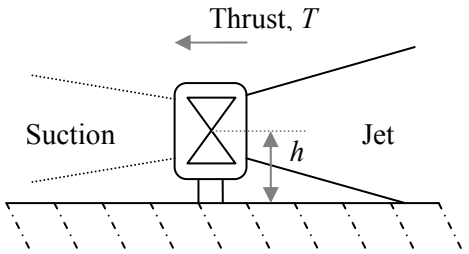

Figure 4.14 – Schematic of the Interaction between an External Thruster and the Hull (h: thruster-hull separation).

Figure 4.15 gives the percentage of the desired thrust force that is lost primarily due to the increased frictional effects. Figure 4.16 gives the lateral force induced by the suction effects, which tries to pull the vehicle in the direction of the thruster as a percentage of the desired thrust force. Both of these figures show trends of the induced forces being a fairly consistent proportion of the desired thrust force across the range of thruster power tested. These results show that the increased friction effects cause a loss of thrust of less than 10% of the desired thrust force. The lateral force induced by the suction effects is between 8% and 20% of the desired thrust.

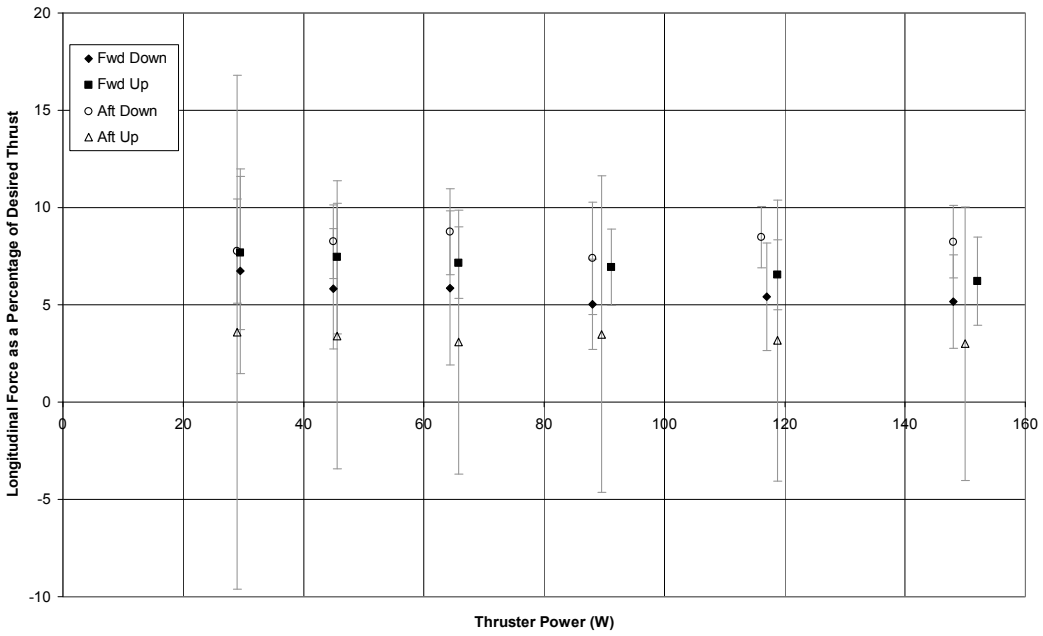

Figure 4.15 – Longitudinal Force induced by the Operation of an External Thruster mounted near a Vehicle as a function of Thruster Location (Fwd/Aft), Jet Direction (Up/Down) and Thruster Power.

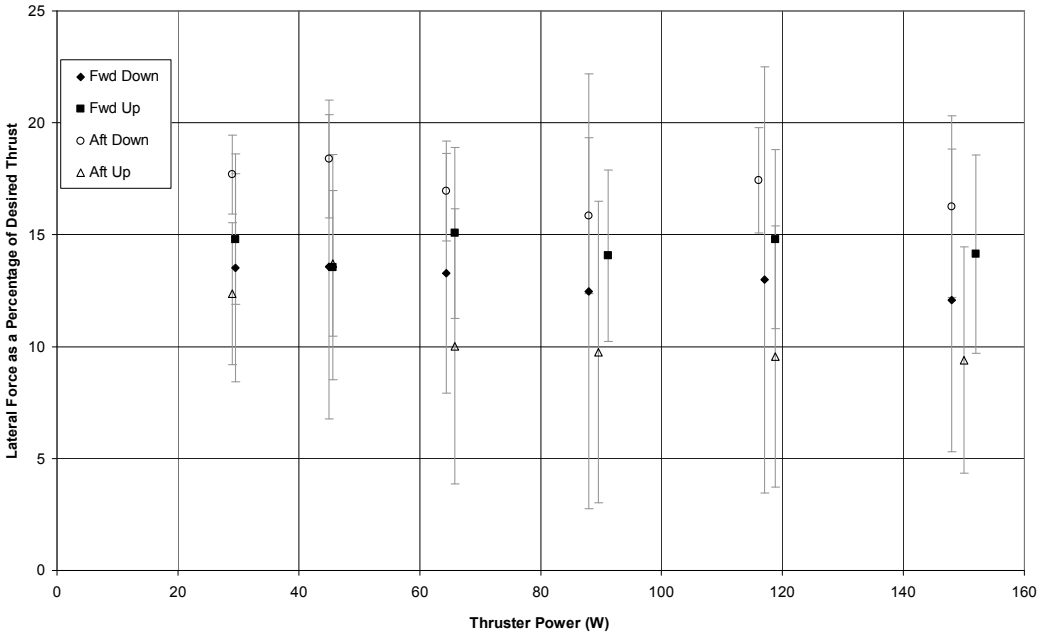

Figure 4.16 – Lateral Force induced by the Operation of an External Thruster mounted near a Vehicle as a function of Thruster Location (Fwd/Aft), Jet Direction (Up/Down) and Thruster Power.

There are variations in the proportions of the desired thrust force as a function of the location of the thruster and the direction of the jet. The results show larger induced forces when the thruster jet is not flowing along the majority of the vehicle, that is, when the jet is directed upstream from the forward position and downstream from the aft position. For the lateral forces, this implies a greater influence of the suction effects induced upstream rather than the suction effects downstream. For the thrust loss effects it is possible that the shape of the vehicle at the nose or tail means that some of the suction effects are also contributing to the loss of thrust. In general the conclusions drawn relating to the average forces acting on the vehicle still apply when the experimental uncertainty is considered. However, the distinctions between the induced forces as a function of the jet direction and the location of the thruster become less clear and hence it is suggested that an average value is adopted that is independent of the jet direction and thruster location.

These tests were undertaken with the thruster mounted close to a stationary vehicle so that these experiments represent a worst case scenario condition. (The induced forces on the vehicle are expected to decrease at larger thruster to vehicle separations (h) and on a moving vehicle.) Despite this, these results show that the induced forces are a small proportion of the desired thrust. The thrust losses are small but can, for simulation purposes, be modelled as a constant proportion of the desired thrust force. The information about the thrust losses may also be of use during the design of the thruster units to ensure the desired forces can be achieved. The lateral forces are larger but are likely to be matched by an opposite force induced by suction effects caused by a thruster on the other side of the vehicle, thus reducing their impact. Again, for simulation purposes, these interaction effects can be modelled as a constant proportion of the desired thrust force.

4.4.5 External Thruster Conclusions

The performance of external thrusters has been discussed in both open water conditions and on a vehicle. The availability of a substantial body of open water data on a series of thrusters (including curve fits) means that it is unnecessary to develop a new performance model for this work. Thus the performance characteristics of a Ka4-70 with p_B/d = 1.0 in a 19A duct, taken from [36] and scaled appropriately, can be used as a representative external thruster.

The preceding discussion on the interactions between thrusters and their surroundings has highlighted two particular types of interaction which may occur on an AUV. These are the interaction between two aligned thrusters and the interaction between a thruster and the hull when the thruster is mounted close to the hull. Models for these interactions have been

suggested – using a jet velocity prediction model with thruster open water data and using experimental results. Additional data on the development of thruster jets has also been provided to facilitate simple analysis of potential thruster configurations. This data and the developed models can be used during the design phase of an AUV or during the development of a simulation of an AUV.

4.5 Tunnel Thrusters

A through-body tunnel thruster is a propeller based device mounted in a tunnel running through a vehicle from one side to the other. On surface vessels these devices are called lateral thrusters or bow thrusters. These thrusters are mounted in transverse tunnels and are used to provide manoeuvring forces at low forward speeds. The tunnels are placed towards the ends of a vessel to maximise the turning capabilities offered, with the most common location being in the bow. The tunnel itself is a housing for the thruster and does not influence the performance of the device in the same way as a duct does for a ducted propeller. Applications for these thrusters include marine vehicles where good low speed manoeuvring capabilities are essential, for example, on a ferry during berthing operations.

4.5.1 Open Literature Information

The published literature on tunnel thrusters is mainly focussed on surface vessel applications, however recently there have been a limited number of publications on AUV applications. Research into tunnel thrusters on surface vessels has focussed on two key areas – the design of the thruster and the response of the vessel. The design research focuses on the variations in thruster performance characteristics as a function of, amongst other factors, the design of the blades, the gearing and shafting mechanism used, the shape of the tunnel and the entrances to the tunnel, and, the influence of the placement within the surrounding hull form. The vessel response research can be divided into two areas, namely, measurements of the forces and moments generated during captive model testing and the turning performance achieved on free swimming vessels. Similar areas have also been investigated for AUV tunnel thrusters. However, the body of work is considerably smaller and no published free swimming trials have been found.

4.5.1.1 Design

The design of tunnel thrusters has been investigated in detail by many authors. The most comprehensive experimental data set was published in [86]. In this work the influence of the

blade shape, blade area ratio and hub diameter were investigated. In general, the design of the blades is limited by the necessity for symmetric performance. A common conclusion is that a minimal hub size is preferable to minimise the restriction to the flow through the tunnel.

Recent advances in thruster technology, such as the development of rim-driven thruster units [87], have, to some extent, superseded some of this original research. The rim-driven thruster has many advantages including the small hub size and symmetrical performance as well as the simple and robust mounting this technology facilitates.

The research regarding the influences of tunnel shape and the entrance fairings remains important. Theoretically it would be beneficial to employ a tunnel shape with some diffusion, however this leads to an asymmetry in the design and, for a typical surface vessel tunnel thruster, the duct would be fairly inefficient. The reasons for this inefficiency relate to the small length to diameter ratio of the tunnel and hence this approach may be more suited to an AUV tunnel thruster. Furthermore, [86] tested a straight walled tunnel, a concave tunnel and a convex tunnel and found that the straight walled tunnel offered the best performance. The selection of the entrance fairing shape is a compromise between enhancing the flow into the thruster at the inlet, maximising the strength of the jet at the outlet and minimising the drag impact on the vehicle. These requirements conflict greatly for a symmetrical tunnel and hence a usual compromise is a tunnel with rounded entrances [61].

The design of tunnel thrusters for an AUV is a similar task to that for a surface vessel, albeit there are difficulties relating to the size and scale of the device. The length to diameter ratio of an AUV tunnel thruster is usually larger than that of a surface vessel (due to the differing locations adopted and hence differing relative tunnel lengths) and the size of the device means that it can be difficult to economically achieve an optimal design. The characteristics of small diameter tunnel thrusters were examined in [88, 89, 90] and, in general, the conclusions agreed with those for surface vessels. The key difference reported relates to the influence of tunnel length. An increase in tunnel length was found to decrease the thrust, albeit by a small amount due to frictional effects, with a more significant influence relating to the dynamic effects. Here, a lag in the dynamic performance of the thruster was found to occur as a function of the tunnel length.

4.5.1.2 Performance Characterisation

To compare propeller designs the performance is usually given in terms of the efficiency. A tunnel thruster is usually only used at low and zero forward speeds and thus the advance coefficient of the thruster is (usually) zero. When the advance coefficient of a thruster is zero the usual definitions of efficiency (see Equation (3.5)) give a value of zero, despite a thrust force still being produced. Therefore definitions based upon the momentum theory relationship given in Equation (3.6) are used [10]. Two commonly used coefficients are the Bendemann static thrust factor, ζ, defined as:

$$\zeta = \frac{T}{P_S^{2/3} d^{2/3} (\rho\pi/2)^{1/3}} = \frac{K_T}{K_Q^{2/3}} \frac{1}{\pi(2)^{1/3}} \tag{4.16}$$

and the static merit coefficient, C, given as:

$$C = \frac{0.00182 T^{3/2}}{SHP\sqrt{\rho\pi d^2/4}} = \frac{K_T^{3/2}}{\pi^{3/2} K_Q} \equiv \sqrt{2}\zeta^{3/2} . \tag{4.17}$$

For a non-ducted propeller the ideal values are $\zeta = 1$ and $C = \sqrt{2}$. For a ducted propeller with no duct diffusion the ideal values are $\zeta = 2^{⅓}$ and $C = 2$. To characterise these thrusters using a normalised scale, that is, from zero to unity, the device performance can be compared to the ideal performance (in terms of the Bendemann static thrust factor) giving an 'efficiency', τ, defined as:

$$\tau = \frac{T}{(\rho\pi)^{1/3} (P_S d)^{2/3}} . \tag{4.18}$$

A survey of published thruster data found that τ is usually in the range $0.5 \leq \tau \leq 0.6$ [91].

4.5.2 Physics and Performance

The experimental analysis of the performance of tunnel thrusters on marine vehicles includes both captive testing and free swimming trials. The results and conclusions of these test programmes will be considered in the following sections.

4.5.2.1 Vessel Response

The ability of a thruster to manoeuvre a vehicle is characterised in terms of the forces and moments experienced by the vehicle under different conditions in comparison with the forces and moments generated by the thruster whilst the vehicle is stationary. Captive testing programmes have been carried out on a variety of surface vessels [92, 73] and a limited number of free swimming tests have been undertaken [61, 93]. The general

conclusion from these tests, and from full scale experience, is that tunnel thrusters become ineffective at forward speeds above 1 – 1.5m.s^{-1} [61]. The particular performance characteristics of these devices and the reasons for these characteristics will be discussed in Section 4.5.2.2.

The performance of a tunnel thruster on a moving AUV has been investigated in [93] and [94]. In [93] the performance of a thruster on a submersible undergoing forward motion is provided without any details of the vehicle or thruster characteristics. In [94] the full scale C-SCOUT vehicle underwent a comprehensive testing programme for the full range of forward speeds and yaw angles in the range ±90º. These results will be discussed in more detail in Section 4.5.2.3.

4.5.2.2 Captive Testing

Early captive testing programmes were designed to characterise the performance of tunnel thrusters on a surface vessel. The performance was found to reduce as the forward speed increased and so investigations were undertaken to attempt to determine the reasons for the reduction in effectiveness. These investigations included pressure measurements on the hull form around the tunnel (at model scale) and qualitative flow visualisation experiments.

The first conclusion of these tests was that the loss of performance of the device was not due to a variation in the performance of the thruster itself, rather the cause relates to the interaction of the accelerated fluid from the thruster with the ambient flow around the vehicle. Thus, in a simplified representation, the details of the thruster itself can be ignored and the thruster is considered as a jet producing device. The jet produced can be characterised in terms of the thrust of the jet and the diameter of the jet, allowing a representative jet velocity, u_j, to be determined. (The swirl in the jet is ignored in this simplified representation.)

When the vehicle is stationary the thruster produces a jet of accelerated fluid and this flows away from the vehicle. As the jet develops downstream, fluid is entrained into the jet as it mixes with the ambient stationary fluid. The vehicle experiences a force equal to that generated by the thruster (the thrust of the jet).

When a jet emits into a crossflow the jet is deflected as a function of the relative strength of the jet to the crossflow. Empirical equations have been developed to predict the path of the jet centreline as a function of the relative strength, for example [95]:

$$\frac{x}{d} = \omega\left(\frac{z}{d}\right)^{\xi}\left(\frac{u}{u_j}\right)^{\gamma} . \tag{4.19}$$

The relative strength of the jet to the crossflow is given in terms of a speed ratio u/u_j for a common incompressible fluid.

When the vehicle is moving with a forward speed the thruster jet is deflected by the ambient flow over the vehicle, as a function of the relative strength, see Figure 4.17. At low to medium speed ratios, where the jet dominates the ambient flow, a flow pattern similar to that of the flow past a solid cylinder is observed. This flow pattern, giving a low pressure region downstream of the tunnel (cylinder), coupled with the entrainment of fluid into the jet, causes a low pressure region to act on the hull surface aft of the tunnel exit (illustrated as the shaded area in Figure 4.17). This low pressure region induces a force on the vehicle which acts opposite to the desired thruster force and consequently reduces the effectiveness of the thruster. The influence of this low pressure region is a function of the relative strength of the jet to the ambient flow and the entrainment into the jet. At higher speed ratios the jet is washed downstream along the body giving a larger area of low pressure and hence increased thruster performance degradation. Furthermore, the offset between the centre of action of the thruster force (the thruster axis) and the centre of action of the low pressure region causes a variation in the moment experienced by the vehicle compared to the expected moment.

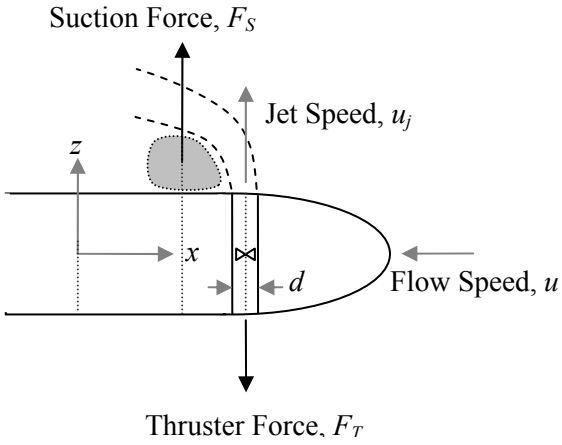

Figure 4.17 – Tunnel Thruster Jet Deflection on a Vehicle Moving with a Forward Speed

There are variations in the pressure distributions around the inlet to the tunnel and upstream of the tunnel exit as a function of the flow conditions. These regions have not been found to have a significant impact on the performance of the thruster [92].

A sample set of results for a tunnel thruster on a tanker model [96] showing the order of magnitude of the reduction in performance is given in Figure 4.18. The coefficients used are a force coefficient, K_F, giving the ratio of the actual force experienced by the vehicle to the expected (zero forward speed) force and a moment coefficient, K_N, giving the ratio of the actual moment experienced by the vehicle to the expected (zero forward speed) moment. These coefficients are plotted against the speed ratio of forward speed to jet speed, u/u_j.

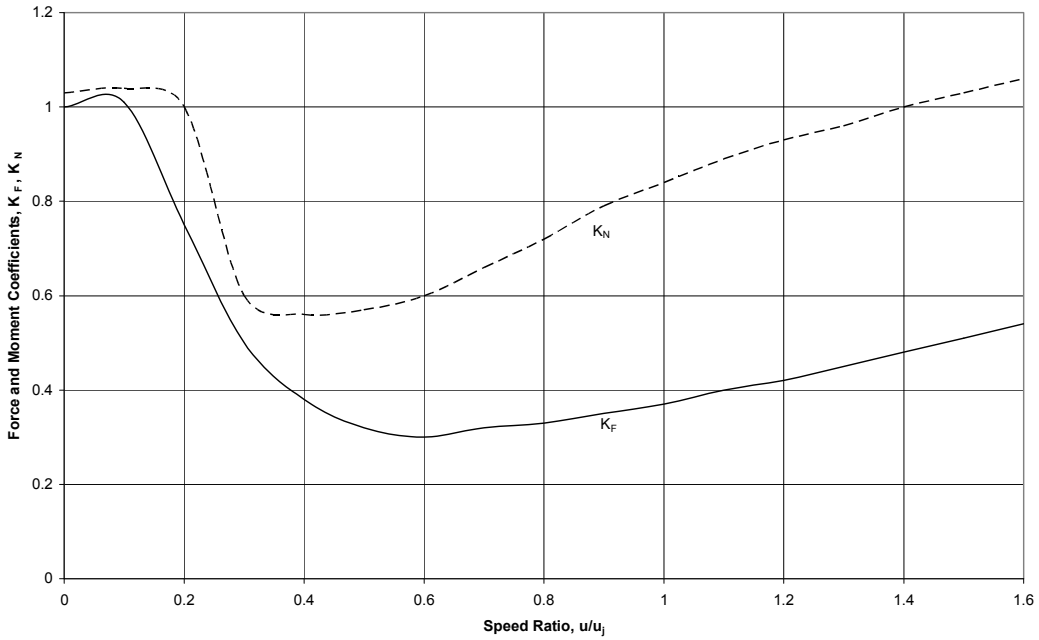

Figure 4.18 – Tunnel Thruster Performance on a Model Scale Tanker [96]
(Solid line shows force coefficient K_F, dashed line shows moment coefficient K_N)

These results show that the force decreases to 30% of the expected force at a speed ratio of 0.6 before a slight recovery at higher speed ratios. The decrease in the moment experienced is less severe and a full recovery is observed at high speed ratio. The recovery at higher speed ratios is thought to be caused by the dominance of the ambient flow over the jet and hence the jet and, to some extent, the suction effects are washed away. The results used to produce Figure 4.18 show consistent trends as a function of speed ratio, whereas other authors have suggested that the reduction in forces and moments is solely a function of the forward speed and thus independent of the thrust force [97]. This conclusion is drawn at low speed ratios where the entrainment of fluid into the jet is not a significant factor in the low pressure region, which is solely caused by the flow pattern around the jet. The factors, and the relevant magnitudes, affecting this functionality are uncertain and hence this will need to be investigated further.

Other experimental results for surface vessels (e.g. [92, 73]) exhibit trends similar to those illustrated in Figure 4.18. The differences between the results indicate a dependency on the particular thruster-tunnel-vehicle configuration concerned. That is, the results for each different configuration are unique as they are dependent upon the interaction between the flow over the vessel, the jet generated by the thruster and the interaction of the generated low pressure region with the hull form.

There have been a limited number of published experimental programmes looking at the forces and moments on the vehicle when operating at non-zero yaw (drift) angles [73, 98]. In general these results show a fairly consistent performance across the range of yaw angles apart from a large decrease in force coefficient, K_F, when the ambient flow (current) is directed towards the thruster exit (in direct opposition to the thruster jet, that is, drift angles between 90º and 180º), see Figure 4.19. The magnitude of the performance decrease across the range of yaw (drift) angles is a function of the speed ratio. Further experimental investigations have also been undertaken to examine the influence of shallow and confined waters [73] and the influence of waves [99].

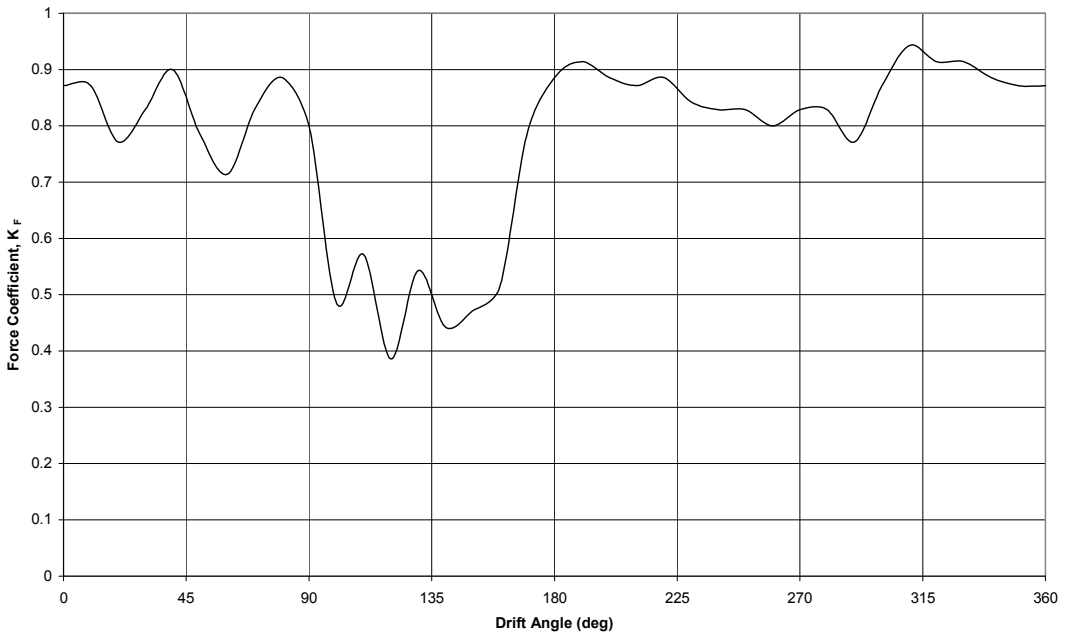

Figure 4.19 – Variation of Tunnel Thruster Performance on a Seabed Operations Vessel as a function of Drift Angle at a Speed Ratio of 0.2 [98]
(A drift angle of 180º implies forward travel)

4.5.2.3 Underwater Vehicle Results

The results for a tunnel thruster on a submersible from [93] are plotted in Figure 4.20 using the same coefficients as Figure 4.18. [93] does not provide any details of the vehicle or thruster tested.

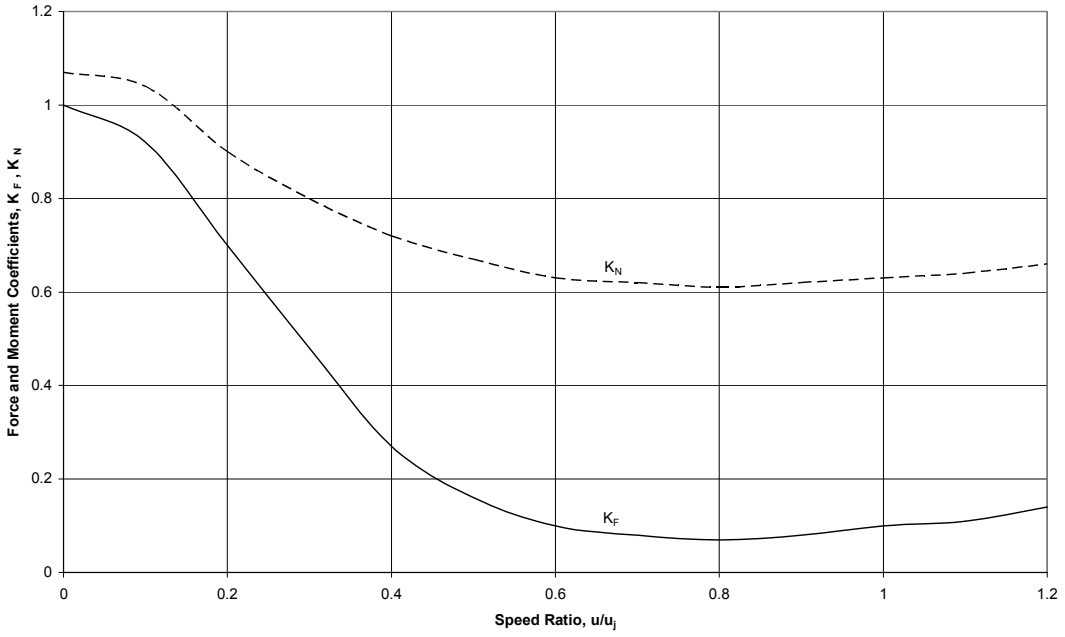

Figure 4.20 – Tunnel Thruster Performance on a Submersible [93]
(Solid line shows force coefficient K_F, dashed line shows moment coefficient K_N)

These results show similar trends to the performance illustrated in Figure 4.18 except the decreases in magnitude of the force and moment are larger and the recovery in performance at higher speed ratios does not occur.

The results for a tunnel thruster on an AUV presented in [94] cover the range of yaw angles from -90º to +90º and the full speed range of the (torpedo-shaped) C-SCOUT AUV. The force results at zero yaw (drift) angle and low forward speeds are shown in Figure 4.21. (The high speed results were found to be unusable as the vehicle appeared to be misaligned.) The results over the range of yaw angles showed that the performance of the thruster was only sensitive to the yaw angle at very large angles and was far more sensitive to increases in the forward speed.

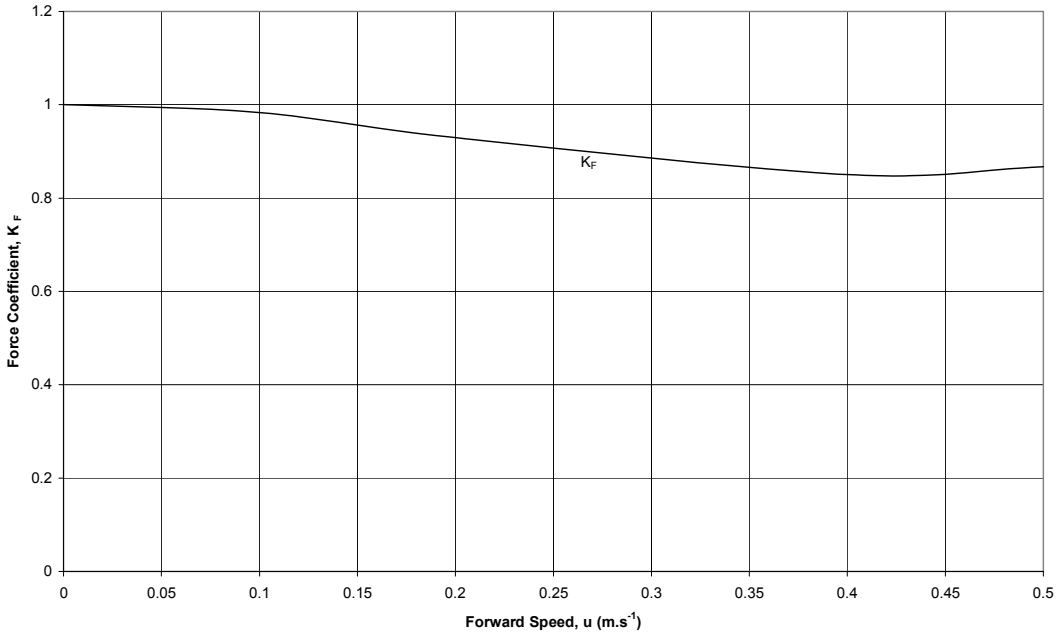

Figure 4.21 – Tunnel Thruster Performance on the C-Scout AUV [94]

These results show a decrease in performance however the magnitude of this decrease is considerably reduced compared to that observed in Figures 4.18 and 4.20. The reasons for this low reduction in performance are thought to be due to the design of the experiments. The thruster was mounted in the hull, but kept isolated from the hull form, and the forces measured were those generated by the thruster, rather than those experienced by the vehicle. Therefore these results do not include the jet interaction effects discussed earlier. The results do provide some confirmation of the conclusion previously noted, namely, the loss of performance is not due to a substantial change in the performance of the thruster itself.

4.5.2.4 Free Swimming Trials

Free swimming trials have been carried out using model and full scale surface vessels [61, 92, 100]. The trials measure the turning performance of the vessel when travelling at a given forward speed with the application of a particular (constant) thruster rotational speed (or power). This type of test is similar to the manoeuvring trials undertaken for surface vessels using rudders. The results are presented in terms of the rate of change of yaw angle and the time taken to turn through given yaw angles. The results show a good correlation with the captive testing, that is, the performance degrades as speed ratio increases before showing a recovery at higher speed ratios. The results of [61] show the highly variable performance to be a function of the particular vessel investigated.

4.5.2.5 Resulting Developments

Over the years of experimental testing with tunnel thrusters there have been surprisingly few major developments in the design of these devices. In fact, the only major development is the Anti-Suction Tunnel (AST) [92]. A small tunnel is placed just downstream of the thruster tunnel and is designed to facilitate a flow from one side of the vehicle to the other and consequently reduce the impact of the low pressure region. An AST is found to have a significant influence on the performance of the thruster and the manufacturers claim an improvement in performance of up to 50% at speeds up to 8 knots [101].

4.5.2.6 Alternative Analysis Approaches

The preceding review of the literature on tunnel thruster design and performance is based solely on the results of experimental investigations. This is due to the unique performance of each different configuration as a function of the particular flow conditions and the lack of a standard series type approach to published investigations. Another approach that is commonly employed to analyse similar problems is CFD. However, there are significant difficulties in undertaking such an analysis. These difficulties lie in trying to combine the flow over the vehicle with the jet flow from the thruster. Recent CFD results using Direct Numerical Simulation (DNS) on round (non-swirling) jets in a crossflow have shown the difficulties in achieving accurate quantitative results [102]. Furthermore, the difficulties in obtaining velocity measurements in a highly turbulent flow leads to a lack of available data for validation of the predicted flow features. In [102] the authors state that modelling these flows using a RANSe approach is a 'formidable' task due to the steep gradients involved.

Recent CFD analyses of the performance of tunnel thrusters have focussed more on the performance of the tunnel thruster itself [103, 104] and thus ignore the hydrodynamic effects discussed above. These analyses provide information on the performance of the device as a function of different thruster design parameters. The results can provide useful information on the velocity distribution downstream of the thruster. There has been one recent published attempt to assess the performance of a stern tunnel thruster on a surface vessel and its interaction with a twin screw propulsion system [105]. However, the inability of the simulation to accurately model the interaction between the thruster jet and the ambient flow (even at low speed ratio) means that the results do not match the experimental data.

As a result of the difficulties in using a CFD simulation to investigate the performance of a tunnel thruster, experimental approaches remain the favoured choice for analysing this type of device.

4.5.3 Experimental Testing

The preceding discussion has highlighted the unique performance of each different tunnel thruster configuration and noted that experimental testing is the favoured option for performance analysis. Therefore an experimental programme was designed and undertaken to characterise the performance of forward and aft mounted tunnel thrusters on a survey-style AUV form.

The area of interest in this research relates to the use of tunnel thrusters to extend the capabilities of survey-style AUVs by adding low speed control. Therefore the focus of these experiments is the performance of the thruster at low and transitional range forward speeds including a range of small pitch (or by symmetry, yaw) angles. The particular ranges chosen are designed to cover the transitional region between survey operation and low speed manoeuvring to facilitate investigation of the feasibility of using tunnel thrusters, and the resultant vehicle performance, during this phase.

Thus the aims of the experimental testing are:

1. Characterise the drag of a survey-style AUV body with and without thruster tunnels throughout the entire speed range.
2. Characterise the performance of forward and aft tunnel thrusters on a stationary vehicle.
3. Characterise the performance of forward and aft tunnel thrusters on a vehicle moving with a forward speed.
4. Characterise the performance of forward and aft mounted tunnel thrusters working concurrently on an AUV.
5. Characterise the performance of forward and aft tunnel thrusters on a moving vehicle working at small yaw angles.

4.5.3.1 Details of the Experimental Facility

The experiments were undertaken at the Southampton Solent University Towing Tank. The tank particulars are shown in Table 4.2. The data acquisition set up has automatic triggers to

record data over the constant speed section of the tank. The length of time taken to cover this distance is recorded and converted to give the constant carriage speed.

Table 4.2 – Southampton Solent University Towing Tank Particulars

Length	60.0m
Width	3.7m
Depth	1.85m
Maximum Carriage Speed	4.00m.s^{-1}
Length of Constant Speed Section	15.24m

4.5.3.2 Model

The model used is a 0.357-scale model of the Autosub AUV originally constructed for experimental testing aiming to characterise the drag of the vehicle in different operational configurations [106]. The model comprises three parts – a nosecone, a midbody and a tail section. The nosecone and tail section are floodable. The tail section has four movable flapped control surfaces and a dummy propeller hub (without blades). The construction used gives a smooth finish (without discontinuities between sections) to the model. However, the previous experimental testing has caused some small blemishes to the surface finish. The details of the model are given in Table 4.3.

Table 4.3 – Autosub Model Details

Length	2.5m
Diameter (max)	0.33m
Volume	0.184m^3
Linear Scale Factor	0.357

The model is mounted onto a specially designed dynamometer that is attached to the towing carriage. The model is mounted using two cylindrical posts attached to either end of the midbody section. The posts have a range of depth settings. For these tests the model was mounted with the centre of the vehicle at 0.72m depth.

The original model was modified to accommodate two thruster tunnels in the horizontal plane – one in the nosecone and one in the tail. The forward thruster tunnel is placed as far forward as possible to maximise the turning moment generated whilst minimising the drag penalty by restricting the tunnel to the cylindrical part of the nosecone as shown in Figure 4.22. The aft tunnel thruster is located so that the two thrusters are symmetrical about the

midbody section. The selection of the aft tunnel location is more flexible as long as the stern propulsion system and control surfaces are avoided. The separation of the forward and aft tunnel thruster centrelines is approximately 18.7*d*, where *d* is the thruster diameter. The relevant locations and dimensions for the model are illustrated in Figure 4.23. The tunnels are straight with a diameter equal to that of the propeller. The tunnels are faired into the hull form using a 0.1*d* radius, selected as a compromise between thruster performance and drag minimisation. The cables providing power to the thrusters are connected to the carriage via the mounting posts through holes in the midbody section as close to the posts as possible. The cables are cable-tied to the rear of the mounting posts to reduce their effect on the flow conditions, see Figure 4.24.

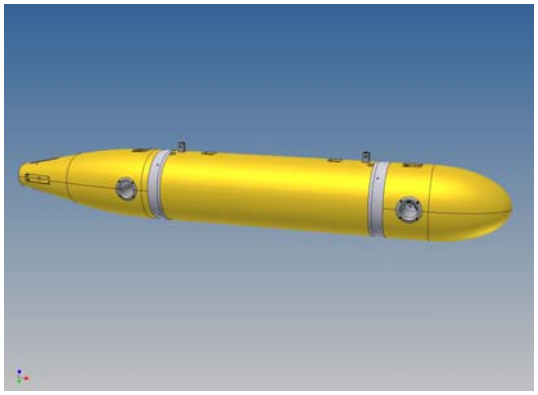

Figure 4.22 – CAD Representation of the Autosub Model

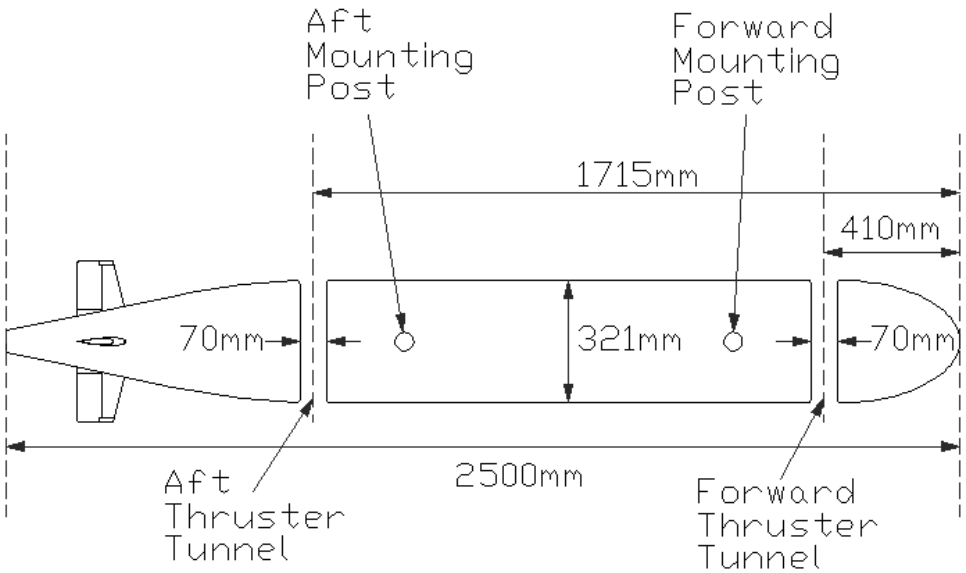

Figure 4.23 – Diagram of the Autosub Model showing Tunnel Locations and Dimensions

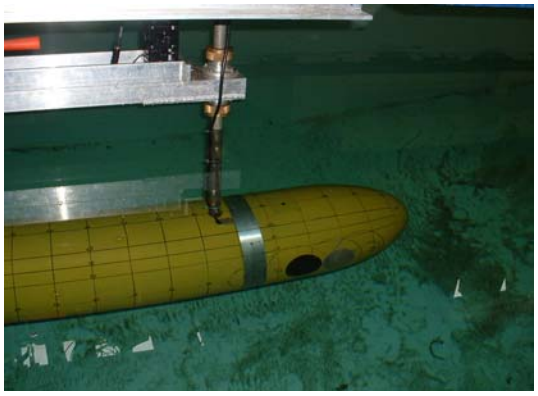

Figure 4.24 – Photograph of the Autosub Model Nosecone in the Southampton Solent University Towing Tank

To facilitate testing of the differences between the drag of the vehicle with and without thruster tunnels, a set of plugs were machined which can be used to block the thruster tunnels. These plugs have the same shape as the original unmodified hull form.

4.5.3.3 Thruster

The thruster used for the tests is a 70mm diameter four-bladed rim-driven DC brushless thruster manufactured by TSL Technology Ltd [107]. The thruster was selected as it is an appropriate size for the model, has a low hub-to-diameter ratio and offers symmetrical performance. The thruster is shown in Figure 4.25. The thruster is controlled using a Castle Creations Barracuda 80 electronic speed controller connected to a laptop using a Parallax USB Servo Controller Board. The controller was set to a constant setting and the speed of the thruster was controlled by varying the voltage (with unlimited current). This set up ensured a good quality output signal that allowed the frequency of the signal to be counted using a frequency counter to provide a measure of the rotational speed of the thruster. The voltage and current drawn were recorded from the power supply display.

Figure 4.25 – Photograph of a TSL Rim-Driven Thruster

4.5.3.4 Dynamometry

The forces on the model are measured using four force blocks – two measure the longitudinal force and two measure the transverse force. The force blocks are mounted in pairs – one longitudinal and one transverse – at each end of the dynamometer and above the mechanism used to set the yaw angle. This means that the forces measured are always in the same (tank-based) axes regardless of the yaw angle used. The mounting arrangement means the force blocks need to be individually calibrated before installation. A multi-point calibration procedure using loads up to 50N was used with all four force blocks providing a linear response to the increasing (and decreasing) load. The data from the force blocks was recorded at a rate of 60Hz. Once mounted in place the response of the combined force blocks was checked to ensure the calibration was not affected by the installation. Figure 4.26 shows the forces recorded (D_A, D_F, F_A, F_F) and how the data is reduced into a drag, D, side force, F_V, and yaw moment, N. The centre of action of the effective force is denoted as CoA.

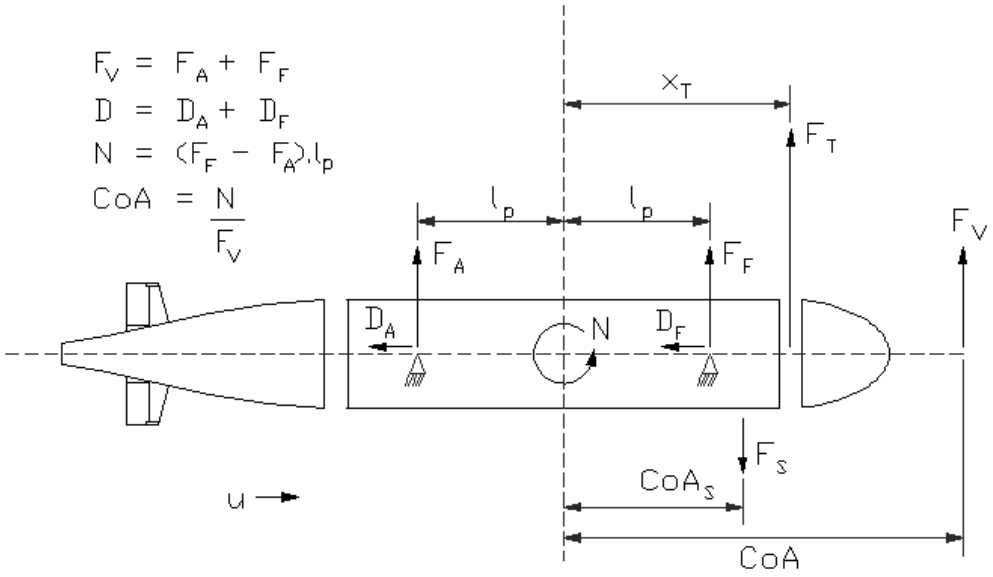

Figure 4.26 – Diagram illustrating the Processing of Experimental Data into Forces and Moments

4.5.3.5 Testing Procedures

The experiments were undertaken following appropriate International Towing Tank Conference (ITTC) Recommended Procedures [108]. The temperature of the water in the tank was recorded to allow determination of the correct density and viscosity for use in data

processing. The water in the tank was allowed to settle for a sufficient length of time to ensure the conditions were the same for all experiments. The measuring equipment was re-zeroed before each experiment. The thruster was started at the same time as the carriage for each run.

Test runs were undertaken to assess the acceleration of the carriage and the influence of this on the measured data. This allowed confirmation that no effects of the acceleration periods are found during the constant speed data acquisition section of the run. The dynamic performance (response to input signal) of the thruster was also tested to ensure that the thruster was operating at constant speed for the duration of the data acquisition section. These tests confirmed that the thruster achieves constant speed operation during the acceleration phase of the carriage and that the thruster control set-up employed was able to maintain constant thruster rotational speed.

4.5.3.6 Test Matrix

The mounting pole drag (including dummy thruster cables) and the vehicle drag were measured over the full speed range of the carriage, from 0.43m.s^{-1} up to 4.00m.s^{-1}. The minimum speed was set to be the lowest speed at which the carriage was able to maintain a steady speed. The tests with the tunnel thrusters operating were undertaken at the four different forward speeds of 0.43m.s^{-1}, 0.64m.s^{-1}, 0.83m.s^{-1} and 1.03m.s^{-1}. During these tests the thrusters were operated at voltages between 10V and 24V. More data points were recorded for the forward thruster as this thruster was chosen for the initial exploratory investigations into the performance characteristics. The yaw angles used were limited by the dynamometer frame and the size of the tank. Tests were undertaken at 5˚, 10˚, 15˚ and 20˚. Additional tests were run for the forward thruster at 2˚, 7˚ and 9˚ and a symmetry check was performed at -5˚. For all yaw angle tests the thrusters were operated in both directions to simulate both ‘positive’ and ‘negative’ yaw angle operation. Repeat runs were randomly selected to confirm the validity of the presented results.

4.5.4 Presentation of Results

The processed results from the experiments outlined are now presented. For clarity versions of Figures 4.27 to 4.46 are presented in Appendix A6 without error bars.

4.5.4.1 Drag Testing

The drag of the vehicle equipped with plugs and with thruster tunnels at zero yaw was tested over the entire speed range achievable by the carriage. The measured forces have been corrected for the drag of the mounting poles, which accounts for approximately two-thirds of the total measured drag force. These results are presented in Figure 4.27, along with the data using the same model from the original testing programme [106] and a drag estimate based upon a volumetric drag coefficient of 0.045 [38].

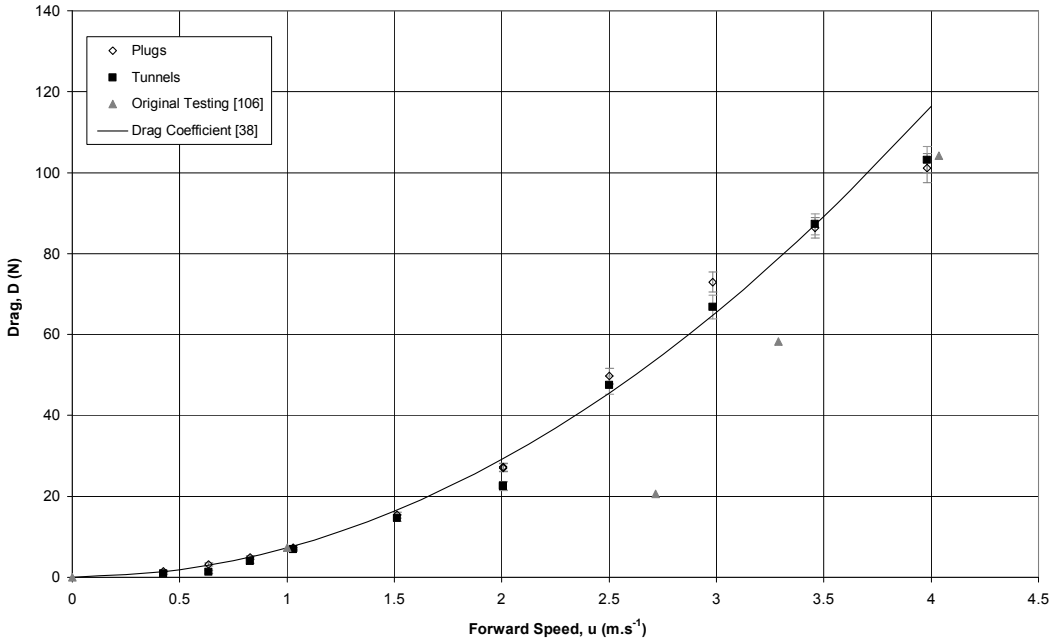

Figure 4.27 – Variation of Vehicle Drag with Forward Speed

The drag of the vehicle with plugs has the same form as the drag of the vehicle with tunnels. Both sets of results follow the drag coefficient curve well but do not match the data from the original test results [106] at the mid-range speeds. [106] only recorded the data points shown and thus no confirmation of the accuracy of the mid-range speed drag values is available, thus, given the comparison with the new results, it is assumed that the data from [106] is unreliable.

The drag of the vehicle is marginally larger for the majority of the speed range with the plugs in place of the tunnels. In fact, only the data points for the two highest speeds tested show a small increase in drag caused by the presence of the tunnels. However, when the experimental uncertainties are considered the differences between the drag of the vehicle with tunnels and without tunnels are less significant. The results are in agreement with the data recorded in [62] and confirm that there is no, or only a very small, increase in drag due

to the presence of the thruster tunnels and hence no significant reduction in survey efficiency. It should be recalled that the thruster tunnels were faired into the hull form with a radius of $0.1d$, selected as a compromise between minimising drag and maximising thruster performance.

The drag results have been non-dimensionalised using a volumetric drag coefficient given by:

$$C_D = \frac{D}{0.5\rho\nabla^{2/3}u^2}. \tag{4.20}$$

The speed of vehicle has been non-dimensionalised using the Reynolds Number given by:

$$Re = \frac{ul}{\upsilon}. \tag{4.21}$$

Using the non-dimensional representation of the data gives Figure 4.28. The data for the vehicle with plugs is compared with the data for the vehicle with tunnels.

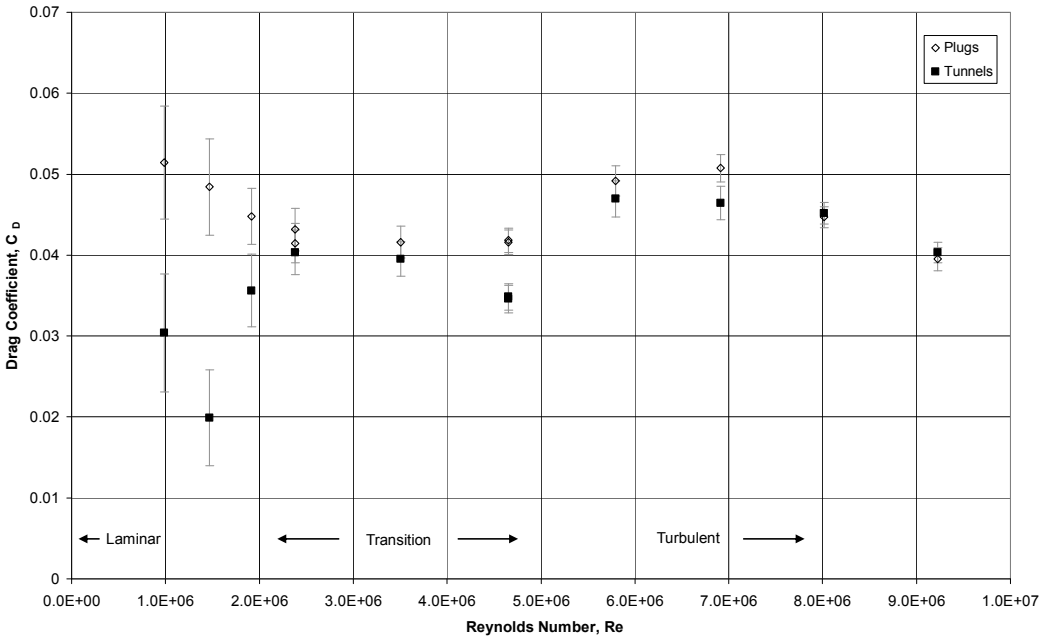

Figure 4.28 – Variation of Vehicle Drag Coefficient with Reynolds Number

The drag coefficient data for the vehicle with plugs shows a more consistent trend in comparison with the data for the vehicle with tunnels. There are some considerable variations in the drag coefficient as a function of Reynolds Number with these being attributed to the considerable influence of the transition into fully turbulent flow in this Reynolds Number range.

4.5.4.2 Thruster Tests at Zero Speed

The performance of the thrusters at zero speed was measured throughout the operating range used. The results are provided in Figure 4.29 together with the manufacturer published performance [107]. Figure 4.29 gives the force generated by the thruster and the corresponding rotational speed at a given power. The measured results indicate the performance of both thrusters to be similar to that published by the manufacturer. This confirms that the mounting of the thruster into a straight tunnel in the vehicle does not substantially affect the steady state performance of the thruster. The thrust coefficients calculated from the data adopt a consistent value indicating the expected linear dependency on the square of the thruster rotational speed.

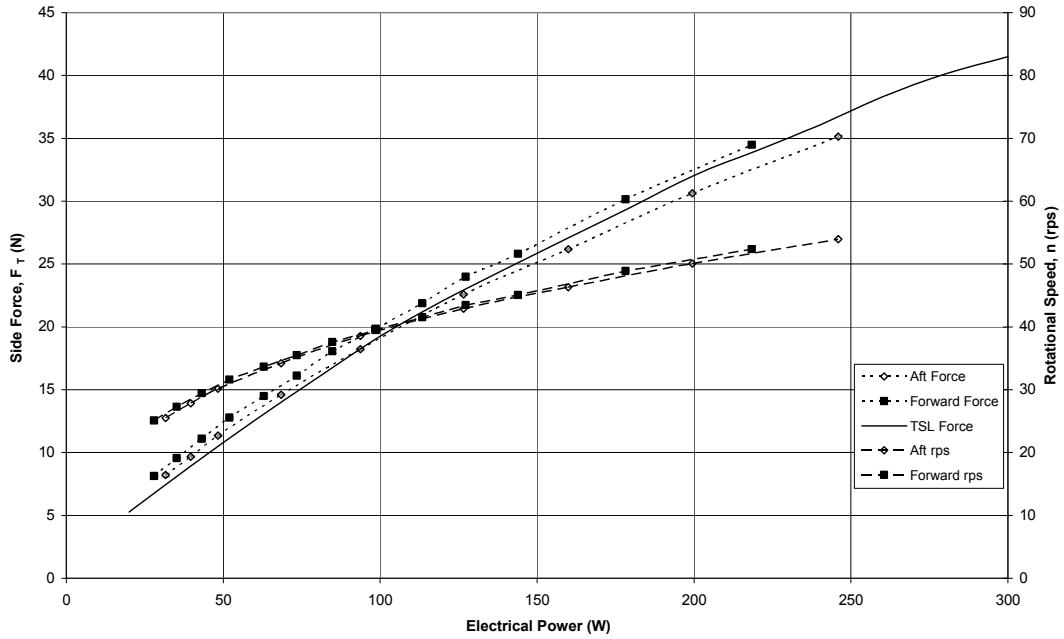

Figure 4.29 – Tunnel Thruster Performance at Zero Speed

4.5.4.3 Tunnel Thruster Performance on a Vehicle Moving with a Forward Speed

Tests were carried out at a range of vehicle speed with varying thruster loads to determine whether the expected decrease in force occurs and whether the decrease is a function of the forward speed or a function of the forward speed and jet speed. The results confirmed that the decrease in force is a function of both the forward speed and jet speed.

Throughout these tests the recorded values of rotational speed and power (current) drawn were monitored. These values showed no, or only minimal, change as a function of the operational conditions. That is, no increase in power was required to maintain the rotational

speed of the thruster. This confirms that the operational conditions do not impact on the performance of the thruster unit itself.

The side force measured on the vehicle with a forward speed has been non-dimensionalised by the zero speed side force given by:

$$K_F = \frac{F(u,n)}{F(0,n)} \hat{=} \frac{F(u,n)}{\rho A u_j^2}. \tag{4.22}$$

The yaw moment has been non-dimensionalised in a similar fashion, namely:

$$K_N = \frac{N(u,n)}{N(0,n)} \hat{=} \frac{N(u,n)}{\rho A u_j^2 x_T}. \tag{4.23}$$

The speed of the vehicle is non-dimensionalised using the speed ratio of forward speed to jet speed defined as:

$$\frac{u}{u_j} = \frac{u}{\sqrt{\frac{F(0,n)}{\rho A}}}. \tag{4.24}$$

Non-dimensionalising the data in this way leads to Figure 4.30 which illustrates a clear reduction of side force and yaw moment with increasing speed ratio. The aft thruster results (solid symbols) and the forward thruster results (hollow symbols) are compared with the data (dotted and solid lines) from [93].

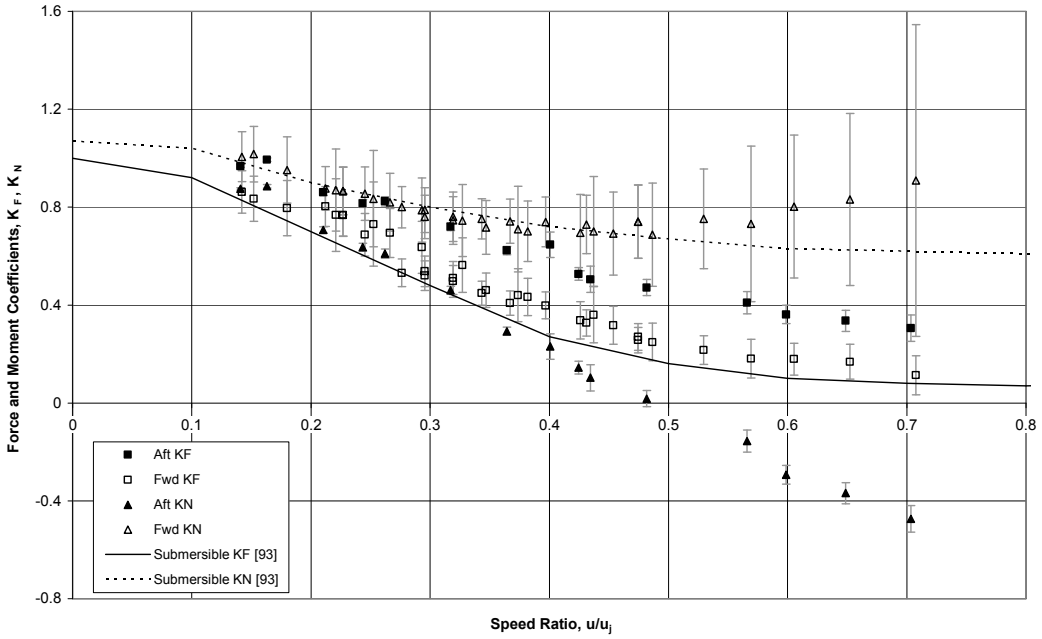

Figure 4.30 – Tunnel Thruster Performance on a Moving Vehicle

The results for both thrusters show decreases in side force and yaw moment with increasing speed ratio. The results for the forward thruster show similar trends to the data from [93].

The decrease in side force for the aft thruster is smaller than for the forward thruster due to a lesser influence of the suction force generated by the interaction of the thruster exit jet with the ambient flow. These results show that a tunnel thruster can be used to generate control forces on an underwater vehicle at low speed ratios.

The decrease in yaw moment for the aft thruster is far greater than that for the forward thruster. This is due to the differing influence of the suction force. For the forward thruster the suction force acts aft of the thruster exit, closer to the centre of the vehicle than the thruster and thus has a smaller moment arm. For the aft thruster the suction force acts aft of the thruster exit, further away from the centre of the vehicle than the thruster, giving the suction force a larger moment arm. Therefore the suction force has a greater influence leading to a far greater decrease in yaw moment and hence no recovery at the higher speed ratios. In fact, at high speed ratios ($u/u_j > 0.5$) the aft thruster yaw moment changes direction (sign) as the suction moment begins to dominate the moment generated by the thruster force.

4.5.4.4 Additional Drag caused by the Operation of a Tunnel Thruster

The additional drag on the vehicle caused by operating the thrusters is shown as a change in vehicle drag coefficient in Figure 4.31. The results plotted show the data from all the individual thruster tests as plotted in Figure 4.30.

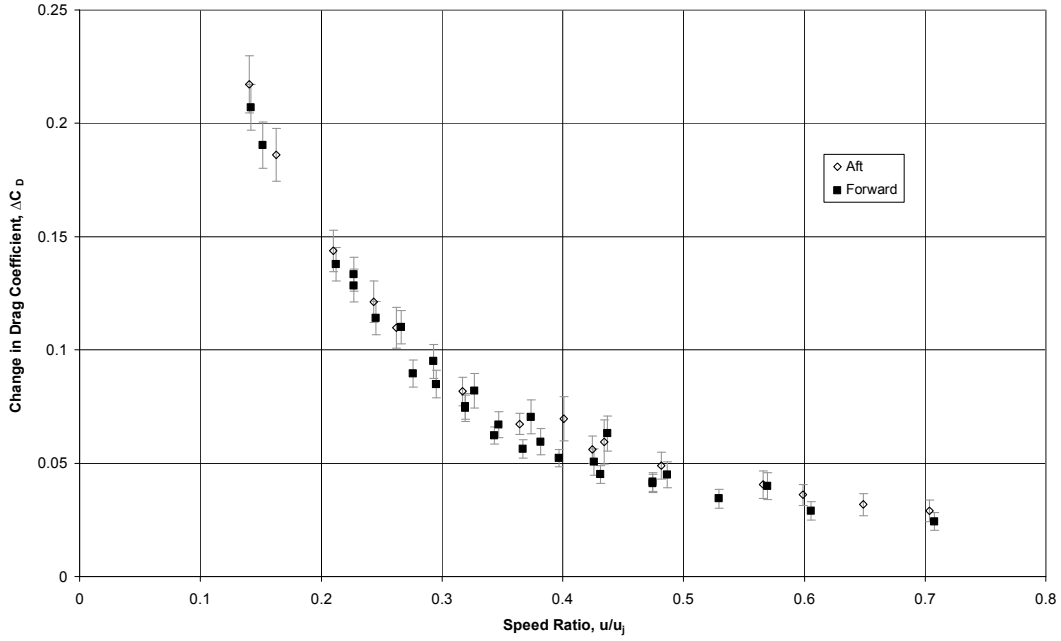

Figure 4.31 – Variation of Vehicle Drag Coefficient with Speed Ratio caused by Thruster Operation

This data indicates the increase in drag when constrained to a fixed heading and is not expected to translate to free swimming manoeuvring performance (when the vehicle heading would change as a result of the thruster force). This data serves to indicate the influence of the relative strengths of the jet and the ambient flow as a function of speed ratio.

Figure 4.31 shows the same increase in drag coefficient is caused by operating the aft thruster as caused by operating the forward thruster. The overall trend of the data is that the increase in drag coefficient is greatest at low speed ratios. This is thought to be due to the increased deflection of the jet at higher speed ratios. That is, at low speed ratios, where the jet is strong relative to the ambient flow, the jet can be considered as a (solid) cylinder forming an obstruction to the flow, whereas at high speed ratios the jet is swept away and thus has a lower drag penalty.

4.5.4.5 Centre of Action of the Yaw Moment

The centre of action of the yaw moment generated by a thruster is given by:

$$CoA = \frac{N(u,n)}{F(u,n)}. \tag{4.25}$$

These values are plotted on Figures 4.32 and 4.33 for the forward and aft thrusters respectively.

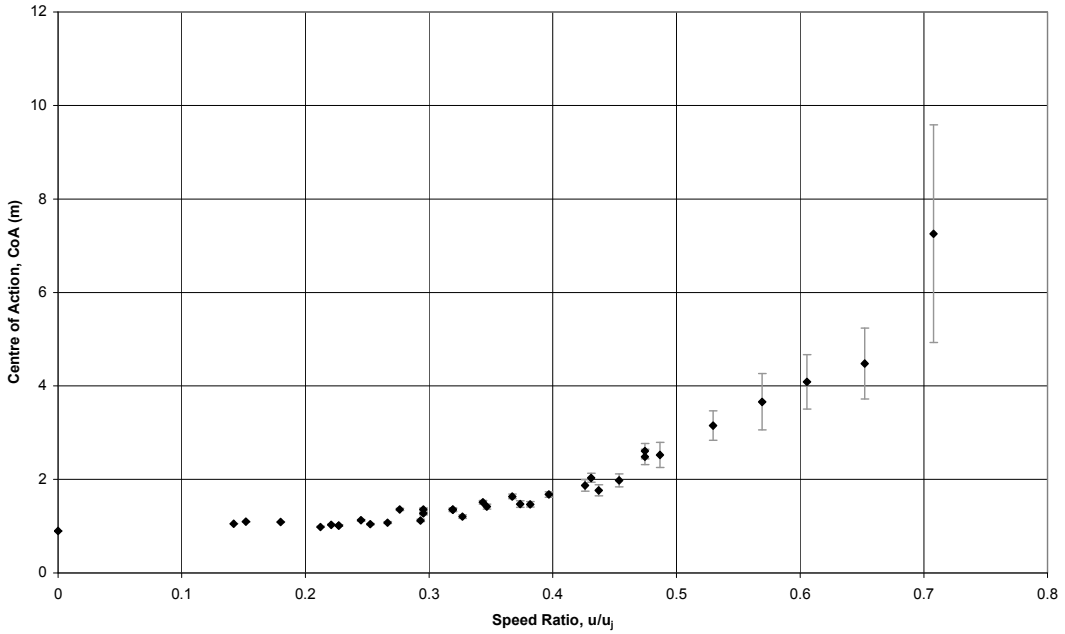

Figure 4.32 – Variation of the Centre of Action of the Yaw Moment with Speed Ratio for the Forward Thruster

The data points at a speed ratio of zero indicate the location of the thruster relative to the pivot point of the vehicle as determined from the static testing results. Figures 4.32 and 4.33 demonstrate that the centre of action of the yaw moment when moving with a forward speed is always forward of the location of the thruster. This conclusion is the same for both thrusters and indicates that there are a number of forces acting on the vehicle. Figure 4.32 shows that the centre of action of the yaw moment for the forward thruster even extends beyond the physical length of the vehicle. The values at high speed ratios ($u/u_j > 0.5$) have larger experimental uncertainties associated with them due to the small magnitudes of the forces measured. The magnitude of the movement of the centre of action for the aft thruster is much lower than that of the forward thruster. As an example the movement of the centre of action from a speed ratio of 0 up to 0.5 is approximately 1m for the aft thruster compared to approximately 1.9m for the forward thruster.

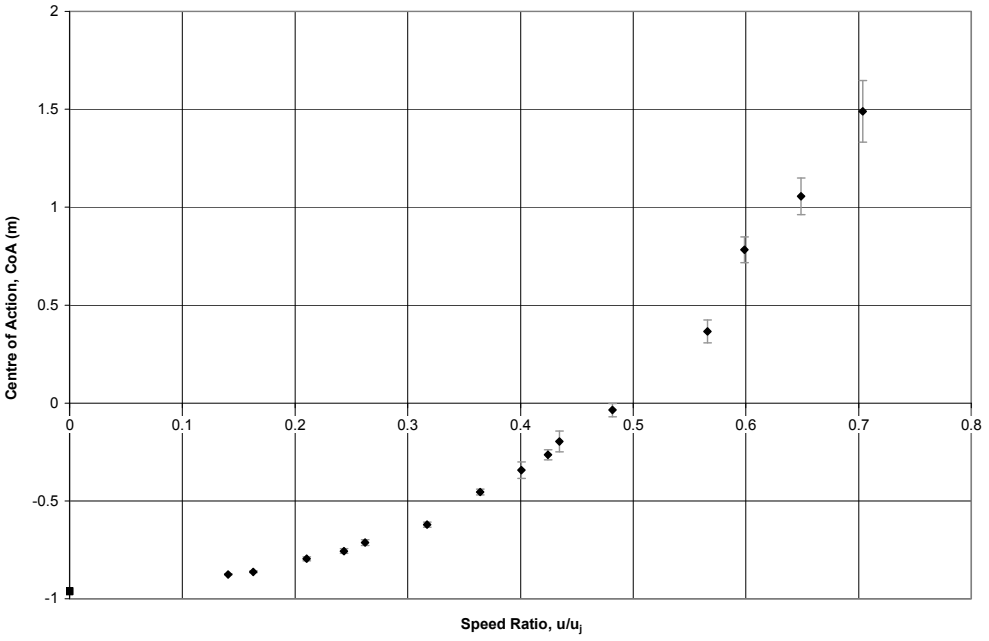

Figure 4.33 – Variation of the Centre of Action of the Yaw Moment with Speed Ratio for the Aft Thruster

4.5.4.6 Centre of Action of the Suction Force

A simplified representation of the forces acting in this operational condition uses two forces. These two forces are the thruster force and a suction force. The suction force is defined as the difference between the expected force from the thruster and the actual force on the vehicle,

$$F_S(u,n) = F(0,n) - F(u,n), \tag{4.26}$$

with the corresponding suction moment defined as the difference between the expected moment and the actual moment,

$$N_S(u,n) = N(0,n) - N(u,n). \tag{4.27}$$

Hence the centre of action of this suction force is defined as

$$CoA_S = \frac{N_S(u,n)}{F_S(u,n)}. \tag{4.28}$$

The centre of action of the suction force for the forward thruster is shown in Figure 4.34 and the aft thruster is shown on Figure 4.35.

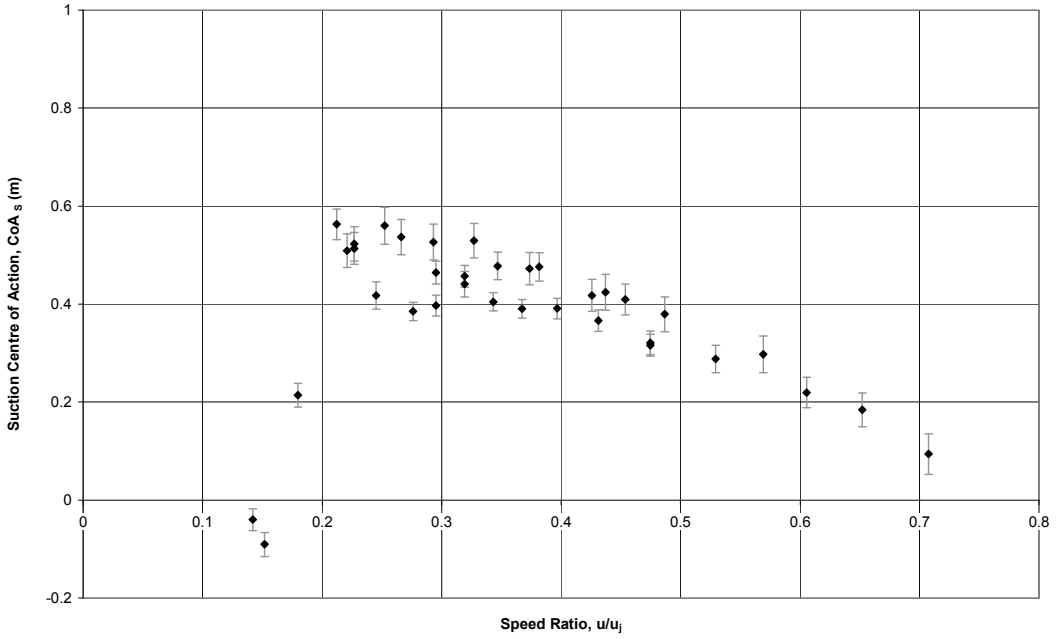

Figure 4.34 – Variation of the Centre of Action of the Suction Force with Speed Ratio for the Forward Thruster

The results at low speed ratios are not necessarily reliable due to the similar magnitudes of the values being compared in these calculations. The forward thruster results show some agreement with the conclusions of [96] that the centre of action of the suction force moves linearly aft along the vehicle with increasing speed ratio. This conclusion is used as an explanation for the recovery in the moment experienced, see Figure 4.18, as the centre of action of the suction force passes through the pivot point of the vessel. The centre of action of the suction force for the aft thruster is far more consistent than for the forward thruster and does not move linearly aft with speed ratio. The consistency of this location is thought to be due to the proximity of the thruster to the vehicle tail, giving the suction force a limited area on which to act.

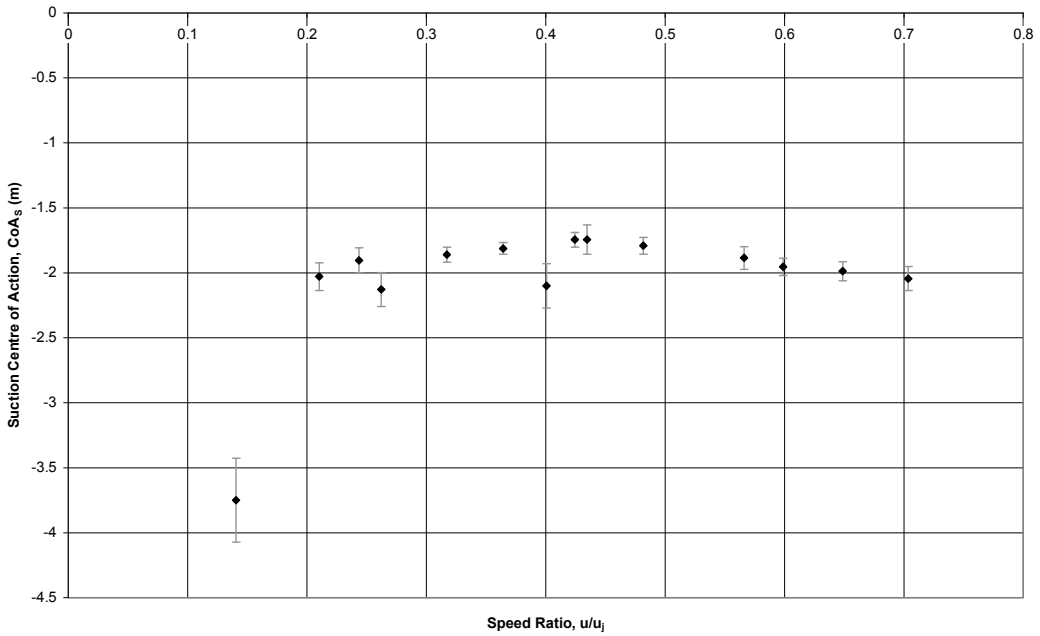

Figure 4.35 – Variation of the Centre of Action of the Suction Force with Speed Ratio for the Aft Thruster

4.5.4.7 Dual Thruster Testing

The thrusters were tested concurrently at zero speed, and then in two different forward speed scenarios, to assess whether the operation of one thruster has any effect on the performance of the other. The first of these forward speed scenarios aims to generate a side force with no yaw moment and the second aims to generate a yaw moment with no side force. That is, firstly, with the thrusters operating in the same direction, and, secondly, with the thrusters operating in opposite directions. In both scenarios the thrusters are generating approximately equal thrust forces.

The zero speed tests showed, as expected, that the performance of the two thrusters at zero speed is independent of each other. That is, the performance of the two thrusters operating concurrently is equal to the sum of the performance of each thruster operating alone. The results from the forward speed tests are shown in Figures 4.36 and 4.37 for the first and second case respectively. The results are compared with data calculated using the sum of the performance of each thruster operating alone.

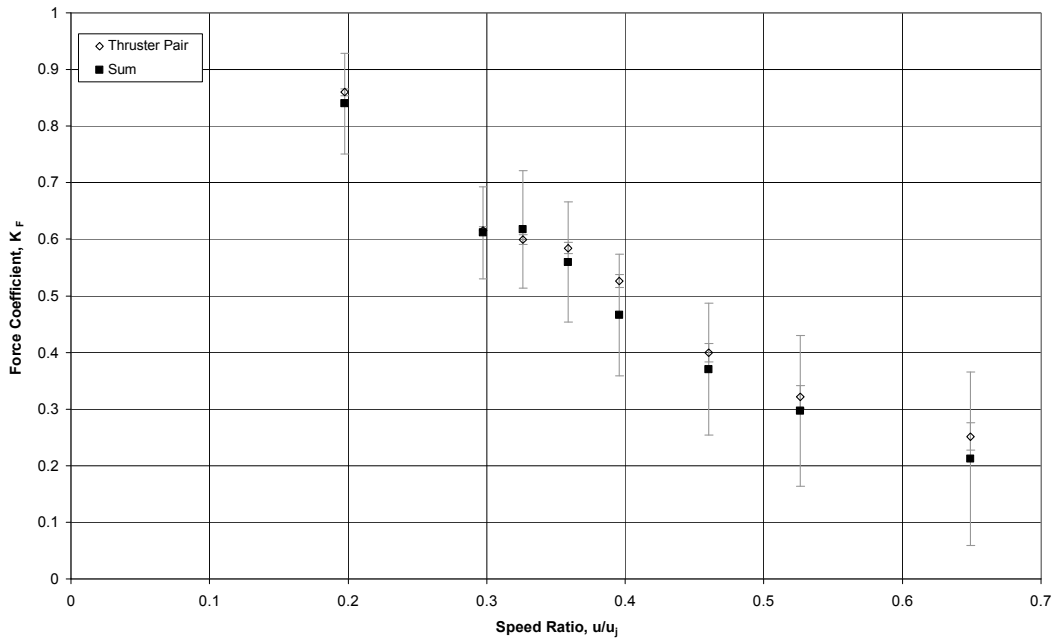

Figure 4.36 – Variation of Generated Side Force with Speed Ratio using a Thruster Pair

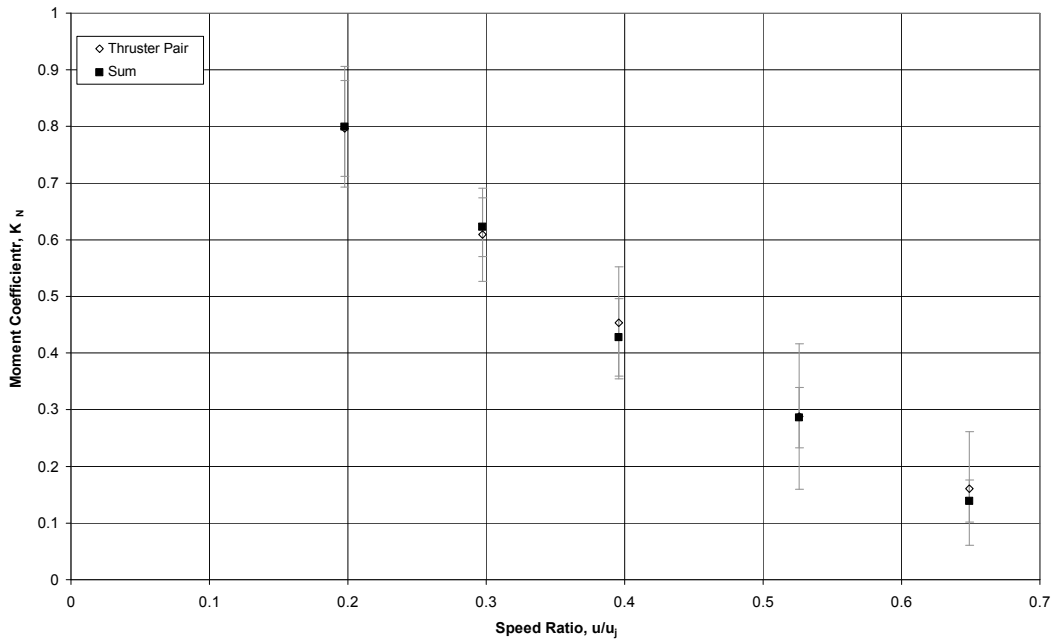

Figure 4.37 – Variation of Generated Yaw Moment with Speed Ratio using a Thruster Pair

Figures 4.36 and 4.37 show little change in the performance characteristics caused by the concurrent thruster operation in comparison with the sum of the individual results. This means that the thrusters can be considered independent of each other across the range of operating conditions, with their performance additive, thus simplifying control system

design. Furthermore, Figure 4.38 shows that the change in drag coefficient is also equal to the sum of the individual thruster drag penalties.

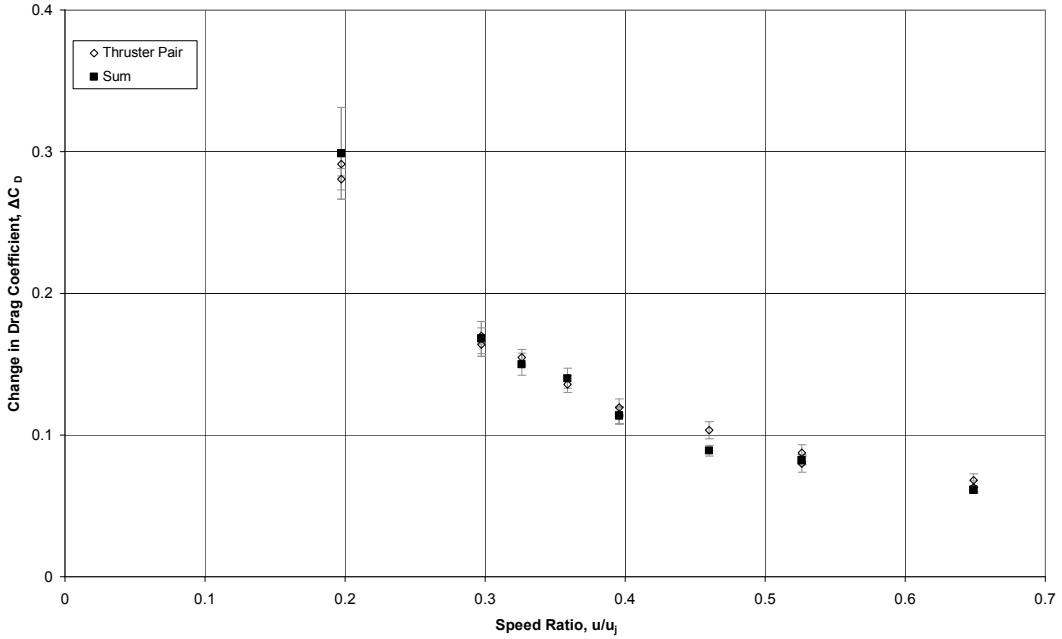

Figure 4.38 – Variation of Vehicle Drag Coefficient with Speed Ratio using a Thruster Pair

It should be noted that the separation of the thrusters is a fairly substantial 18.7*d*. Interaction effects have been experienced with bow thrusters on surface vessels when two thrusters are placed very close together [92], but it is unknown what minimum separation is required to avoid interaction effects. (Configurations including closely spaced thrusters are unlikely to be employed on an AUV).

4.5.4.8 Performance of a Tunnel Thruster on a Moving Vehicle at an Angle of Yaw

The performance of both the forward and aft thrusters was measured at yaw angles up to ±20º. This range exceeds the usual range of ascending (or diving) angles for an AUV (±10º) to attempt to determine performance trends and to gain insight into the performance of the thrusters as a manoeuvring device in the horizontal plane. The results have been analysed assuming that the thruster operation is intended to generate a force perpendicular to the direction of forward carriage motion. This simulates the condition of attempting to generate a force in the vertical plane whilst operating with a pitch angle. The results are shown in the usual force and moment coefficient form in Figures 4.39 to 4.46. A positive yaw angle implies that the jet is emitting into the oncoming flow and a negative yaw angle implies that the jet exit is shielded by the vehicle (and the oncoming flow gives a small inflow component to the thruster).

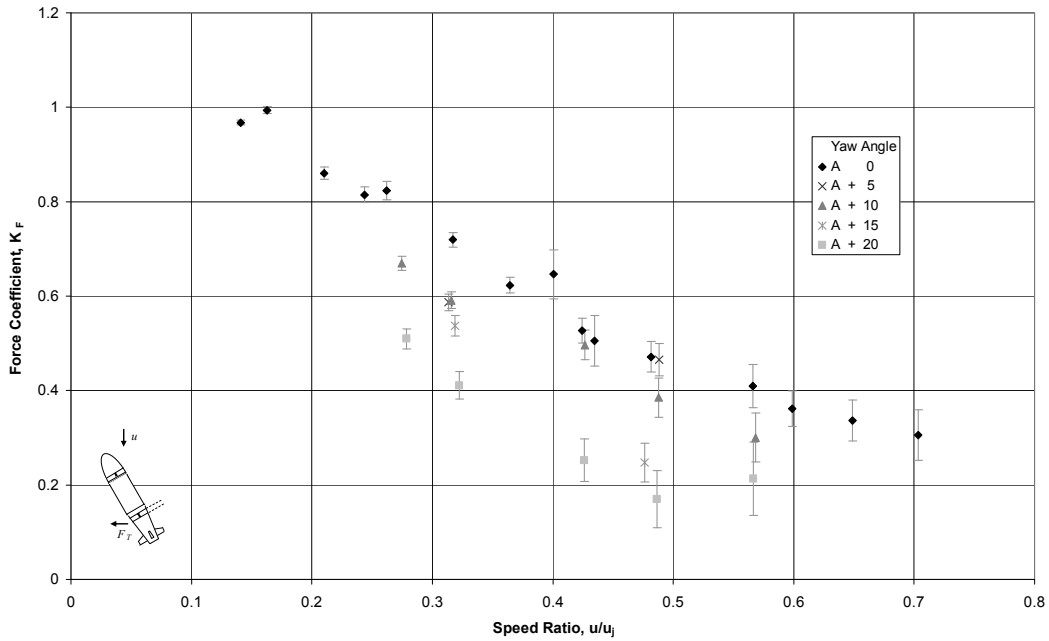

Figure 4.39 – Variation of Aft Thruster Side Force Performance with Speed Ratio at Positive Yaw Angles

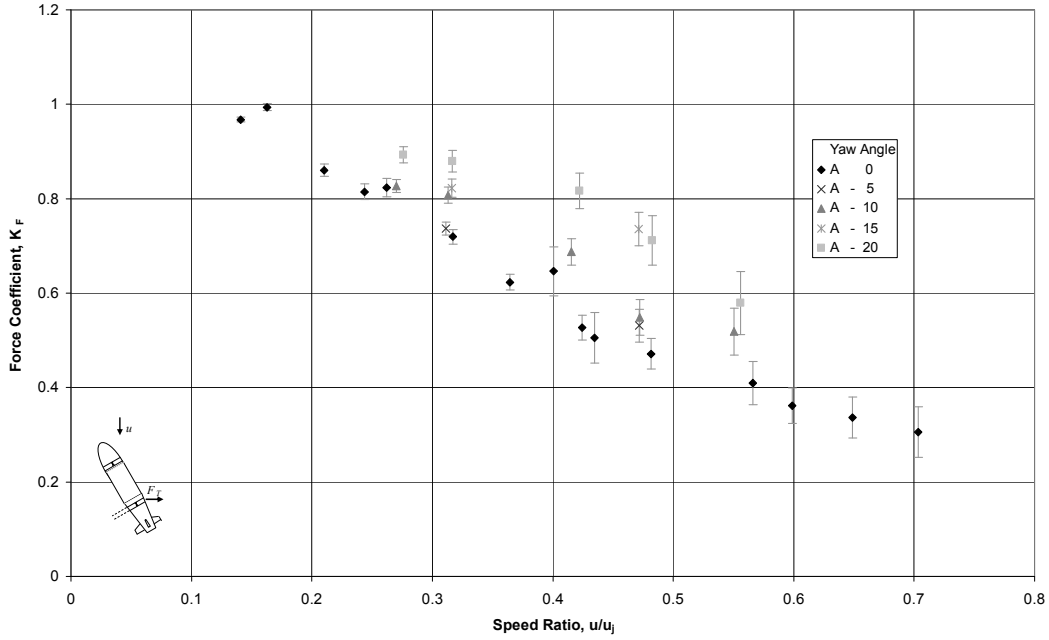

Figure 4.40 – Variation of Aft Thruster Side Force Performance with Speed Ratio at Negative Yaw Angles

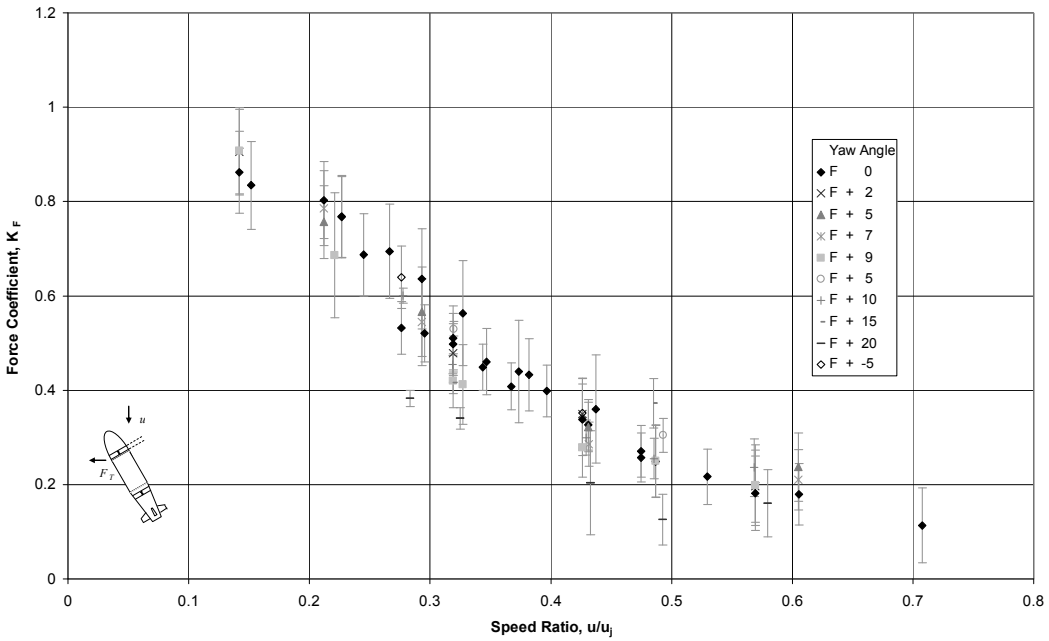

Figure 4.41 – Variation of Forward Thruster Side Force Performance with Speed Ratio at Positive Yaw Angles

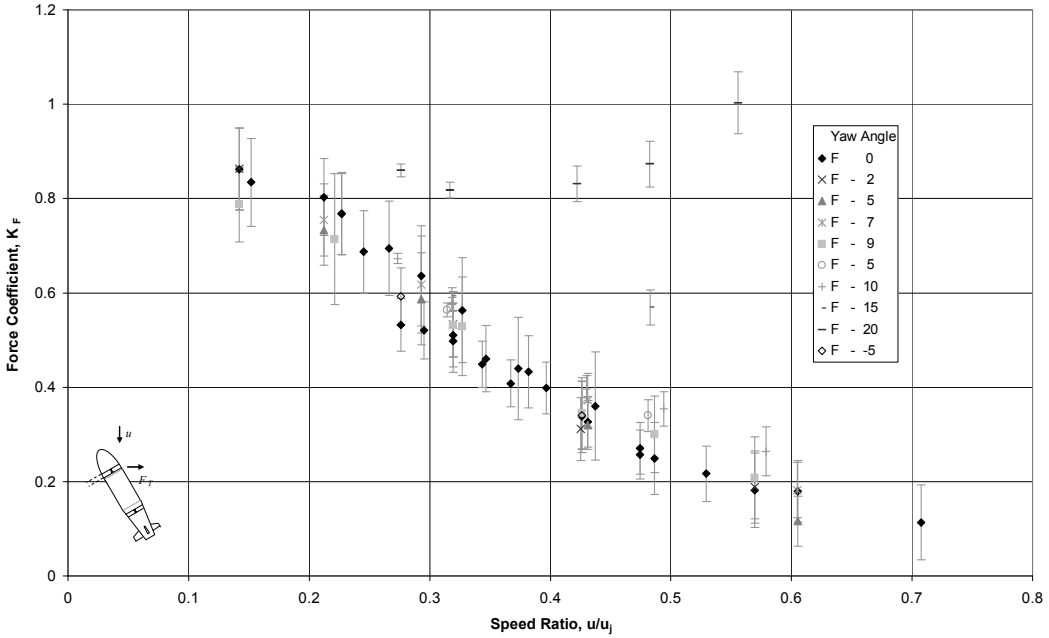

Figure 4.42 – Variation of Forward Thruster Side Force Performance with Speed Ratio at Negative Yaw Angles

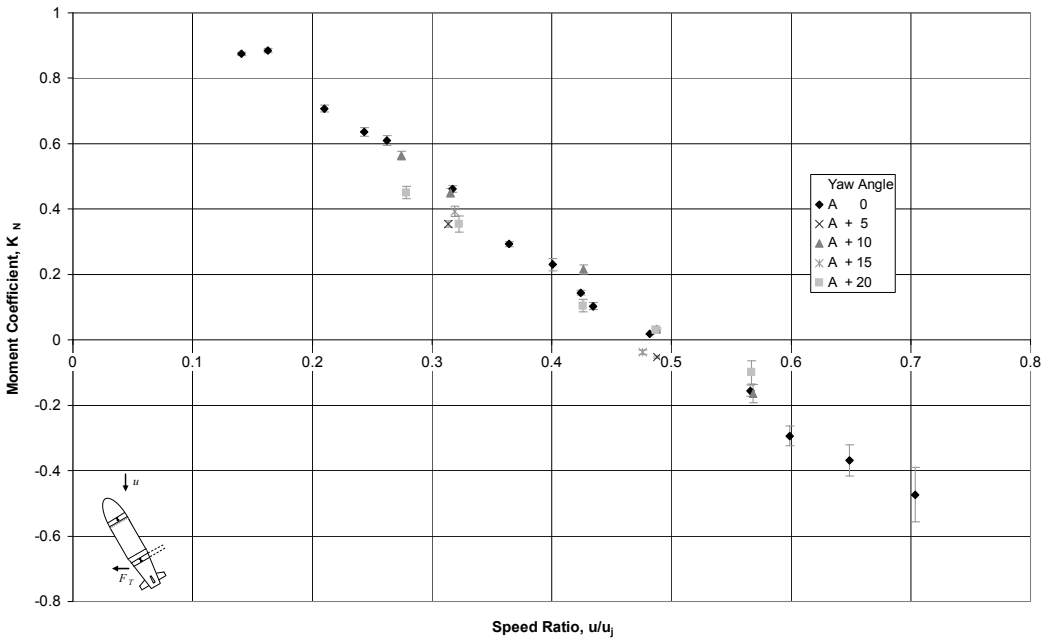

Figure 4.43 – Variation of Aft Thruster Moment Performance with Speed Ratio at Positive Yaw Angles

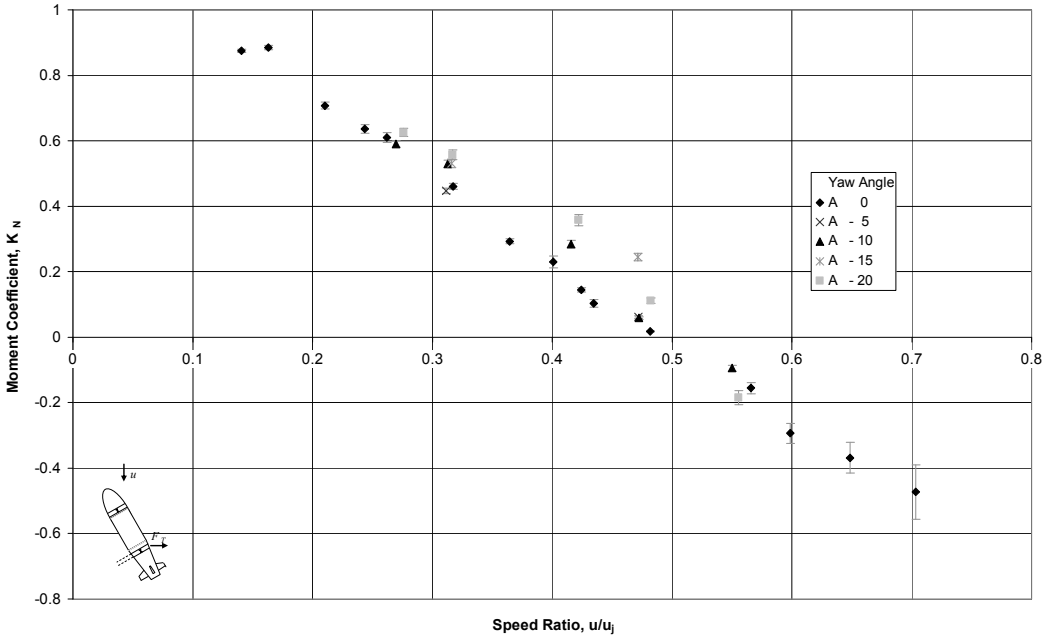

Figure 4.44 – Variation of Aft Thruster Moment Performance with Speed Ratio at Negative Yaw Angles

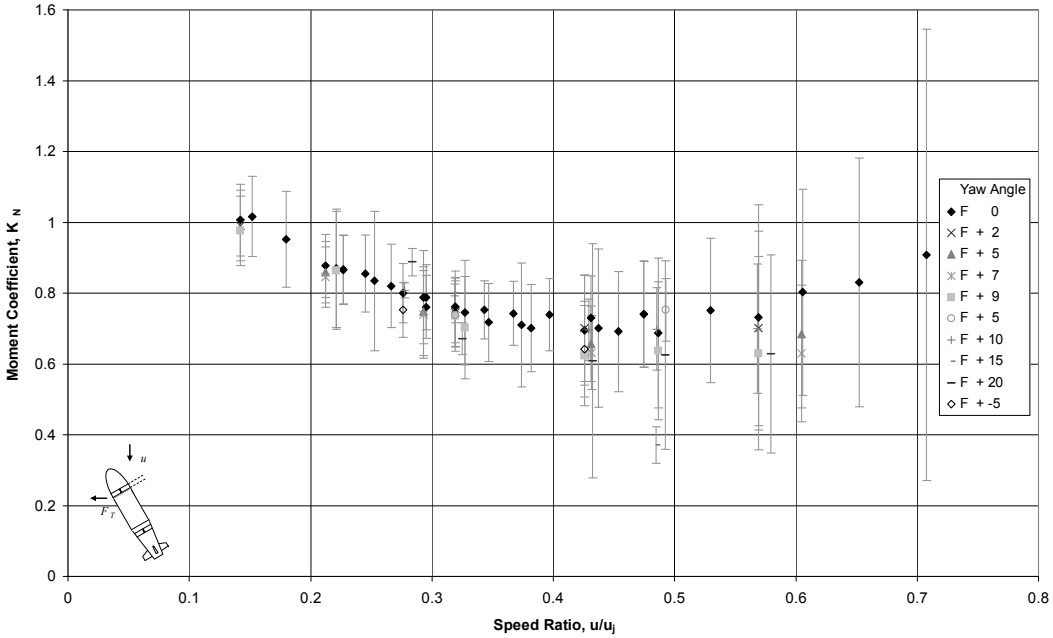

Figure 4.45 – Variation of Forward Thruster Moment Performance with Speed Ratio at Positive Yaw Angles

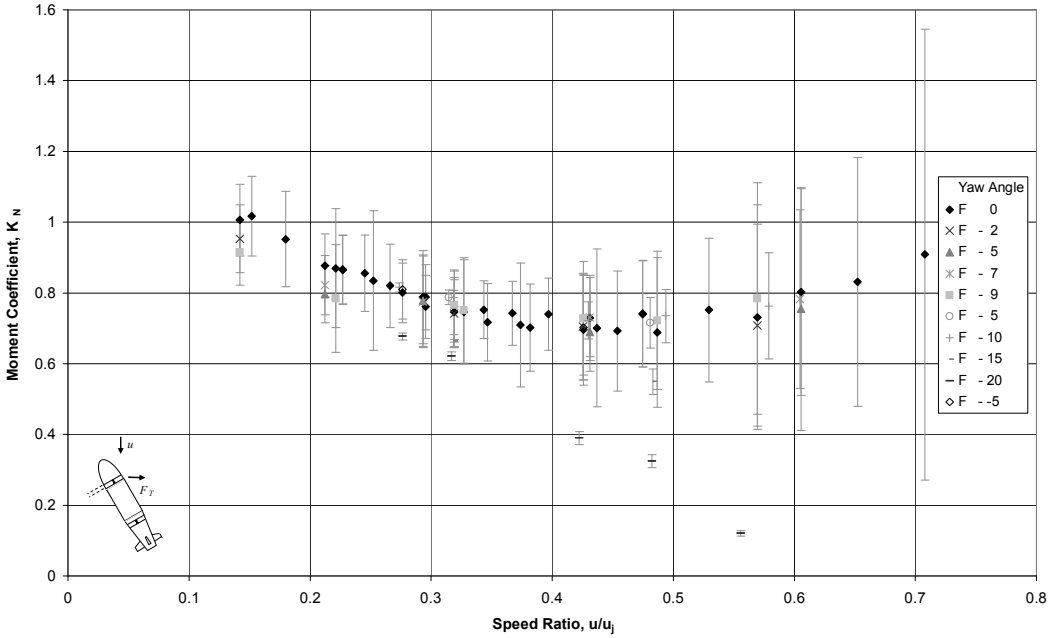

Figure 4.46 – Variation of Forward Thruster Moment Performance with Speed Ratio at Negative Yaw Angles

Figures 4.39 to 4.42 indicate that the side force performance is improved when the jet exit is shielded by the vehicle and the performance similarly decreases when the jet emits into the oncoming flow. These effects are more noticeable in the aft thruster results in comparison with the forward thruster results. When the thruster is operating with the jet shielded by the vehicle, the oncoming flow provides a small inflow component to the thruster. An inflow component should cause a reduction in the thrust generated, however, in these results the performance actually improves. This shows that the shielding of the jet has a larger influence on the performance than the influence of any small inflow component. The magnitude of any change of performance caused by the inflow effects was small as it is not shown in a change of thruster rotational speed or power (current) drawn.

Figures 4.43 and 4.44 illustrate that the moment performance for the aft thruster is not greatly affected by the yaw angle. The moment is practically unchanged for the jet emitting into the flow and slightly increased in the shielded condition. In general, Figures 4.45 and 4.46 show a small decrease in moment generated by the forward thruster for both conditions.

There is one set of conditions for which the results presented exhibit much greater variation than any other set of results. This condition relates to the performance of the forward thruster operating at -20º (with the jet exit shielded by the vehicle nose). Figure 4.42 shows much improved side force performance (including an occurrence of $K_F > 1$) and Figure 4.46 shows a corresponding large decrease in the moment experienced. Due to the separation of these results from the other values, the data samples were investigated to find out if there were any abnormalities in these particular data sets. None could be found as illustrated by the error bars.

After further investigation of all the data samples involved in the analysis procedure (the zero speed test, the zero thrust test and combined speed and thrust run) it was found that the zero thrust tests show the effects of stall on the control surfaces at both 15º and 20º. At 15º the aft side force reading shows a considerable decrease but by 20º this reading has recovered. The aft drag values also show an increase for these angles. These results correspond to the performance characteristics of the NACA0015 aerofoil section used for the rudder at the Reynolds Number (based on chord) of approximately 9.5×10^4, see Figure 4.47 [109].

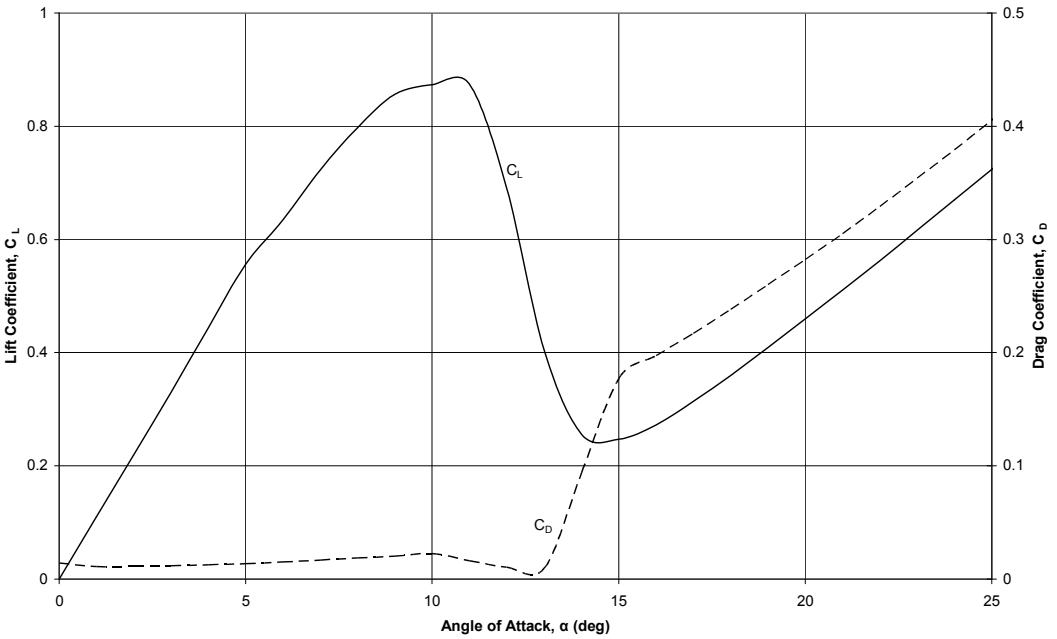

Figure 4.47 – Lift and Drag Characteristics of a NACA0015 Aerofoil Section at a Reynolds Number of $9.5x10^4$

Analysis of the combined speed and thrust runs shows that the majority of data samples include the effects of rudder stall, where expected. Those test results that do not follow the general trends correspond to the forward thruster at -20º (see Figure 4.42) and the forward thruster at +15º (see Figure 4.41). These samples do not show the expected rudder stall characteristics, and hence, the comparison of these results with the zero thrust runs is not valid. It is not expected that the operation of the thruster causes a significant variation in the performance of the rudder, being out of phase by 90º, however there were no other differences between the tests. The control surfaces were held fixed at zero deflection angle for all tests. All the test runs for a given angle were made consecutively to ensure the yaw angle was consistent and the experimental conditions were the same. Furthermore, all the yaw angle runs were made at a constant speed of $0.83m.s^{-1}$ giving a constant rudder Reynolds Number for all tests.

It is important to note that the expected range of operation of the vehicle does not include operating at -20º at high speeds (speed ratios). The most likely operation of the tunnel thruster at higher speeds and large yaw angles is undertaking the control of the hydrostatic balance during the transition between survey operation and low speed operation. This condition corresponds to a positive yaw angle in this sign convention.

As a result of this analysis it has been shown that the results can only be considered reliable if the conditions at, and performance of, the rudder can be assumed to be consistent across the zero thrust and combined speed and thrust runs. This is the case in the range ±10º, where stall is unlikely to occur. Therefore the conclusions from these tests are limited to this range. Hence, in conclusion, there is limited influence of yaw angle on the performance of the thrusters in the ±10º range of operation. The conclusion from those results at yaw angles greater than ±10º is that the performance variation is still limited, especially at low speed ratios. These conclusions are in agreement with the limited surface vessel data available (see Figure 4.19) and show a greater influence of the speed ratio in comparison with the influence of the yaw angle, which agrees with the conclusions from [94, 98].

4.5.5 Experimental Testing Conclusions

The following conclusions may be drawn from the experimental investigation into the performance of tunnel thrusters mounted into a torpedo shaped AUV:

1. The drag of a torpedo shaped AUV is not substantially affected by the addition of through-body thruster tunnels.
2. The performance of a rim-driven thruster unit at zero speed is unaffected by mounting the thruster in a through-body tunnel. The performance can be characterised using a standard thrust coefficient as the thrust varies linearly with the square of thruster rotational speed.
3. The performance of a thruster unit itself is not significantly affected by the operational conditions (forward speed and small yaw angle).
4. A decrease in effective force and moment when moving with a forward speed is observed. These decreases are a function of the speed ratio of forward speed to jet speed. Despite the observed decreases in performance, the tunnel thruster can be used to control an AUV at low speeds.
5. The performance of an aft mounted thruster on a vehicle moving with a forward speed differs substantially when compared with a forward mounted thruster.
6. The influence of the suction force is much greater for the aft thruster than the forward thruster due to the location of the centre of action of the suction force. This increased influence causes a change in direction of the yaw moment for the aft thruster at high speed ratios.
7. The centre of action of the total moment moves forward with increasing speed ratio for both the forward and aft mounted thrusters.
8. The centre of action of the suction force moves linearly aft for the forward thruster, but has a consistent location across the range of non-zero speed ratio for the aft

thruster. This difference is due to the considerably smaller area of hull downstream of the aft thruster.

9. The increase in vehicle drag coefficient due to the operation of the thrusters is the same for the forward and aft thrusters and decreases with increasing speed ratio.
10. The performance of a pair of thrusters working together at a separation of 18.7*d* is independent of the operation of either thruster. At this separation the total performance can be predicted by summing the individual contributions.
11. The performance of tunnel thrusters working on a vehicle at an angle of yaw shows limited influence of yaw angle up to ±10º. In general the performance increases when the jet is shielded and decreases when the jet emits into the oncoming flow with these effects having a greater influence on the aft thruster compared to the forward thruster.

4.5.6 Modelling Tunnel Thruster Performance

Modelling the forces and moments generated by a tunnel thruster on an AUV is important as it allows further insight to be gained into how a vehicle will perform when using these thrusters. This insight is necessary for control system design and mission planning. No common modelling procedure is readily available in the published literature, although a few models have been published and will be reviewed next. These models aim to capture the hydrodynamic effects observed during the experimental testing programme.

Several authors have suggested curve fits to the force and moment coefficients (K_F and K_N) for a model tanker published in [96]. One example of these curve fits is [110]:

$$K_F = g_1\left(\frac{u}{u_j}\right) \tag{4.29}$$

and

$$K_N = g_2\left(\frac{u}{u_j}\right). \tag{4.30}$$

For $0 \le \frac{u}{u_j} \le 0.1$ then $g_1 = g_2 = 1$

whereas for $0.1 \le \frac{u}{u_j} \le 1.6$ then

$$g_1 = 1.33\exp\left(-4.917\frac{u}{u_j}\right) + 0.309\frac{u}{u_j} + 0.042 \tag{4.31}$$

and

$$g_2 = 1.79\exp\left(-4.466\frac{u}{u_j}\right) - 0.399\left(\frac{u}{u_j}\right)^2 + 1.450\frac{u}{u_j} - 0.269. \tag{4.32}$$

An additional relationship is also provided to account for the roll moment in the form of the product of the side force and an appropriate moment arm (not based on [96]). These curve fits match the experimental data [96] well but do not offer a suitable structure for the development of a simple model for a different configuration or experimental data set.

A model developed in [99] from a data set mainly focussing on the influence of waves on the performance of a tunnel thruster on a surface vessel is presented in the form:

$$K_F = 1 - \frac{C_P}{2}\left(\frac{u}{u_j}\right)^2 \tag{4.33}$$

with

$$C_P = \frac{\Delta T_T}{0.5\rho A u^2} = g_3\left[\left(\frac{u}{u_j}\right)^{g_4-2} - g_5\left(\frac{u}{u_j}\right)\right] \tag{4.34}$$

and

$$g_5 = \frac{g_4}{3}\left[\left(\frac{u}{u_j}\right)^*\right]^{g_4-3}. \tag{4.35}$$

Here g_3 and g_4 are constants and $(u/u_j)^*$ is the velocity ratio corresponding to the minimum value of K_F. This model offers a simpler approach to modelling the forces, but the functional form of this model does not match the trends observed for a tunnel thruster on an AUV. The selection of the coefficient, g_5, sets a minimum on the curve, after which the performance is seen to increase. This type of performance is characteristic for surface vessels, but is not seen in the data reported here (see Figure 4.30) or in the submersible data from [93] (see Figure 4.20).

A surface vessel model developed in [111] suggests that the thrust loss up to $u/u_j = 0.3$ satisfies:

$$K_F = 1 - 1.4\frac{u}{u_j}\left(\frac{u}{u_j} + 1\right)^2 \tag{4.36}$$

and for $u/u_j \geq 0.3$ K_F is held constant. The moments on the vehicle are given, for the forward thruster by:

$$N = F_T\left[x_T - 1.4\frac{u}{u_j}\left(\frac{u}{u_j} + 1\right)^2 + \frac{u}{u_j}\frac{l_T}{2}\right] \tag{4.37}$$

and for the aft thruster by:

$$N = F_T\left[x_T - \frac{u}{u_j}\frac{l_T}{2}\right]. \tag{4.38}$$

Here l_T is tunnel length. This model is much simpler in form than the previous models, albeit it does not show a sufficient decrease in thrust force. The representation of the moments for the forward and aft thrusters shows some agreement with the results recorded here as it acknowledges a difference between the two. However, the shape of the results given does not correlate with the results recorded here.

The results from [73] are used to provide performance characteristics for a set of basis surface vessels at the MArine Research Institute Netherlands (MARIN) for simulations of vessel performance. A simulation of a vessel used for the development of control systems states that the forces from the tunnel thruster should be factored by $\exp(-g_6u^2)$ to account for the ambient flow effects [112].

All of the models discussed focus on marine surface vessels. Another field where similar thruster installations are found is Vertical / Short Take-Off and Landing (V/STOL) aircraft. These aircraft use thrusters mounted in the wings to provide forces in the vertical plane to enable vertical and short take-off, in effect enhancing their low speed manoeuvring characteristics. Discussions in research on the forces from these thruster configurations state that experimental testing is the only way to ensure that the performance is accurately characterised [113]. A complex modelling structure for the performance of such a configuration is provided. The structure of this model is heavily linked to aircraft applications and the trends captured show considerably different performance characteristics to those observed on an AUV (or a marine surface vessel).

The original AUV tunnel thruster models developed in [88] and [89] were modified in [94]. The modifications involve a look-up table of experimental results to give the steady state performance of the thruster as a linear function of the square of the thruster rotational speed. However, these modifications serve only to incorporate the limited variations in thruster performance observed during the reported experiments.

A variety of models have been suggested in the literature using differing structures and these are usually based on a particular set of experimental results. Therefore since no common modelling procedure has been found it becomes necessary to attempt to develop a model using the experimental results and insight gained.

4.5.6.1 AUV Tunnel Thruster Modelling Procedure

To develop a simple modelling procedure requires an understanding of the operation of a tunnel thruster on an AUV under various conditions. In this context a simple model is one that can be easily adapted to cover a range of thrusters and hull forms. That is, a model that uses only a small number of coefficients that require a detailed understanding of the operation to select an appropriate value. The aim of the development of a modelling procedure is to allow AUV designers and operators to include the general characteristics of tunnel thrusters when predicting vehicle response.

The models noted above represent the influence of the interaction between the thruster jet and the ambient flow and not the forces generated by the thruster itself. The force from the thruster is assumed to be obtainable from simple static performance models, for example:

$$F_T = K_3 n|n| = K_T \rho d^4 n|n| . \tag{4.39}$$

More complex representations of the forces from a tunnel thruster are widely available in the literature, for example [55] and [10]. These models also include the dynamic performance of the thruster and these can be combined with a modelling procedure for tunnel thrusters. It was concluded in [94] that the dynamic performance of a tunnel thruster was unaffected by the operational conditions. A series of tests undertaken with the experimental set up detailed in Section 4.5.3 confirmed this conclusion. Therefore existing models for thruster dynamics can be employed for this purpose.

The results in Section 4.5.4 show that the variations in the performance of a tunnel thruster are a function of the speed ratio and thus the model will be based on this parameter. The speed ratio can be easily calculated using Equation (4.24) and the thruster performance model (Equation (4.39)). Furthermore, the results in Section 4.5.4 show that there is only a limited influence of yaw angle on the performance of the tunnel thruster. Therefore the model developed will be assumed to hold over the small range of yaw (or pitch) angles to be experienced.

For the development of a model of tunnel thruster performance a simplified representation of the operation is to be used. This representation uses two forces, namely, the thruster force and a suction force as discussed in Section 4.5.4. The thruster force is modelled using a simple thruster model, for example Equation (4.39), and is assumed independent of the operational conditions. The suction force represents the sum of all of the suction effects acting on the vehicle and is the difference between the thruster force and force experienced

by the vehicle, see Equation (4.26). The thruster force is assumed to act along the thruster axis and the suction force acts at a variable location. The variables and definitions are as illustrated in Figure 4.48.

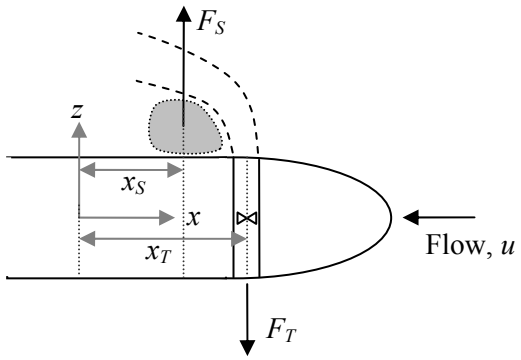

Figure 4.48 – Tunnel Thruster Model Definitions

To determine the value of the suction force requires a model of relationship between the force coefficient, K_F, and the speed ratio, u/u_j. The results shown in Figure 4.30 can be represented by an exponential model of the form:

$$K_F = \exp\left[-c\left(\frac{u}{u_j}\right)^2\right] \tag{4.40}$$

Figure 4.49 shows the agreement between the exponential model and the experimental results. The coefficient, c, is selected for each thruster using a least squares approach. Note that in comparison with the surface vessel models, Equation (4.40) does not give any recovery of performance at high speed ratios.

The moment acting on the vehicle can be determined using the following relationship, see Figure 4.48:

$$N = F_T x_T + F_S x_S \,. \tag{4.41}$$

The only remaining component of Equation (4.41) to be determined is the centre of action of the suction force, x_S. The results shown in Figures 4.34 and 4.35 show how the centre of action of the suction force varies with speed ratio. For the forward thruster the centre of action moves linearly aft with increasing speed ratio, hence:

$$x_S = x_T - k_4 d \frac{u}{u_j} \,. \tag{4.42}$$

However, the centre of action of the suction force for the aft thruster is roughly constant with speed ratio, hence:

$$x_S = x_T + k_5 d \,. \tag{4.43}$$

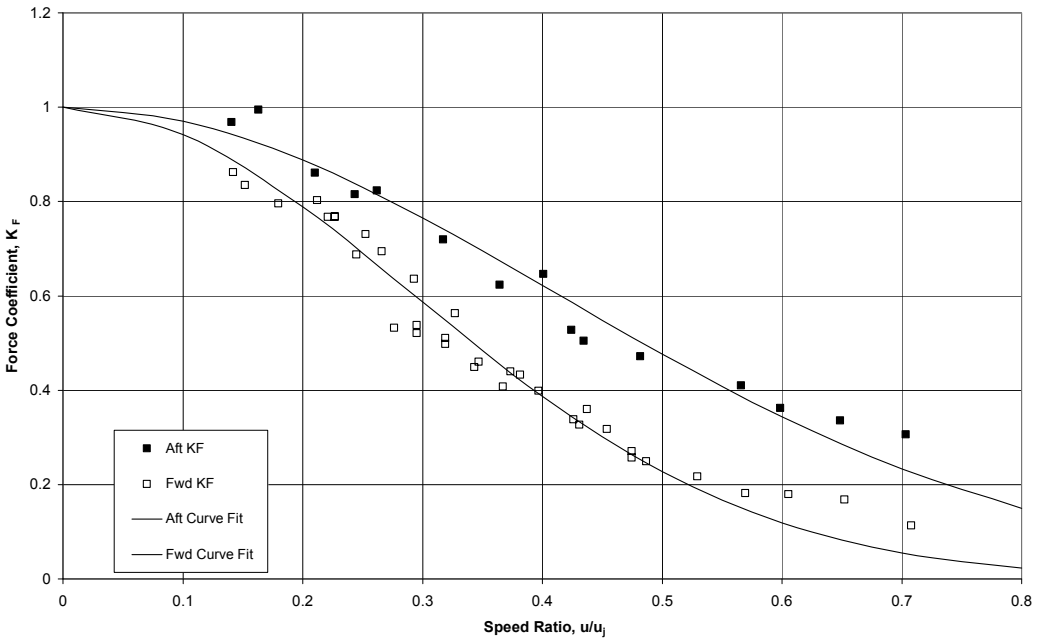

Figure 4.49 – Comparison of Exponential Model with Experimental Results

These equations can be combined to form a complete model of the performance of a through-body tunnel thruster on an AUV over the range of operational forward speeds and a range of small yaw or pitch angles. The model can be summarised as follows:

The force generated by the tunnel thruster is:

$$F_T = K_3 n|n|, \tag{4.44}$$

here K_3 is a thruster specific constant. The force experienced by the vehicle is:

$$F_V = F_T \exp\left[-c\left(\frac{u}{u_j}\right)^2\right], \tag{4.45}$$

where c is a configuration specific constant. The moment experienced by the vehicle is:

$$N = F_T x_T + (F_T - F_V) x_S . \tag{4.46}$$

Here x_T is the distance between the pivot point of the vehicle and the thruster axis and x_S is defined for a forward mounted thruster as:

$$x_S = x_T - k_4 d \frac{u}{u_j} . \tag{4.47}$$

Here k_4 is a configuration specific constant. x_S for an aft mounted thruster is defined as:

$$x_S = x_T + k_5 d \tag{4.48}$$

and k_5 is a configuration specific constant.

The above model describes the performance of a tunnel thruster on a survey-style AUV and requires the specification of 3 constants per thruster. The first of these constants (K_3) should be obtainable from the data provided by the manufacturer. The data provided in Section 4.5.4 provides a suitable basis for the selection of the remaining constants for initial design studies, that is, Figure 4.49 for c and Figures 4.34 and 4.35 for k_4 and k_5 respectively.

Prior to the experimental testing detailed in Section 4.5.3, a preliminary model of the performance of tunnel thrusters was developed using the existing published data. The development of this model is given in [114], which is provided in Appendix B1. For zero yaw (pitch) motion this model takes a similar form to Equation (4.45). The model also covers motion at yaw angles of up to ±90º. This part of the model was based upon the data in [98], [94] and [73] however the experimental results presented in Section 4.5.4 do not provide sufficient data to validate the form of this model.

4.5.7 Model Validation

The model described by Equations (4.44) to (4.48) has been developed using theoretical arguments and experimental results. The experimental results have been obtained using captive experimental testing, that is, with a constrained model in a confined body of water. For this model to be of use in the development of real vehicles it is important to consider how these captive experimental results, and hence the model, relate to the free swimming performance of an AUV.

To consider the free swimming scenario, data from a series of lake trials with the Delphin AUV [115] was assessed. Delphin is a 2m long manoeuvrable AUV with a hull form corresponding to a scaled version of Autosub6000 but limited to an immersion of 10m depth. Delphin has a stern mounted propeller and a cruciform of control surfaces similar to those on Autosub6000, as illustrated in Figure 4.50. In addition, Delphin is equipped with two vertical and two horizontal tunnel thrusters to provide low speed manoeuvring control.

The tunnel thrusters used on Delphin are the same thrusters as used in the experimental testing programme of Section 4.5.3. Delphin was equipped with a Global Positioning System (GPS) antenna and ballasted to operate just below the surface to allow visual contact with the vehicle to be maintained and to ensure the GPS antenna could communicate with the required satellites. The GPS co-ordinates were recorded on the vehicle, but not used for control or navigation. Delphin was commanded to travel forwards subject to a constant stern propeller demand and after a given time had elapsed the control system sent a demand to the

forward horizontal tunnel thruster. This set point demand remained constant for the remainder of the trial. Consequently, Delphin began to turn in a circle. The form of this trial is similar to those used to examine the performance of surface vessels under rudder control.

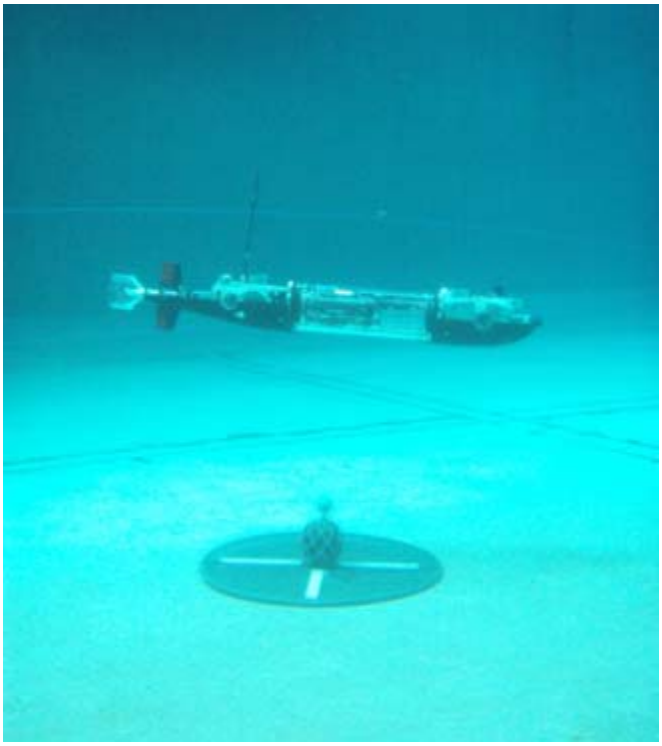

Figure 4.50 – The Delphin AUV Hovering above a Bottom Target at the Student Autonomous Underwater Challenge – Europe 2009

Three trial runs were possible using Delphin. These trials were undertaken with a common stern thruster demand corresponding to an average forward speed of 0.65m.s^{-1} (calculated from the GPS data). This speed corresponds to the low speed manoeuvring range for the full scale Autosub6000 and thus represents a realistic operating condition for manoeuvring the vehicle with tunnel thrusters. The three trials were undertaken using thruster 'set points' designated 600, 1200 and 1800 giving a range of speed ratio from 0.4 to 1.35. The resulting turning circles determined from the GPS data are provided in Figures 4.51, 4.52 and 4.53.

Figures 4.52 and 4.53 show consistent and repeatable turning circles. Figure 4.51 shows most of a turning circle, however the turning circle was too large and thus the vehicle collided with the side of the lake. The averaged non-dimensional turning radii, R', calculated from the GPS data are given in Table 4.4.

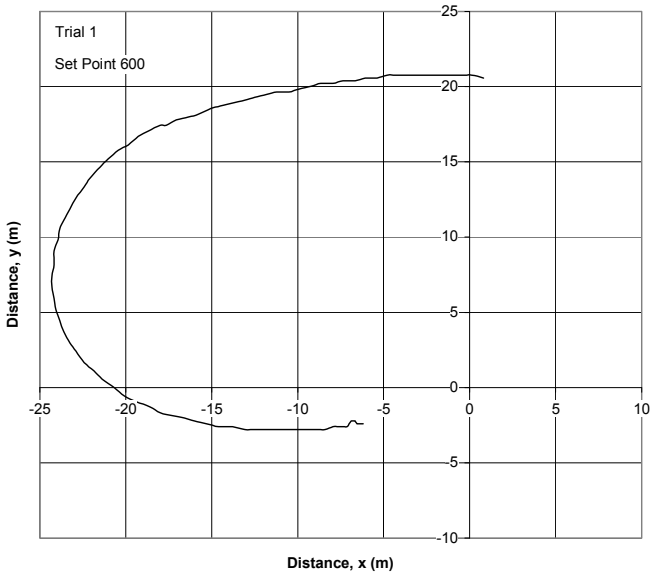

Figure 4.51 – Delphin GPS Trace with Thruster Set Point 600

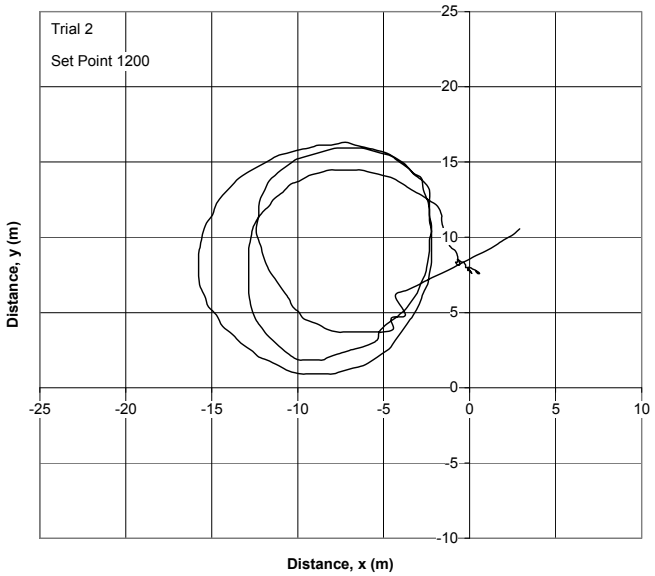

Figure 4.52 – Delphin GPS Trace with Thruster Set Point 1200

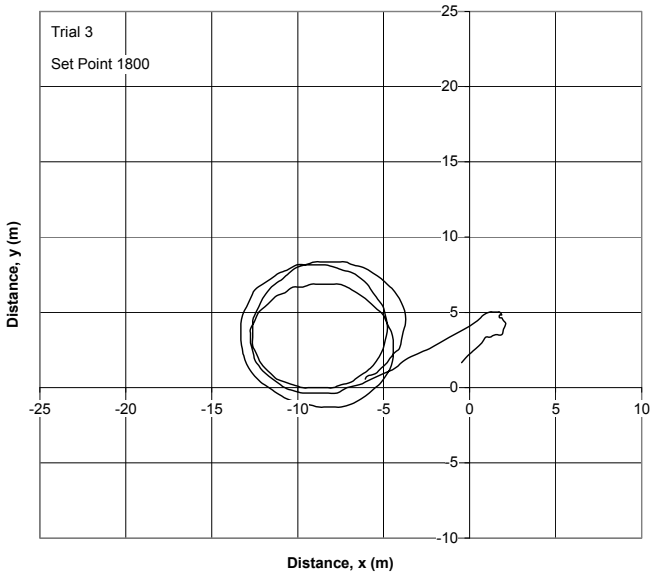

Figure 4.53 – Delphin GPS Trace with Thruster Set Point 1800

Table 4.4 – Averaged Non-Dimensional Turning Radii from Lake Trials

Trial	Thruster Set Point	Non-Dimensional Turning Radius
1	600	5.61
2	1200	3.09
3	1800	2.10

To compare the performance of Delphin with the model developed in Section 4.5.6.1, Equation (4.49) is used to calculate the non-dimensional turning radius based on the linearised equations of motion in the horizontal plane with the assumption of a steady turning rate. The coefficients used are those given in Appendix A3.

$$R' = \frac{1}{r'} = \frac{(-Y'_r + m')N'_v - (-N'_r + m'x'_G)Y'_v}{(F'_V N'_v - N'Y'_v)} \tag{4.49}$$

The non-dimensional turning force F'_V and the non-dimensional turning moment N' are determined using the model developed in Section 4.5.6.1. The thruster set points are converted into a rotational speed, using an experimentally determined correlation, allowing the thrust generated by the thruster to be estimated using Equation (4.44). Equation (4.45) is used to determine the force on the vehicle due to the operation of the thruster and Equation (4.46) with Equation (4.47) is used to determine the corresponding moment. The coefficients used in Equations (4.44), (4.45) and (4.47) are those determined from the captive experimental testing (detailed in Section 4.5.4). The results of these calculations are illustrated in Figure 4.54 and compared with the trials data.

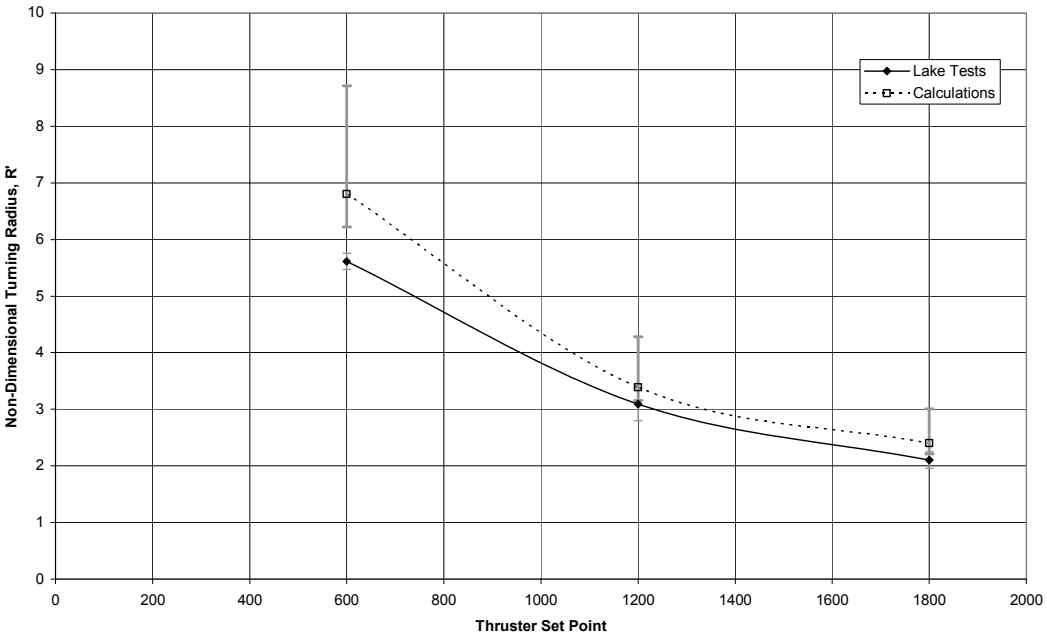

Figure 4.54 – Comparison of the Trials Results and Model Predictions of the Delphin AUV Turning Radii

Figure 4.54 illustrates a good agreement between the experimentally determined turning radii and those predicted by the model. The calculated turning radii are larger than those determined experimentally. However, given the unquantifiable uncertainties in the calculations, the agreement between the results, in terms of both the trend and magnitudes, is encouraging. These unquantifiable uncertainties relate to the applicability of the modelling parameters used to the Delphin AUV.

4.5.8 Tunnel Thruster Conclusions

This section has introduced the tunnel thruster, its performance characteristics and the physics behind these characteristics. An experimental programme has been undertaken to determine the particular performance characteristics for a tunnel thruster on a torpedo-shaped survey-style AUV. The results of these experiments demonstrate that a tunnel thruster can be used to generate low speed control forces for a survey-style AUV. A modelling procedure has been developed using the insight and experimental results gained to aid in the design and development of AUVs and their control systems. This modelling procedure has been validated against results from free swimming trials and shows excellent agreement.

4.6 Concluding Remarks

This chapter has introduced the general issues relating to the use of propeller based thrusters to provide the additional low and zero speed control for a multi-purpose AUV. The performance characteristics of external thrusters and through-body tunnel thrusters have been considered in detail, both in open water conditions and onboard a survey-style AUV.

The performance of external thrusters and the flexibility offered make them a good choice for providing low and zero speed control for an underwater vehicle. Hence they are commonly employed on ROVs and modular AUVs for this purpose. Similarly, it has been shown that through-body tunnel thrusters can also provide the required low and zero speed control. Therefore a decision needs to be made between the two options available.

In the development of a multi-purpose AUV the importance of maintaining the survey efficiency has been stressed. Therefore, given the substantial negative impact of the external thrusters on the survey efficiency and the demonstrated low speed performance of tunnel thrusters, the decision has been made to explore the capabilities of tunnel thrusters further. Consequently, the following analysis of the transition phase and the performance during low speed manoeuvres is based upon a survey-style AUV equipped with tunnel thrusters.

Chapter 5 – Performance Simulation

5.1 Introduction

The development of a multi-purpose AUV requires an understanding of the performance and operability of the proposed configuration to examine whether the vehicle is capable of achieving the design aims and to aid in mission design. One of the ways of obtaining the required insight is to use a simulation of the performance of the AUV. To be able to construct such a simulation requires knowledge of the AUV response to different motions and control forces. In [25] a series of experiments were undertaken to ascertain the required information to facilitate a simulation of the Autosub AUV response. In this research the development of a multi-purpose AUV is based upon adding new control capabilities to an existing survey-style AUV. The details of the developed simulation will be explained and then a series of performance simulations will be undertaken to investigate the performance characteristics of a multi-purpose AUV.

5.2 Simulation Details

A six degree-of-freedom simulation of Autosub was developed using Matlab Simulink [116]. The simulation facilitates the examination of the performance of Autosub with different control strategies for undertaking different manoeuvres. The basic model has four key blocks, namely, a model block that calculates the AUV responses, a speed control block, a depth control block and a heading control block. The three control blocks are adapted to match the vehicle performance being investigated. The simulation is constructed as illustrated in Figure 5.1. Details of the four component blocks will now be discussed.

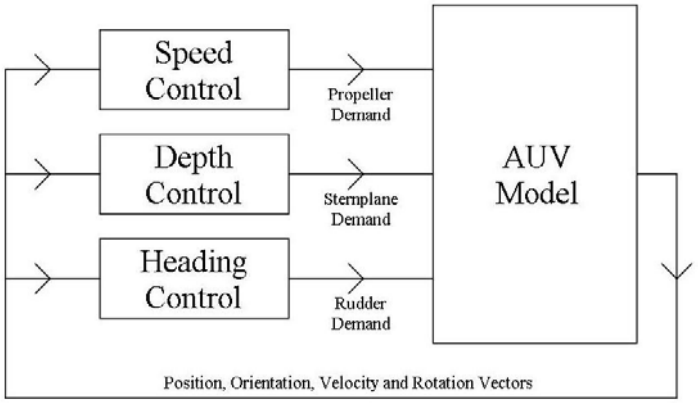

Figure 5.1 – AUV Simulation Overview

5.2.1 AUV Model Block

The AUV model block simulates the response of the vehicle using the equations of motion for the AUV. The equations of motion used are the Booth et al. [117] submarine equations with hydrodynamic derivatives assigned as determined from experiments [25]. The equations are arranged so that the inertial contributions, X_{ACCEL}, are equated to the appropriate forces and moments acting on the AUV, see Equation (5.1).

$$X_{ACCEL} = \left(X_{HYD} + X_{HYDST} + X_{RB}\right) + \left(X_{CS} + X_{PROP}\right) \tag{5.1}$$

The AUV model block is split into several parts to calculate different contributions to the forces and moments on the vehicle. These forces and moments are attributed to the hydrodynamic (HYD), hydrostatic (HYDST) and rigid body (RB) effects, and the control forces and moments generated by the control surfaces (CS) and propeller (PROP). These contributions are summed and then integrated using a fourth order Runge-Kutta scheme. At each time step the state vector, which contains the vehicle position, orientation, velocity and rotation vectors, is updated. These newly calculated vectors are passed onto the control blocks and the simulation progresses until a user-specified endpoint has been reached. The simulations are undertaken using the Matlab Simulink variable time step approach, which varies the time step, limited by a maximum value, according to the noted changes in the state vector.

The hydrodynamic derivatives determined in [25] facilitate the evaluation of the performance of the original Autosub survey-style vehicle configuration. The development of the equations, and the definition of the hydrodynamic derivatives, is based on the assumption of limiting the vehicle to small deviations from a given condition. That is, the equations, with a particular set of derivatives, accurately simulate the performance of the vehicle at the particular condition and in a small range around this condition. For these equations and derivatives the particular condition is survey operation. Therefore it would be inappropriate to use these equations to simulate substantially different conditions, for example, low speed six degree-of-freedom manoeuvres. Therefore the assessment of performance using the simulation will be limited to scenarios similar to survey operation, that is, where the predominant direction of motion is forwards.

The simulation was restricted to motions in the vertical plane alone as the simulation is to be used to analyse the performance of the vehicle during the transition phase where the key interest relates to the control of depth. That is, the sway, yaw and roll motions were neglected and the rudder was held fixed with zero deflection angle. Therefore the heading

control block is redundant in these simulations. The simulation continues to model the surge, heave and pitch motions controlled by the speed and depth control blocks.

The reduced equations of motion used in the simulation are given as Equations (5.2), (5.3) and (5.4). (Note that the vehicle is 0.3% positively buoyant in these simulations, unless otherwise stated.)

Surge:

$$\begin{aligned} m\left[\dot{u} + wq - x_G q^2 + z_G \dot{q}\right] &= 0.5\rho l^2 \left(X'_{uu} u^2 + X'_{ww} w^2 + X'_{uu\delta\delta} u^2 \delta S^2\right) \\ &\quad + 0.5\rho l^3 \left(X'_{\dot{u}} \dot{u} + X'_{wq} wq\right) \\ &\quad + 0.5\rho l^4 X'_{qq} q^2 \\ &\quad + (B - mg)\sin\theta + X_{PROP} \end{aligned} \tag{5.2}$$

Heave:

$$\begin{aligned} m\left[\dot{w} - uq - z_G q^2 - x_G \dot{q}\right] &= 0.5\rho l^2 \left(Z'_{uw} uw + Z'_{w|w|} w|w| + Z'_{uu\delta} u^2 \delta S\right) \\ &\quad + 0.5\rho l^3 \left(Z'_{\dot{w}} \dot{w} + Z'_{uq} uq + Z'_{u|q|\delta S} u|q|\delta S\right) \\ &\quad + 0.5\rho l^3 \left(Z'_{w|q|} w|q|\right) \\ &\quad + 0.5\rho l^4 Z'_{\dot{q}} \dot{q} \\ &\quad + (mg - B)\cos\theta \end{aligned} \tag{5.3}$$

Pitch:

$$\begin{aligned} I_{YY}\dot{q} + m\left[z_G\left(\dot{u} + wq\right) - x_G\left(\dot{w} - uq\right)\right] &= 0.5\rho l^3 \left(M'_{uw} uw + M'_{uu\delta} u^2 \delta S + M'_{w|w|} w|w|\right) \\ &\quad + 0.5\rho l^4 \left(M'_{\dot{w}} \dot{w} + M'_{uq} uq + M'_{q|w|} q|w|\right) \\ &\quad + 0.5\rho l^4 \left(M'_{u|q|\delta S} u|q|\delta S\right) \\ &\quad + 0.5\rho l^5 M'_{\dot{q}} \dot{q} \\ &\quad - \left(mgx_G - Bx_B\right)\cos\theta - \left(mgz_G - Bz_B\right)\sin\theta \end{aligned} \tag{5.4}$$

The stern propeller is assumed to generate a force in the vehicle longitudinal direction (x) alone and the propeller torque is not modelled. This represents a simplified model of the propeller performance and provides an appropriate force to simulate operation at a selected forward speed. The model block uses a quadratic representation of the propeller thrust characteristics expressed in terms of a rotational speed ratio, defined as:

$$n' = \frac{n}{k_0 u} = \frac{u_{req}}{u}. \tag{5.5}$$

Here k_0 is the ratio of the rotational speed of the propeller to the vehicle speed at self propulsion; hence $k_0 u$ gives the rotational speed necessary to maintain the vehicle speed. Using this ratio the propeller force model is:

$$X_{PROP} = 0.5\rho l^2 u|u|\left(b'_j + b'_{j+1} n' + b'_{j+2}\left(n'\right)^2\right). \tag{5.6}$$

The coefficient set, b'_j, b'_{j+1} and b'_{j+2}, used with j = 1, 4 or 7, depends upon the regime of operation for the propeller as determined by the value of n'. The coefficient sets reflect the differing propeller performance in differing regimes of operation and are determined from simplified propeller characteristics.

5.2.2 Speed Control Block

The speed control block allows the user to select a constant operational forward speed as the input and outputs a command to increase or decrease the propeller force as appropriate. Alternatively the user may define a simple relationship that determines the variation of vehicle forward speed over time. An example relationship is a constant gradient increase (or decrease) of speed. The required vehicle speed is used in the propeller model as detailed in Equations (5.5) and (5.6). The speed control block includes a feedback loop to ensure that the required speed is achieved.

5.2.3 Depth Control Block

The depth control is undertaken using a simple control module, which combines both depth and pitch control [118]. This is schematically illustrated in Figure 5.2.

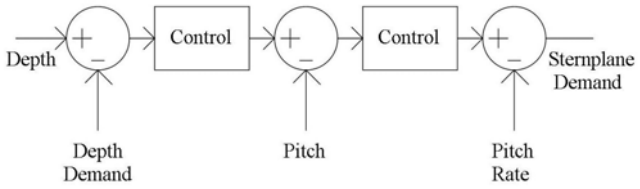

Figure 5.2 – Schematic Illustration of the Depth Controller

The depth control module takes a demand depth as its input and compares this with the actual vehicle depth to calculate a depth error. This depth error is then converted into a pitch demand by a control operator. This pitch demand is compared with the actual pitch and sent through another control operator to determine a demand pitch rate. This is compared with the actual pitch rate and the result is sent to the sternplane controller, which determines the demand to be sent to the servo controlling the sternplane. The demand sternplane angle is limited by a maximum deflection angle for the control surfaces. This depth control module is designed for survey speed operation as it converts a depth demand into an equivalent pitch angle, which relies on the force generation capabilities of the vehicle hull form to overcome the positive buoyancy and hence control vehicle depth.

5.2.4 Heading Control Block

The heading control block is redundant in these simulations as the analysis is restricted to the vertical plane. The heading control block is replaced by a command to hold the rudder with a fixed zero deflection angle.

5.2.5 Sensors and Data

The described AUV simulation calculates the response of the vehicle to the given control demands. On a real vehicle these control demands are sent to the appropriate actuators and the corresponding response is measured using onboard sensors. These sensors include, for example, a compass to measure the heading of the vehicle and a Doppler Velocity Log (DVL) to estimate the vehicle velocity. This represents a significant difference between the simulation and the operation of the real vehicle. The simulation calculated responses are reliable and free from noise whereas sensor data is less reliable and susceptible to noise and interference. Simulations have been reported in the literature that add random noise to the calculated responses to investigate the robustness of the controllers used and the ability to control the vehicle subject to a loss of data (from particular sensors). However, this is not the aim of this particular study and thus the simulations will be performed using the unmodified responses calculated by the model.

5.3 Survey Depth Control Performance

The survey performance of the vehicle can be investigated using the simulation in its current form. The restriction of the simulation to the vertical plane limits the scope of these investigations. However, the performance characteristics of the vehicle in terms of its depth control abilities can be demonstrated. Figure 5.3 shows the response of the vehicle to a step change in depth demand of 50m at t = 500s while travelling at a survey speed of 1.5m.s^{-1}.

Figure 5.3 shows a smooth and gradual change of depth from 300m to 350m between t = 500s and t = 600s. The sternplane angle increases to its maximum value to set a pitch angle to enable the vehicle to dive. Once this pitch angle has been achieved the sternplane angle is reduced to maintain this pitch angle. As the depth approaches its target value, the sternplane angle returns to the original value to set the vehicle pitch angle to that required to maintain depth. These results demonstrate the ability of the control surfaces to set, maintain and change depth at survey speeds.

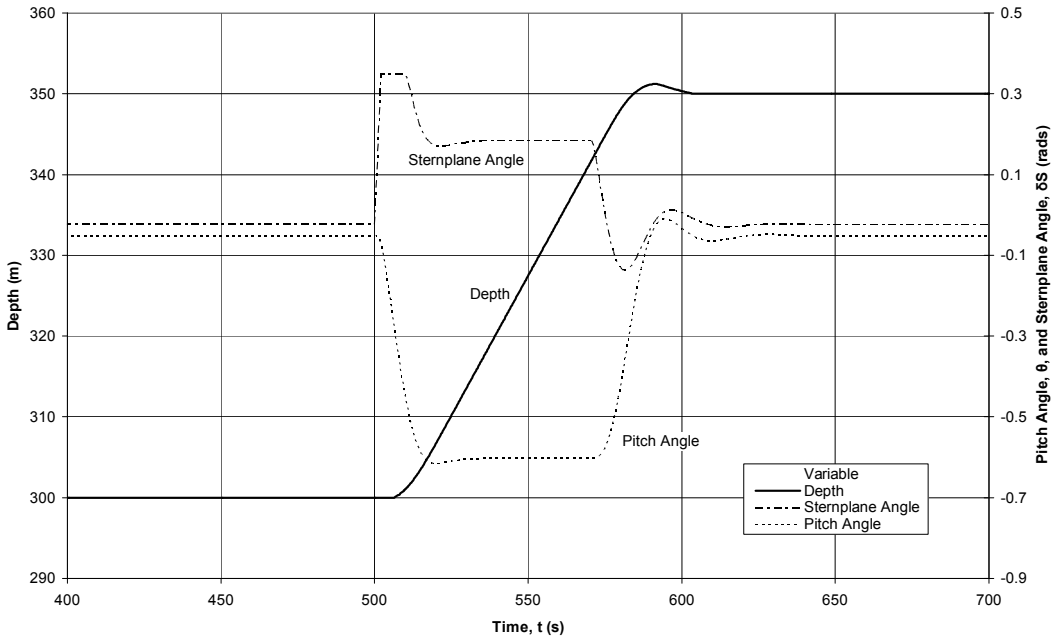

Figure 5.3 – Depth Control at Survey Speed using Control Surfaces

5.4 Depth Control in the Transition Phase

The simulation tool is now used to demonstrate the behaviour of the AUV, in its original survey configuration, as the operational mode changes from constant speed survey operation to the zero forward speed (hover) condition. The reduction in required forward speed is taken at a constant rate. Figure 5.4 shows the sternplane, pitch and depth response of the vehicle as the forward speed is reduced.

The vehicle starts at a depth of 300m travelling at $1.5 m.s^{-1}$ with a small sternplane deflection and corresponding pitch angle to generate the force required to counteract the inherent positive buoyancy. As the vehicle begins to slow down the speed dependence of the generated hydrostatic balance control force means that the pitch angle must increase to maintain depth. Therefore the depth control block alters the sternplane deflection angle to increase the pitch angle. As the speed continues to reduce the maximum deflection of the control surfaces is reached, marked by the control threshold at point A. Here the control surfaces can no longer generate sufficient force to maintain the required pitch angle to operate at constant depth. Hence the vehicle depth decreases indicating that the vehicle is rising towards the surface. Furthermore, the pitch angle returns towards zero due to the vehicle's righting moment. This simulation shows that in order to operate at speeds below $0.73 m.s^{-1}$ (point A) an alternative method of controlling the hydrostatic balance is required.

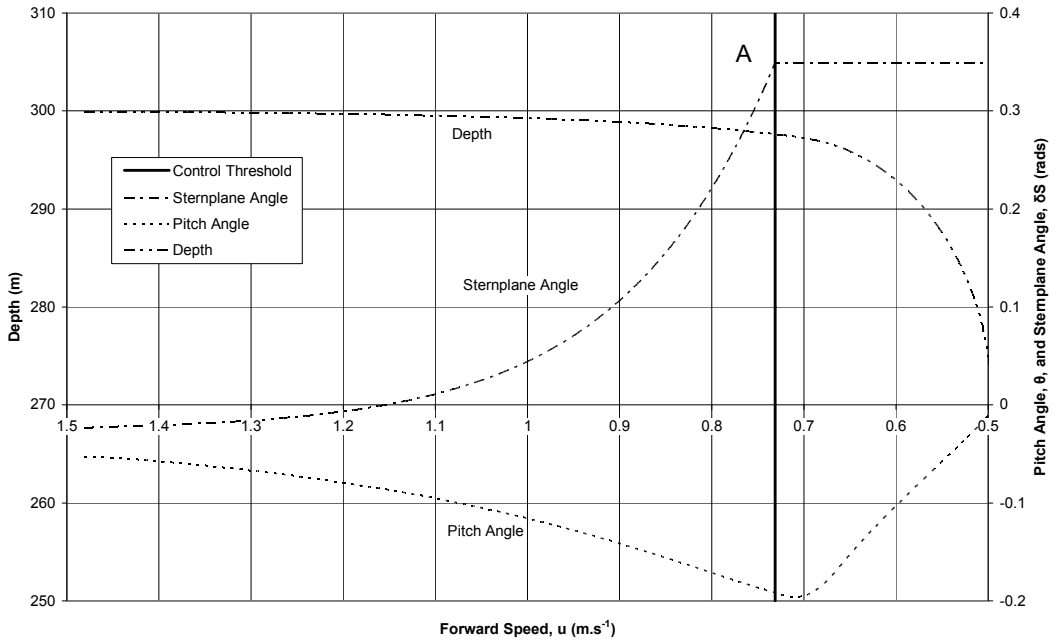

Figure 5.4 – Transition Zone using the Original Survey AUV Configuration

Figure 5.4 shows a small gradual loss of depth before point A. This is caused by the reactive nature of the control system used, that is, the control system reacts to a change in depth and does not pre-empt the change in depth despite this change being caused by the change of vehicle speed, as commanded by the controller.

The maximum deflection angle for the control surfaces is set at 20˚ (for practical reasons) to try to avoid the onset of stall. The simulations do not model stall and the stall angle (and hence maximum lift force obtainable) will reduce with decreasing Reynolds number.

5.5 Low Speed Depth Control

Figure 5.4 illustrates that the control surfaces cannot maintain control over depth at forward speeds below 0.73m.s^{-1} for the particular vehicle configuration represented in the simulation. Therefore an additional control approach is required. The selected control approach is that of a through-body tunnel thruster. Tunnel thrusters will be used in two different configurations in the vertical plane, firstly, a single centrally mounted tunnel thruster, and secondly, a pair of tunnel thrusters with one mounted at each end of the vehicle, equispaced about the vehicle centre. The depth control capabilities of the chosen tunnel thruster configurations need to be investigated to ensure that they are capable of providing sufficient control throughout the low and transitional speed ranges. The experimental results detailed in Section 4.5.4 show that the effectiveness of a tunnel thruster decreases with increasing

forward speed. Hence it is important to determine what the limiting forward speed is for tunnel thruster depth control. This will now be investigated using the simulation tool.

The forces and moments generated by the tunnel thrusters, X_{TT}, are added to the AUV model in the simulation to give an updated version of Equation (5.1):

$$X_{ACCEL} = \left(X_{HYD} + X_{HYDST} + X_{RB}\right) + \left(X_{CS} + X_{PROP} + X_{TT}\right) \tag{5.7}$$

The influence of the tunnel thrusters is calculated using the model based on the experimental data as described in Section 4.5.6.1. The remaining parts of the AUV model are unaltered and thus no account of the influence of the presence of the tunnel thruster on survey operation is made. That is, no drag correction is made for the addition of the tunnel thruster and no additional allowance is made for any influence of the modified flow conditions induced by the presence of the tunnel thruster.

The depth control performance of the tunnel thruster will be investigated using two different models. The first model only includes the forces generated by the tunnel thruster, that is, neglecting the variation in moment induced by the offset of the centre of action of the suction force. In effect the suction force is assumed to act at the thruster axis (i.e. $x_S = x_T$). The second approach uses the complete model described in Section 4.5.6.1, that is, with the suction centre of action variable. The comparison of the results from these approaches will provide insight into the performance of the vehicle and the mechanisms influencing the particular performance characteristics exhibited.

The simulation requires a tunnel thruster control block to determine the demand operating point. There are many different options for the type of controller selected, for example controlling the power to the thruster or controlling the rotational speed of the thruster. The chosen option is to control the rotational speed of the thruster as this allows accurate control and provides a simple relationship between the control variable and the generated thrust force.

Different controllers were developed for the two configurations to be considered. For the single thruster, the rotational speed is determined using a Proportional-Integral-Derivative (PID) controller, which takes the depth error as its input. This controller only controls the depth of the vehicle as the single centrally mounted thruster offers no direct control over pitch. For the thruster pair, the single thruster controller is used to determine a total rotational speed (force) required to maintain depth. This total rotational speed is then

allocated to the two thrusters with the aim of maintaining zero pitch. The allocation is determined using a factor, k_6, which is calculated using the following relationship:

$$k_6 = 0.5 \tanh\left(\frac{GP_d}{P_{dL}}\right) + 0.5 \,. \tag{5.8}$$

Here P_d is the pitch error (the difference between target and actual pitch), P_{dL} is a pitch limit (setting the extents of the allowed pitch range) and G is a constant that sets the steepness of the allocation. A high value of G sets a steeper, more responsive allocation. The rotational speed for each thruster is determined by multiplying the total rotational speed by k_6 for the aft thruster and $(1-k_6)$ for the forward thruster.

For these simulations $G = 1$, however the influence of G was tested over the range $0.01 \leq G \leq 10$. Equation (5.8) effectively gives a proportional pitch controller with gain G. The asymmetry of the thruster performance (as indicated by the experimental results presented in Section 4.5.4) dictates that the required forward and aft thruster rotational speeds to maintain depth are not equal. Thus the use of a proportional controller gives a small steady state pitch error as a function of the gain, G. Increasing the value of G reduces the steady state pitch error.

Simulations were performed using the described control strategies over a range of forward speed to demonstrate the depth control capabilities of the tunnel thrusters. The simulations were performed using the two different thruster configurations and the two different modelling approaches. The resulting variations in rotational speed and pitch angle (when maintaining constant depth) are shown in Figures 5.5 and 5.6 respectively. Here 'NP' implies the use of the modelling approach without the pitch moment (with the suction centre of action held fixed ($x_S = x_T$)).

The simplest example to consider is the single central tunnel thruster without the pitch moment (denoted 'Single NP'). In this case the pitch remains at zero throughout the speed range for which depth is controlled. At the highest speeds (0.9m.s^{-1} and 1.0m.s^{-1}) the thruster has reached its maximum rotational speed, however the resultant force acting on the vehicle is insufficient to maintain control over depth. Figure 5.5 shows that the rotational speed of the thruster is gradually increased to attempt to combat the loss of performance of the thruster as the forward speed increases. In this case the entire depth control force is being generated directly by the tunnel thruster.

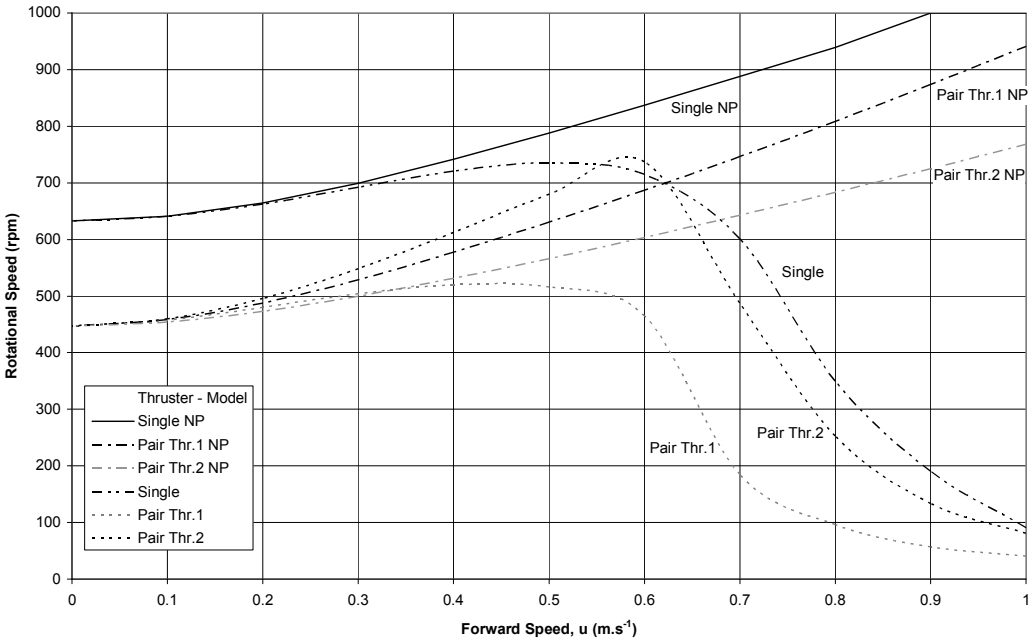

Figure 5.5 – Variation of Thruster Rotational Speed for Tunnel Thruster Depth Control as a function of Forward Speed

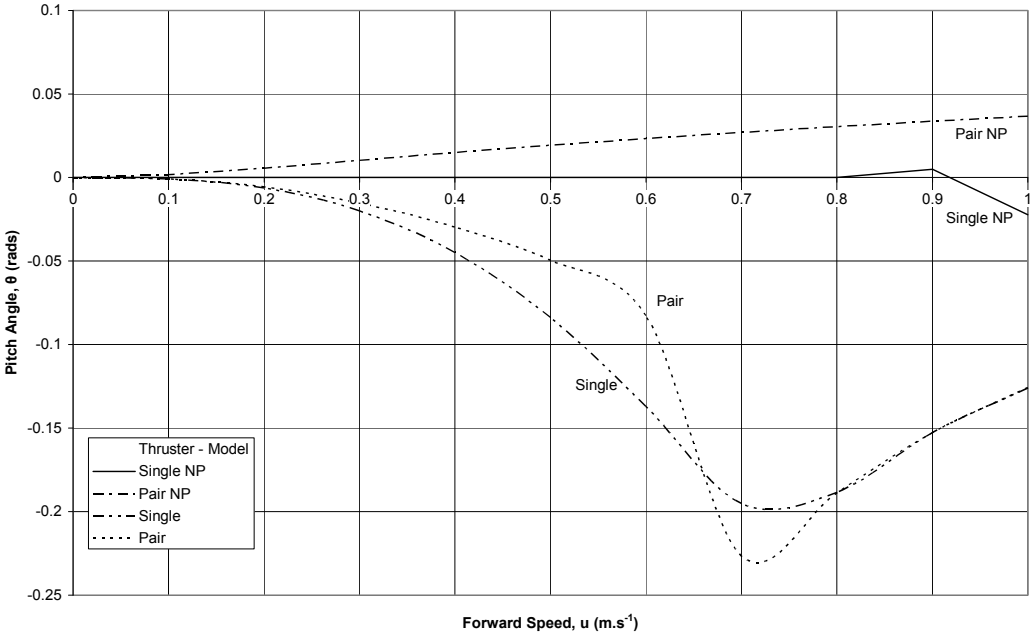

Figure 5.6 – Variation of Pitch for Tunnel Thruster Depth Control as a function of Forward Speed

When the single thruster is considered with the pitch moment included (Single), noting that the controller has no direct control over the pitch angle, the pitch angle increases up to a forward speed of approximately 0.7m.s^{-1}. This is caused by the increasing pitch moment induced by the tunnel thruster as the forward speed (speed ratio) increases. The rotational speed of the thruster is gradually increased up to a forward speed of approximately 0.6m.s^{-1}. Thereafter the rotational speed begins to decrease.

In the speed range between 0.4ms^{-1} and 0.8m.s^{-1} there is an interchange of the dominant depth control force from the tunnel thruster force to the hydrodynamic force generated by the vehicle, see Figure 5.7. Essentially, as the vehicle speed increases, the pitch moment generated by the tunnel thruster induces a nose down pitch angle. This nose down pitch angle causes the vehicle to generate a hydrodynamic control force and when this force becomes sufficient to maintain the depth of the vehicle, the load on the tunnel thruster is decreased. The thruster load and required pitch angle continue to decrease as the speed increases beyond 0.7m.s^{-1}. By 0.8m.s^{-1} the tunnel thruster is effectively producing no useful control force and is solely inducing a pitching moment to control the depth of the vehicle in a survey-style manner.

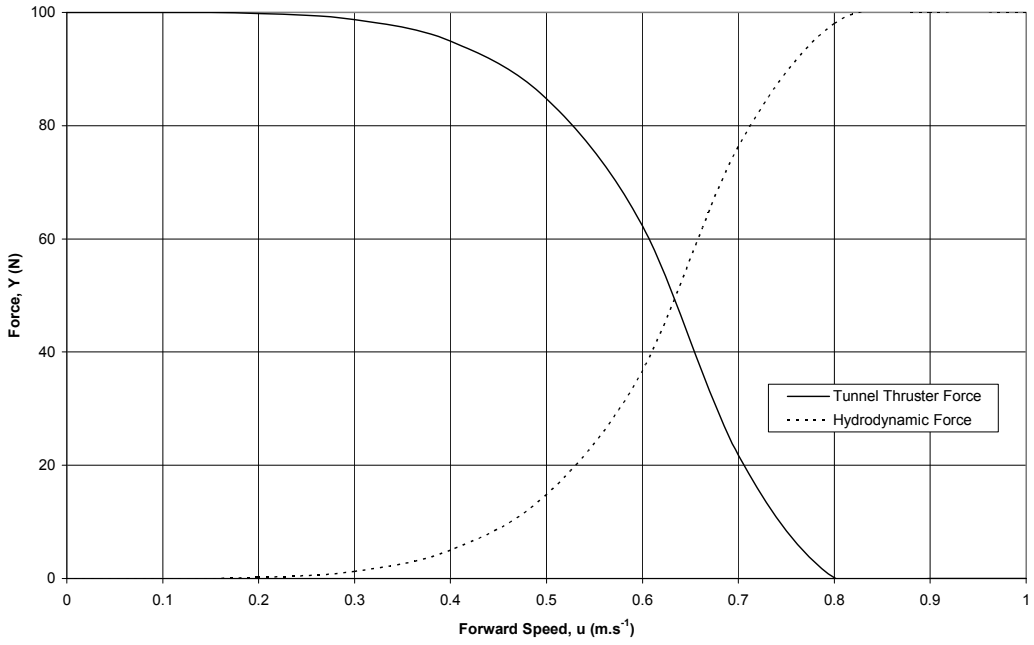

Figure 5.7 – Variation of Forces in the Vertical Plane for Single Tunnel Thruster Depth Control as a function of Forward Speed

When the thruster pair is considered with the pitch moment included (Pair) the pitch angle increases at a slower rate than for the 'Single' thruster case. This is due to the conflicting influences of the pitching moments induced by the forward and aft thrusters. The differences

are caused by the differing variations in the forces generated by the forward and aft thrusters and the differing centres of action for the induced suction forces. The controller has no knowledge of this differing performance other than through the response of the vehicle to control demands. At a forward speed of $0.6m.s^{-1}$ the centre of action of the forward thruster suction force moves past the centre of the vehicle. The suction force now adds to the nose down pitch moment of the aft thruster, as predicted by the tunnel thruster model (see Equation (4.47)). Hence the large increase in pitch angle after $0.6m.s^{-1}$, with a corresponding increase in hydrodynamic force evidenced by a relaxation of the thruster load (similar to that shown in Figure 5.7 for the single thruster). The interchange between the control methods is complete at the minimum point on the pitch curve and from this point forward the thrusters are solely inducing a pitch moment to maintain the required angle for constant depth operation.

It should be recalled that the tunnel thruster controller for the pair of thrusters is set to aim for a pitch angle of zero. Hence in the simulations for the thruster pair without the pitch moment included (Pair NP), the AUV performs in a similar manner to the single thruster without pitch moment. The form of the pitch controller (Equation (5.8)) gives a steady state pitch error, which is positive due to the differing reductions in performance of the forward and aft thrusters. Note that the maximum rotational speed of the thrusters is not reached by $1.0m.s^{-1}$ indicating that depth control can continue into the survey speed range. In fact, to maintain depth the thrusters are producing a force greater than the positive buoyancy due to the necessity to overcome the sum of the positive buoyancy force and the hydrodynamic force generated by operating with a nose-up pitch angle.

For the thruster pair case with the pitch moment included the best solution, in terms of minimising thruster use (energy) was found by relaxing the pitch control (reducing G in Equation (5.8)) so that the pitch control is dominated by the thruster induced pitch moment. This allows the vehicle to pitch nose down and consequently generate a hydrodynamic depth control force and thus reduce the load on the thrusters. Increasing the gain on the pitch control reduced the pitch angle towards the desired value of zero (and reduces the steady state pitch error) but serves only to increase the thruster load required.

To achieve the results shown in Figures 5.5 and 5.6 required fortuitous thruster selection in terms of the thrust density selected for the speed range and required forces, to allow the depth control to be undertaken using the hydrodynamic control force. To ensure the validity of the results presented a check was made on the range of speed ratio utilised to give the performance illustrated. When the majority of the depth control force is provided by the

tunnel thruster the speed ratio is always within the bounds of the experimental results detailed in Section 4.5.4. However, when the tunnel thruster is used in a pseudo-survey-style depth control approach, that is, when the thruster is not generating a considerable proportion of the depth control force, but is inducing a moment that sets a nose-down pitch angle, the range of speed ratio used exceeds the bounds of the experimental results. That is, these simulations extrapolate the experimental results in the manner predicted by the modelling procedure developed. Consequently these results may not be reliable and such performance may not be achievable in practice. With this uncertainty the low speed depth control must be designed to use the tunnel thruster to generate a depth control force directly. This demonstrates that an interchange between control strategies is required to allow a vehicle to transition from survey-style depth control using control surfaces to low speed depth control using tunnel thrusters.

These results demonstrate that tunnel thrusters (of this size) can provide sufficient control to maintain depth throughout the required low speed range and into the transitional speed range, exceeding the limit of control surface control. The limiting speed for the tunnel thruster, when providing the depth control force directly, is $0.9 m.s^{-1}$ for a single thruster (calculated using the thruster model of Equation (4.45)) and exceeds $1.0 m.s^{-1}$ for the thruster pair. The single tunnel thruster configuration cannot maintain control over the pitch of the vehicle, and consequently, for pitch control a tunnel thruster pair must be used.

5.5.1 Low Speed Depth Control with External Thrusters

Depth control with external thrusters is simpler than for tunnel thrusters as it is assumed that the outflow from the thruster (when working in the vertical plane) will not interact with the vehicle. Therefore the only requirement is to select a thruster that can generate the required forces for the operational conditions. The data in [36] shows that the thrust generated by an external thruster, operating at 90º to the ambient flow, is fairly consistent across the range of advance angle. Therefore this subject will not be given any further attention.

5.6 Transition Phase Control

The previous discussion has shown that tunnel thrusters cannot be used to control the depth of the vehicle throughout the speed range. Furthermore, tunnel thrusters require considerable amounts of energy and, on an energy limited vehicle, their use is to be restricted to situations where they are the only suitable method of control (see Section 5.7.1.1). Hence they will only be used to control the hydrostatic balance during low speed operation, when

the control surfaces can no longer undertake this task, and for hovering. Therefore, for these reasons, an interchange between the methods of controlling the hydrostatic balance as the vehicle goes through the transition phase is required. The interchange is between using the tunnel thrusters to provide the depth control force at low speed and using the control surfaces in a survey-style depth control system at high speed.

5.6.1 Requirements for Transition Phase Control

The transition phase has not previously been investigated in detail in the open literature. Hence there is a lack of established performance standards and requirements. In general, the aim is to maintain a suitable level of depth and pitch control without unnecessarily draining the limited energy supply. It is not expected that mission objectives would be undertaken during this phase and thus exact depth and pitch control would not necessarily be required.

The only published attempts at undertaking a necessary autonomous transition between different control approaches (due to the limitations of the chosen approach) have been made with the Nereus AUV, shown in Figure 5.8 [45]. The Nereus AUV is a hybrid AUV/ROV. In AUV mode, Nereus is primarily used for terrain following and can be used throughout the speed range, including hover. The vehicle is ballasted to be neutrally buoyant and has two hulls, each with a fixed rear propulsor. In between the two hulls there are two control foils, one aft and one central. The central control foil has a thruster attached to it.

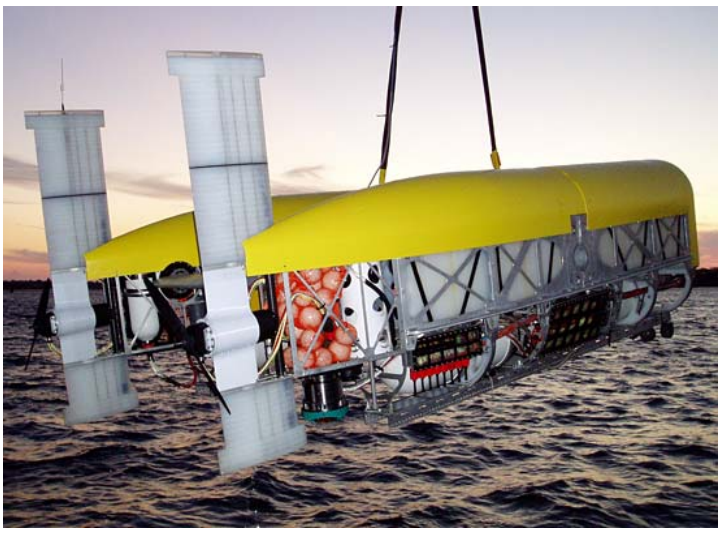

Figure 5.8 – Photograph of the Nereus AUV [45]

A simulation model [45] was developed using results from [119] to demonstrate that Nereus could operate with four modes of changing depth (used as determined by the forward speed range). These are, in increasing order of forward speed, foils fixed hover, vectored thrust

(using the central thruster), zero pitch flight (using the foils to change depth) and zero *w* flight (using the foils to set a pitch angle to change depth) [120]. Nereus is designed to use these different control options as the control surfaces suffer from the same speed limitations as those on Autosub. Thus Nereus needs to switch between the control approaches to undergo the depth changes required for terrain following. Nereus was initially designed to undergo 'discrete switching' between the modes of depth control. One of the aims of the full scale testing of the vehicle was to calibrate the simulation tool to allow investigation of smoother transition approaches between depth change methods, however no results have been published to date [121].

5.6.2 Interchange Control

The aim of this study is to examine the performance of an AUV undertaking the transition phase using various control options; hence a more flexible approach than discrete switching is desired. The approach adopted here uses an interchange function [122] to determine the proportion of the depth control given to each system. This function was developed to allow switching between control strategies. However, it has only been tested in simulations with consistent actuator performance as a function of the operational conditions. For example, variations in tunnel thruster performance as a function of forward speed are not accounted for to simplify the modelling required and due to a lack of available performance data.

The proportion of the depth control given to the thruster (TT) and control surfaces (CS) respectively at time step, *i*, is:

$$\sigma_{i,TT} = 1 - 0.5\left[\tanh\left(\frac{u_i - u^*}{\Delta\sigma}\right) + 1\right]$$

and (5.9)

$$\sigma_{i,CS} = 1 - \sigma_{i,TT}\,.$$

The proportion of the control is determined as a function of the vehicle forward speed and two user-defined parameters, namely, the mid-transition speed, u^*, and the 'steepness' of the transition zone, $\Delta\sigma$. A low value of the 'steepness' parameter gives a step change in the control demand at the mid-transition speed, whereas a high value gives a longer smooth transition (centred about the mid-transition speed). Hence this function provides the flexibility to assess the performance of the vehicle undergoing transition with a range of control options, from discrete switching to much smoother interchanges. The depth error is factored by the proportion of the control for each system and is sent to the individual controllers.

5.6.3 Modifications to the Depth Control Block

The original depth control block has now been split into two parts, namely, a tunnel thruster control module and a control surface control module. They have joint control over depth. The simulations will initially be undertaken using a single centrally mounted tunnel thruster. Therefore the control surface control module will retain the pitch control elements of the original depth control block.

The structure of the two controllers is the same as outlined previously, however, the integral terms are modified with a variable gain and a reset function. The integral gain is factored by the result of the interchange function, Equation (5.9), to increase or decrease the amount of integral control used depending on the speed of the vehicle. The integrator reset is activated by the vehicle speed becoming higher than the upper limit (for the tunnel thruster) or lower than the lower limit (for the control surfaces) of the transition zone.

5.7 Transition Simulations

The performance of the AUV during the transition phase was investigated using the simulation tool. Initially these investigations were undertaken using the single centrally mounted tunnel thruster without the pitch moment included. The simulations have been undertaken at five different decelerations, with five different values of the transition 'steepness' and eight different values of the mid-transition speed. The decelerations used were chosen to represent gradual flight-path-style transition phases and the mid-transition speeds are chosen to cover the entire range of operability for the control surfaces. The specific values used are given in Table 5.1.

Table 5.1 – Control Variables for Transition Simulations

Deceleration	**Steepness**	**Mid-Transition Speed**
($m.s^{-2}$)	**$\Delta\sigma$**	**u^*** ($m.s^{-1}$)
0.005	0.01	0.5
0.0075	0.10	0.5625
0.01	0.15	0.625
0.0125	0.20	0.75
0.015	0.30	0.875
		1.0
		1.125
		1.25

The results of the simulations have been analysed in two different ways. Firstly, the ability of the vehicle to control itself has been assessed by examining the variations in depth and pitch. Secondly, the amount of energy required for the different approaches has been calculated. Energy is chosen as a measure of the performance, as this is a key factor for an energy limited vehicle and hence an understanding of the impact of control approaches is necessary.

To calculate the energy it is necessary to define the limits for the calculation. The start point is simple, that is, the point at which the vehicle begins to slow down. The end point is less well defined. The choice is based upon whether (a) the transition period is considered to end at a common point in time, regardless of the intervening events, or, (b) the transition period ends when the vehicle reaches a steady state hovering condition. The latter will inevitably be a function of how the transition is undertaken and will be different for each simulation. Both of these conditions were examined and the results are discussed next.

Here option (a) was implemented as the latest time, of the entire set, for the steady state hovering condition (zero forward speed) to be achieved during a set of simulations. Option (b) is taken as the time in an individual simulation when the steady state hovering condition is achieved. The hovering condition is assumed to have been achieved when the AUV is within a certain distance of the target depth, arbitrarily set at ±2cm. A 'set of simulations' is defined as those runs with a common level of deceleration and steepness, that is, only mid-transition speed is variable.

The energy required by the thruster is calculated by numerically integrating the power drawn over the time period selected according to option (a) or (b). The thrust, F_T, is calculated in accordance with Equation (4.44) and is converted to thruster power using the momentum theory based relationship [10]:

$$P = \frac{F_T^{3/2}}{2\tau^{3/2}\sqrt{\rho A}}. \tag{5.10}$$

Here τ is a measure of the performance of the thruster, compared to an ideal thruster, taken to be 0.55 using a review of available commercial thruster performance and surface vessel bow thruster data [91]. That is, the required energy is given by:

$$E = \sum_{i=1}^{\kappa} \frac{\left(K_3\left(\frac{n_i + n_{i-1}}{2}\right)^2\right)^{3/2}}{2\tau^{3/2}\sqrt{\rho A}}\left(t_i - t_{i-1}\right). \tag{5.11}$$

κ is a counter corresponding to the number of time steps required to reach the end of the transition zone.

5.7.1 Transition with a Single Tunnel Thruster without Pitch Moment Effects

Figures 5.9 and 5.10 provide depth time histories and their variation with mid-transition speed and steepness for the vehicle undergoing transition with a deceleration of $0.01 m.s^{-2}$. The simulation starts with the vehicle travelling at $1.5 m.s^{-1}$ and the deceleration starts at t = 200s with zero forward speed being reached at approximately t = 350s. The variations in depth up to t = 200s illustrate the initialisation period for the simulation. Figure 5.9 also shows an example of the typical variation in forward speed during the transition phase. The form of the forward speed variation is a function of the variation in pitch angle which slows the rate of loss of speed around the mid-transition speed (in the case shown $u^* = 0.5 m.s^{-1}$).

These figures show that the depth change is more sensitive to mid-transition speed (u^*) than steepness ($\Delta\sigma$). In general the depth changes are small in magnitude (relative to the size of the vehicle) and larger for lower mid-transition speeds and smoother transitions. These depth changes are not expected to be a problem unless the transition zone is undertaken in restricted waters or this zone coincides with other depth sensitive mission operations. It should be noted that the illustrated changes in depth show the vehicle rising which is usually safer than descending in the underwater environment.

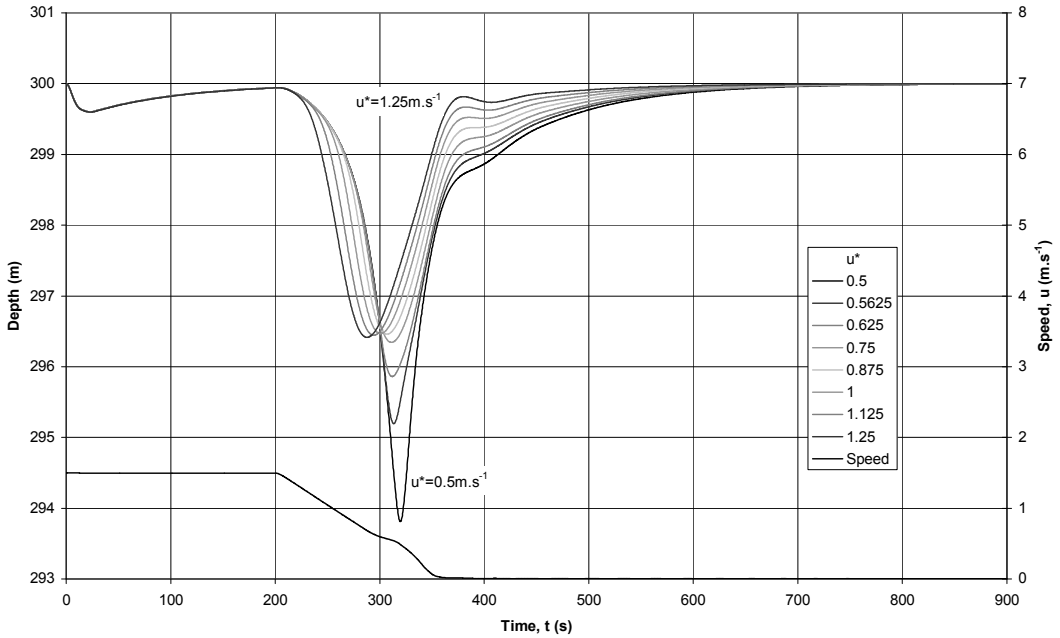

Figure 5.9 – Depth Time History for Fixed $\Delta\sigma = 0.1$ and Variable u^* using a Single Tunnel Thruster

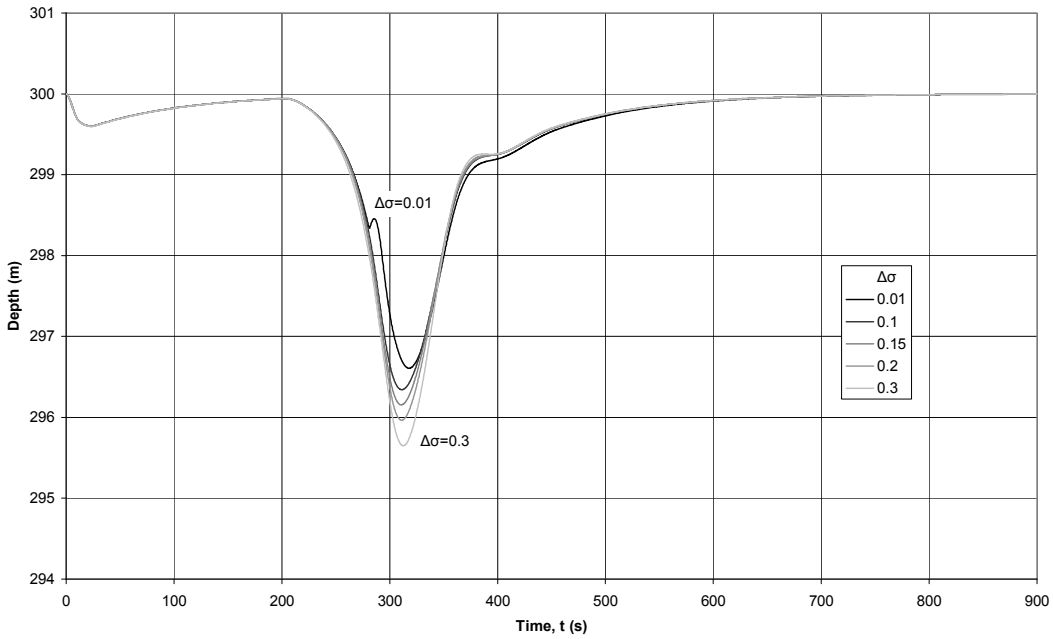

Figure 5.10 – Depth Time History for Fixed $u^* = 0.75 m.s^{-1}$ and Variable $\Delta\sigma$ using a Single Tunnel Thruster

Figures 5.11 and 5.12 show the pitch time histories for the same simulations. These figures yield similar conclusions to the depth time histories, with a much greater dependence on mid-transition speed and larger pitch changes for lower mid-transition speeds. However, a smoother transition gives a smaller pitch change. Once the pitch change has been recovered from the initial speed reduction all the simulations show small amplitude pitch oscillations that continue into the steady state hovering operation. The amplitude of the oscillations is generally lower with higher mid-transition speeds. The continued oscillations in pitch once the hovering condition is achieved are due to the numerical procedure used and would be damped out more rapidly on a real vehicle.

Examining the results presented, and those for the other decelerations, shows that in order to maintain control over pitch, that is, to ensure a smooth variation in pitch and reduce the pitch oscillations, the transition zone should be taken slowly and with a high mid-transition speed. In effect this approach allows the control surfaces a certain length of time (while the majority of the depth control is undertaken by the tunnel thruster) when the forward speed is high enough so that the pitch fluctuations can be successfully controlled.

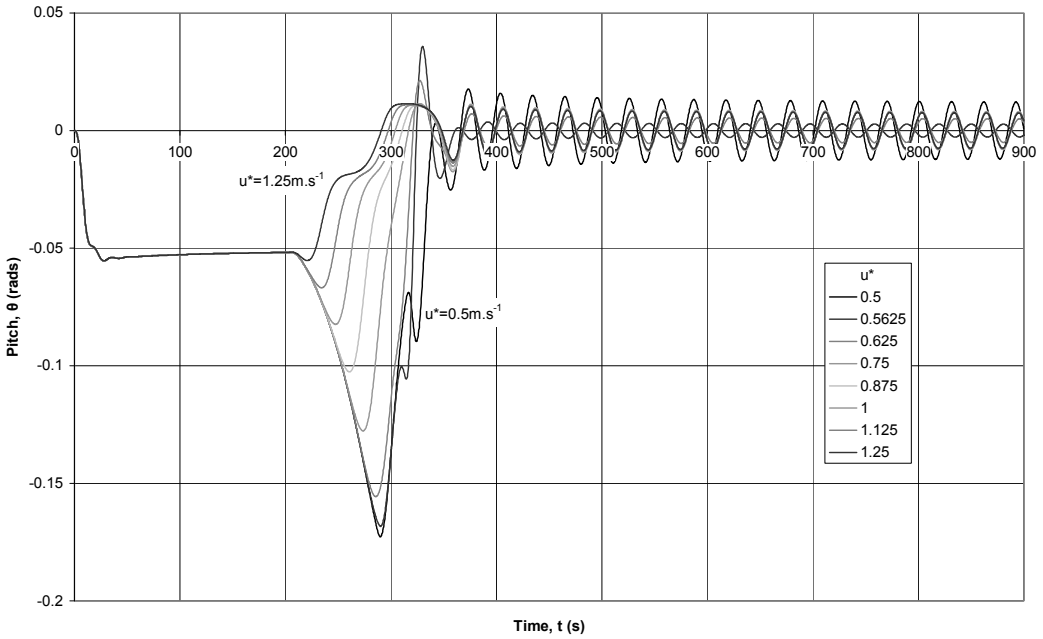

Figure 5.11 – Pitch Time History for Fixed $\Delta\sigma = 0.1$ and Variable u^* using a Single Tunnel Thruster

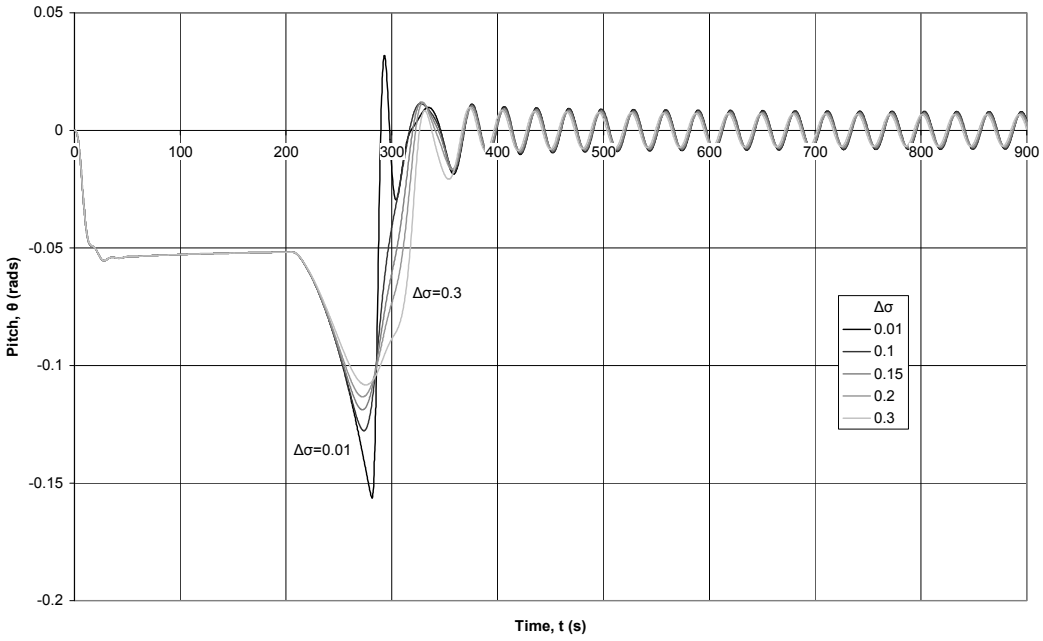

Figure 5.12 – Pitch Time History for Fixed $u^* = 0.75\text{m.s}^{-1}$ and Variable $\Delta\sigma$ using a Single Tunnel Thruster

Examination of the depth, pitch, thruster rotational speed and control surface deflection time histories across the cited range of decelerations show variations are greater according to the length of time spent at a particular speed rather than the rate of change of speed. That is, the lower decelerations mean a greater time at each speed and hence the overall depth and pitch changes are the largest, but these changes are then recovered at a higher speed than for higher deceleration rates.

5.7.1.1 Variation of Energy Requirements

A representative set of calculated energy results are presented in Figures 5.13 and 5.14 for a deceleration of $0.01 m.s^{-2}$, for calculation options (a) and (b) respectively. To place the energy required by the transition phase in context, the propulsion power required to propel the vehicle at $1.5 m.s^{-1}$ is 373W.

Both Figures 5.13 and 5.14 show that the steepest transition ($\Delta\sigma = 0.01$) is the most costly approach in terms of energy consumption. Investigation of the time histories of the thruster rotational speed allows identification of the higher energy levels to be attributed to the sudden jump in demand on the tunnel thruster. Both figures also show that there is little difference caused by variation of the steepness parameter. Figure 5.14 shows that there is little variation between the energy required across the range of mid-transition speeds when the individual transition periods are considered. If a global transition period (option (a)) is considered then there is a minimum energy point around $0.55 m.s^{-1}$ as shown in Figure 5.13. The differences between the two figures illustrate the amount of energy that would be used in waiting for the global transition period to end. One reason that the transition energy is fairly flat in Figure 5.14 is that it is easier to achieve transition at higher speeds, in terms of the magnitude of the depth change to correct, but the interaction of the thruster jet with the higher speed flow means the thruster requires more energy to control the vehicle.

A series of tests was undertaken to investigate the dependency of the energy on the force required, that is, by how much the vehicle is positively ballasted. The results of this set of simulations (for positive buoyancy varying from 0.15% to 0.6%) found little variation in the general form of the energy results on the force required.

The conclusion from these simulations is that there is little variation in the required energy and thus the transition zone control parameters should be selected on a basis of the levels of controllability required. To maintain controllability the transition zone should be taken slowly with a high mid-transition speed.

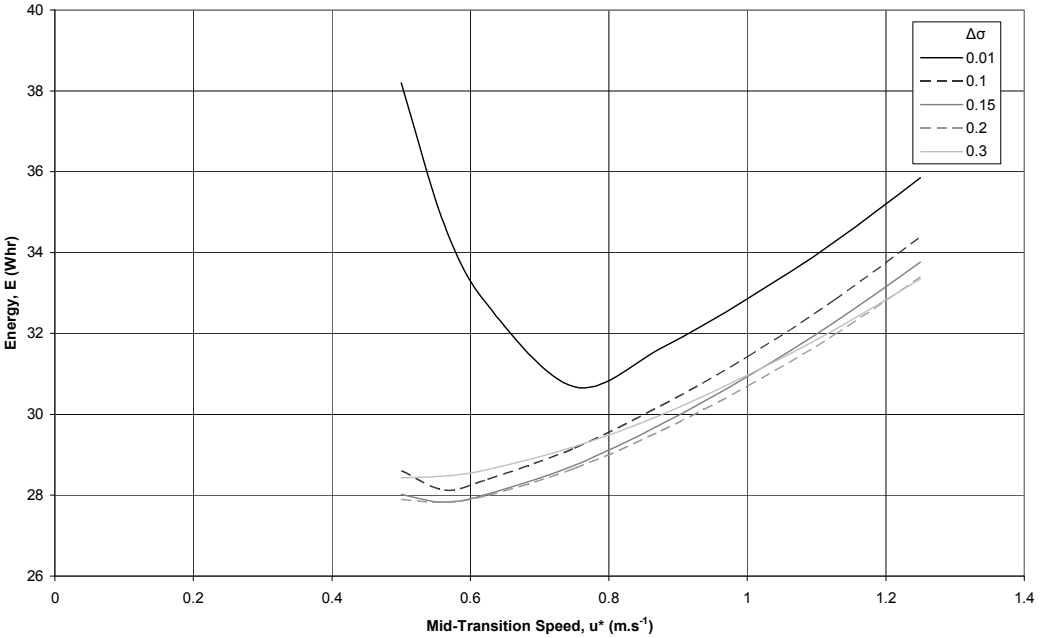

Figure 5.13 – Energy Calculation Results using Option (a) for the Transition Phase using a Single Tunnel Thruster

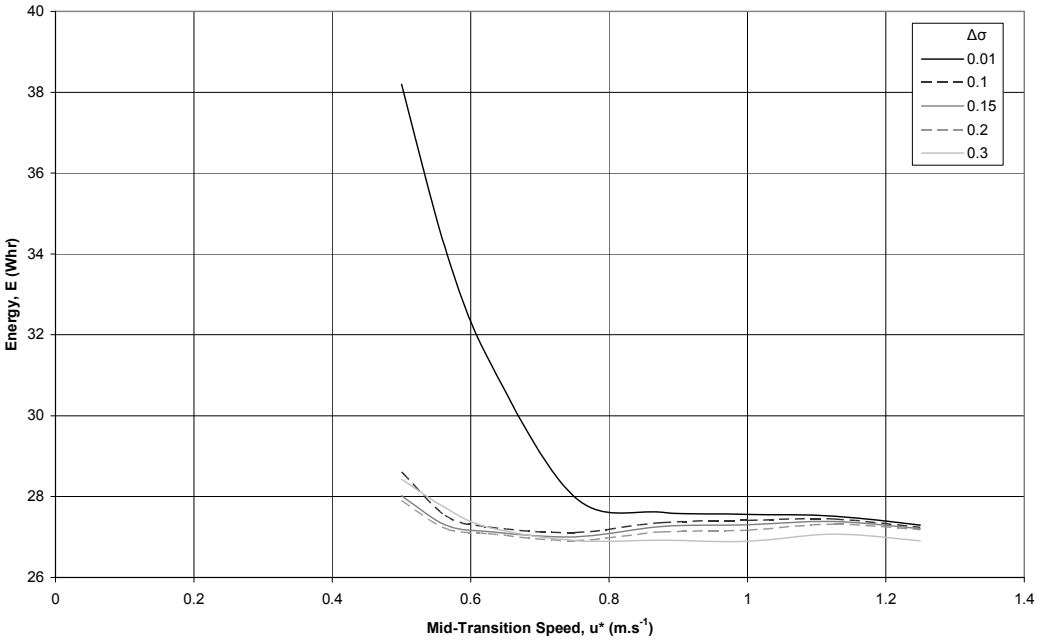

Figure 5.14 – Energy Calculation Results using Option (b) for the Transition Phase using a Single Tunnel Thruster

The steepness of the transition zone does not have a large impact provided a step change (discrete switch) is avoided. However, larger values of steepness increase the speed range included in the transition zone. Hence the steepness value selected may be influenced by a desire to have a small transition zone to simplify the overall control and enlarge the operating range of the AUV.

5.7.2 Transition with a Single Tunnel Thruster with Pitch Moment Effects

The simulation tool will now be used with the single tunnel thruster configuration and inclusion of the pitch moment caused by the thruster generated suction forces. Simulations were undertaken across the full range of mid-transition speeds and transition steepness at one deceleration, namely, $0.01 m.s^{-2}$. No alterations were made to the control strategy used. The depth profiles, see Figure 5.15, show a reduced depth change with a more consistent return to the target depth across the range of mid-transition speeds.

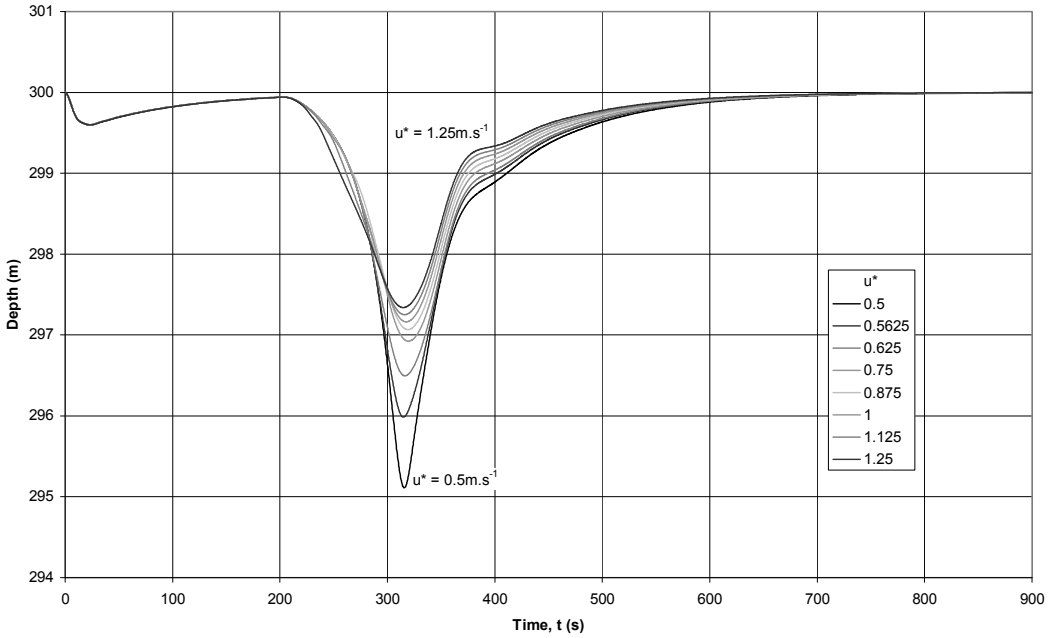

Figure 5.15 – Depth Time History for Fixed $\Delta\sigma = 0.1$ and Variable u^* including Pitch Moment Effects

The pitch variations, see Figure 5.16, show a larger maximum pitch angle with a longer time spent with a larger negative pitch angle caused by the suction moment generated. The pitch oscillations still occur, but have a more consistent magnitude that is approximately equal to the average magnitude from the simulations without the suction moment included.

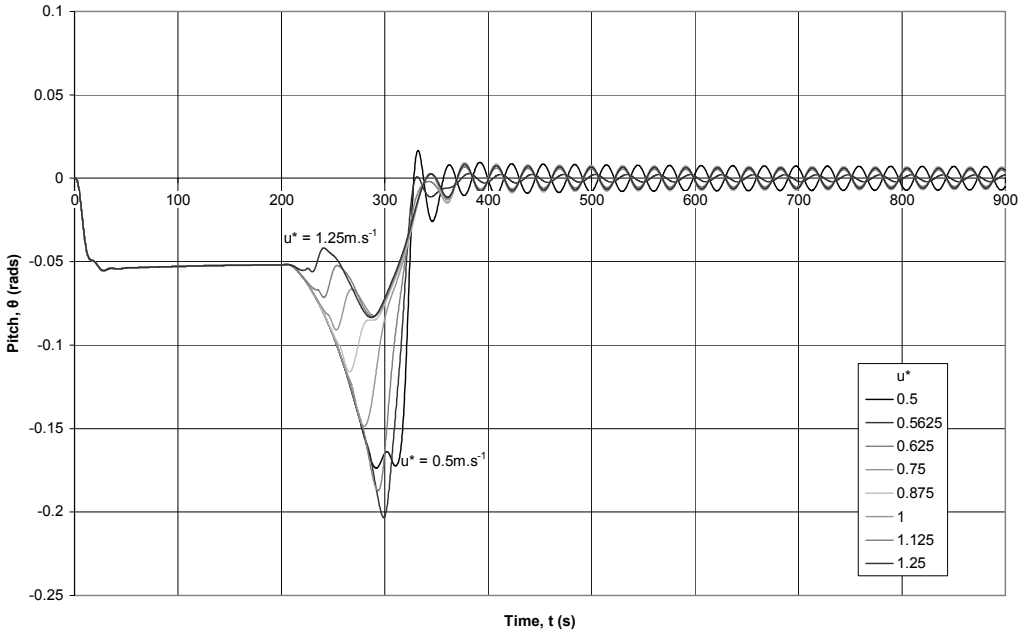

Figure 5.16 – Pitch Time History for Fixed $\Delta\sigma = 0.1$ and Variable u^* including Pitch Moment Effects

The energy variations, see Figure 5.17, show an overall decrease in energy usage attributable to the increased pitch angles and the smaller depth changes, meaning the thruster is required to do less work. The shape of the energy variations is altered with a decrease in the energy for higher mid-transition speeds (using both calculation approaches) showing that there may be a small energy benefit to transitioning at higher speeds. This can be attributed to the assistance to the control surfaces provided by the thruster induced pitch moment. It should be noted that the speed ratios used here are within the bounds of the earlier reported experimental results, excepting the initial short acceleration (start up) phase for the thruster.

The overall conclusion from these simulations is that the thruster induced pitch moment can have quite a substantial effect by inducing large pitch angles. However, in this case, these pitch angles benefit the operation of the vehicle and this is shown in an overall reduced energy cost. These conclusions concur with those from the tunnel thruster depth control tests described in Section 5.5.

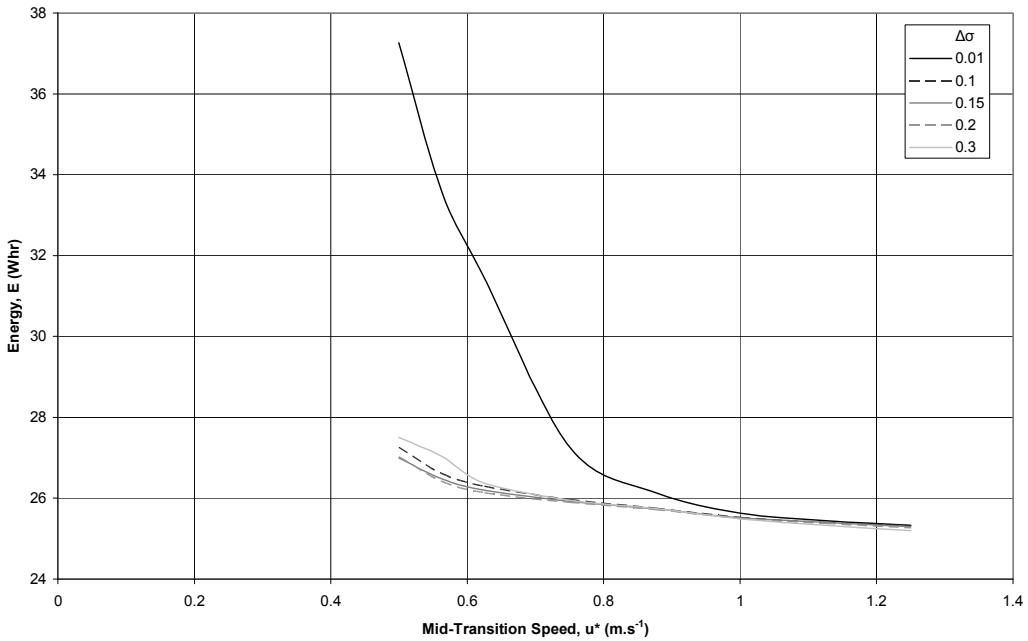

Figure 5.17 – Energy Calculation Results using Option (b) for the Transition Phase including Pitch Moment Effects

5.7.3 Transition with a Single Tunnel Thruster with No Hydrodynamic Effects

Having considered the transition phase with a single thruster and two different modelling approaches, an interesting comparison can be made by assuming that there are no hydrodynamic effects. These simulations allow a comparison to be made which demonstrates the importance of accurate actuator modelling. In these simulations the thruster produces a force that is proportional to the square of the rotational speed, simply that in accordance with Equation (4.44). The depth profiles across the range of mid-transition speeds are shown in Figure 5.18.

These depth profiles show smaller depth changes than for the simulations without the pitch moment. In comparison with the simulations including the pitch moment, these simulations show slightly larger overall depth changes for the low mid-transition speeds and slightly smaller overall depth changes for the higher mid-transition speeds. This highlights the beneficial effect of the pitch moment on the transition phase.

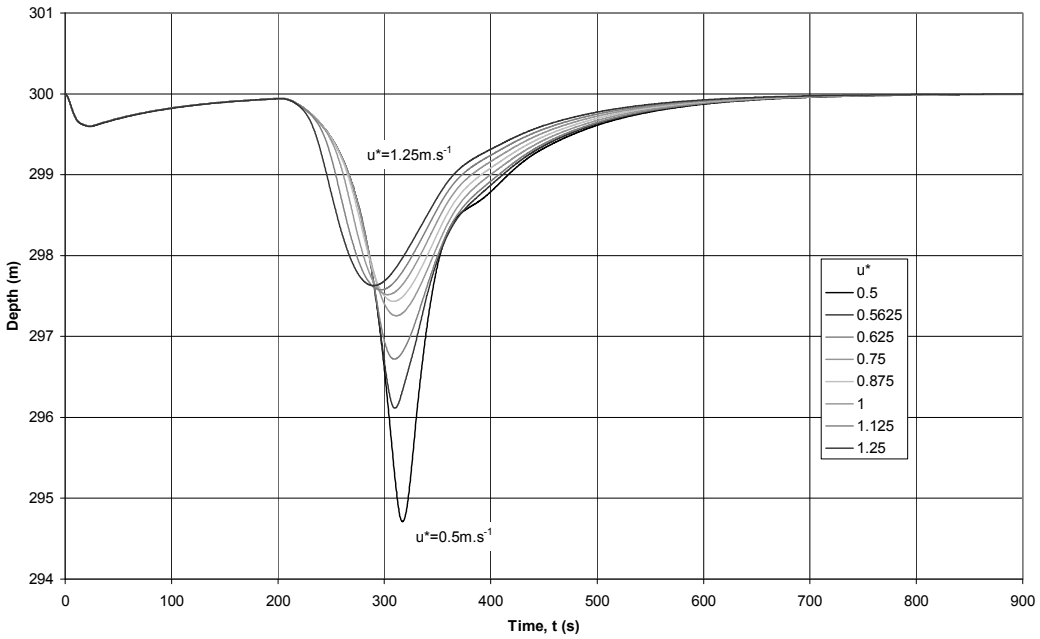

Figure 5.18 – Depth Time History for Fixed $\Delta\sigma = 0.1$ and Variable u^* without Hydrodynamic Effects

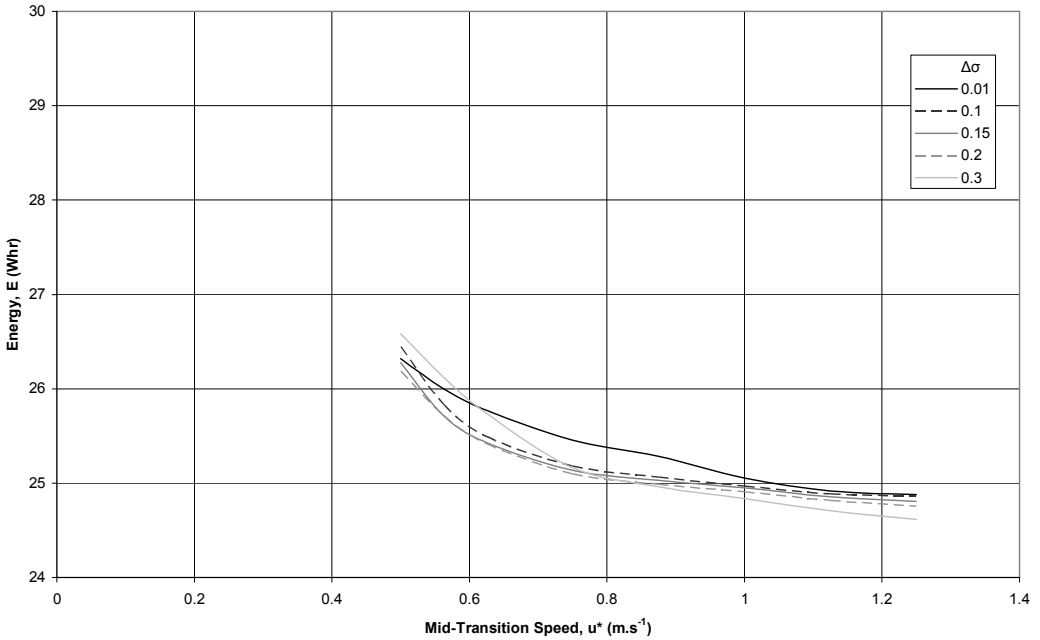

Figure 5.19 – Energy Calculation Results using Option (a) for the Transition Phase without Hydrodynamic Effects

With respect to the energy required to undertake the transition phase, the simulations without the hydrodynamic effects show small decreases in energy requirement compared to the previous simulations with and without the pitch moment, see Figure 5.19. The trends in the required energy are similar to the simulations with the pitch moment, showing a small gradual decrease in required energy with increasing mid-transition speed. These results also agree with the high mid-transition speed results from the earlier simulations, which showed little difference between the results for $\Delta\sigma = 0.01$ and other transition steepness values.

5.7.4 Transition with a Tunnel Thruster Pair

The simulation tool will now be used to evaluate the transition performance of the AUV with a tunnel thruster pair. This configuration allows control of the vehicle pitch to be maintained throughout the speed range. A key focus of this analysis so far has been the energy requirements for the transition phase. Manipulations of Equation (5.10) show that the energy used by two tunnel thrusters of the same diameter as the single tunnel thruster is a factor of $(1/\sqrt{2})$ less than that required by a single tunnel thruster. The diameter of the tunnel thrusters would need to be reduced by the same factor for the energy required by both approaches to be the same. However, these requirements may not be practical in terms of the available locations and space onboard the vehicle.

A complete set of simulations at a deceleration of $0.01 m.s^{-2}$ were run for this configuration with the complete model including suction induced pitch effects. The results showed a depth change similar in magnitude to that for the single tunnel thruster (without pitch moment), see Figure 5.20, but with a more consistent return to the target depth, as found when including the pitch moment.

The pitch curves are consistent across the range of mid-transition speeds and show a fairly large pitch angle followed by a rapid recovery to zero pitch with significantly reduced oscillations. Figure 5.21 shows a comparison of the pitch variations for the single tunnel thruster with and without the pitch moment and the tunnel thruster pair. This illustrates the large pitch angle experienced with the thruster pair and the significant reduction in the oscillations. The thruster pair curve has a non-smooth nature due to the simplicity of the thruster controller used in this complex situation. (A simple controller was used to ensure that the mechanisms influencing the vehicle response could be easily identified and were not masked by the controller.)

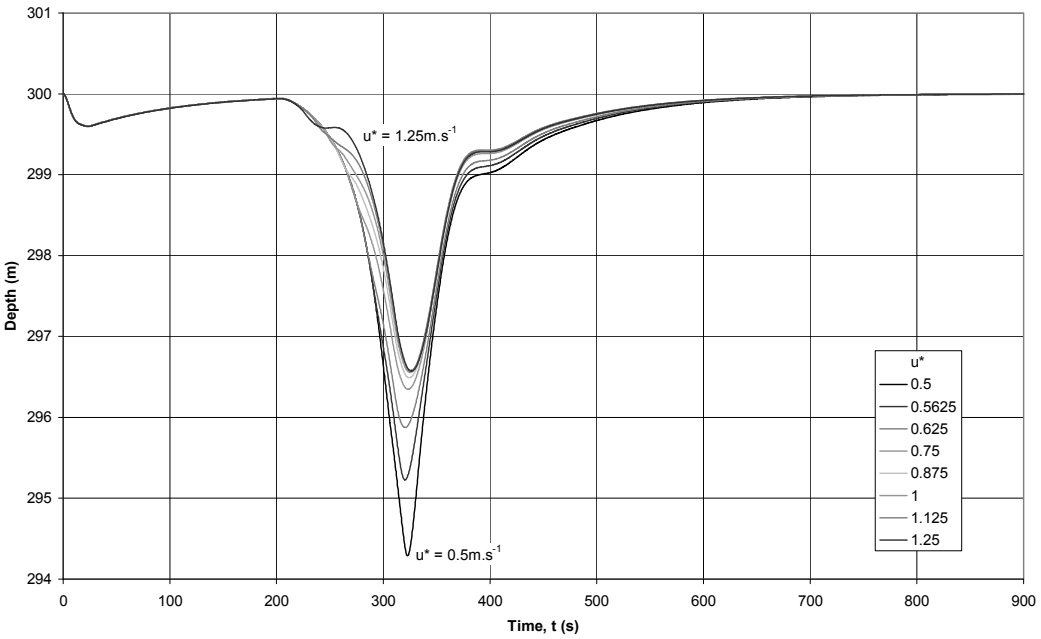

Figure 5.20 – Depth Time History for Fixed $\Delta\sigma = 0.1$ and Variable u^* using a Tunnel Thruster Pair

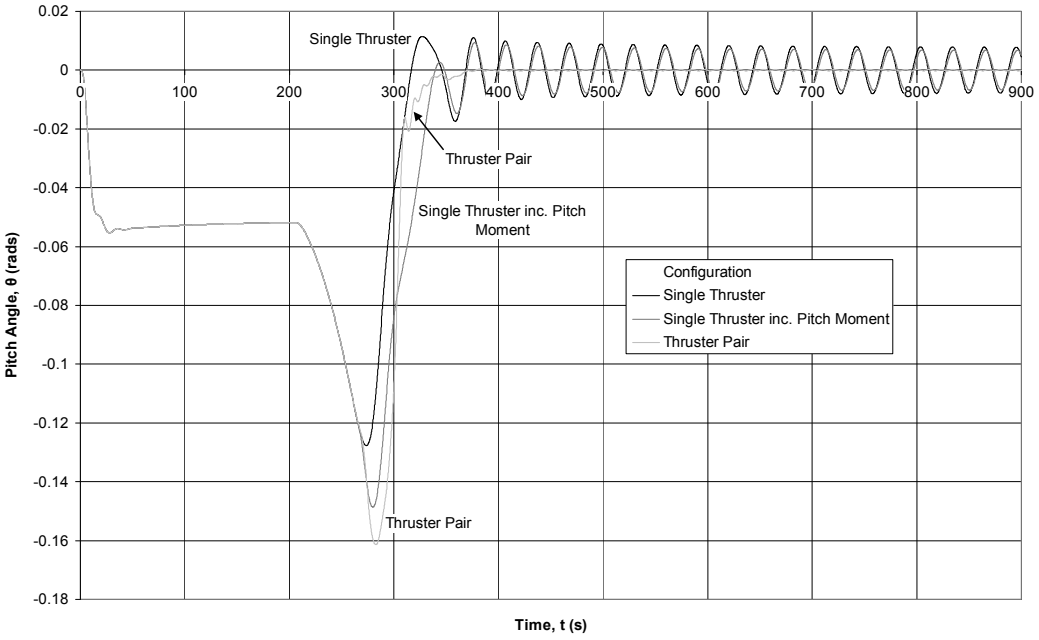

Figure 5.21 – Comparison of Pitch Time History for the Transition Phase using a Single Thruster, a Single Thruster including Pitch Moment Effects and a Thruster Pair

The energy cost is similar in shape to the results for the single thruster when including the pitch moments, compare Figure 5.17 with Figure 5.22. The energy magnitude is much reduced, but in line with that predicted by the manipulations of Equation (5.10), that is, reduced by a factor of approximately $(1/\sqrt{2})$. Overall these simulations demonstrate the ability of the selected approach to maintain the controllability of the AUV using a pair of tunnel thrusters to provide pitch control.

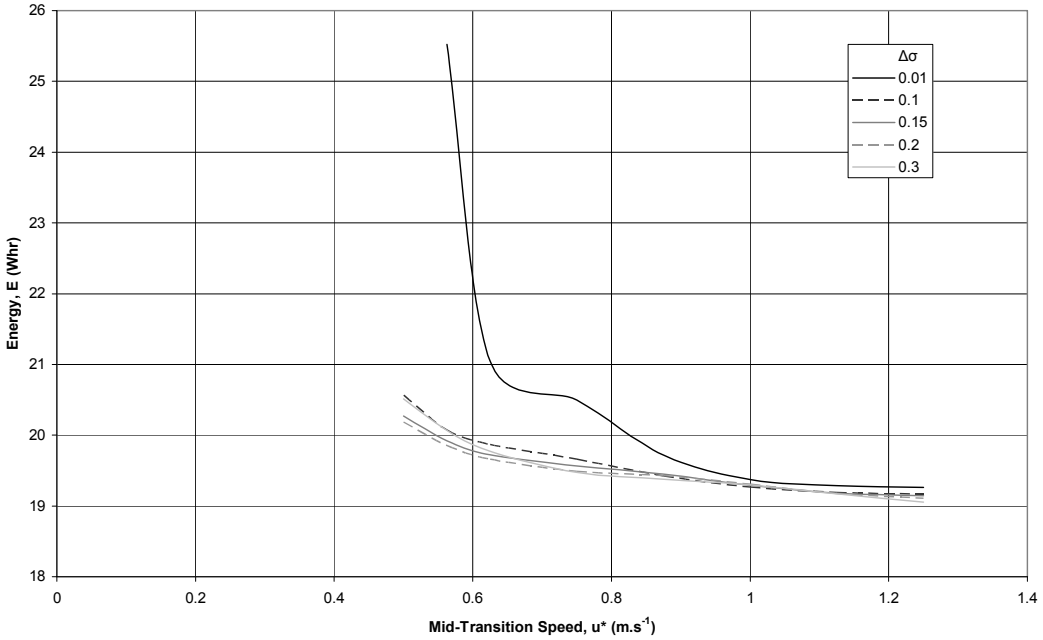

Figure 5.22 – Energy Calculation Results using Option (b) for the Transition Phase using a Tunnel Thruster Pair

5.7.5 The Transition Phase from Low Speed to Survey Speed

The preceding discussions on the transition phase for an AUV have focussed on the transition from survey speed operation to low speed operation. Obviously for the AUV to complete a mission similar to that discussed in Section 3.2 there will be a second transition phase – the transition from low speed operation to survey speed operation. The simulation was used to investigate the performance of the AUV during this acceleration phase. Simulations were performed across the range of mid-transition speeds at an acceleration of $0.01 m.s^{-2}$ with the steepness held constant at 0.1. The transition starts at t = 500s and survey speed is reached at approximately t = 650s. The vehicle was tested in the single tunnel thruster configuration both with and without the contributions caused by the pitch moment induced by the thruster. The depth profiles from the sets of simulations are shown in Figures 5.23 and 5.24. Within the first 500s, since initially the thruster rotational speed is zero, the

depth changes are a consequence of the controller matching the desired low speed operation at $u = 0.1\text{m.s}^{-1}$.

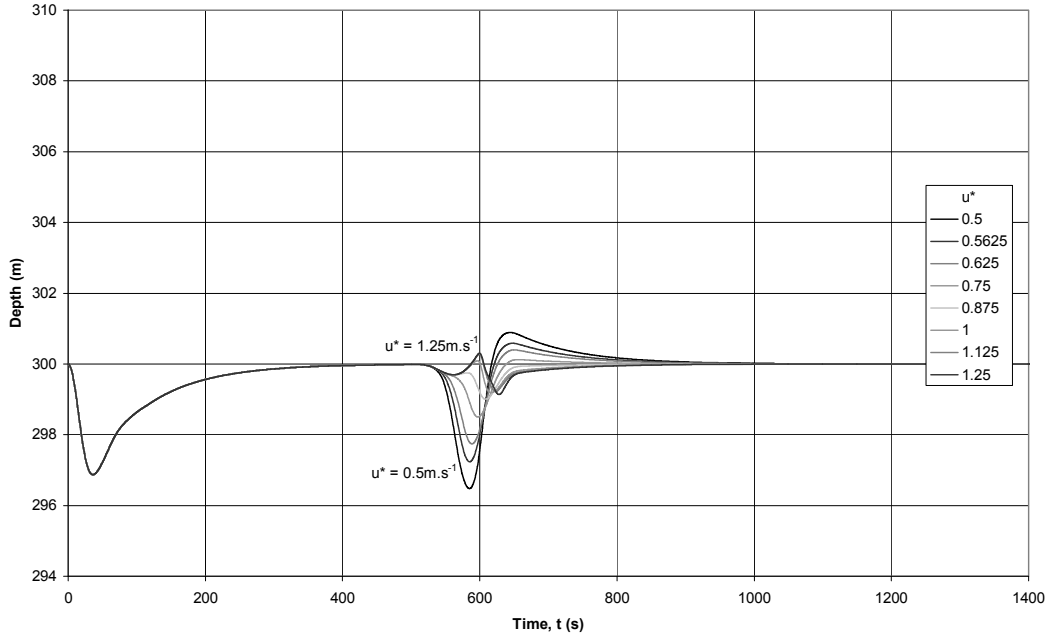

Figure 5.23 – Time History of Depth during the Transition Phase from Low Speed to Survey Speed without Pitch Moment Effects

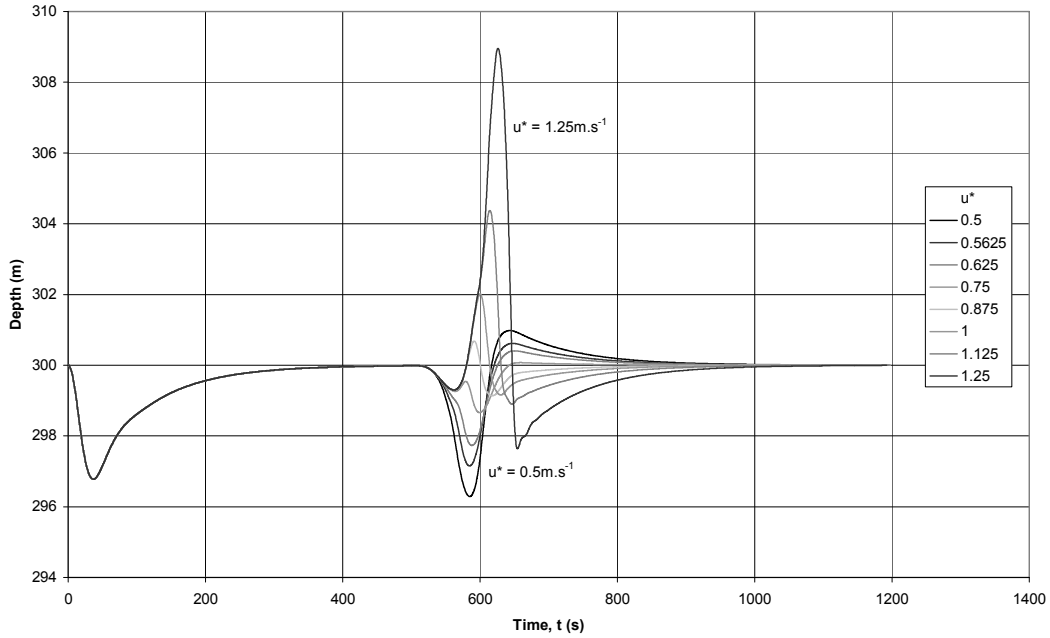

Figure 5.24 – Time History of Depth during the Transition Phase from Low Speed to Survey Speed including Pitch Moment Effects

The simulations without the pitch moment show initial changes in depth as the tunnel thruster begins to lose effectiveness. The depth changes are the largest for the lower mid-transition speeds where the control surfaces are not able to provide the required forces to set a pitch angle. Eventually the control surfaces begin to be able to control the depth and return the vehicle to the desired depth (with an overshoot). At the higher mid-transition speeds there is still an initial loss of depth before the tunnel thruster recovers this loss of control prior to interchanging control with the control surfaces. The higher mid-transition speeds show much lower overall changes in depth compared to the lower speeds.

The simulations that include the pitch moment show similar results for the low mid-transition speeds but a notable difference for the higher speeds. Here the vehicle gains in depth due to the pitch moment induced by the tunnel thruster before the interchange in the control allows the control surfaces to return the depth to the desired value. As for the initial depth control studies the pitch moment generated is a function of the speed ratio and, at the higher mid-transition speeds, the speed ratio is unrealistically high. Thus the results for the pitch moment can only be considered reliable for the low to mid-range mid-transition speeds (up to $u^* = 1.0 \text{m.s}^{-1}$).

These conclusions are backed up by the pitch variations and the thruster rotational speed variations. The acceleration phase using a pair of tunnel thrusters is well controlled due to the control over pitch available throughout the speed range. These results show that this simple control system can control the vehicle through both parts of the transition phase, that is, the transition from survey speed operation to low speed operation and vice versa. Given the possibility that the vehicle may descend during the transition phase it is advised that the vehicle is well above the seafloor before undertaking this manoeuvre to ensure the safety of the vehicle.

5.7.6 Selection of Transition Phase Parameters

The simulations have demonstrated that sufficient levels of controllability can be maintained using tunnel thrusters with the control approach described. The control interchange approach adopted provides the operator with the freedom to select the speed range included within, and the form of, the transition phase. The mid-transition speed is likely to be selected on a basis of mission objectives, since it is not advisable to undertake key mission objectives whilst operating in the transition phase. The steepness is likely to be selected as a compromise between having a smoother transition, which reduces the energy cost and

improves controllability, versus the desire to use a lower steepness to reduce the extent, in terms of speed range, of the transition zone.

5.8 Performance Enhancement

During the transition phase, the AUV consumes a considerable amount of energy to maintain control over the depth and pitch. For the single tunnel thruster example considered, the energy required for the vehicle to hover is equivalent to the propulsion power required to propel the vehicle at $1.2 m.s^{-1}$ (using a simplified estimate of propulsion power [123]). Whilst undertaking the transition phase the power load required by the tunnel thruster is higher than the hovering load due to the increased forces required to overcome the depth change and the loss of effectiveness of the tunnel thruster at higher forward speeds. This high power load leads to an increased interest in reducing the use or the energy requirement of the tunnel thrusters. A few options will be discussed next, including a practical approach and an examination of the thruster design features.

5.8.1 Dive First

A large component of the power requirement is attributable to the power needed to overcome the depth error induced by the loss of performance of the control surfaces (when decelerating). This gives a wide range of required thruster rotational speed for a short period of time. Normally the thruster will be required to operate at a near constant rotational speed to maintain depth at low and zero speeds (see Figure 5.5).

Therefore an interesting approach to the transition phase is to try to maintain a fairly consistent operating point for the thruster. This eases the power load on the thruster and batteries and simplifies the design of the thruster unit. Clearly, using this approach the thruster cannot overcome large depth errors and hence an alternative solution to the loss of depth is required. One possible option is to make a small dive on the approach to the transition phase whilst the control surfaces are still able to control the vehicle. Simultaneously the thruster is turned on at a value approximately equal to that required to maintain depth (control the positive buoyancy) at low and zero speeds. As the vehicle slows down the control surface performance reduces and the vehicle will begin to rise due to the positive buoyancy. At the same time the thruster induced force increases providing greater control over the depth of the vehicle. The change in depth induced by the lack of control from both the control surfaces and thruster must be smaller than the change in depth caused by the initial dive. Once the tunnel thruster has achieved a suitable level of control it can be

used to correct a small depth error as appropriate. A sample depth time history for this type of transition phase is shown in Figure 5.25, which shows an initial dive at 400s followed by the thruster guiding the vehicle back to the desired depth. The oscillations in depth (after t = 600s) illustrate the attempts by the thruster controller to set the desired depth.

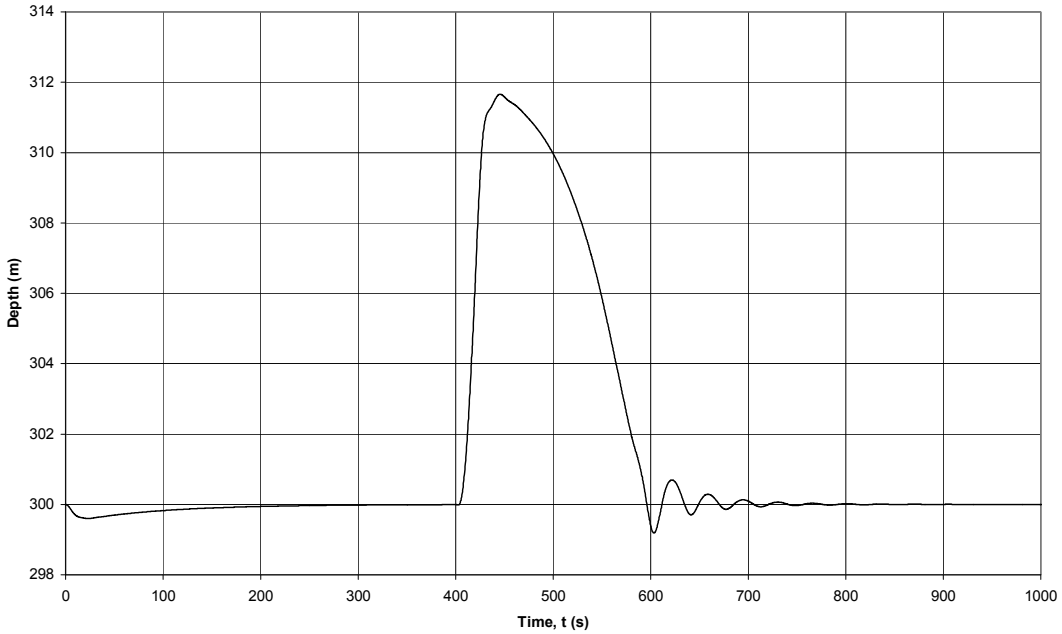

Figure 5.25 – Time History of Depth for the Transition Phase with an Initial Control Surface induced Dive

The advantage of this approach is that the tunnel thruster has a near constant operating point, simplifying the design of the thruster and providing a smoother and more predictable power requirement. The total energy required by the thruster operating at a constant rotational speed throughout the transition phase is approximately the same as when using the interchange controller. An energy saving can be made by delaying the initial command to the thruster until the thruster control force is required (defined by an estimated forward speed).

This approach does have some drawbacks. The change of vehicle depth is quite substantial and this may not be suitable given the mission objectives or surrounding terrain. The lack of pitch control with the single centrally mounted tunnel thruster leads to considerable oscillations in pitch using this approach. This approach would also not be suitable for the transition phase from low speed operation to survey speed operation, since the pre-transition dive would need to be undertaken by the tunnel thrusters, at a substantial energy cost. Hence, if a change in depth is considered acceptable then the vehicle could be allowed to rise

due to the loss of tunnel thruster control and this could be recovered by the control surfaces once a sufficient forward speed is achieved.

5.8.2 Design Features

The simulations undertaken use thrusters with selected design characteristics, however these characteristics were chosen when the particular performance required for the transition phase was not well understood. One potential way in which the performance could be improved is to select a different thruster using the insight gained. The thruster characteristics for the transition phase relate to the operational speed ratio range. The speed ratio is given by:

$$\frac{u}{u_j} = \frac{u}{\sqrt{\frac{F_T}{\rho A}}}. \tag{5.12}$$

The three variables in this formulation (forward speed, u, thrust, F_T, and thruster area, A) offer different approaches to improving the performance of the vehicle during the transition phase by shifting the range of speed ratio used towards zero. These are:

1. Reduce the forward speed of the vehicle at which the vehicle undergoes transition. This can be achieved by extending the range of control provided by the control surfaces. There are two options, firstly, reduce the force required by decreasing the positive buoyancy, and secondly, enhance the performance of the control surfaces (by using a higher lift section or increasing the size).
2. Reduce the required thruster load. This can be achieved in the same ways as reducing the forward speed for transition.
3. Reduce the size of the thruster. A smaller thruster would generate a stronger jet for a given thruster force and hence reduce the speed ratio. The drawback to this approach is a decrease in the efficiency of the thruster and consequently an increased power requirement (see Figure 4.3).

These simple approaches relate to the design and selection of the actuators for a given vehicle demonstrating the need for a considerate and well informed approach.

5.8.2.1 Tunnel Shape

Throughout this research a simple and logical constraint has been applied requiring symmetrical tunnel thruster performance. This constraint implies the use of a symmetrical tunnel. In the horizontal plane this can be justified by noting that there is no predominant direction of force generation. However, on a positively buoyant AUV there is a predominant direction in the vertical plane. This means that an asymmetric tunnel could be justifiably

employed to enhance the performance of the thruster in the downwards direction, whilst using the positive buoyancy to provide a control force in the upwards direction. It should be recalled that the highest tunnel thruster efficiency was reported with a straight tunnel [86].

To enhance the performance, a downstream contracting nozzle could be attached to the tunnel to accelerate the flow downstream of the propeller. The speed ratio for the thruster, as given in Equation (5.12), has a proportional dependence on the diameter of the thruster. The potential improvements have been estimated using a simple calculation. The intended nozzle is schematically illustrated in Figure 5.26. At a forward speed of 0.75m.s^{-1} and with a nozzle contraction ratio of 2, the value of K_F increases from 0.2 to 0.45, a 125% increase in the force experienced by the vehicle. The variation of K_F with contraction ratio is shown in Figure 5.27 using the Autosub configuration at forward speeds of 0.5m.s^{-1}, 0.75m.s^{-1} and 1.0m.s^{-1}.

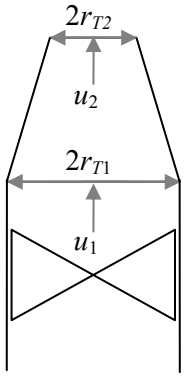

Figure 5.26 – Diagram showing a Contracting Nozzle Downstream of the Propeller in a Thruster Tunnel

The results shown in Figure 5.27 show that considerable improvements in the force experienced by the vehicle can be achieved using moderate contraction ratios across the range of forward speeds. These calculations assume that the flow in the tunnel is non-swirling and neglect boundary layer separation. That is, the acceleration of the flow is calculated using the conservation of mass:

$$\frac{u_2}{u_1} = \frac{r_{T1}^2}{r_{T2}^2}. \tag{5.13}$$

However, the flow is the tunnel will have a considerable swirl component generated by the rotation of the propeller. The effects of this swirl component can be considered using the equation developed in [124]:

$$\frac{u_2}{u_1} = 1 + \left(\frac{r_{T1}^2}{r_{T2}^2} - 1 \right) \frac{0.5kr_{T2}}{J_1(kr_{T2})}. \tag{5.14}$$

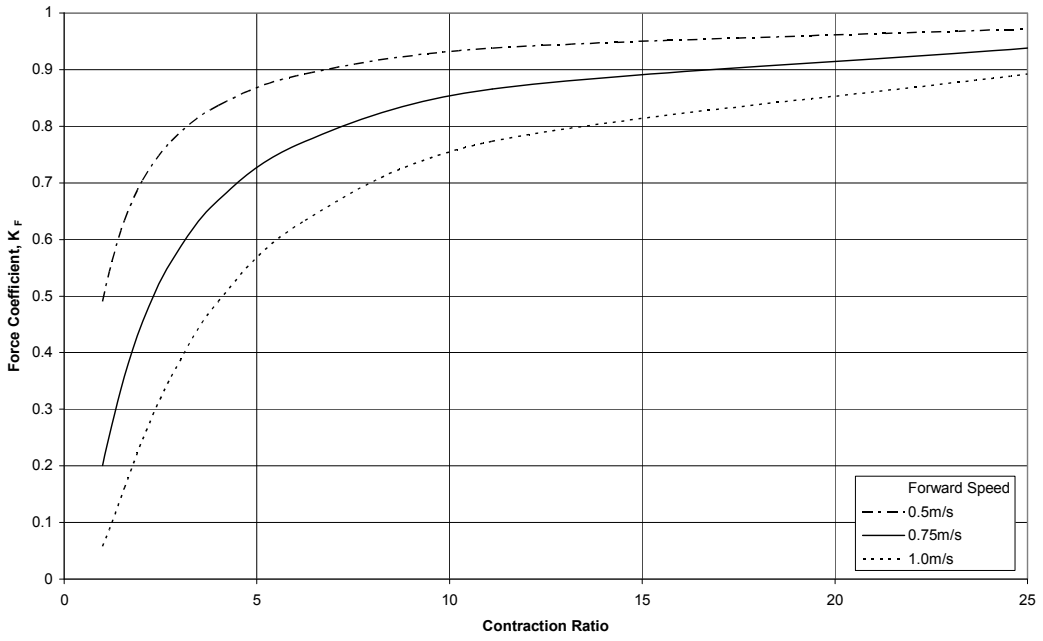

Figure 5.27 – Tunnel Thruster Performance Enhancement using a Downstream Nozzle as a function of Contraction Ratio and Forward Speed

Equation (5.14) gives the increase in velocity on the tunnel centreline, where r_{T1} and r_{T2} are the inlet and outlet radii, k is twice the ratio of the angular and axial velocities in the flow and J_1 is a Bessel function of the first kind. Solutions of this type give a maximum velocity on the centreline with the variation in the velocity off the centreline being characterised by the shape of the Bessel function $J_0(k\chi)$, where χ is the radial co-ordinate.

Equation (5.14) shows that the increase in velocity is enhanced by the presence of a swirl component. This equation assumes that wall separation and vortex breakdown are both avoided. These phenomena only occur at high swirl, but wall separation can be induced at lower swirl numbers if the contraction ratio is too high [125].

The results above show that a moderate contraction ratio will offer a performance enhancement that provides a large energy saving for the AUV. Limited results reported in [61] indicate that performance improvements of this order can be achieved. However, it would be necessary to build and test such a device to ensure that the performance enhancements suggested by these calculations can be realised for propeller type flows at this scale.

5.8.2.2 Alternative Design Options

Alternative performance enhancement options include the installation of an Anti-Suction Tunnel (AST), as discussed in Section 4.5.2.5 and the use of a grid across the tunnel entrances. A grid can be designed using aerofoil sections, which effectively increases the strength of the jet as it leaves the tunnel. If well designed this leads to a decrease in speed ratio and hence improved performance.

5.8.3 Performance Enhancement Conclusions

This short discussion on enhancing the performance of the actuators on an AUV during the transition phase has considered several approaches. The most important conclusion from this discussion is the need for well informed design of the actuators used, that is, both the control surfaces and the thrusters to enable an efficient transition phase. The potential for performance enhancement through the use of a nozzle on the thruster tunnel offers an interesting investigation, which could potentially save considerable amounts of energy.

5.9 Transition with External Thrusters

Depth control with external thrusters is not as complex as tunnel thruster control assuming that the inflow and outflow from the thruster do not interact with the vehicle. Such an assumption would be valid on an AUV design with thrusters mounted on wings. Hence a fairly simple control solution could be employed similar to that for the single centrally mounted tunnel thruster. The only difficulty relates to the ability of the controller to control the forces generated from the thruster with an effective inflow angle of 90º.

A more interesting investigation is to examine the transition performance of an AUV with a vectored external thruster. In this case the thruster would be used for survey propulsion. On the approach to the transition phase the thruster would begin to be rotated at a controlled rate to allow a component of the thruster force to provide a depth control force. The rotation of the thruster would simultaneously reduce the forward propulsion force and hence slow the vehicle at the same time.

A drawback of this approach is the loss of surge control when the thrusters are rotated to 90º (solely providing a force in the vertical plane). It would be possible to provide a surge force by rotating the thruster through a small angle whilst simultaneously increasing the magnitude of the force to ensure that the component in the vertical plane remains sufficient to maintain

depth. This is not a simple control strategy to implement and the disparity between the control forces required to maintain depth and undergo low speed surge motion would mean that a high level of positional accuracy would be required for the thruster.

Nevertheless a simulation was undertaken with the external thruster set to rotate at a constant rate once the forward propulsion force is approximately equal to the positive buoyancy. The control surface depth control was relaxed using the same approach as used in the tunnel thruster simulations. The rotation of the thruster begins at t = 500s. The resulting response is illustrated in Figure 5.28.

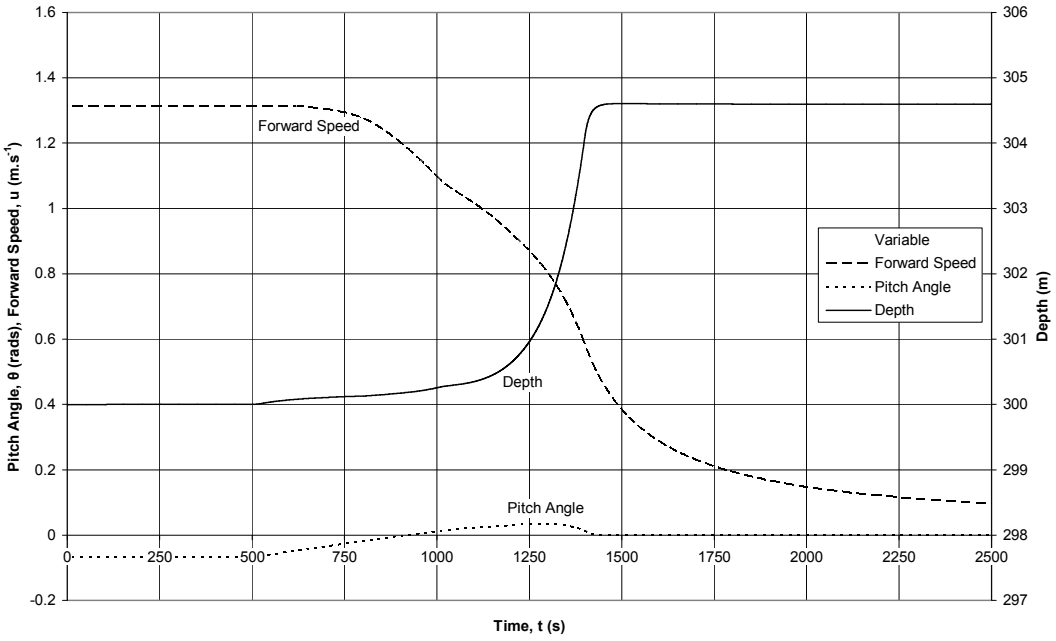

Figure 5.28 – Time History for the Transition Phase with External Thrusters

The results show that the depth is well maintained with a constant error of 4.6m induced by the transition phase. No attempt is made to recover the depth error as the thruster rotational speed is a constant value. In reality dynamic assignment of the thruster rotational speed would be required to allow for the unknown positive buoyancy force and to overcome the induced depth errors. The pitch variations show a smooth return to zero pitch angle and no oscillations in the hovering phase. It should be noted that zero forward speed is not achieved in this simulation due to the lack of surge control available. Despite this encouraging performance this approach does not really represent a feasible control strategy for a multi-purpose AUV due to the difficulties relating to the low speed vehicle control using this configuration.

5.10 Transition Simulation Conclusions

An approach to combining stern plane control and thruster control to reflect the changing requirements as forward speed is reduced, in a flight-style transition phase to a hover condition, has been used to test the vehicle performance and assess the feasibility of using tunnel thrusters to control the hydrostatic balance at low speeds.

Simulations of a survey-style AUV undertaking the transition phase have been performed for a range of decelerations and control interchange parameters to assess their influence on the performance of the vehicle and the associated energy cost. The results demonstrate that the selection of the control parameters can be made on a basis of the levels of vehicle performance and controllability desired, since the energy cost is relatively consistent for smooth transitions.

Overall these results demonstrate the ability of the tunnel thruster configurations tested to maintain vehicle control throughout the transition phase and provide a means of estimating the associated energy cost to the vehicle. The practical issues associated with using tunnel thrusters have also been considered showing the estimated power loads required.

Potential performance enhancements have also been considered using a variety of approaches. The most promising of these approaches involves the addition of a downstream nozzle to accelerate the tunnel thruster jet and thus reduce the speed ratio.

5.11 Low Speed Manoeuvring

The preceding simulations have focussed on the transition between survey speed operation and low and zero speed operation. The simulation tool uses a set of hydrodynamic coefficients that were determined through an experimental testing programme undertaken at survey speeds. Therefore it would be inappropriate to assess the performance of the AUV during (high angle of attack) low speed manoeuvres using the simulation tool.

Hence it is necessary to consider alternative approaches to examining the low speed manoeuvring performance of a multi-purpose AUV. A literature survey was undertaken to find performance measures for low speed manoeuvres. No common standards were found for underwater vehicles. ROV performance is usually given in terms of autopilot accuracy and the bollard pull thrust available in given directions. [126] comments on the manoeuvring performance of underwater vehicles in qualitative terms, for example, ‘easy

and rapid' changes in position and 'stable' position-keeping. Consequently, the literature search was expanded to include surface vessels. The measures used to describe surface vessel manoeuvring performance are well defined for manoeuvring at speed, however no measures were found for low speed operation. In fact, the standard International Maritime Organisation (IMO) manoeuvring measures are all defined for operation at speed [127].

The definition of low speed manoeuvring measures for surface vessels is a current topic of international research and discussion. [128] suggests a series of measures and manoeuvres including crash stop manoeuvres, a minimum rudder angle for effective yaw checking and combinations of accelerations and decelerations to assess the transition between different quadrants of propulsor operation. [129] notes that a commonly used test requires the vessel to turn on the spot within a box two vessel lengths square within a certain time. [130] suggests two sets of indices, one which gives geometric features, for example, rudder area ratios, and one which gives operational characteristics, for example, the thrust density of the thrusters.

These suggested measures may not be appropriate for an AUV. Some of the proposed surface vessel measures (for example, ability to move away from a bank [128]) are designed to include the effects of confined and shallow waters where the majority of low speed manoeuvres take place. Confined and shallow waters can have a significant impact on the performance of a vessel. A multi-purpose AUV will not be limited to undertaking low speed manoeuvres in confined and shallow waters and more general performance measures are desired.

The surface vessel manoeuvres suggested, and the associated measures from these trials, focus on the ability of the vessel to undertake the manoeuvre assuming that the vessel cannot easily undertake the manoeuvre. For example, the turn on the spot manoeuvre within a two vessel length square box implies that the vessel cannot turn 'on the spot'. In this case there is likely to be some translation of the centre of rotation of the vessel from its original location.

The multi-purpose AUV is expected to be able to turn on the spot, without a translation of the centre of rotation of the vehicle from its original location. There may be an overshoot on a required heading which can be controlled using a well designed and tuned control system. This overshoot provides a measure of performance but does not characterise the complete abilities of a vehicle to turn on the spot. The speed of rotation could be used, but it would be difficult to define a performance metric based on the rotation speed. The multi-purpose

AUV control system should be able to set the speed of rotation within a range determined by the minimum and maximum forces available from the thrusters. This range of rotation speed is likely to exceed the band of useful rotation speeds for the completion of mission objectives.

The classification of the performance in this case is a complex problem incorporating the control system, the dynamics of the available thrusters and the response of the vehicle. There is no simple and reliable way of assessing this performance without resorting to experimental trials.

Therefore, it is important to separate the low speed manoeuvring performance into two categories. The first category is those manoeuvres that it is assumed the AUV can undertake directly and without difficulty. The second category is those manoeuvres that the AUV cannot undertake directly and where some measure of ability or error would be appropriate. An example of this case is the less manoeuvrable vehicle discussed in Section 3.2, where the ability of the vehicle to sway (using a combination of surge and yaw) could be described using measures similar to those discussed for surface vessels.

For a multi-purpose AUV designed to meet the requirements set out in Table 3.1, it is assumed that the majority of the required low speed manoeuvres fall into the first category. Therefore the low speed manoeuvring performance of a multi-purpose AUV can be assessed using the following two criteria:

1. Capability

   The ability of the vehicle to generate forces and moments in the required directions to undertake a given manoeuvre. The first measure of the capability is the thruster configuration on the vehicle. This capability should be given in terms of the degrees of freedom that can be actively controlled using the thruster configuration on the vehicle and the manoeuvres that this configuration enables the vehicle to undertake. These manoeuvres should be simple building-block style manoeuvres, for example, sway translation and yaw rotation in the horizontal plane. Experimental trials could be used to determine the maximum and minimum translation or rotation speeds for these simple manoeuvres (however these may not be of much use as they are likely to exceed the useful range). Furthermore, the maximum thrust capabilities of the vehicle could be given to assess the bollard pull available and the magnitude of the current in which the vehicle could maintain attitude and position.

2. Accuracy

   The accuracy with which the vehicle can undertake the desired manoeuvre. This is a measure of the performance of the control system on the vehicle and its ability to control the response of the vehicle given the thruster configuration onboard. This should be measured in terms of an overshoot on the desired position or heading (or the time taken) to undertake the simple building-block style manoeuvres discussed. The major characteristic to be assessed using these measures is how well the control system can control the dynamic response of the thrusters and the thruster deadbands.

These two criteria are similar to those already used for ROVs. The important point here is the use of the basic set of building-block style manoeuvres rather than using autopilot accuracy. This facilitates the comparison of the performance of different vehicles, control systems and thruster configurations to provide sufficient information to allow the potential user of a multi-purpose AUV to select a vehicle which is most suited to a desired mission profile. Furthermore, this information can be used to aid the mission design process.

5.11.1 Demonstration of Low Speed Manoeuvring Performance

The ability of a tunnel thruster equipped AUV to undertake low speed manoeuvres has been demonstrated during the validation of the tunnel thruster modelling procedure in Section 4.5.7. The ability of a tunnel thruster equipped AUV to undertake simpler building-block style low speed manoeuvres will now be demonstrated using the Delphin AUV [115]. For further details of the Delphin AUV, the control system and its performance, see [131].

In terms of low speed manoeuvring capability the Delphin AUV is equipped with:

1. A stern mounted propeller giving direct control over surge.
2. A pair of vertical tunnel thrusters giving direct control over heave and pitch.
3. A pair of horizontal tunnel thrusters giving direct control over sway and yaw.

This thruster configuration allows the Delphin AUV to undertake manoeuvres involving direct control over surge, sway and heave translation and pitch and yaw rotation. Roll is passively controlled. The thrusters provide sufficient forces to manoeuvre the vehicle with a range of translation and rotation velocities that is greater than required to complete the original design mission objectives.

To illustrate a simple building-block style manoeuvre, Figure 5.29 shows the positively buoyant Delphin undergoing heave motion. Delphin starts from operation on the surface and dives to a desired depth of 2.5m. Figure 5.29 indicates an overshoot on the depth demand of

0.27m and it takes approximately 15s to control the depth to within 10cm (~ 0.5*d*) of the depth demand.

Figure 5.29 provides the depth and thruster rotational speed time histories as Delphin uses the forward and aft vertical tunnel thrusters to dive directly downwards from the surface. Delphin is quickly within range of the desired depth and is shown to be able to maintain this depth accurately. The initial large value of the thruster rotational speed is due to the need to overcome the inefficiency of the tunnel thrusters when operating on the surface. The difference between the rotational speed for the forward and aft thrusters indicates the differing forces required to control the asymmetric vehicle.

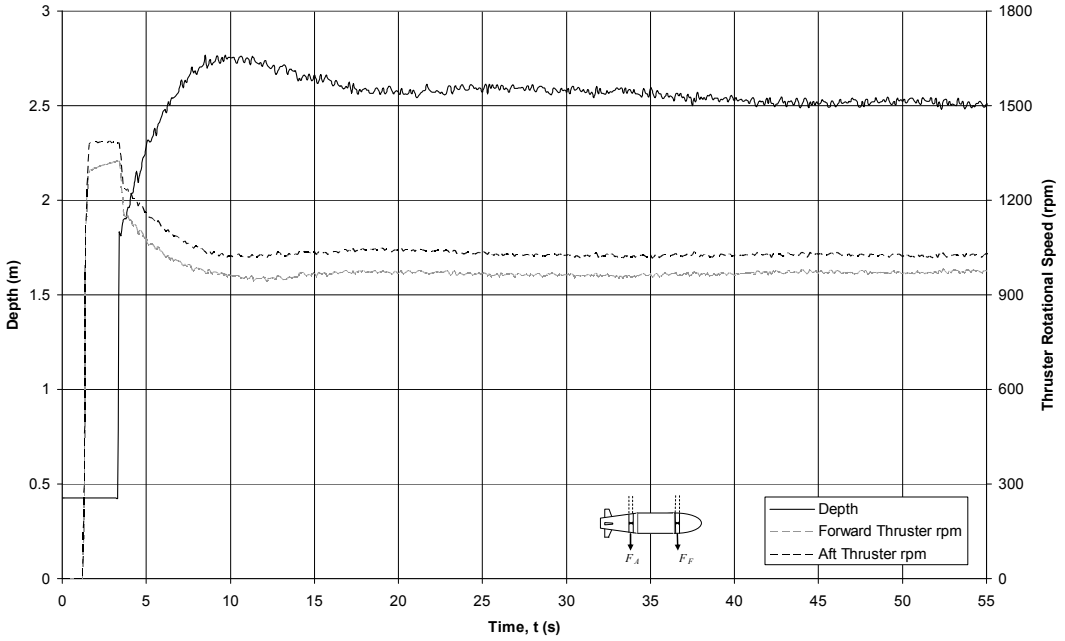

Figure 5.29 – Depth Time History for the Delphin AUV

Figure 5.30 shows Delphin undergoing pure yaw rotation in a zero current environment. This manoeuvre was undertaken as part of a search pattern during which the vehicle stops, hovers and then turns on the spot (for a given time) to scan the area using the forward looking camera. Hence in this case there is no 'desired' heading to measure an overshoot against.

Figure 5.30 shows the thruster rotational speeds for the forward and aft horizontal tunnel thrusters which maintain an approximately constant value. The resulting performance shows the vehicle rotating at a constant rate of approximately 4.5deg.s^{-1}.

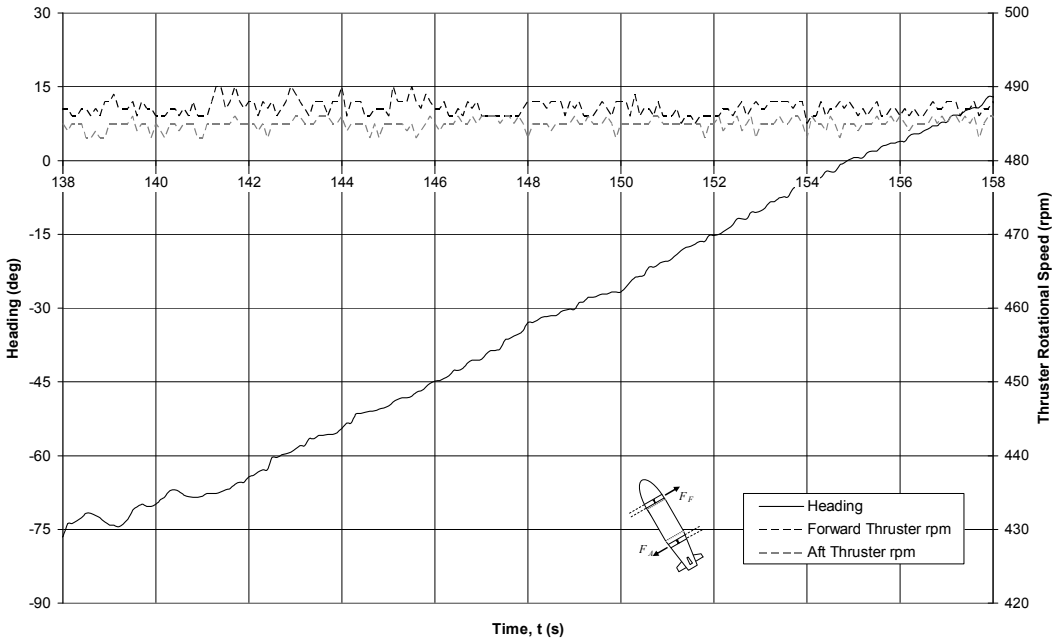

Figure 5.30 – Heading Time History for the Delphin AUV

5.11.2 Low Speed Manoeuvring Conclusions

The definition of low speed manoeuvring measures has been discussed and it has been shown that the measures used need to be specific to the particular operational characteristics of the vehicle type concerned. That is, the ability of a vehicle to undertake a manoeuvre needs to be assessed before determining an appropriate measure. For a multi-purpose AUV it is assumed that most manoeuvres can be undertaken directly. Thus it is suggested that the low speed manoeuvring performance is determined in terms of the capabilities offered by the vehicle and the ability of the control system to command the thrusters to undertake building-block style manoeuvres. The latter is a complex problem involving the dynamic performance of the thrusters and the performance of the control system which must be determined using experimental trials. The low speed manoeuvring performance of a tunnel thruster equipped AUV has been demonstrated using trials data from the Delphin AUV.

5.12 Concluding Remarks

A numerical simulation has been used to investigate the ability of a survey-style AUV, equipped with through-body tunnel thrusters, to maintain control in the vertical plane at survey speeds and at low speeds using appropriate actuator configurations. These simulations have demonstrated the ability of tunnel thrusters to provide the necessary low and transitional speed control to enable a survey-style AUV to undertake missions

throughout the speed range. Furthermore, the simulation has been used to investigate control strategies for the transition phase between high speed survey to low speed operation. These simulations demonstrate that a smooth interchange between control strategies is the best approach with respect to the response of the vehicle and that the energy demands are relatively consistent across the range of control parameters investigated.

Approaches to improving the performance of the tunnel thrusters have been suggested with the addition of a downstream contracting nozzle found to be the simplest and most promising option where there is a predominant direction of force generation, for example in the vertical plane.

The low speed manoeuvring capabilities of an underwater vehicle and the approaches to characterising this performance have been considered. A method of comparing the performance of different vehicle configurations and controllers has been suggested. This method requires the definition of the capabilities of a vehicle alongside the resulting accuracy with which these capabilities can be employed to undertake simple building-block style manoeuvres at low speed. The low speed manoeuvring abilities of a tunnel thruster controlled AUV have been demonstrated using trials data from the Delphin AUV.

Chapter 6 – Conclusions and Further Work

6.1 Introduction

The reported research has focussed on two areas of the design and operation of AUVs. These areas are the assessment of the survey performance of an AUV and the development of a multi-purpose AUV. The conclusions from these two areas will now be briefly revisited before outlining some suggestions for further research.

6.2 Assessment of Survey Performance Conclusions

The components of the propulsion and manoeuvring systems used on a survey-style AUV were reviewed and the key factors influencing their performance identified. The external components of these systems, that is, those that interact with the surrounding fluid to generate control forces were selected as the focus of the analysis. A model of the Autosub propeller was developed using the boundary element method and the performance of the control surfaces was characterised using existing experimental data.

The use of hybrid devices on a survey-style AUV was examined to determine whether they would offer improvements to the existing survey performance. A hybrid device is defined as one that can produce both propulsion and manoeuvring forces. Two particular devices were investigated, namely, a vectored thruster and a collective and cyclic pitch propeller. The performance of a vectored thruster was examined using simplified approaches to estimating the forces generated. The performance of a collective and cyclic pitch propeller was investigated using the developed Autosub propeller model. The performance of both devices, in terms of the manoeuvring capabilities, was found to be inferior to that of the existing systems and the benefits these systems offered were considered insufficient to justify the additional engineering complexity.

6.3 Development of a Multi-Purpose AUV Conclusions

A multi-purpose AUV was defined as an AUV capable of combining high speed survey operation and low speed investigation tasks. These characteristics would allow the multi-purpose AUV to explore a wide area and investigate in detail any features of interest discovered. Following on from the examination of the survey characteristics of an AUV and the demonstration of the importance of the survey efficiency of a multi-purpose AUV, the

design approach adopted was to consider the addition of low and zero speed control to a survey-style AUV.

The available options for low speed control were assessed and propeller based thrusters were chosen for further investigation due to their simplicity, robustness, responsiveness and ability to generate control forces throughout the entire speed range. A major influence on the performance of a propeller based thruster mounted on an AUV was determined to be placement of the thruster. Two types of mounting were considered, namely, with the thruster attached to the outside of the vehicle (an external thruster) and with the thruster placed in a through-body tunnel. The literature concerning external thrusters and through-body tunnel thrusters was reviewed and gaps were found relating to the performance characteristics when mounted on survey-style AUV hull forms. Therefore a series of experiments was undertaken to determine the forces induced on an AUV by propeller based thrusters.

The interactions between an external thruster and its surroundings were considered and the two most prevalent interactions were selected for further investigation. The interactions between a pair of thrusters mounted one behind the other were assessed and a model based on a simplified representation of a propeller jet was developed to represent the variation in thrust force as a function of the thruster separation. The interactions between a thruster and the hull form were examined experimentally. The longitudinal and lateral forces on a vehicle induced by an external thruster mounted close to the hull form were measured and found to be less than 20% of the desired thrust force in all cases tested.

An experimental programme was undertaken to characterise the performance of forward and aft mounted through-body tunnel thrusters on an AUV hull form over a range of forward speeds and yaw angles. The experiments demonstrated that there is no, or only a very small, increase in drag caused by the addition of thruster tunnels and hence no significant variation in survey efficiency. The magnitude of the force induced on a vehicle by a tunnel thruster was found to reduce with increasing forward speed (for a constant thruster operating point). In fact, the performance of the tunnel thrusters was determined to be a function of the speed ratio; the ratio of vehicle speed to thruster jet speed. The variation in performance of the forward and aft thrusters was found to differ, with the decrease in effectiveness of the forward thruster occurring at a faster rate than for the aft thruster. The influence of a vehicle yaw angle on thruster performance was determined to be small, with a marginal increase in performance when the thruster exit is shielded by the vehicle and a similar decrease in performance when the thruster jet emits directly into the oncoming flow.

These tunnel thruster results were used to develop a new, simple modelling procedure that requires the specification of only three constants per thruster. The model was validated using turning circle trials data from the Delphin AUV. As a result of the experiments undertaken and the review of the available literature, it was decided to continue the development of a multi-purpose AUV focussing on the use of through-body tunnel thrusters. The primary reason for this choice was the widely different survey efficiency impact of the two approaches considered.

The developed model of the performance of a through-body tunnel thruster was incorporated into a numerical simulation of Autosub. The aim of the investigation using this simulation was to examine the performance of a survey-style AUV throughout the speed range. Initially, the operational speed ranges for survey-style control surface depth control and tunnel thruster depth control were determined, demonstrating that tunnel thrusters offer sufficient control in the low and transitional speed ranges. Consequently the performance of the AUV during the transition phase between depth control methods was investigated including assessing different approaches to the required control interchange. The investigations were made using models incorporating differing levels of physical representation to facilitate identification of the particular mechanisms causing the observed performance characteristics. The results of this investigation determined that the selection of the interchange control parameters can be made as a function of the desired vehicle performance since the required energy is relatively insensitive to the chosen parameters provided the transition is smooth.

Approaches to improving the performance of the tunnel thrusters to reduce the energy requirements were suggested and briefly examined. The most promising of these approaches was considered to be the addition of a downstream contracting nozzle to the thruster tunnel.

The low speed manoeuvring performance of a tunnel thruster equipped survey-style AUV could not be determined using the developed simulation tool. No common approach to characterising the low speed manoeuvring performance of underwater vehicles could be found in the literature and hence a method was devised. This method involves the definition of the capabilities of the vehicle configuration, in terms of the forces available and hence simple building-block style manoeuvres achievable, and the accuracy with which these manoeuvres can be realised. The ability of a tunnel thruster equipped AUV to undertake basic low speed manoeuvres was demonstrated experimentally using trials data from the Delphin AUV.

6.4 Further Work

The suggestions for further work from this research mainly originate from the investigations into the development of a multi-purpose AUV. This is due primarily to the disappointing performance of the hybrid devices assessed, however an interesting investigation could be undertaken into furthering the understanding of stern mounted vectored thruster performance on an AUV.

The suggested avenues for further work from the research undertaken into the development of a multi-purpose AUV include:

- A combined experimental and CFD programme to characterise in greater detail the inflow to and, more importantly, the outflow from a propeller based thruster and to develop an analytical model of these flows.
- An experimental examination of the interaction of propeller jets with a crossflow and the resulting interaction with a body to aid the development of CFD models of a simplified scenario before the inclusion of real vehicle characteristics.
- An experimental investigation of different AUV depth control systems and actuator configurations to determine their performance and the limits of their operability.
- An experimental study of the performance of an AUV during the transition phase as a function of the control interchange approach adopted.
- An experimental assessment of the performance benefits offered by the addition of a contracting nozzle to a tunnel thruster.

References

[1] Newman, P., Westwood, R. & Westwood, J. (2007) *Market Prospects for Autonomous Underwater Vehicles*, Proceedings of the 9th Unmanned Underwater Vehicle Showcase - UUVS, Southampton, UK.

[2] Hagen, P.E., Storkersen, N.J. & Vestgard, K. (1999) *HUGIN - Use of UUV Technology in Marine Applications*, Proceedings of the MTS/IEEE Oceans Conference, vol. 2, pp967-972, Seattle, WA, USA.

[3] Stokey, R.P., Roup, A., Von Alt, C., Allen, B., Forrester, N., Austin, T., Goldsborough, R., Purcell, M., Jaffre, F., Packard, G. & Kukulya, A. (2005) *Development of the REMUS 600 Autonomous Underwater Vehicle*, Proceedings of the MTS/IEEE Oceans Conference, Washington, DC, USA.

[4] Ferguson, J. & Pope, A. (2000) *Explorer – A Modular AUV for Commercial Site Survey*, Proceedings of the IEEE International Symposium on Underwater Technology – UT'00, pp129-132, Tokyo, Japan.

[5] Collar, P.G. (1990) *The AUTOSUB Project - Autonomous Underwater Vehicles for Data Collection in the Deep Ocean***,** Proceedings of the IEE Colloquium on 'Monitoring the Sea', pp3/1-3/4, London, UK.

[6] Stevenson, P., Millward, N.W., McPhail, S.D., Riggs, J., White, D., Pebody, M., Perrett, J.R. & Webb, A.T. (2003) *Engineering an Autonomous Underwater Vehicle for Under Ice Operations*, Proceedings of the 22nd ASME International Conference on Offshore Mechanics and Arctic Engineering – OMAE, vol. 3, pp445-452, Cancun, Mexico.

[7] McPhail, S.D., Furlong, M., Huvenne, V., Perrett, J. & Pebody, M. (2009) *Autosub6000: Its First Deepwater Trials and Science Missions*, Underwater Technology, vol. 28, no. 3, pp91-98.

[8] Natural Environment Research Council. (2006) *Oceans 2025: Overview of the NERC Marine Centres' Proposed Strategic Research Programme 2007-2012*, Natural Environment Research Council.

[9] Hornfeld, W. (2006) *Status of the Atlas Elektronik's Modular AUV Family*, Proceedings of the 25th ASME International Conference on Offshore Mechanics and Arctic Engineering – OMAE, Hamburg, Germany.

[10] Carlton, J.S. (2007) *Marine Propellers and Propulsion*, Second Edition, Butterworth-Heinemann, Oxford, UK.

[11] Zorbas, D. (1989) *Electric Machines: Principles, Applications, and Control Schematics*, West Publishing Company, St Paul, MN, USA.

[12] Burcher, R. & Rydill, L. (1994) *Concepts in Submarine Design*, Cambridge Ocean Technology Series, Cambridge, UK.

[13] Abbott, I.H. & von Doenhoff, A. (1959) *Theory of Wing Sections: Including a Summary of Airfoil Data*, McGraw-Hill, New York, USA.

[14] Sileo, L. (2007) *Low Reynolds Number Turbulent Flow Past Thrusters of Unmanned Underwater Vehicles*, Proceedings of the 2nd International Conference on Marine Research and Transportation – ICMRT'07, Naples, Italy.

[15] Merry, S.L., Large, M.J., Whitten, T.J., Wilkinson, M.R. & Babb, R.J. (1996) *Control Surface and Actuator Design for a Low Drag, Laminar Flow AUV*, Proceedings of the IEEE Symposium on Autonomous Underwater Vehicle Technology – AUV'96, pp57-64, Monterrey, CA, USA.

[16] McKee, A.I. (1959) *Recent Submarine Design Practices and Problems*, Trans. SNAME, vol. 67, pp623-652.

[17] Arentzen, E.S. & Mandel, P. (1960) *Naval Architectural Aspects of Submarine Design*, Trans. SNAME, vol. 68, pp622-692.

[18] Breslin, J.P. & Andersen, P. (1993) *Hydrodynamics of Ship Propellers*, Cambridge University Press, Cambridge, UK.

[19] Hess, J.L. (1990) *Panel Methods in Computational Fluid Dynamics*, Annual Review of Fluid Mechanics, vol. 22, pp255-274.

[20] Kerwin, J.E. (1986) *Marine Propellers*, Annual Review of Fluid Mechanics, vol. 18, pp367-403.

[21] Turnock, S.R. (2000) *Palisupan User Guide*, Ship Science Report, no. 100, University of Southampton.

[22] Molland, A.F. & Turnock, S.R. (2007) *Marine Rudders and Control Surfaces: Principles, Data, Design and Applications*, Butterworth-Heinemann, Oxford, UK.

[23] Palmer, A.R. (2007) *Improved Propulsion and Manoeuvring of Autonomous Underwater Vehicles*, Engineering Doctorate Mini-Thesis, University of Southampton.

[24] Hughes, A.W. (2000) *Investigation of Tip Driven Thrusters and Waterjet Propulsion Systems*, PhD Thesis, University of Southampton.

[25] Kimber, N.I. & Marshfield, W.B. (1993) *Design and Testing of Control Surfaces for the Autosub Demonstrator Test Vehicle*, DRA Haslar Technical Report.

[26] Allen, B., Vorus, W.S. & Prestero, T. (2000) *Propulsion System Performance Enhancements on REMUS AUVs*, Proceedings of the MTS/IEEE Oceans Conference, vol. 3, pp1869-1873, Providence, RI, USA.

[27] Fish, F.E. (2006) *Limits of Nature and Advances of Technology: What does Biomimetics have to offer to Aquatic Robots?*, Applied Bionics and Biomechanics, vol. 3, no. 1, pp49-60.

[28] Bandyopadhyay, P.R. (2005) *Trends in Biorobotic Autonomous Undersea Vehicles*, IEEE Journal of Oceanic Engineering, vol. 30, no. 1, pp109-39.

[29] http://www.bluefinrobotics.com – Bluefin Robotics Website. Viewed 22/09/06.

[30] Zimmerman, R., D'Spain, G.L. & Chadwell, C.D. (2005) *Decreasing the Radiated Acoustic and Vibration Noise of a Mid-size AUV*, IEEE Journal of Oceanic Engineering, vol. 30, no. 1, pp179-187.

[31] Chocron, O. & Mangel, H. (2008) *Reconfigurable Magnetic-Coupling Thrusters for Agile AUVs*, Proceedings of the IEEE/RSJ International Conference on Intelligent Robots and Systems, pp3172-3177, Nice, France.

[32] Cavallo, E. (2003) *Parallel Wrist for the Guidance of an Underwater Vehicle*, PhD Thesis, University of Genoa.

[33] Quackenbush, T., Usab, W. & Carpenter, B. (2004) *Ducted Propulsors with Steerable Outflow using Smart Materials Technology*, Proceedings of the RINA Advanced Marine Materials Conference, London, UK.

[34] Le Page, Y.G. & Holappa, K.W. (2000) *Simulation and Control of an Autonomous Underwater Vehicle Equipped with a Vectored Thruster*, Proceedings of the MTS/IEEE Oceans Conference, vol. 3, pp2135-2140, Providence, RI, USA.

[35] Ackermann, L.E.J. (2007) *Thrust Response of a Vectored Thruster Unmanned Underwater Vehicle*, MS Thesis, Florida Atlantic University.

[36] Oosterveld, M.W.C. (1973) *Ducted Propeller Characteristics*, Proceedings of the RINA Symposium on Ducted Propellers, paper 4, pp35-70, London, UK.

[37] Le Page, Y.G. & Holappa, K.W. (2000) *Hydrodynamics of an Autonomous Underwater Vehicle Equipped with a Vectored Thruster*, Proceedings of the MTS/IEEE Oceans Conference, vol. 3, pp2129-2134, Providence, RI, USA.

[38] Stevenson, P., Furlong, M. & Dormer, D. (2009) *AUV Design – Shape, Drag and Practical Issues*, Sea Technology, vol. 50, no.1, pp41-44.

[39] Humphrey, T.C., Bose, N., Williams, C. & Snow, M. (2004) *Design and Fabrication of a Collective and Cyclic Pitch Propeller*, Proceedings of the 23rd ASME International Conference on Offshore Mechanics and Arctic Engineering - OMAE, vol. 3, pp653-659, Vancouver, Canada.

[40] Haselton, F.H., Wilson, W.G. & Rice, R.S. (1966) *Tandem Propeller Concept of Submarine Propulsion and Control*, Journal of Aircraft, vol. 3, no. 2, pp180-184.

[41] Joosen, W.P.A., Van Manen, J.D. & Van Der Walle, F. (1963) *Large Hub to Diameter Ratio Propellers with Programmed Blade Control*, International Shipbuilding Progress, vol. 10, no. 101, pp3-11.

[42] Nagashima, Y., Taguchi, N. & Ishimatsu, T. (2006) *Development of a Compact Hybrid Underwater Vehicle using Variable Vector Propeller*, Proceedings of the JSCE International Symposium on Automation and Robotics in Construction, Tokyo, Japan.

[43] Gabriel, R. & Atlar, M. (1998) *Calculation of the Performance of a Ship Propeller with Cyclic Blade Pitch Control*, International Shipbuilding Progress, vol. 45, no. 443, pp201-223.

[44] Jackson, H.A. (1983) *Submarine Parametrics*, Proceedings of the RINA International Symposium on Naval Submarines, vol. 1, paper 3, London, UK.

[45] Bowen, A.D., Yoerger, D.R., Taylor, C., McCabe, R., Howland, J., Gomez-Ibanez, D., Kinsey, J.C., Heintz, M., McDonald, G., Peters, D.B., Fletcher, B., Young, C., Buescher, J., Whitcomb, L.L., Martin, S.C., Webster, S.E. & Jakuba, M.V. (2008) *The Nereus Hybrid Underwater Robotic Vehicle for Global Science Operations to 11,000m Depth*, Proceedings of the MTS/IEEE Oceans Conference, Quebec City, QC, Canada.

[46] Engineering Sciences Data Unit. (1986) *Mean Forces, Pressures and Flow Field Velocities for Circular Structures: Single Cylinder with Two-Dimensional Flow*, ESDU 80025, ESDU International, London, UK.

[47] Thornton, B., Ura, T., Nose, Y. & Turnock, S.R. (2007) *Zero-G Class Underwater Robots: Unrestricted Attitude Control using Control Moment Gyros*, IEEE Journal of Oceanic Engineering, vol. 32, no.3, pp565-583.

[48] Jakuba, M.V. (2003) *Modeling and Control of an Autonomous Underwater Vehicle with Combined Foil/Thruster Actuators*, MS Thesis, Massachusetts Institute of Technology.

[49] Tangirala, S. & Dzielski, J. (2007) *A Variable Buoyancy Control System for a Large AUV*, IEEE Journal of Oceanic Engineering, vol. 32, no. 4, pp762-771.

[50] Worrall, M., Bagley, P., Jamieson, A., Holford, A., Player, M. & Nielson, R.D. (2006) *The Development of a Variable Buoyancy System*, Proceedings of the 2nd IMarEST World Maritime Technology Conference - WMTC, London, UK.

[51] Kirkwood, W.J. & Steele, D.E. (1994) *Active Variable Buoyancy Control System for MBARI's ROV*, Proceedings of the MTS/IEEE Oceans Conference, Brest, France.

[52] Blanke, M., Lindegaard, K.-P. & Fossen, T.I. (2000) *Dynamic Model for Thrust Generation of Marine Propellers*, Proceedings of the 5th IFAC Conference on Maneuvering and Control of Marine Craft - MCMC, pp363-368, Aalborg, Denmark.

[53] Kim, J. & Chung, W.K. (2006) *Accurate and Practical Thruster Modeling for Underwater Vehicles*, Ocean Engineering, vol. 33, pp566-586.

[54] Yoerger, D.R., Cooke, J.G. & Slotine, J.-J.E. (1990) *The Influence of Thruster Dynamics on Underwater Vehicle Behavior and their Incorporation into Control System Design*, IEEE Journal of Oceanic Engineering, vol. 15, no. 3, pp167-178.

[55] Healey, A.J., Rock, S.M., Cody, S., Miles, D. & Brown, J.P. (1995) *Toward an Improved Understanding of Thruster Dynamics for Underwater Vehicles*, IEEE Journal of Oceanic Engineering, vol. 20, no. 4, pp354-361.

[56] Bachmayer, R., Whitcomb, L.L. & Grosenbaugh, M.A. (2000) *An Accurate Four-Quadrant Nonlinear Dynamical Model for Marine Thrusters: Theory and Experimental Validation*, IEEE Journal of Oceanic Engineering, vol. 25, no. 1, pp146-159.

[57] Whitcomb, L. & Yoerger, D.R. (1999) *Development, Comparison, and Preliminary Experimental Validation of Nonlinear Dynamic Thruster Models*, IEEE Journal of Oceanic Engineering, vol. 24, no. 4, pp481-494.

[58] Vonnet, M., Ait-Ahmed, N. & Loron, L. (2008) *Marine Propeller Dynamics Modeling using a Frequency Domain Approach*, Proceedings of the 5th IEEE International Multi-Conference on Systems, Signals and Devices - SSD'08, Amman, Jordan.

[59] Stuntz, G.R. & Taylor, J.R. (1964) *Some Aspects of Bow-Thruster Design*, Trans. SNAME, vol. 72, pp336-373.

[60] Holtrop, J. (2001) *Extrapolation of Propulsion Tests for Ships with Appendages and Complex Propulsors*, Marine Technology, vol. 38, no. 3, pp145-157.

[61] English, J.W. (1963) *The Design and Performance of Lateral Thrust Units for Ships*, Trans. RINA, vol. 105, no. 3, pp251-279.

[62] Heron, A., Duncan, A. & Anderson, B. (2000) *Hydrodynamic Testing of Underwater Vehicles at the Australian Maritime Engineering Co-operative Research Centre*, Proceedings of the IEEE International Symposium on Underwater Technology – UT'00, pp475-479, Tokyo, Japan.

[63] Toumelin, N. & Lemaire, J. (2001) *New Capabilities of the REDERMOR Unmanned Underwater Vehicle*, Proceedings of the MTS/IEEE Oceans Conference, vol. 2, pp1032-1035, Honolulu, HI, USA.

[64] Anderson, J.M. (1992) *Model Development for Control of the Autonomous Benthic Explorer*, Proceedings of the 2nd International Offshore and Polar Engineering Conference - ISOPE, Colorado, USA.

[65] Stettler, J., Hover, F.S., Triantafyllou, M.S. & Hutchison, B.L. (2005) *Investigating the Steady and Unsteady Maneuvering Dynamics of an Azimuthing Podded Propulsor*, Trans. SNAME, vol. 113, pp122-148.

[66] Baltazar, J. & Falcão de Campos, J.A.C. (2009) *On the Modelling of the Flow in Ducted Propellers With a Panel Method*, Proceedings of the 1st International Symposium on Marine Propulsors – smp'09, pp614-622, Trondheim, Norway.

[67] Lewis, E.V. (editor) (1967) *Principles of Naval Architecture*, Society of Naval Architects and Marine Engineers, New York, USA.

[68] Liang, H. & Maxworthy, T. (2008) *Experimental Investigations of a Swirling Jet in both Stationary and Rotating Surroundings*, Experiments in Fluids, vol. 45, pp283-293.

[69] Piquet, J. (2001) *Turbulent Flows: Models and Physics*, Springer, Berlin, Germany.

[70] Schlichting, H. (1960) *Boundary Layer Theory*, Fourth Edition, McGraw Hill, New York, USA.

[71] Gilchrist, R.T. & Naughton, J.W. (2005) *Experimental Study of Incompressible Jets with Different Initial Swirl Distributions: Mean Results*, AIAA Journal, vol. 43, no. 4, pp741-751.

[72] Shiri, A., George, W.K. & Naughton, J.W. (2008) *Experimental Study of the Far Field of Incompressible Swirling Jets*, AIAA Journal, vol. 46, no. 8, pp2002-2009.

[73] Nienhuis, U. (1992) *Analysis of Thruster Effectivity for Dynamic Positioning and Low Speed Manoeuvring*, PhD Thesis, Delft University.

[74] Young, A.D. & Rao, K.N. (1978) *Some Low Speed Experimental Results on the Effects of Swirl and Velocity Distribution on an Axi-Symmetric Jet*, Aeronautical Quarterly, vol. 29, pt. 4, pp270-284.

[75] Abramovich, G.N. (1963) *The Theory of Turbulent Jets*, MIT Press, Cambridge, MA, USA.

[76] Dang, J. & Laheij, H. (2004) *Hydrodynamic Aspects of Steerable Thrusters*, Proceedings of the Dynamic Positioning Conference, Marine Technology Society, Houston, TX, USA.

[77] van Dijk, R.R.T. & Aalbers, A.B. (2001) *What Happens in Water*, Proceedings of the Dynamic Positioning Conference, Marine Technology Society, Houston, TX, USA.

[78] Brown, D.T. & Ekstrom, L. (2005) *Vessel Thruster-Thruster Interactions during Azimuthing Operations*, Proceedings of the 24th ASME International Conference on Offshore Mechanics and Arctic Engineering - OMAE, vol. 1B, pp991-996, Halkidiki, Greece.

[79] Lehn, E. (1980) *Thruster Interaction Effects*, NFSI Report-102.80, The Ship Research Institute of Norway, Trondheim, Norway.

[80] Di Felice, F., Di Florio, D., Felli, M. & Romano, G.P. (2004) *Experimental Investigations of the Propeller Wake at Different Loading Conditions by Particle Image Velocimetry*, Journal of Ship Research, vol. 48, no. 2, pp168-190.

[81] Bosland, R., Huijsmans, R. & Dijk, J.M. (2009) *Numerical Prediction of Thruster-Thruster Interaction*, Proceedings of the 28th ASME Ocean, Offshore and Arctic Engineering Conference - OMAE, Honolulu, HI, USA.

[82] El Lababidy, S.A., Bose, N. & Lui, P. (2006) *Experimental Evaluation of a Dynamic Positioning Thruster Prohibited Operating Zone using Stereoscopic Particle Image Velocimetry (SPIV)*, Proceedings of the 25th ASME International Conference on Offshore Mechanics and Arctic Engineering – OMAE, Hamburg, Germany.

[83] Felli, M. (2009) *On the Hydrodynamic of an Impinging Swirling Jet: Effect of the Impingement Distance and the Swirl Number*, Proceedings of the 28th ASME Ocean, Offshore and Arctic Engineering Conference - OMAE, Honolulu, HI, USA.

[84] Prasad, J. & Elgamiel, H. (2006) *Model Tests for the DP System of a Drilling Semi-Submersible*, Proceedings of the Dynamic Positioning Conference, Marine Technology Society, Houston, TX, USA.

[85] Faltinsen, O.M. (1990) *Sea Loads on Ships and Offshore Structures*, Cambridge University Press, Cambridge, UK.

[86] Taniguchi, K., Watanabe, K. & Kasai, H. (1966) *Investigations into Fundamental Characteristics and Operating Performances of Side Thrusters*, Mitsubishi Technical Bulletin.

[87] Abu Skarkh, S.M., Turnock, S.R. & Hughes, A.W. (2003) *Design and Performance of an Electric Tip-Driven Thruster*, Proceedings of the Institution of Mechanical Engineers, Journal of Engineering for the Maritime Environment, vol. 217, pt. M, pp133-147.

[88] McLean, M.B. (1991) *Dynamic Performance of Small Diameter Tunnel Thrusters*, MS Thesis, Naval Postgraduate School.

[89] Cody, S.E. (1992) *Experimental Study of the Response of Small Tunnel Thrusters to Triangular and Square Wave Inputs*, MS Thesis, Naval Postgraduate School.

[90] Whitney, J.W. (1998) *An Experimental Investigation of the Design and Performance of Small Diameter Tunnel Thrusters*, MS Thesis, Florida Atlantic University.

[91] Norrby, R.A. (1974) *Evaluation of Side Thruster Performance*, International Shipbuilding Progress, vol. 21, no. 240, pp252-256.

[92] Brix, J.E. & Bussemaker, O. (1973) *Lateral Thrusters with Anti-Suction Tunnels*, Proceedings of the 1st North American Tug Convention, day 4, paper 5, pp263-284, Vancouver, Canada.

[93] Beveridge, J.L. (1972) *Design and Performance of Bow Thrusters*, Marine Technology, vol. 9, no. 4, pp439-453.

[94] Saunders, A. & Nahon, M. (2002) *The Effect of Forward Vehicle Velocity on Through-Body AUV Tunnel Thruster Performance*, Proceedings of the MTS/IEEE Oceans Conference, vol. 1, pp250-259, Biloxi, MS, USA.

[95] Margason, R.J. (1968) *The Path of a Jet Directed at Large Angles to a Subsonic Free Stream*, NASA-TN-D-4919.

[96] Chislett, M.S. & Björheden, O. (1966) *Influence of Ship Speed on the Effectiveness of a Lateral-Thrust Unit*, Report Hy-8, Hydro-og Aerodynamisk Laboratorium, Lyngby, Denmark.

[97] Karlikov, V.P. & Sholomovich, G.I. (1998) *Some Features of Body-flow Interaction in the Presence of Transverse Jets*, Fluid Dynamics, vol. 33, no. 3, pp313-317.

[98] Symons, P.J.R. & Sadden, J.A. (1982) *The Design of the Seabed Operations Vessel*, Trans. RINA, vol. 124, pp41-61.

[99] Minsaas, K.J., Thon, H.J. & Kauczynski, W. (1987) *Estimation of Required Thruster Capacity for Operation of Offshore Vessels under Severe Weather Conditions*, Proceedings of the 3rd International Symposium on Practical Design of Ships and Mobile Units - PRADS, vol. 1, pp411-433, Trondheim, Norway.

[100] Norrby, R.A. & Ridley, D.E. (1981) *Notes on Thrusters for Ship Maneuvering and Dynamic Positioning*, Trans. SNAME, vol. 88, pp 377-402.

[101] Schottel. *Schottel Transverse Thruster Catalogue*, Available at http://www.schottel.de/. Viewed 24/09/08.

[102] Muppidi, S. & Mahesh, K. (2007) *Direct Numerical Simulation of Round Turbulent Jets in Crossflow*, Journal of Fluid Mechanics, vol. 574, pp59-84.

[103] Steden, M., Hundemer, J., Müller, S.-B. & Abdel-Maksoud, M. (2007) *Untersuchung der Umströmung von aus Mehrkomponenten bestehenden Schiffsantrieben*, (*Geometrical Parameterisation and Investigation of the Flow around Ship-Propulsors consisting of Multi-Components*), 102. Hauptversammlung der Schiffbautechnischen Gesellschaft, Berlin, Germany. (In German)

[104] Kinnas, S.A., Chang, S.-H., He, L. & Johannessen, J.T. (2009) *Performance Prediction of a Cavitating Rim Driven Tunnel Thruster*, Proceedings of the 1st International Symposium on Marine Propulsors – smp'09, pp435-442, Trondheim, Norway.

[105] Sileo, L. & Steen, S. (2009) *Numerical Investigation of the Interaction Between a Stern Tunnel Thruster and Two Main Ducted Propellers*, Proceedings of the 1st International Symposium on Marine Propulsors – smp'09, pp129-138, Trondheim, Norway.

[106] Fallows, C.D. (2004) *Characterisation of the Propulsion Systems of Underwater Vehicles*, PhD Thesis, University of Southampton.

[107] http://www.tsltechnology.com/ - TSL Technology Limited Website. Viewed 24/06/2008.

[108] International Towing Tank Conference. (2006) *ITTC Recommended Procedures*, (*Resistance Tests* 7.5-02-02-01, *Density and Viscosity of Water* 7.5-02-01-03, *Uncertainty Analysis Guidelines for Resistance Towing Tank Tests* 7.5-02-02-02) ITTC.

[109] Sheldahl, R.E. & Klimas, P.C. (1981) *Aerodynamic Characteristics of Seven Symmetrical Airfoil Sections through 180-Degree Angle of Attack for use in Aerodynamic Analysis of Vertical Axis Wind Turbines*, SAND80-2114, Sandia National Laboratories, Albuquerque, NM, USA.

[110] Lewandowski, E.M. (2004) *The Dynamics of Marine Craft: Maneuvering and Seakeeping*, World Scientific, Singapore.

[111] Nikolaev, E.P., Pershits, R.Y. & Russetzky, A.A. (1972) *Estimation of the Effectiveness of Lateral Thrust Units*, Journal of Mechanical Engineering Science, vol. 14, no. 7, supplementary issue, paper 21, pp155-160.

[112] Godhavn, J.-M., Fossen, T.I. & Berge, S.P. (1998) *Nonlinear and Adaptive Backstepping Designs for Tracking Control of Ships,* International Journal of Adaptive Control and Signal Processing, vol. 12, no. 8, pp649-670.

[113] Kuhn, R.E., Margason, R.J. & Curtis, P. (2007) *Jet Induced Effects: The Aerodynamics of Jet and Fan Powered V/STOL Aircraft in Hover and Transition*, AIAA, Reston, VA, USA.

[114] Palmer, A.R., Hearn, G.E. & Stevenson, P. (2008) *Modelling Tunnel Thrusters for Autonomous Underwater Vehicles,* Proceedings of the IFAC Workshop on Navigation, Guidance and Control of Underwater Vehicles - NGCUV, Killaloe, Ireland.

[115] Cousturier, R., Eddy, N., Furlong, M., Harris, C., Liu, J., Palmer, A., Phillips, A., Sharkh, S. & Turnock, S. (2009) *Delphin: The University of Southampton Entry into the 2009 Student Autonomous Underwater Challenge – Europe*, Proceedings of the 4th Student Autonomous Underwater Challenge – Europe, Gosport, UK.

[116] Furlong, M. (2005) *System Identification of the Hydrodynamic Characteristics of Underwater Vehicles*, EngD Thesis, University of Southampton.

[117] Booth, T.B., Randall, J.W. & Hirom, C.P.J. (1980) *Dynamic Characteristics of Submarines*, Second Edition, Technical Report, AMTE Haslar, UK.

[118] McPhail, S.D. & Pebody, M. (1997) *Autosub-1. A Distributed Approach to Navigation and Control of an Autonomous Underwater Vehicle*, Proceedings of the 7th IEEE International Conference on Electronic Engineering in Oceanography - Technology Transfer from Research to Industry, pp16-22, Southampton, UK.

[119] Hoerner, S.F. (1965) *Fluid Dynamic Drag*, Published by the Author.

[120] Jakuba, M.V., Yoerger, D.R., Whitcomb, L.L. & Gobat, J.I. (2007) *Longitudinal Control Design and Performance Evaluation for the Nereus 11,000m Underwater Vehicle*, Proceedings of the MTS/IEEE Oceans Conference, Vancouver, Canada.

[121] Whitcomb, L.L., Jakuba, M.V., Kinsey, J.C., Martin, S.C., Webster, S.E., Howland, J.C., Taylor, C.L., Gomez-Ibanez, D. & Yoerger, D.R. (2008) *Navigation and Control of the Nereus Hybrid Underwater Vehicle for Global Ocean Science to 11,000m Depth: Preliminary Results*, Proceedings of the 14th Yale Workshop on Adaptive and Learning Systems, New Haven, CT, USA.

[122] Breivik, M. & Fossen, T.I. (2006) *A Unified Control Concept for Autonomous Underwater Vehicles*, Proceedings of the IEEE American Control Conference, Minneapolis, MN, USA.

[123] Furlong, M.E., McPhail, S.D. & Stevenson, P. (2007) *A Concept Design for an Ultra-Long-Range Survey Class AUV*, Proceedings of the MTS/IEEE Oceans Conference, Aberdeen, UK.

[124] Batchelor, G.K. (1967) *An Introduction to Fluid Dynamics*, Cambridge University Press, Cambridge, UK.

[125] Rusak, Z. & Meder, C.C. (2004) *Near-critical Swirling Flow in a Slightly Contracting Pipe*, AIAA Journal, vol. 42, no. 11, pp2284-2293.

[126] Allmendinger, E.E. (1990) *Submersible Vehicle Systems Design*, Society of Naval Architects and Marine Engineers, New York, USA.

[127] Hochbaum, A.C. (2008) *The Manoeuvring Committee: Final Report and Recommendations to the 25th ITTC*, Proceedings of the 25th International Towing Tank Conference, Fukuoka, Japan.

[128] Hwang, W.Y., Jacobsen, B.K., Barr, R.A., Ankudinov, V.K., Fuller, N.R., Vest, L.C., Morris, M.A., McGovern, A.W. & Landsburg, A.C. (2003) *An Exploratory Study to Characterize Ship Maneuvering at Slow Speed*, Proceedings of International Conference on Marine Simulation and Ship Maneuverability – MARSIM'03, Kanazawa, Japan.

[129] Quadvlieg, F.H.H.A. & van Coevorden, P. (2003) *Manoeuvring Criteria: More than IMO A.751 Requirement Alone*, Proceedings of International Conference on Marine Simulation and Ship Maneuverability – MARSIM'03, Kanazawa, Japan.

[130] Dand, I. (2003) *Low Speed Manoeuvring Criteria: Some Considerations*, Proceedings of International Conference on Marine Simulation and Ship Maneuverability – MARSIM'03, Kanazawa, Japan.

[131] Liu, J., Furlong, M., Palmer, A., Phillips, A., Turnock, S. and Sharkh, S. (2009) *Design and Control of a Flight-Style AUV with Hovering Capability*, Proceedings of the 16th AUSI International Symposium on Unmanned Untethered Submersible Technology - UUST, Durham, NH, USA.

Appendix A – Additional Calculations, Derivations and Data

Appendix A1 Autosub Propeller Particulars

Table A1.1 – Autosub Propeller Design Parameters

Parameter	**Value**
Design Drag Coefficient (Volumetric)	0.045
Design Wake Fraction	0.15
Design Thrust Deduction Factor	0.10
Hub Diameter	0.22m

Table A1.2 – Autosub Propeller Particulars

Parameter	**Value**
Autosub Design Survey Speed	$1.75 m.s^{-1}$
Design Shaft Rotational Speed	300rpm
Propeller Diameter	0.70m
Number of Propeller Blades	2
Average Blade p_B / d	0.54
Maximum Blade Chord	35mm
Blade Angle of Attack	3º
Basis Propeller Section	NACA 65(2)-415 (a=0.5)

Table A1.3 – Autosub Control Surface Particulars

Parameter	**Value**
Basis Section	NACA 0015
Area	$0.1162 m^2$
Taper Ratio	0.7337
Outreach	0.3714m
Flap Area	$0.06664 m^2$

Figure A1.1 – Photograph showing the Autosub Propeller and Control Surfaces

Appendix A2 Results of Potential Flow Calculations with Autosub Hull

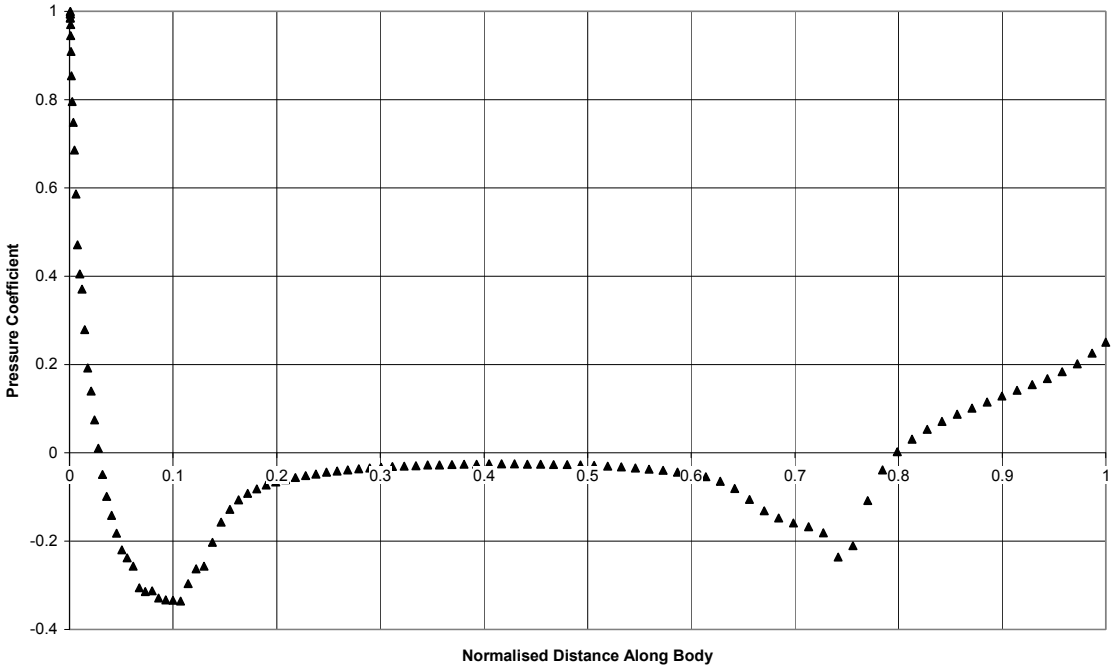

Figure A2.1 – Longitudinal Distribution of Pressure Coefficient along Autosub

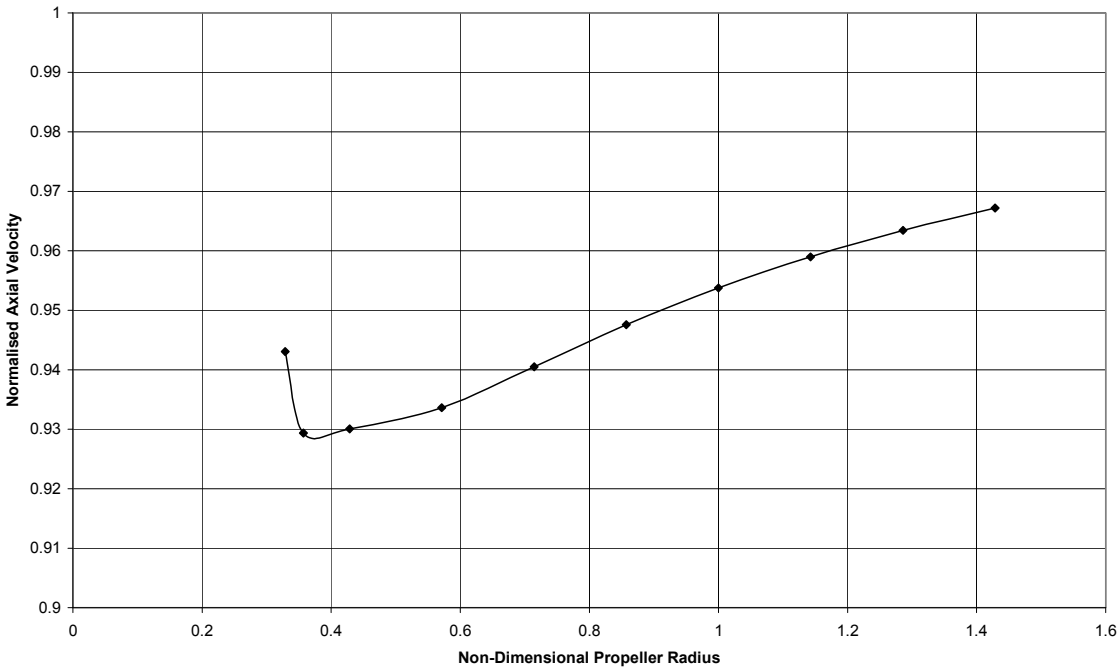

Figure A2.2 – Axial Velocity Distribution at the Propeller Plane

Appendix A3 Calculation of Turning Radii

Consider the steady linearised sway and yaw equations for an AUV equipped with control surfaces:

$$-Y'_v v' + (-Y'_r + m')r' = Y'_\delta \delta$$

$$-N'_v v' + (-N'_r r' + m' x'_G)r' = N'_\delta \delta$$

Eliminating the non-dimensional sway velocity, v', solving for the non-dimensional yaw rate, r', and inverting yields the non-dimensional turning radius as a function of control surface deflection angle, δ:

$$R' = \frac{1}{r'} = \frac{(-Y'_r + m')N'_v - (-N'_r + m' x'_G)Y'_v}{(Y'_\delta N'_v - N'_\delta Y'_v)\delta}.$$

The terms $Y'_\delta \delta$ and $N'_\delta \delta$ represent the control surfaces generated non-dimensional sway force and yaw moment respectively. Hence these terms can be replaced as appropriate to develop similar relationships for alternative actuator configurations.

Table A3.1 – Linearised Hydrodynamic Coefficient Values in the Horizontal Plane [25]

Coefficient	Value
Y'_r	0.01122
Y'_v	-0.02913
Y'_δ	0.01016

Coefficient	Value
N'_r	-0.00504
N'_v	-0.00468
N'_δ	-0.00442

Appendix A4 Calculation of Depth Control Limiting Speed

Consider the steady linearised heave equation for an AUV equipped with control surfaces:

$$Z_w w + Z_\delta \delta = B\theta .$$

Rearranging for the heave velocity, w, yields;

$$w = \frac{B\theta - Z_\delta \delta}{Z_w} .$$

The steady linearised pitch equation for an AUV equipped with control surfaces is:

$$M_w w + M_\theta \theta + M_\delta \delta = 0 ,$$

with $M_\theta = mg\overline{BG}$.

Substituting the rearranged heave equation into the pitch equation and rearranging for the pitch angle, θ, gives:

$$\theta = \frac{Z_\delta \delta Z_w \left[\frac{M_w}{Z_w} - \frac{M_\delta}{Z_\delta} \right]}{M_w B + mg\overline{BG} Z_w} .$$

Using the limiting condition for depth control that $\theta = -\frac{w}{U_c}$ gives:

$$0 = \frac{(B + Z_w U_c) Z_w \left[\frac{M_w}{Z_w} - \frac{M_\delta}{Z_\delta} \right]}{M_w N + mg\overline{BG} Z_w} .$$

Non-dimensionalising the hydrodynamic derivatives and rearranging yields the critical speed for depth control, U_c, as a function of the mass, m, and buoyancy, B:

$$U_c^2 = \frac{M'_w lB + mg\overline{BG} Z'_w - BZ'_w l \left[\frac{M'_w}{Z'_w} - \frac{M'_\delta}{Z'_\delta} \right]}{Z'^2_w 0.5\rho l^3 \left[\frac{M'_w}{Z'_w} - \frac{M'_\delta}{Z'_\delta} \right]} .$$

Table A4.1 – Linearised Hydrodynamic Coefficient Values in the Vertical Plane [25]

Coefficient	Value
Z'_w	-0.02913
Z'_δ	-0.01062

Coefficient	Value
M'_w	0.00468
M'_δ	0.04416

Appendix A5 Derivation of Zero Speed Thruster Power Relationship

Consider the simplified representation of a propeller as a disk which imparts a uniform acceleration to the fluid passing through it, as illustrated in Figure A5.1, where u is the propeller speed of advance and a_m is defined as the axial inflow factor:

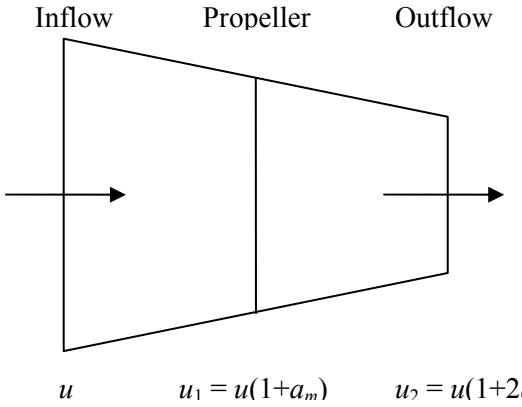

Figure A5.1 – Momentum Theory Representation of a Propeller

The thrust generated is given by:

$$T = \dot{m}(\Delta u) = \rho A u_1 (u_2 - u) = \rho A u^2 (1 + a_m) 2a_m .$$

Now, defining a slip ratio, s, as the velocity increase compared to the speed of advance:

$$s = \frac{2a_m u}{u} = 2a_m .$$

Considering the ideal efficiency of the propeller in terms of the slip ratio gives:

$$\eta_{IDEAL} = \frac{Useful\ Work}{Work\ Done} = \frac{Tu}{Tu_1} = \frac{1}{1 + a_m} = \frac{2}{2 + s} .$$

Inserting the slip ratio into the generated thrust yields:

$$T = \rho A u^2 \left(1 + \frac{s}{2}\right) s .$$

Now, defining the thrust coefficient, C_T, in terms of the slip ratio:

$$C_T = \frac{T}{\frac{1}{2}\rho A u^2} = s(2 + s) .$$

Rearranging this to give the slip ratio in terms of the thrust coefficient:

$$s = \sqrt{C_T + 1} - 1 .$$

Inserting this into the ideal efficiency and assuming that at low speed $C_T >> 1$ gives:

$$\eta_{IDEAL} = \frac{2}{C_T^{1/2}}.$$

The power required by a propeller is given by:

$$P = \frac{Tu}{\eta_{IDEAL}} = \frac{TuC_T^{1/2}}{2} = \frac{Tu}{2}\sqrt{\frac{T}{0.5\rho A u^2}} = T\sqrt{\frac{1}{2}}\sqrt{\frac{T}{\rho A}}.$$

Rearranging this gives the ideal power per unit thrust required to develop a given thrust from a propeller of a given area:

$$\frac{P}{T} = \sqrt{\frac{1}{2}}\sqrt{\frac{T}{\rho A}}.$$

Note that some authors neglect the $\sqrt{\frac{1}{2}}$ term for convenience.

Appendix A6 Experimental Results

The following figures are repeats of those given in the main text as Figures 4.15 and 4.16 and Figures 4.27 to 4.46 presented without error bars for clarity.

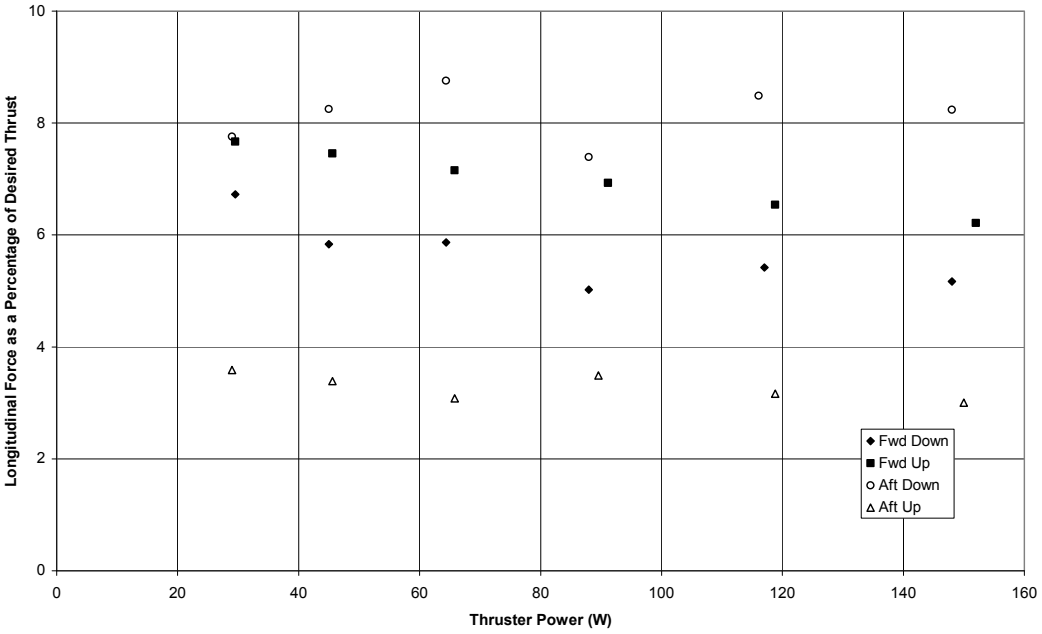

Figure A4.15 – Longitudinal Force induced by the Operation of an External Thruster mounted near a Vehicle as a function of Thruster Location (Fwd/Aft), Jet Direction (Up/Down) and Thruster Power.

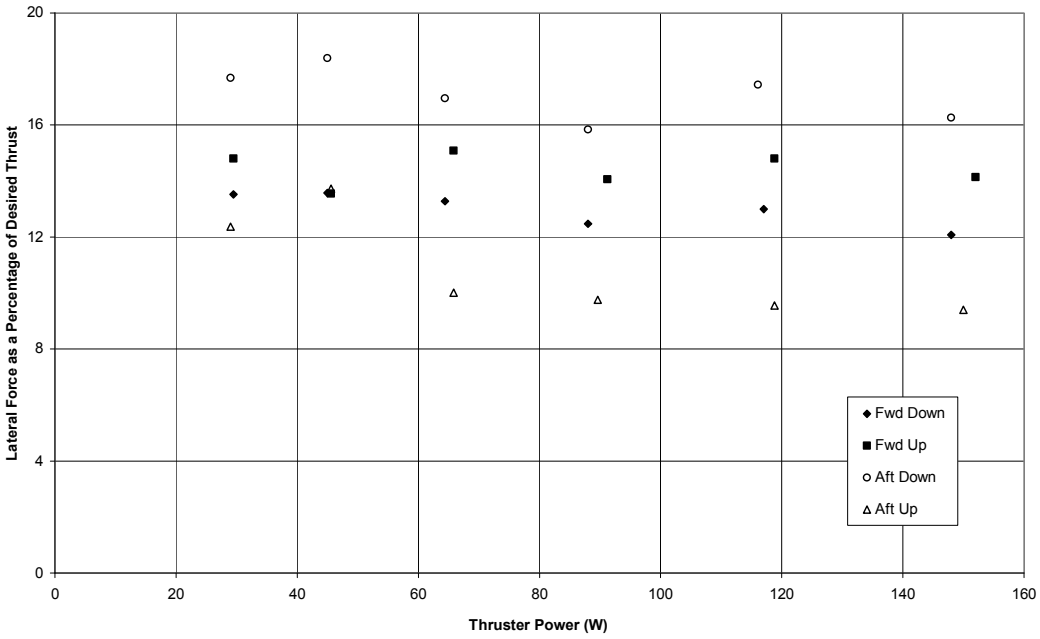

Figure A4.16 – Lateral Force induced by the Operation of an External Thruster mounted near a Vehicle as a function of Thruster Location (Fwd/Aft), Jet Direction (Up/Down) and Thruster Power.

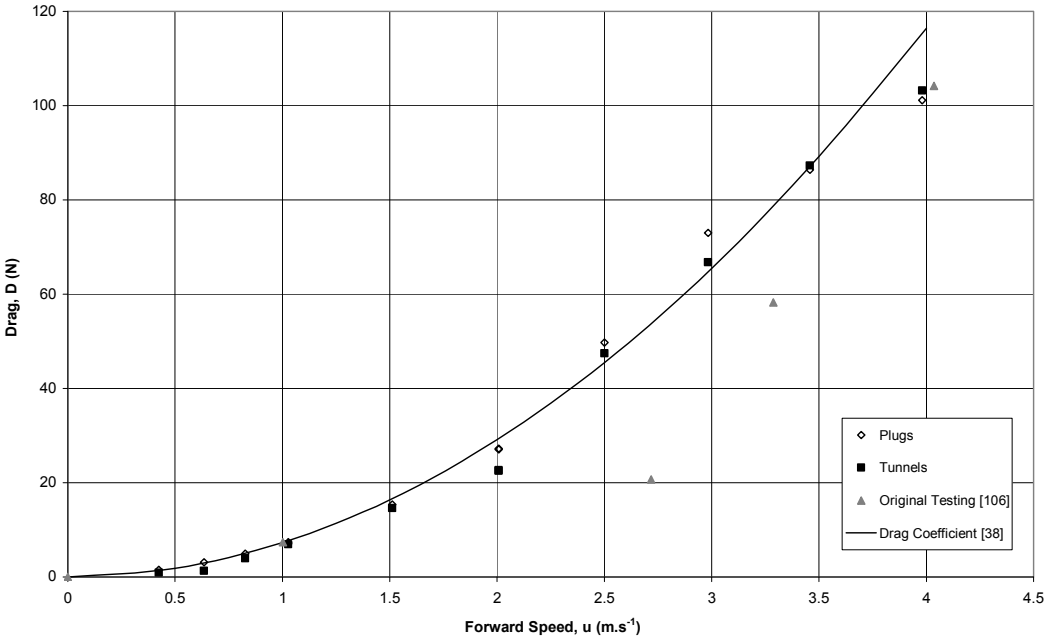

Figure A4.27 – Variation of Vehicle Drag with Forward Speed

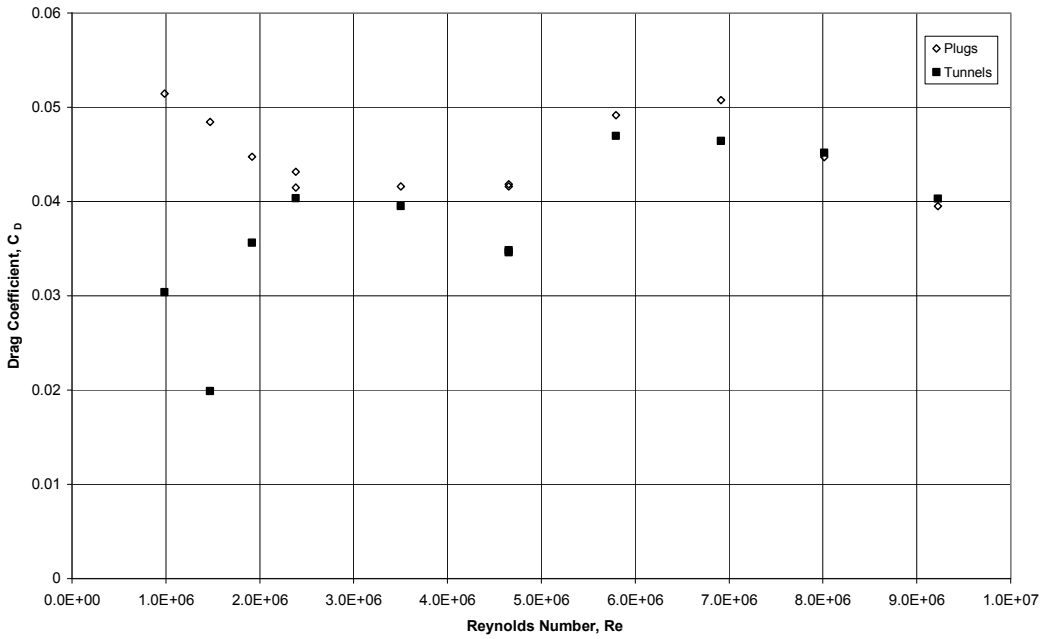

Figure A4.28 – Variation of Vehicle Drag Coefficient with Reynolds Number

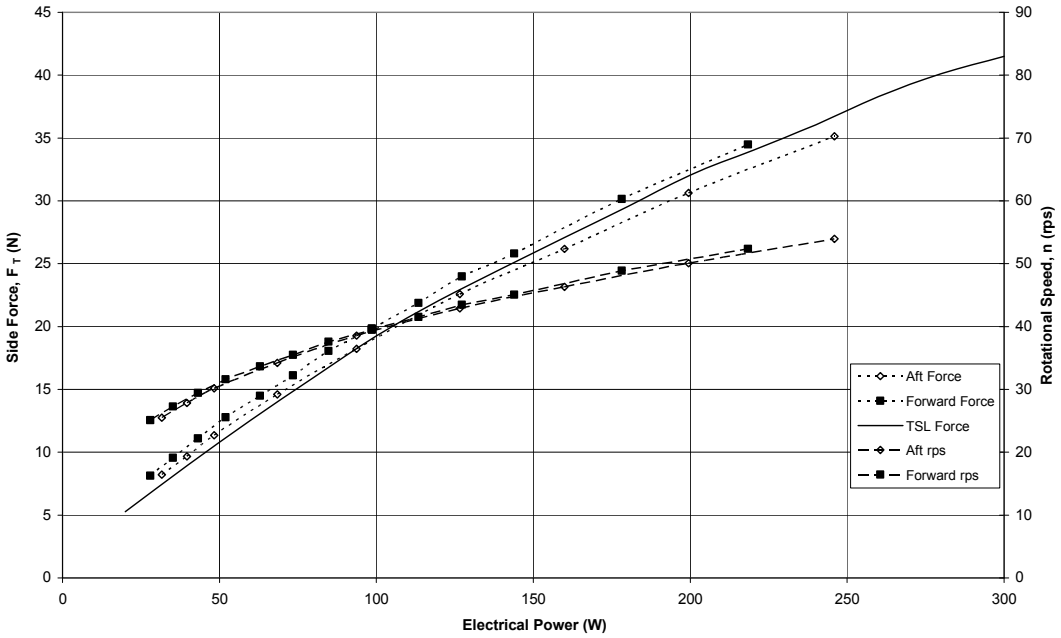

Figure A4.29 – Tunnel Thruster Performance at Zero Speed

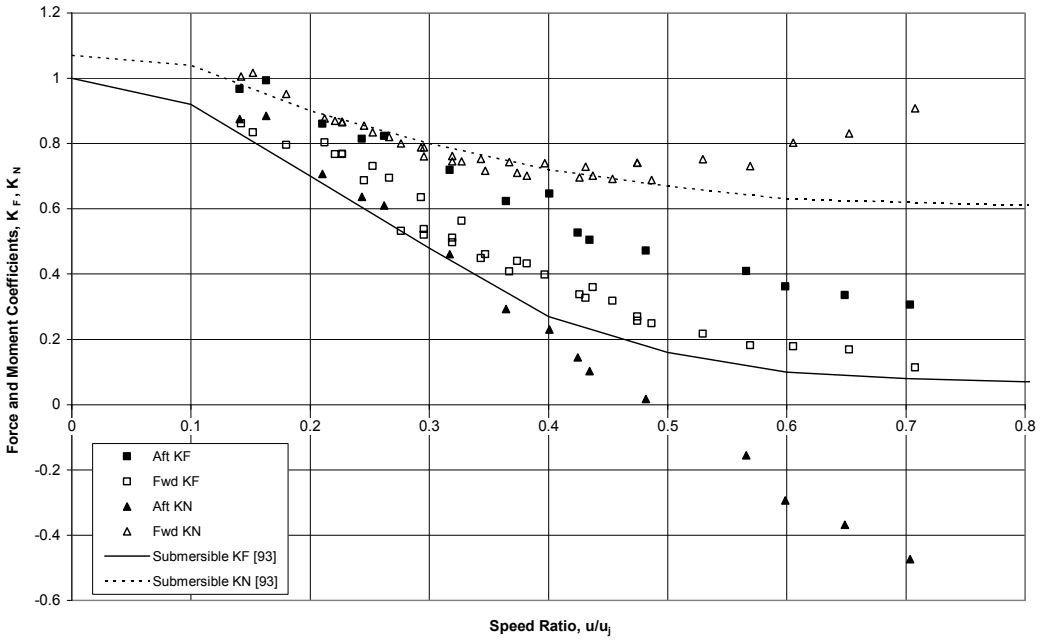

Figure A4.30 – Tunnel Thruster Performance on a Moving Vehicle

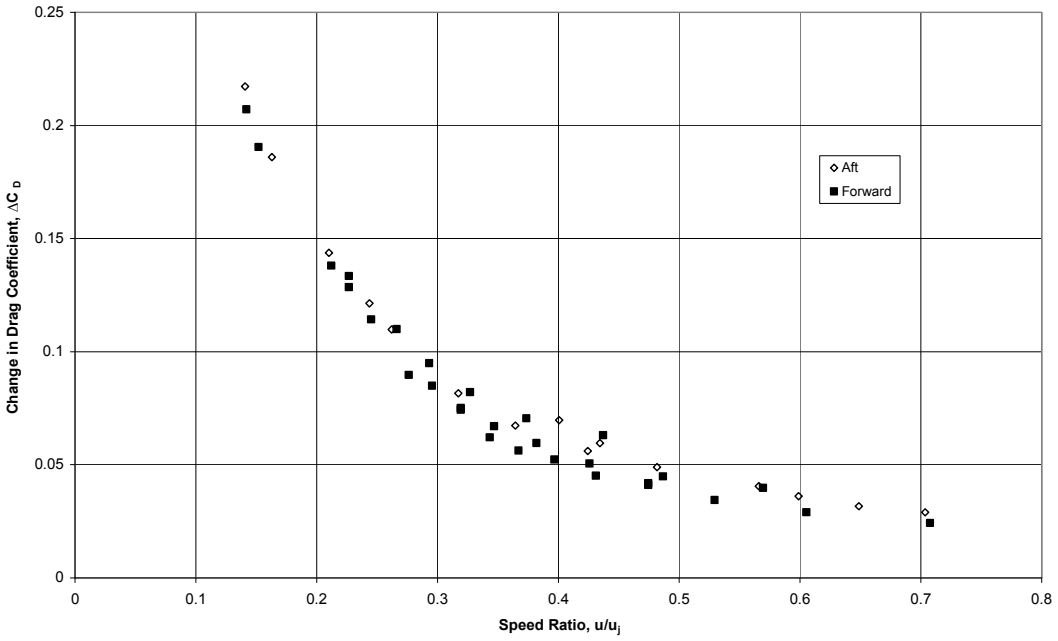

Figure A4.31 – Variation of Vehicle Drag Coefficient with Speed Ratio caused by Thruster Operation

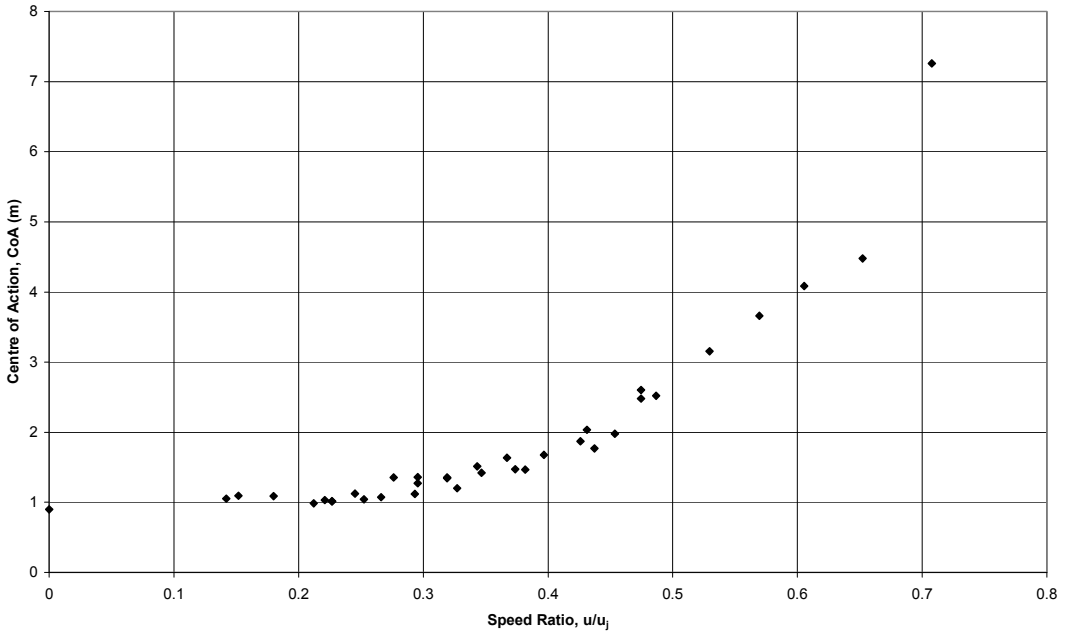

Figure A4.32 – Variation of the Centre of Action of the Yaw Moment with Speed Ratio for the Forward Thruster

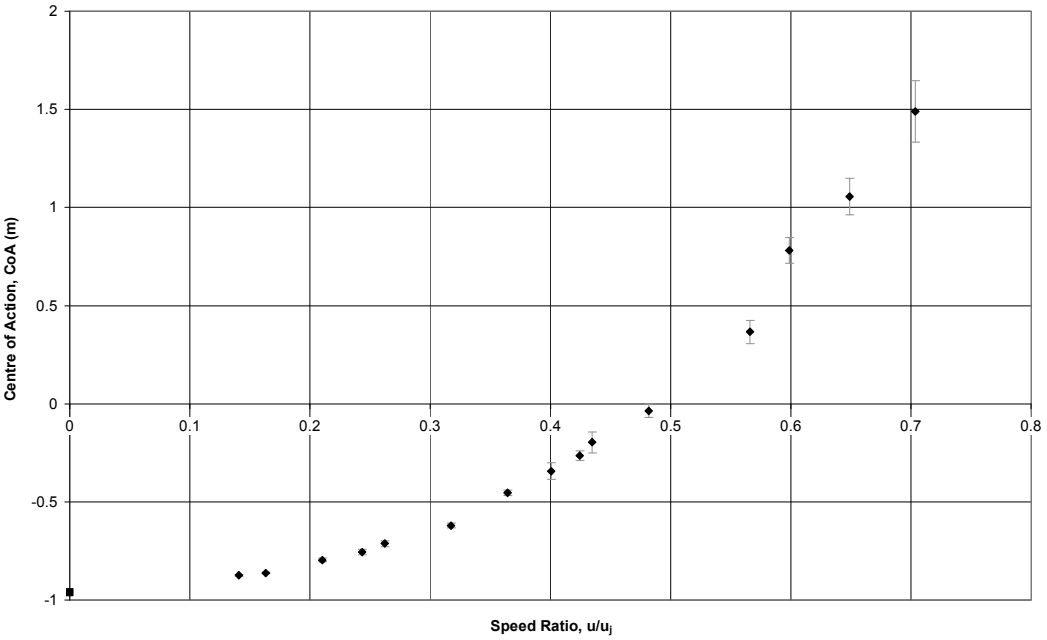

Figure A4.33 – Variation of the Centre of Action of the Yaw Moment with Speed Ratio for the Aft Thruster

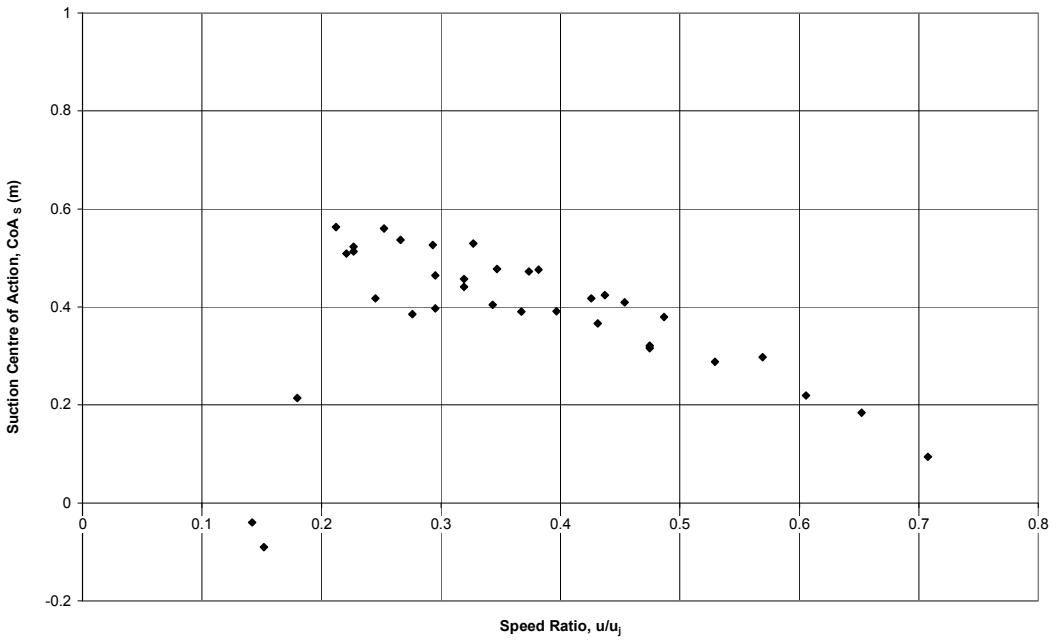

Figure A4.34 – Variation of the Centre of Action of the Suction Force with Speed Ratio for the Forward Thruster

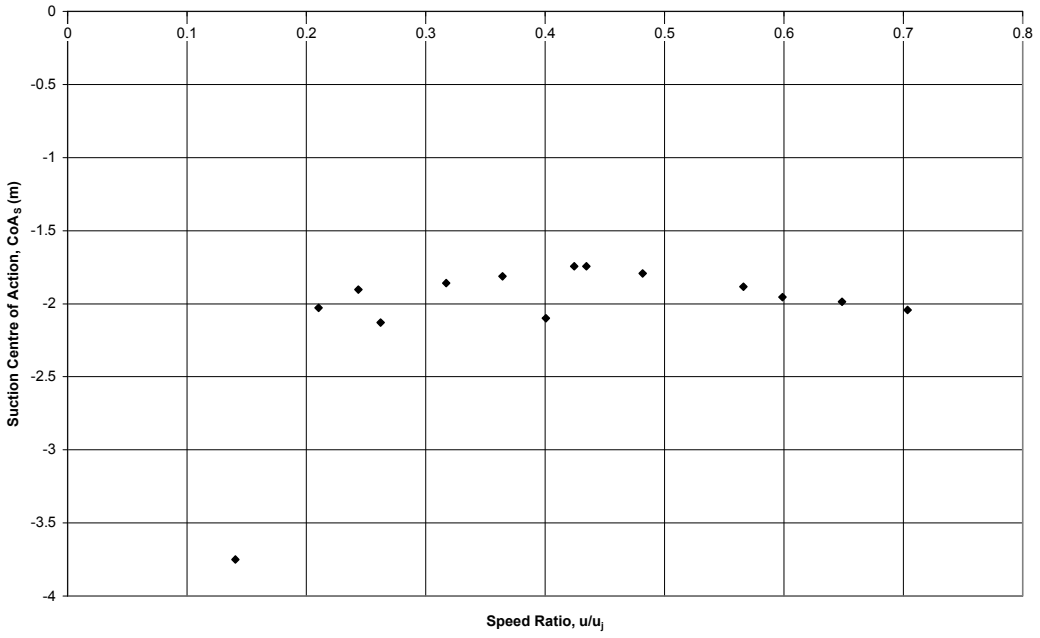

Figure A4.35 – Variation of the Centre of Action of the Suction Force with Speed Ratio for the Aft Thruster

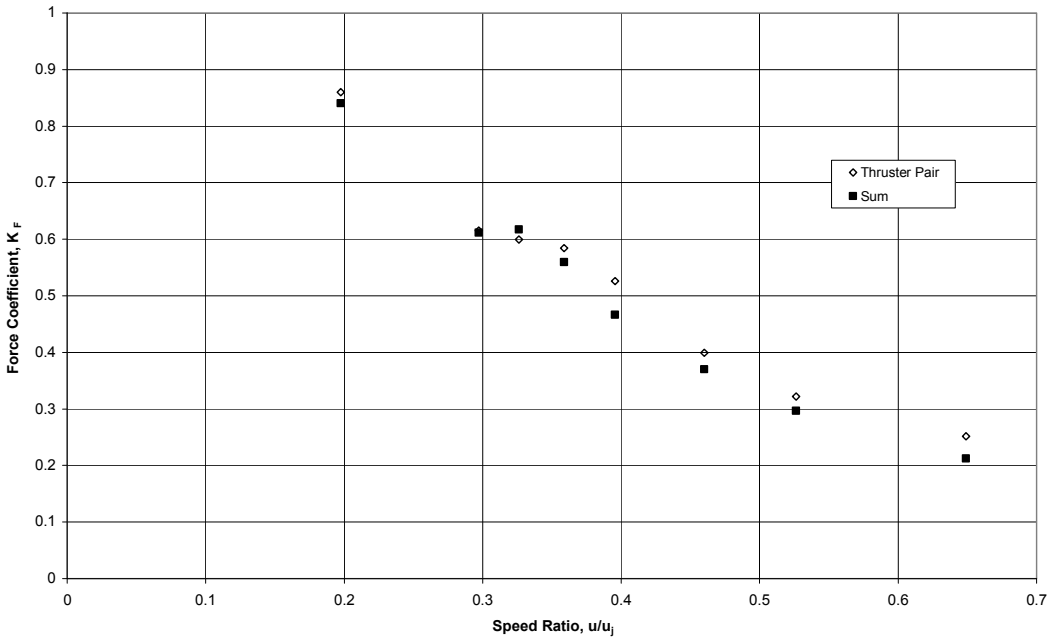

Figure A4.36 – Variation of Generated Side Force with Speed Ratio using a Thruster Pair

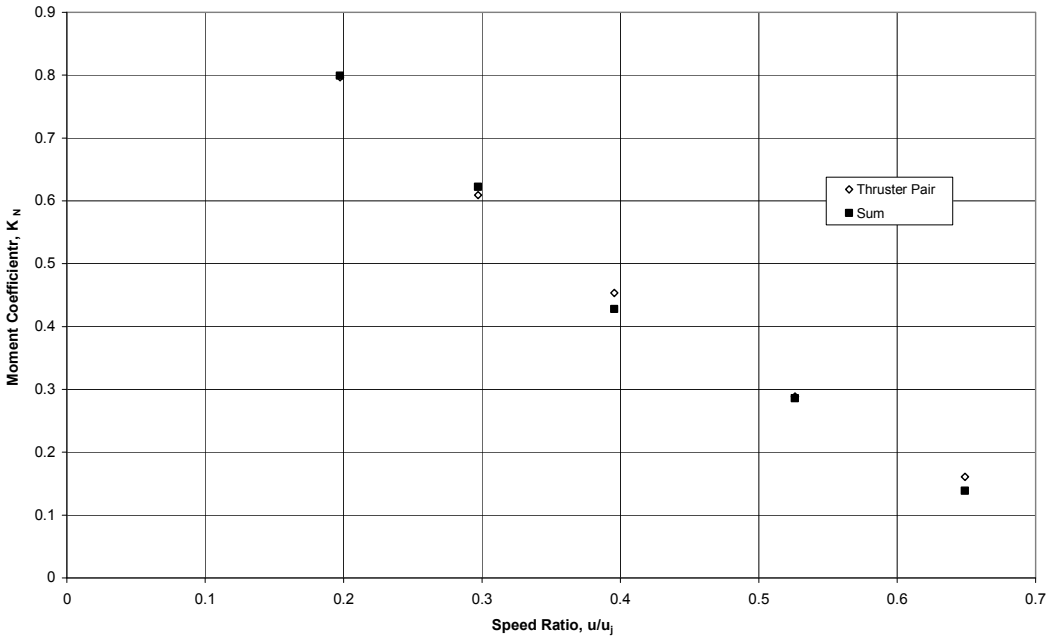

Figure A4.37 – Variation of Generated Yaw Moment with Speed Ratio using a Thruster Pair

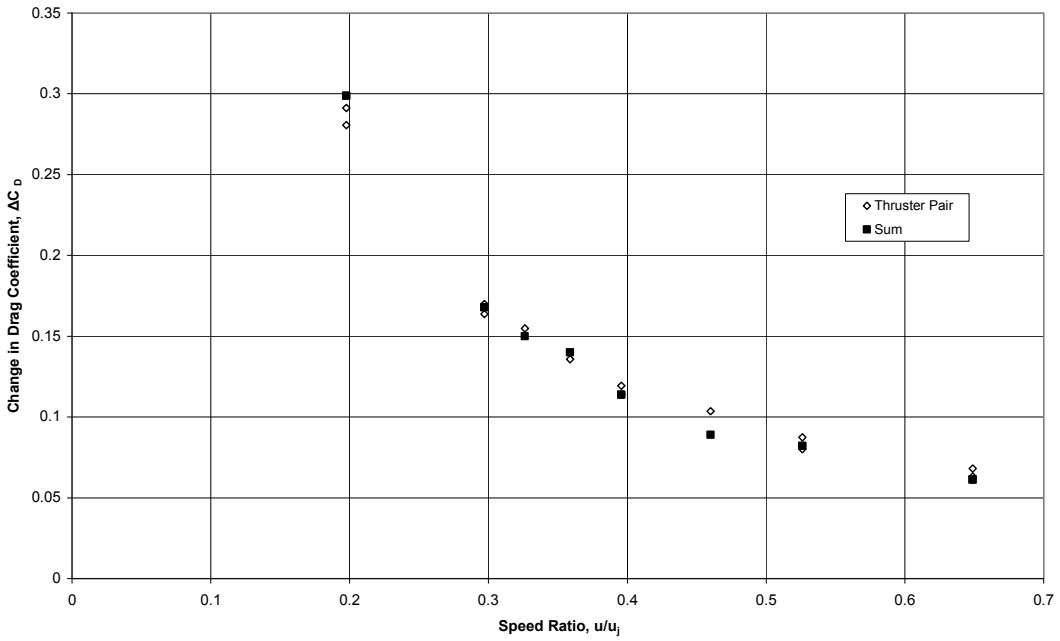

Figure A4.38 – Variation of Vehicle Drag Coefficient with Speed Ratio using a Thruster Pair

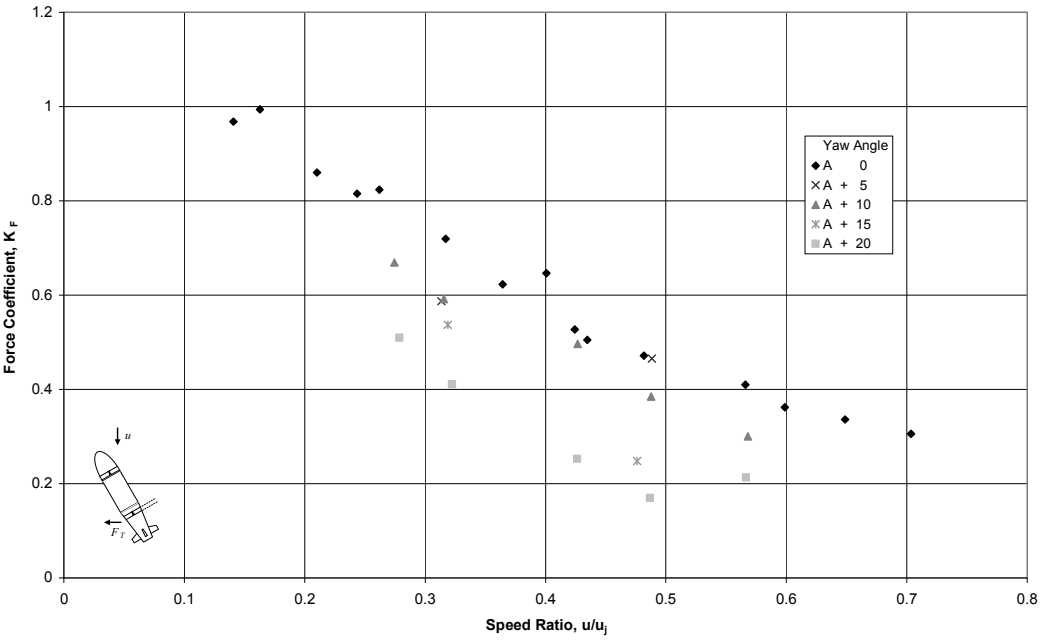

Figure A4.39 – Variation of Aft Thruster Side Force Performance with Speed Ratio at Positive Yaw Angles

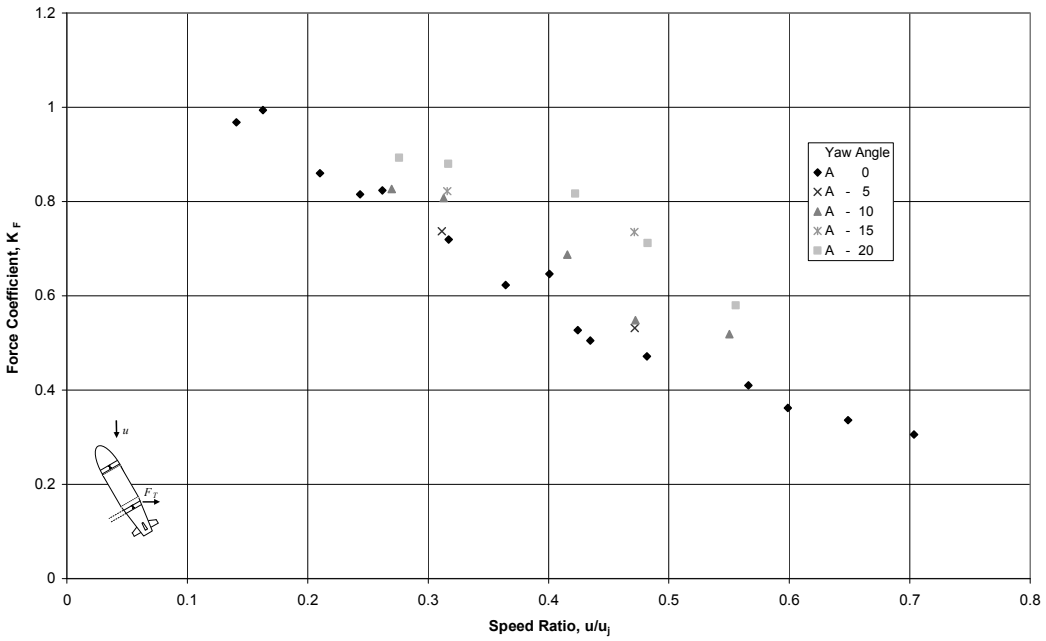

Figure A4.40 – Variation of Aft Thruster Side Force Performance with Speed Ratio at Negative Yaw Angles

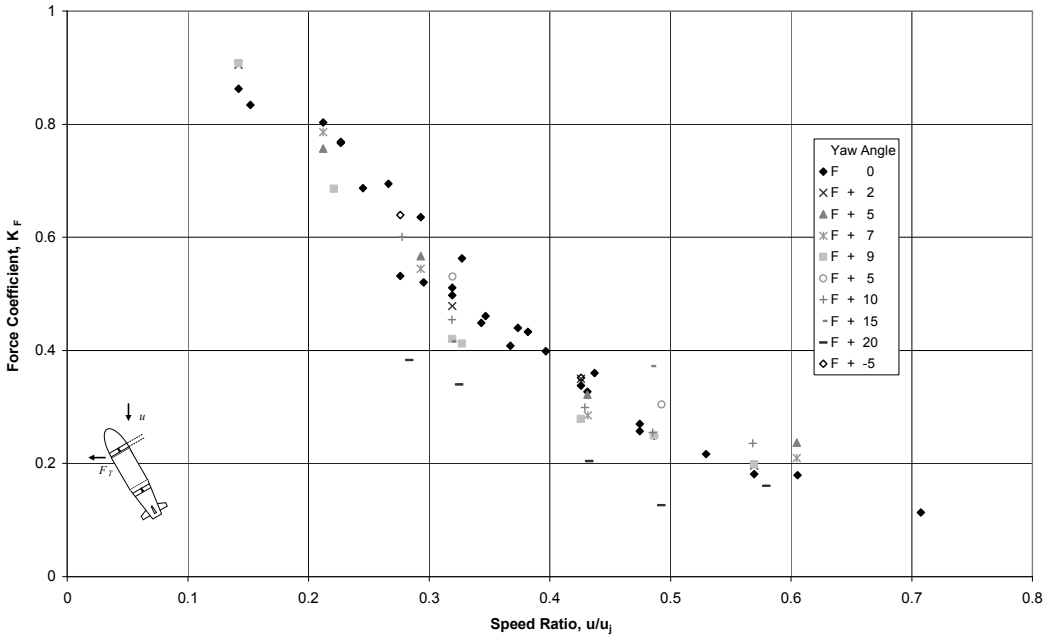

Figure A4.41 – Variation of Forward Thruster Side Force Performance with Speed Ratio at Positive Yaw Angles

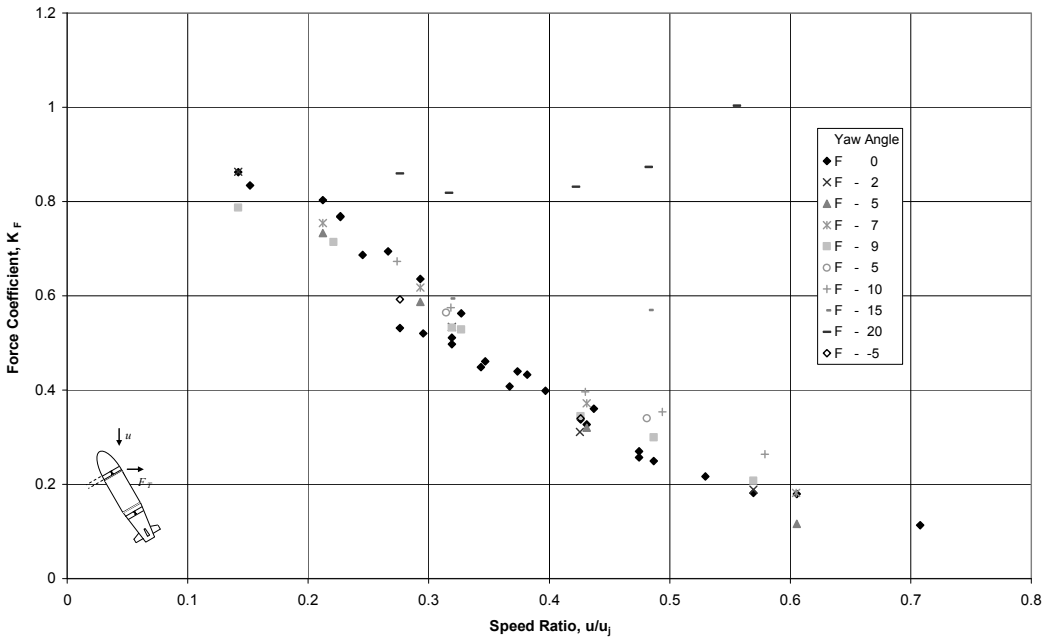

Figure A4.42 – Variation of Forward Thruster Side Force Performance with Speed Ratio at Negative Yaw Angles

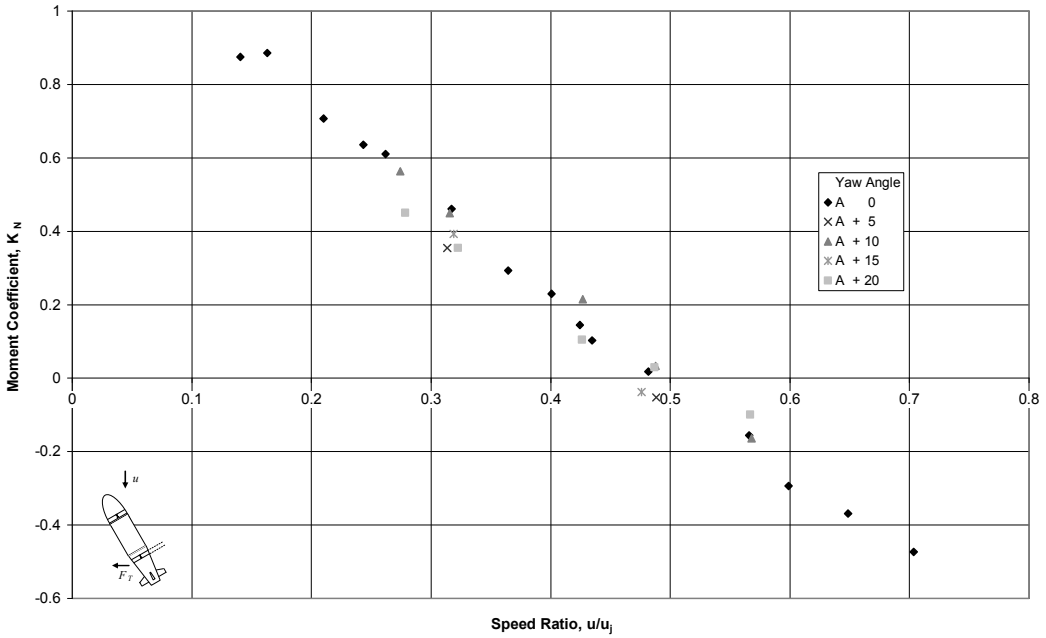

Figure A4.43 – Variation of Aft Thruster Moment Performance with Speed Ratio at Positive Yaw Angles

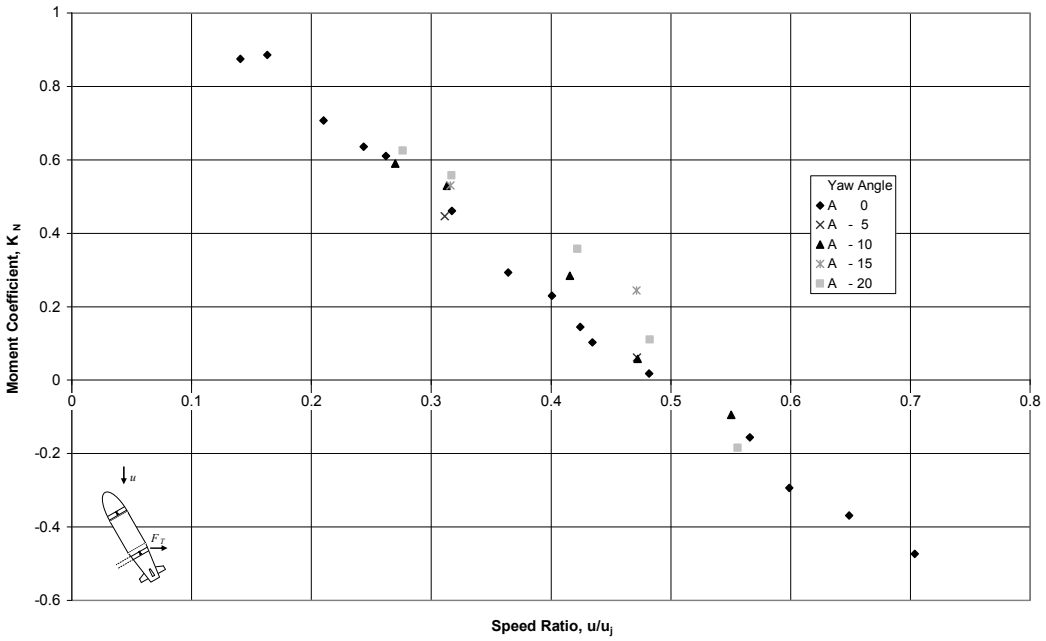

Figure A4.44 – Variation of Aft Thruster Moment Performance with Speed Ratio at Negative Yaw Angles

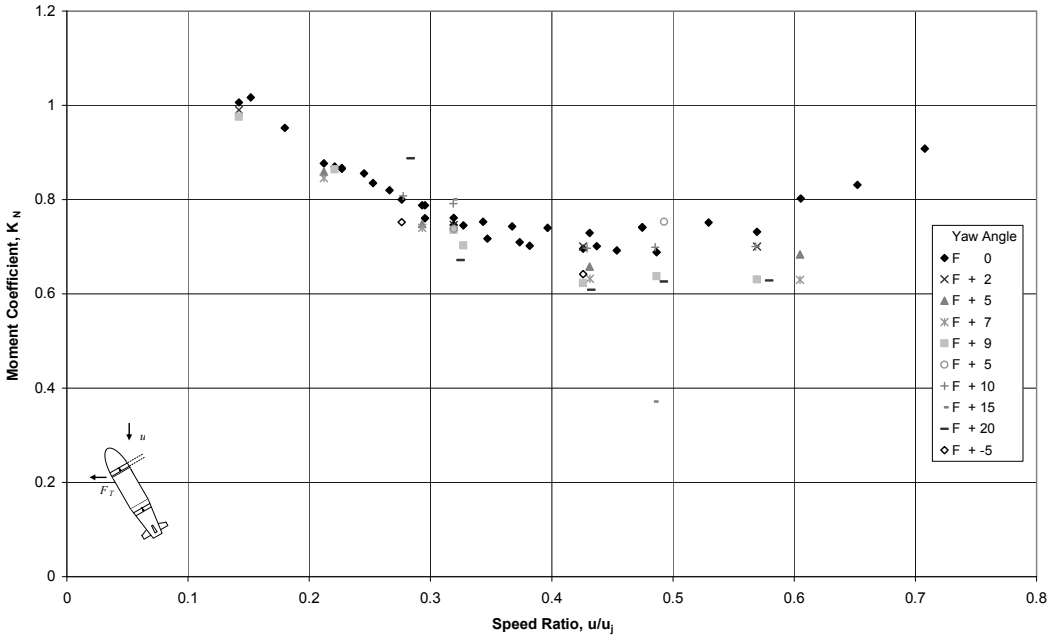

Figure A4.45 – Variation of Forward Thruster Moment Performance with Speed Ratio at Positive Yaw Angles

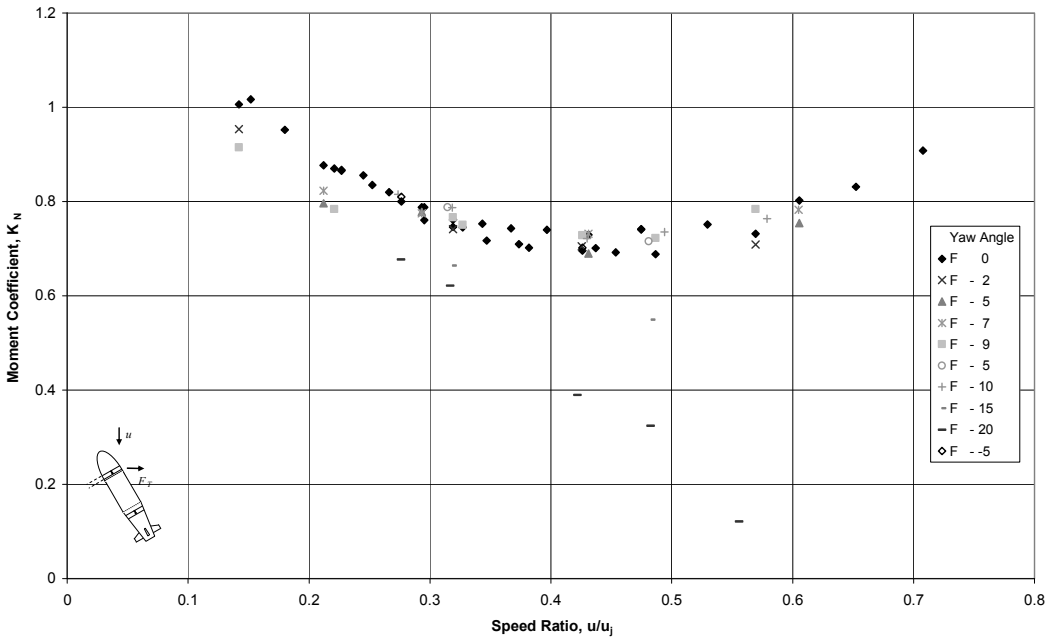

Figure A4.46 – Variation of Forward Thruster Moment Performance with Speed Ratio at Negative Yaw Angles

Appendix B – Published Work

Published versions of the research reported in this thesis are provided here.

Appendix B1 Modelling Tunnel Thrusters for Autonomous Underwater Vehicles

Pages 207 - 212

Palmer, A.R., Hearn, G.E. and Stevenson, P.

Proceedings of the IFAC Workshop on Navigation, Guidance and Control of Underwater Vehicles (NGCUV), Killaloe, Ireland, 8-10 April 2008

Appendix B2 Thruster Interactions on Autonomous Underwater Vehicles

Pages 213 - 221

Palmer, A.R., Hearn, G.E. and Stevenson, P.

Proceedings of the 28th ASME International Conference on Ocean, Offshore and Arctic Engineering (OMAE2009), Waikiki, Hawaii, USA, 31 May–5 June 2009

Appendix B3 Experimental Testing of an Autonomous Underwater Vehicle Equipped with Tunnel Thrusters

Pages 222 - 228

Palmer, A.R., Hearn, G.E. and Stevenson, P.

Proceedings of the First International Symposium on Marine Propulsion (smp'09), pp569-575, Trondheim, Norway, 22-24 June 2009

Appendix B4 A Theoretical Approach to Facilitating Transition Phase Motion in a Positively Buoyant Autonomous Underwater Vehicle

Pages 229 - 244

Palmer, A.R., Hearn, G.E. and Stevenson, P.

Transactions of the Royal Institution of Naval Architects 2009 (Accepted, to appear)